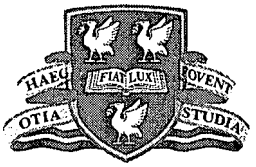

THE UNIVERSITY
of LIVERPOOL

Robust Low-Order Control Techniques with Powertrain Applications

---

Thesis submitted in accordance with the requirements of the
University *of* Liverpool for the
Degree of Doctor in Philosophy

by

Paul Dickinson

November 2007

Acknowledgments

I owe a special thanks to Tom Shenton for his supervision during this work. His guidance and support made this work possible. His enthusiasm for the subject has been a great source of inspiration and made the work throughly enjoyable. I would also like to thank Derek Neary for his technical assistance with the experimental setup.

I would like to thank the many friends I have made during my PhD. Specifically I'd like to thank Christian, Chris, Georgios, Jack, James, Nick and Rick for their (many) constructive arguments and numerous debating sessions in the pub.

Thanks to my parents for their continued support and encouragement. Finally, my ultimate appreciation goes to my loving partner Samantha for all her patience and support.

Statement of originality

This thesis is submitted for the degree of Doctor in Philosophy in the Faculty of Engineering at the University of Liverpool. The research project reported herein was carried out, unless otherwise stated, by the author in the Department of Engineering at the University of Liverpool between August 2003 and August 2006.

No part of this thesis has been submitted in support of an application for a degree or qualification of this or any other University or educational establishment. However, some parts of this thesis have been published, or submitted for publication, in the following papers:

- P. Dickinson and A.T. Shenton, Low order MIMO controller design for an engine disturbance rejection problem, 6th Biennial UKACC International Control Conference, Glasgow, September 2006.
- P. Dickinson and A.T. Shenton, Fixed order time-delay MIMO $\mathcal{H}_\infty$ parameter space controller design, *submitted to* International Journal of Control, November 2006.
- P. Dickinson and A.T. Shenton, Multivariable techniques for S.I. engine idle-speed control, *submitted to* Proceedings of the IMECHE, Part D: Journal of Automobile Engineering, January 2007.
- P. Dickinson and A.T. Shenton, A Parameter Space Method for Two-Term Constrained and Minimum Variance Controller Design, *submitted to* Automatica, January 2007.

P. Dickinson
19th November 2007

Abstract

Powertrain applications require high performance controllers yet are in general restricted to low order solutions due to limitations in the software and hardware. There are many well developed robust feedback techniques which can be applied very successfully to automotive systems, however these are generally high order solutions and are therefore not suited to most commercial powertrain control modules (PCM). Typically, powertrain control strategies are implemented through low order look-up tables. There are only a limited number of robust design methods which can be used for fixed, low order controller design and many of these techniques are limited to single-input-single-output (SISO) problems.

New technology engines are being developed with additional mechanical systems to increase the performance. As these technologies are developed the interactions between system inputs and outputs are increasingly coupled and therefore it is necessary to consider engines as multivariable systems. Accordingly, for high performance control it is necessary to move away from single control loops or sequential SISO loop designs favoured until recently.

To achieve high performance with the constraints of the PCM this thesis develops a series of 'engineer friendly' controller design tools. Two distinct parameter space (PS) control techniques are detailed, which are particularly suited to low and fixed order control. These methodologies are intended to be suitable for non-control experts by offering insights into the design constraints.

The first technique is a novel PS approach to constrained and minimum variance (MV) controller design for both continuous and discrete systems. This technique is successfully applied to the peak pressure position (PPP) control problem using spark advance (SA) as the input.

The second technique developed is a multivariable $\mathcal{H}_\infty$ parameter space technique for designing fixed, low order controllers. This technique uses only frequency response information in the design scheme and is therefore equally suited to both continuous and discrete systems. Controllers are developed by a series of parameter plane iterations, which can be used for re-tuning controllers from alternative design methods. Equally, the technique can be used for

the direct design of controllers, starting with no initial transfer function gains. The method is successfully demonstrated as a direct design technique for a single sensitivity problem with time response criteria. A further example demonstrates the technique for weighted sensitivity reduction using the direct design approach and also for re-tuning a reduced order controller obtained by an algebraic Riccati design.

To facilitate the application of the multivariable PS technique, a novel approach to designing a feedforward fuelling controller for a port fuel injection (PFI) gasoline engine is detailed. The feedforward controller is based on inverse nonlinear auto-regressive moving average (NARMA) ordinary least squares (OLS) identification. The approach is applied successfully to the idle speed region of an engine and has the advantage on linearising the plant dynamics. The system with compensator is subsequently re-identified and coupled with a robust multivariable PS controller for control of the idle speed and air-to-fuel ratio (AFR).

Contents

List of Figures

Nomenclature

ABV Air Bleed Valve

ADC Analogue to Digital Converter

AFR Air-to-fuel ratio

AIC Akaike's Information Criterion

ANN Artificial Neural Networks

ARMAX Auto-Regressive Moving Average with eXogenous

Auto-Regressive Moving Average

BHP Brake Horse Power [550 ft-lb/s]

CCV Cycle-to-Cycle Variation

CR Compression Ratio

DEM Discrete Event Models

DOHC Double Overhead Camshaft

DSP Digital Signal Processing

EGR Exhaust Gas Recirculation

EMS Engine Management System

GA Genetic Algorithms

GDI Gasoline Direct Injection

GM Gain Margin

GMV Generalised Minimum Variance

HC Hydrocarbons

HEGO Heated Exhaust Gas Oxygen

IC Internal Combustion

IEG Induction to Exhaust Gas

IMEP Indicated Mean Effective Pressure

IO Input-Output

IPS Induction to Power Stroke

LFT Lower Fractional Transformation

Linear Matrix Inequality

LMI Linear Matrix Inequality

MAF Mass Air Flow

MAP Manifold Absolute Pressure

MBT Maximum Best Torque

MIMO Multiple Input Multiple Output

MISO Multiple Input Single Output

MPC Model Predictive Control

MV Minimum Variance

MVM Mean Value Models

NARMA Nonlinear Auto-Regressive Moving Average

NOx Nitrous Oxides

NVH Noise and Vehicle-Harshness

OLS Ordinary Least Squares

PCM Powertrain Control Module

PD Proportional Derivative

PFI Port Fuel Injection

PI Proportional Integral

PID Proportional Integral Derivative

PM Phase Margin

PPP Peak Pressure Position

PS Parameter Space

PS PferdeStarke [Kg-m/s]

PWM Pulse Width Modulated

QFT Quantitative Feedback Theory

RGA Relative Gain Array

RON Research Octane Number

SA Spark Advance

SI Spark Ignition

SISO Single-Input-Single-Output

SOHC Single Overhead Cam

TDC Top Dead Centre

TP Throttle Position

UEGO Universal Exhaust Gas Oxygen

WOT Wide Open Throttle

Chapter 1

Introduction

The internal combustion (IC) engine is overwhelmingly the most widely used propulsion source in automobiles to date. Since the earliest automobiles were produced, a stream of technological developments has ensured engine performance has continually increased. Nevertheless, the modern IC engine still has large potential for increases in performance, generally through further advancements in technology coupled with high performance control [45].

Competition between vehicle manufacturers to improve driveability and safety and increasing demands for improved fuel economy and reduced emissions, coupled with decreasing costs, has resulted in a large range of control problems. This thesis focuses on powertrain control of spark ignition (SI) engines. In the sequel an overview of the new and emerging technologies adopted in powertrain systems is presented. The corresponding control challenges are discussed.

1.1 New Technology Engines

With increasingly stringent demands on engine efficiency, fuel economy and emissions the current trend in gasoline engine is plant 'downsizing' [66]. To achieve the corresponding reduction in engine capacities without compromising driveability has seen the development of numerous mechanical innovations. In order to keep development and production costs down a significant amount of research is also underway to improve engine electronics. The latest engine developments include:

Direct Injection

One important recent development in gasoline engines is the introduction of the fuel injector positioned directly into the cylinder. The fuel economy of compression ignition, direct injec-

tion diesel engines has always been superior to the port fuel injection (PFI) gasoline engine. The PFI engine was introduced as an improvement to the carburetor, previously used to meter the flow of fuel into the engine. Electronic injection allowed for improved control of the air-to-fuel ratio (AFR), which was required to ensure catalytic converters would operate efficiently. The PFI engine generally has one injector mounted in each manifold runner directed at the corresponding inlet port. The injected fuel is vapourised by the heat from the port and mixes with the air entering the cylinder. One of the difficulties with this system is that not all the fuel injected enters the cylinder; instead a fuel puddle is develops on the inlet wall.

The higher engine efficiencies that have been achieved in diesel engines are due to higher compression ratios and reduced pumping losses since the air entering the engine is unthrottled. However, despite continual improvements to the diesel engine over recent years, particularly for passenger vehicles, the gasoline engine has remained more popular. The diesel engine has a higher capital cost per unit and exhibits higher noise and vibration characteristics. Furthermore, nitrous oxides (NO_x) and particulate emissions are significantly worse in diesel engines than gasoline equivalents. With these benefits and problems of the diesel engine in mind, technologies for gasoline engines led to the development of high pressure injectors which could spray directly into the cylinder with a fine enough spray to atomise the fuel.

The potential advantages of the gasoline direct injection engine for improved emissions control and fuel efficiency are significant. Since the fuel is injected directly, difficulties in delivering the correct amount of fuel due to wall wetting dynamics are removed. The PFI engine, on the other hand, must always maintain a fuel puddle to ensure the responsiveness of the engine is maintained; this requirement (and the invention of the three way catalytic converter (TWC)) requires the engine to be fuelled at stoichiometric even when minimal torque is required. In the GDI engine the fuel is injected later in the engine cycle and therefore time delays between torque demand and sensor feedback are minimised. Accordingly, GDI engines can operate in either one of two modes; stratified charge or homogeneous charge, since there is no time delay when switching. A detailed survey of the GDI engine can be seen in [113] and [114].

Turbo Chargers

Turbo chargers are becoming more popular in gasoline engines as engine sizes are reduced. Turbo chargers consist of a turbine, powered by high speed exhaust gases, which in turn drive a compressor that delivers the air to the engine intake. This utilisation of the energy in the exhaust gas to increase the amount of air entering the cylinder significantly improves the volumetric efficiency when operating. Accordingly, significant improvements in engine

power and torque over similar volume naturally aspirated engines can readily be achieved. One of the biggest control challenges associated with these devices is they generally display nonlinear characteristics and furthermore, suffer from large time delays when the turbo begins to turn. This time delay or 'turbo-lag' results in low volumetric efficiencies at low speeds and can also cause undesirable driveability problems. An alternative method of increasing the air delivery to the cylinders is achieved by a supercharger. In contrast to the turbocharger the supercharger is driven mechanically from the crankshaft. The principles of compressing the gas to improve the density of the charge are similar. Further details of supercharging for gasoline engines can be found in [9]. The effects of the compression ratio and control challenges are addressed in [64].

Exhaust Gas Recirculation

Exhaust gas recirculation (EGR) systems have been developed to reduce the formation of NO_x. A proportion of exhaust gases from previous combustion events are fed back into the cylinder to part-fill the cylinder with what is effectively an inert gas. The proceeding combustion event produces less heat since there are less combustible gases in the cylinder and the exhaust gas aids in absorbing the heat. Therefore, with lower combustion temperatures the formation of NO_x is reduced. Furthermore, when the engine is running at relatively low loads, EGR can be introduced to effectively reduce the volumetric capacity and therefore improve fuel consumption. Moreover, the throttle can be opened further and therefore reduce pumping losses.

When EGR was first introduced into engines the exhaust gas was carried by a pipe to a solenoid valve in the inlet manifold. More recently, since the introduction of variable valve timing systems (VVT), EGR can be introduced into the cylinder by adjusting the timing of the exhaust valves, such that they remain open during the start of the following induction stroke. The control problems associated with each method are distinct yet challenging. EGR introduced into the inlet manifold will have inherent time delays and therefore fast control of the valve is required for good transient performance. These time delays are removed with VVT systems, however rapid control of the camshafts can result in poor driveability.

Variable Valve Timing

The timing of the inlet and exhaust valves has a significant impact on an engine's performance. Optimisation of the valve timing can improve pumping efficiency, reduce emissions and improve engine performance over the entire operating range. In fixed camshaft engines the timing of the valves is determined by the camshaft(s) which rotate at half the crankshaft speed. Early engines operated with one camshaft that determined the opening and closing

timing of the valves. As the number of valves per cylinder has increased it has become increasingly necessary to use double-overhead camshafts (DOHC) due to space constraints. In these 'fixed camshaft' engines the timing was invariably a compromise between low speed, low load conditions and wide open throttle (WOT), high load conditions.

Recently several mechanical innovations have resulted in the ability to vary the timing of the valve openings. Early systems were based on cam switching, where the cams used to drive the valves would switch to a second profile at a certain engine speed. More recently, systems which allow the timing to be varied continuously across the speed range have been developed. In general these systems allow the phasing of the inlet and outlet camshafts to be varied independently depending on the engine speed and load. An extension to the variable timing systems has been in variable lift technologies to further optimise the breathing dynamics across the operating region. A further advantage of systems which allow for independent control of the exhaust valves is that this facilitates a method of regulating EGR. This 'internal EGR' is controlled by the appropriate exhaust valve timing, which allows some of the exhaust gas to be re-captured from the preceding combustion event.

The range of technologies adopted for the control of the valve timing, including details of timing strategies is well documented in [49]. The effects on VVT on fuel economy and emissions are presented in [57] together with a review of suitable control algorithms.

Variable Volume Engines

Variable engine volume technologies are currently receiving a significant amount of interest. Early attempts to vary the volumetric capacity of engines have been achieved through cylinder switching. This option is used when operating at low load and low speeds, where to improve fuel consumption and emissions, the number of cylinders in operation is reduced. More recently research is focusing on varying the cylinder volumes, however, many of these approaches result in increased compression ratios (CR) and therefore result in a number of control challenges such as preventing engine knock.

1.2 Engine Control

In order to achieve the maximum efficiency across the wide operating region, an engine management system (EMS) is used to control the various outputs. With an increasing number of engine sensors, auxiliary mechanical systems and electronic actuators, the control problems are numerous and non-trivial. Furthermore, requirements on emissions, engine performance and driver perception often require trade-offs since the design constraints often conflict. The engine is controlled by the powertrain control module (PCM) which consists of a modest

microprocessor.

1.2.1 Powertrain Control Module

In general the memory and computational speeds of the microprocessors are low by modern desktop PC standards. The typical architecture is a 16-bit instruction word microcontroller with a clock speed of around 40 MHz. The microcontroller contains various analogue to digital converters (ADC), a range of pulse width modulated (PWM) outputs and around 512KB of flash RAM for storing controller parameters.

The PCM module is usually supplied to the vehicle manufacturers with pre-programmed software or *strategy*. The strategy consists of a series of feedforward, feedback and logic control settings which the vehicle manufacturer *tunes* to suit the vehicle. These settings are in general stored as a set of parameters in look-up tables. The look-up based strategy is generally designed around fixed order controllers and therefore the vehicle manufacturer is faced with the task of populating the tables with fixed structure controller parameters.

The range of input and output signals on a PCM varies depending on the control strategy implemented and complexity of the engine and related systems. A schematic of the typical inputs and outputs on a modern PFI engine [22, 45] are given in figure 1.1.

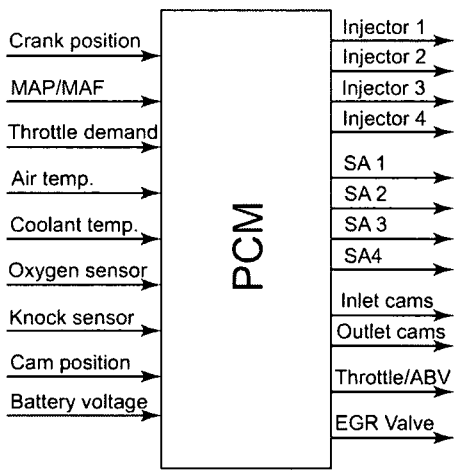

Figure 1.1: Typical PCM inputs and outputs for PFI gasoline engine

1.2.2 Engine Control Challenges

In general the various functions of the PCM can be considered as several distinct control problems.

Idle Control

The idle speed problem remains an active problem in automotive control. At idle the engine speed must be regulated to remain as low as possible to economise on fuel, yet also turn fast enough to minimise low speed vibrations. Furthermore, the system must be able to withstand any speed fluctuations caused by torque disturbances (for example electrical devices which load the alternator, air conditioning pump and/or power steering pumps) without causing the engine to stall [54].

Vehicles in city traffic consume around 30% of their fuel whilst at idle [59]. Under idling conditions reducing the idle speed from 800 to 650 rpm can make fuel savings of approximately 24% [37]. However, at a lower idle speed set-point, the engine becomes more susceptible to disturbances which cause vibration. Excessive vibration are unpleasant for the driver and therefore result in poor driver perception of the vehicle and a low rating of the so-called 'noise and vehicle-harshness' (NVH) .

In the spark ignition (SI) engine the control engineer has three potential channels of actuation available. These are: the amount of air entering the engine, determined by the operation of the air bleed valve (ABV) or increasingly common the electronic throttle; the level of spark advance (SA); and, the mass of fuel injected into each cylinder.

One of the difficulties in rejecting torque disturbances acting on the engine is due to the significant time delays in the system. The air entering the engine is the primary channel for the regulation of the engine speed. Significant time delays exist due to the transport delay from the actuator to the inlet manifold, where the manifold filling dynamics can also delay the air further. Finally there is an induction to power stroke delay due to the discrete operating nature of the engine. Figure 1.2 presents a schematic of the air path in a PFI SI engine from the intake to the exhaust, where it can be seen that the fastest effective actuator is the spark plug since this can affect the next combustion event. The fuel injectors can also be used for control, however in the port-injected engine these suffer from time lags and delays due to wall wetting dynamics and the induction to power stroke delay. In most PCM strategies the primary control effort is the air-flow, controlled by an electronic throttle or ABV. Additionally the SA is often retarded from its optimal setting for maximum best torque (MBT), to allow an even faster increase and decrease in speed forming a two input one output controller. One criticism of this formulation is that to achieve this speed increase from the SA the engine must run sub-optimally for most of the time because the set-point is not MBT. However, this is often deemed necessary since there is significant pure time delay in the air path and without such a set-point the fast spark control would demonstrate no effect. A detailed survey of the idle problem and the many controller design techniques successfully applied are documented in [54].

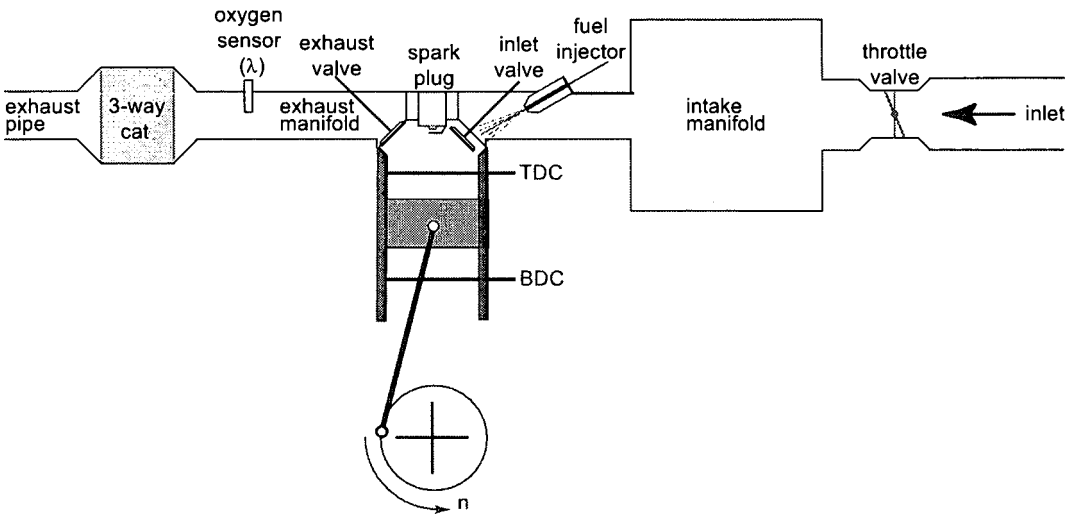

Figure 1.2: Engine schematic of a PFI SI engine

Air-to-Fuel Ratio Control

The control of air-to-fuel ratio (AFR) is one of the most important aspects of the PCM. The introduction of the three way catalytic converter (TWC) required that the AFR be kept at the stoichiometric ratio to ensure it operated efficiently. In PFI engines a significant delay occurs between the injection of the fuel and the measurement of the oxygen remaining in the exhaust gas at the sensor. Accordingly, the fuelling control in an engine requires a fast feedforward element to ensure the system remains responsive, coupled with the slower but precise feedback loop. The AFR control encompasses three main aspects: accurate estimation of air charge; compensation for fuel puddling dynamics in the intake manifold runners and on the intake valves; and, closed-loop regulation of AFR for high catalyst performance [103].

Under transient conditions the fuel must be calculated as soon as a change in air-flow is observed. This information can be obtained by the throttle position (TP), manifold absolute pressure (MAP) or the mass air flow (MAF) entering the engine. Once an estimate of the air charge entering the engine is established, the wall wetting dynamics of the manifold must also be considered. PFI engines take part of the fuel from the puddle which develops in the inlet manifold and therefore, the scheme must also compensate for these wall wetting dynamics. The fast and slow fuelling dynamics in the inlet are generally represented by the so-called *tau-X* model comprising of the fast fuel lag and slow fuel lag sub-system as depicted in figure 1.3. A feedback scheme is also used in conjunction with the feedforward scheme. The TWC must operate within a very narrow band of stoichiometric if it is to remain efficient as illustrated in figure 1.4a. Accordingly, a feedback scheme is used to ensure zero steady state error [45]. Historically, most production vehicles base the feedback on a heated exhaust gas oxygen (HEGO) switching-type sensor mounted at the confluence point in the exhaust. This

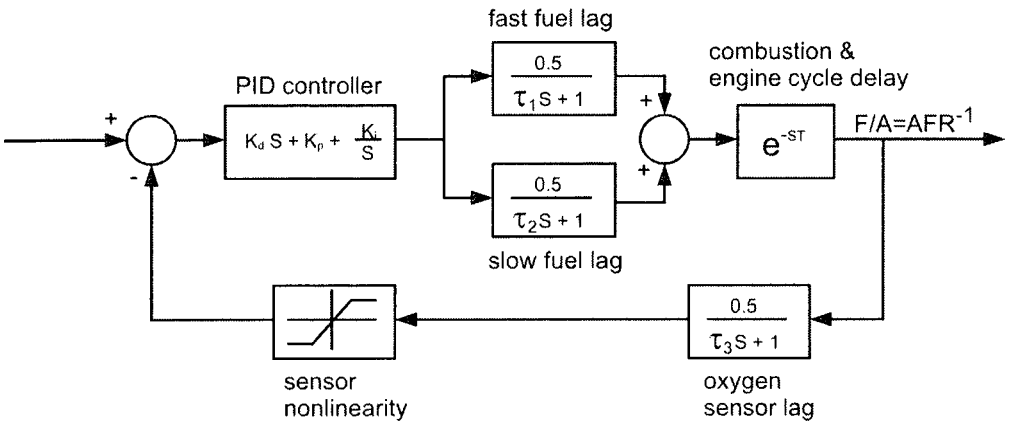

Figure 1.3: Fuel puddle dynamics HEGO sensor feedback control

measures the presence of oxygen in the exhaust gas, however, the sensor displays a very high degree of nonlinearity as shown in figure 1.4b and therefore controllers are often heuristically tuned [103]. The feedback scheme of figure 1.3 is a typical implementation of this approach. An alternative to the HEGO sensor is universal exhaust gas oxygen sensor (UEGO) which

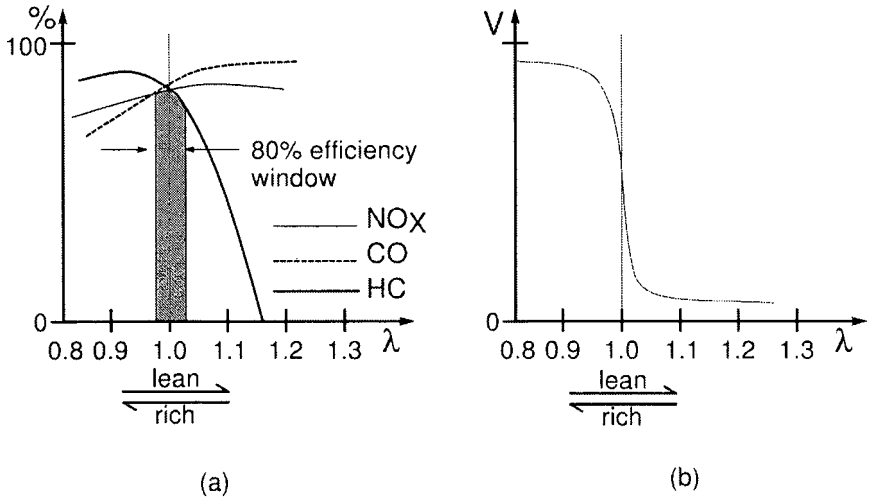

Figure 1.4: Efficiency of TWC (a) HEGO characteristics (b) [48, 94]

is a linear device capable of measuring AFR. These sensors are significantly more expensive and therefore, generally not widely implemented in standard production vehicles, however a significant improvement in AFR control can be achieved by their use. With a UEGO sensor the combined system can be more successfully linearised and therefore standard linear controller design techniques can be applied.

VVT Torque Control

Engines equipped with VVT require careful control to optimise the timing of the valves for maximum torque throughout the speed and load range and also to provide internal EGR when appropriate. Good idle stability requires minimum overlap between the intake and exhaust valves, similarly WOT requires low overlap to ensure maximum air is induced into the cylinders. Speed and loads between these conditions require varying degrees of valve overlap to achieve the required amount of EGR.

Four versions of VVT are used: phasing the intake camshaft only; phasing of the exhaust camshaft only; 'dual equal' phasing of the intake and exhaust camshafts; and, 'dual independent' which allows the camshafts to be varied independently. The camshaft phasing reference is typically scheduled based on the throttle demand and engine speed. However, the control problem is made difficult by transient demands on the throttle. Without compensating for transient throttle demands the response causes large camshaft fluctuations when a transient is applied. Sudden changes in the camshaft positions cause undesirable torque fluctuations in the driveline leading to poor engine response and driveability problems [55, 57, 103].

Combustion Control

Control of the combustion timing is essential to operate the engine at maximum efficiency. Combustion control (and most other powertrain control) is operated in the *crank angle domain* not time domain and therefore, as the engine speed varies the start of combustion must be controlled to ensure the maximum use is made of the energy available in the charge. For example, igniting the charge too early in the compression stroke results in an early expansion of the charge and therefore the work done opposes the direction of the engine. Conversely, a very late spark results in poor use of the energy available since combustions occurs too late in the expansion stroke. Under most operating conditions it has been found empirically that the optimal SA for a particular engine coincides more-or-less with a fixed peak pressure position (PPP) [48].

In production vehicles the SA is scheduled based on the engine speed and load. Primarily, this is because it is deemed uneconomic to install pressure sensors in production vehicles. As a consequence the timing can often be suboptimal cylinder-to-cylinder due to manufacturing variations. Furthermore, with engine wear the engine maps (look-up tables) can become less appropriate. Moreover, since individual cylinder pressure is not monitored alternative sensors are required to prevent engine knock (discussed in more detail below).

In GDI engines the timing of the fuel injection event(s) is also a critical control variable. Good mixing of the fuel and air requires precise control of the fuel injection timing, further-

more, it is possible to have multiple injection events during the compression stroke. GDI engines are also designed to operate in two modes: homogeneous charge (stoichiometric) and stratified charge modes. The torque and emissions characteristics from the two modes are so distinct that different combustion timing strategies are required for each.

Common to all combustion processes are the cycle-to-cycle variations (CCVs). The combustion process is highly chaotic resulting in large variations in the combustion quality, measured using variables including: PPP, work done typically measured as the indicated mean effective pressure (IMEP), value of peak pressure, ignition delay, mass fraction burn rate and heat release. Introducing in-cylinder pressure based measurements allows feedback control schemes such as minimum variance to reduce these CCVs and improve engine performance.

Knock Control

'Engine knock' is a phenomenon which arises by uncontrolled combustion in the cylinder. At sufficiently high pressures, localised high temperatures on the cylinder walls can cause pre-ignition, prior to the flame front initiated by the spark plug [48]. This rapid burning creates excessively high cylinder pressures and can cause significant engine damage if left uncontrolled. The term knock (also known as 'pinking' or 'pinging') derives its name from the metallic sound the engine makes under this situation. Under this condition the engine performance is severely reduced and therefore an anti-knock scheme is required.

Feedback sensors which are typically piezoelectric accelerometers, are used to detect the presence of knock. It is essential that an adaptive control scheme is used on an engine, which immediately retards the SA and/or reduce the turbocharger boost pressure once knock is detected. The control algorithm gradually increases the SA back to the optimal setting until the presence of knock is detected and the process is repeated [94].

1.3 Overview

The remainder of the chapter gives an overview of this thesis and highlights the novel contributions to the subject.

Chapter 2 gives an overview of the controller design process including model generation. A discussion regarding the different modelling approaches is made with reference to powertrain control. Physical modelling approaches are compared to 'black-box' models favoured in the applications within this thesis. System limitations such as controller order and cross channel interaction are discussed. Low order controller generation is considered with possible order reduction processes suggested if high order models are involved. The remainder of the

chapter introduces some robust control techniques where the merits of each technique are evaluated with particular reference to powertrain control.

Chapter 3 discusses the experimental setup used with the practical engine examples implemented in this thesis. The characteristics of the 1.6l Ford gasoline engine and low inertia dynamometer are explained. The main engine sensors and actuators are described together with how these interface with the dSpace digital signal processing unit.

Chapter 4 presents a novel single-input-single-output (SISO) parameter space (PS) design technique for achieving minimum (with regards to a fixed structure controller) and constrained output variance. The method is developed for both continuous and discrete systems. The technique is based on a closed-form SISO PS approach to designing fixed order, two term controllers such as PI or PD, which is readily implementable as a fast and robust numeric algorithm for interactive design. The technique is based on mapping loci of constant variance for continuous and discrete rational systems. White noise coloured by a rational filter is assumed to be the output disturbance to a rational plant. PS mappings are developed from the mean-squared value, evaluated from the spectral density function and Leverrier's algorithm to produce loci for a given closed loop output variance. These loci can be used either on their own or superimposed with other requirements such as sensitivity functions or gain and phase margin boundaries in the parameter plane, thus creating a robust constrained variance PS method. Two examples demonstrate the technique for the continuous and discrete case. The technique is experimentally validated on the University of Liverpool engine and dynamometer for the control of the PPP using SA.

Chapter 5 details the development of a PS technique for square multivariable systems based on $\mathcal{H}_\infty$ constraints. The technique is based on iteratively tuning fixed, second order controller elements. Inspection of the singular values for closed loop transfer functions leads to determinant equations with a set of solutions in the complex plane. The mapping equations which translate these solutions into controller parameter planes are detailed. A suggested design procedure for the technique is described and the method applied to an idle speed problem for a natural gas engine, where the design objectives are primarily time domain criteria. Two alternative multivariable techniques are also detailed for comparative purposes.

Chapter 6 develops the multivariable PS technique for non-square systems such as the multiple-input-single-output (MISO) idle speed problem. Left and right hand weighting functions are included in the theory. Multiple controller elements are considered to allow higher, fixed order controllers to be developed. A first example is presented to highlight the significant advantages of the proposed multiple-input-multiple-output (MIMO) design method over the sequential application of SISO parameter space methods. A second comparative example illustrates the capability of the technique both for direct design of low order, PID

and fourth order controllers and for retuning a reduced order Riccati designed $\mathcal{H}_\infty$ controller, by application to a well known benchmark problem for an experimental highly maneuverable aircraft (HiMAT).

Chapter 7 presents a novel application of inverse nonlinear auto-regressive with moving average (NARMA) ordinary least squares (OLS) identification to generate a feedforward controller for the AFR control problem. Reverse causality input-output data is directly identified using algebraic NARMA models to develop a feedforward fuel map which saves considerable calibration times and furthermore captures dynamic effects. In the forward case different time delays are observed between the inputs: manifold absolute pressure (MAP), engine speed and fuel; and, therefore a compromise between tracking performance and time response was necessary. The resulting inverse model was experimentally demonstrated open loop on the engine and dynamometer as a feedforward controller. The compensator has the added advantage of linearising the AFR path dynamics and subsequently a PS multivariable feedback controller was designed to give zero steady state AFR error and idle speed regulation.

Chapter 8 concludes the thesis by summarising the merits and limitations of PS feedback control. The PS feedback techniques are both transparent and intuitive and can therefore improve engine performance and reduce development time. Suggestions for extending the parameter space techniques are discussed. Alternative powertrain applications for the inverse compensator scheme of Chapter 7 for use as a rapid calibration tool are suggested.

1.4 Contribution

The previous sections demonstrate the breadth of powertrain control problems. Each problem is suited to different control techniques, however in general most share the following features:

- PCM strategies are based on low and fixed order control schemes.
- Production engines exhibit uncertainty in their respective plant models and therefore require a degree of robustness.
- Performance requirements are high.
- Operating conditions (driver, environmental, size of vehicle) vary considerably.

By far, the majority of the powertrain control solutions presented in the literature are for high order controllers. Since in general automotive strategies are based on low order controllers this limits their use in a production PCM. The focus of this thesis is low order controller design suitable for practical implementation. This thesis details the development of two parameter space techniques for the design of robust, fixed order controllers. A novel MISO

rapid calibration technique based on a nonlinear partial inverse model, using input-output data is also developed. The novel contributions of this thesis are:

- The development of a novel closed-form SISO parameter space approach to designing constrained-variance, fixed order, two term controllers such as PI or PD. The interactive, graphical technique is based on mapping loci of constant variance for continuous and discrete rational systems. These loci can be used either on their own or superimposed with other requirements such as sensitivity functions or gain and phase margin boundaries in the parameter plane thus creating a robust constrained variance PS method. Minimum variance subject to additional design constraints can then be obtained by iteratively reducing the variance level until the admissible parameter region is exhausted.

  The technique is successfully applied to a continuous idle speed controller design and simulation results presented. An application of the discrete technique includes the model identification and control of the PPP using the University of Liverpool engine and low inertia dynamometer facilities.

- A multivariable parameter space design technique for robustness and transient performance is presented, suitable for the many powertrain problems which are inherently multivariable. The technique is based on mapping sensitivity constraints for square, invertible systems into the parameter space. A multivariable idle speed and AFR problem demonstrates the technique for a single sensitivity design with time domain performance criteria.

- Left and right hand weighting functions are then included in an extension of the multivariable PS technique for non-square systems. A comparative example illustrates the capability of the technique both for direct design of low order, PID and fourth order controllers and for retuning a reduced order Riccati designed $\mathcal{H}_\infty$ controller, by application to a well known benchmark problem for an experimental highly maneuverable aircraft (HiMAT).

- A system identification approach for the systematic calibration of a fuelling strategy in the PFI SI engine. The technique offers a time-efficient 'one-shot' alternative to traditional fuelling map calibration approaches since it is based entirely on rapidly obtained dynamically perturbed input-output data. Non-linear black-box parameter identification directly produces a dynamic inverse multivariable NARMA feedforward controller and linearising feedback compensator. The controller accurately determines the required fuel pulse width from engine speed and manifold pressure to jointly maintain stoichiometric AFR and engine speed. The methodology is experimentally validated

on the University of Liverpool low inertia dynamometer with and without a parameter space designed feedback controller.

Chapter 2

Robust Feedback Control

2.1 Introduction

As the complexity of engine and powertrain systems increases so does the demand on the controller to realise the potential performance benefits. In many cases there are large interactions between the various control inputs and outputs and therefore, to optimise the system performance a multivariable approach is often required.

One important constraint the control engineer often faces is the controller order. Over 90% of controllers used in industrial applications are proportional integral (PI) or proportional integral derivative (PID) [111]. For reasons of industrial practice, operative understanding or software or hardware limitations, the control engineer is often required to develop such controllers.

This chapter considers the various approaches to developing low order controllers. A discussion on the plant modelling for controller design purposes compares physical based models and black box modelling approaches. Controller constraints and considerations are detailed and a survey of possible linear robust control techniques is included.

2.2 Engine Models

Most systematic controller design methods are based on a representative model of the system under consideration. The accuracy of the model can have a significant effect on the transient performance of the controller on the physical system, indeed it is likely to be the most significant determinant of success. Two distinct approaches to modelling are: physical modelling, where the physical properties of the system are the basis for the model and phenomenological 'black-box' modelling where the physical system is excited and the output response measured to obtain a mathematical representation of the dynamics. A third approach, the so-called

'grey box' modelling combines these techniques, where the parameters of a physical model are obtained by system identification. Each of these approaches are appropriate in different circumstances.

Another consideration when developing a model is its fitness for purpose. In general a control oriented model should represent the input-output behaviour with reasonable accuracy, including relevant transient effects. For many applications the controller order is in-part determined by the model order, therefore, it is also often favoured if the model order is relatively low. Powertrain processes are often inherently nonlinear, yet linear approximations are often necessary for applying linear control. Linearised models can be developed from nonlinear models, or alternatively linear models can be obtained directly from identification.

The two typical physical modelling approaches for the development of powertrain models are: continuous mean value models (MVM) which neglect the discrete engine cycle events and discrete event models (DEM) which explicitly account for the reciprocating nature of the engine. MVM are in general used for relatively slow changing processes, as opposed to crank-based periodic events such as combustion modelling where a DEM is required.

2.2.1 Physical Models

For a given physical system the mechanisms and processes can be used to describe the behaviour. Models based directly on the physical processes are often termed 'white-box' or phenomenological models. The underlying assumption is that the dynamics are clearly understood and physical parameters known with a degree of certainty. With reference to the IC engine there are a large number of complex physical processes occurring including the kinematics, thermodynamics and fluid dynamics and therefore it can be extremely difficult to obtain an accurate model.

One of the merits of physical modelling is that it provides insight into the system. This can be a considerable benefit when determining appropriate control laws or specifications. Furthermore, as stated in [47] a good phenomenological model should be easily adapted to similar systems, such as different capacity engines, whereas black box identified models are only suitable for the system and operating range over which they are identified. An entire SI PFI engine model is given in [47]. Control oriented models which include variable camshaft timing can be found in [56, 102]

2.2.2 Black Box Models

System identification is a behavioural approach to developing a model without requiring a physical understanding of the process. The system can therefore be treated as a 'black box'.

A mathematical model of a system is developed by experimental perturbation of the system with appropriate signals and observation of the response. A wide range of linear and nonlinear identification techniques can subsequently be used to determine the relationships between the input signals and system response.

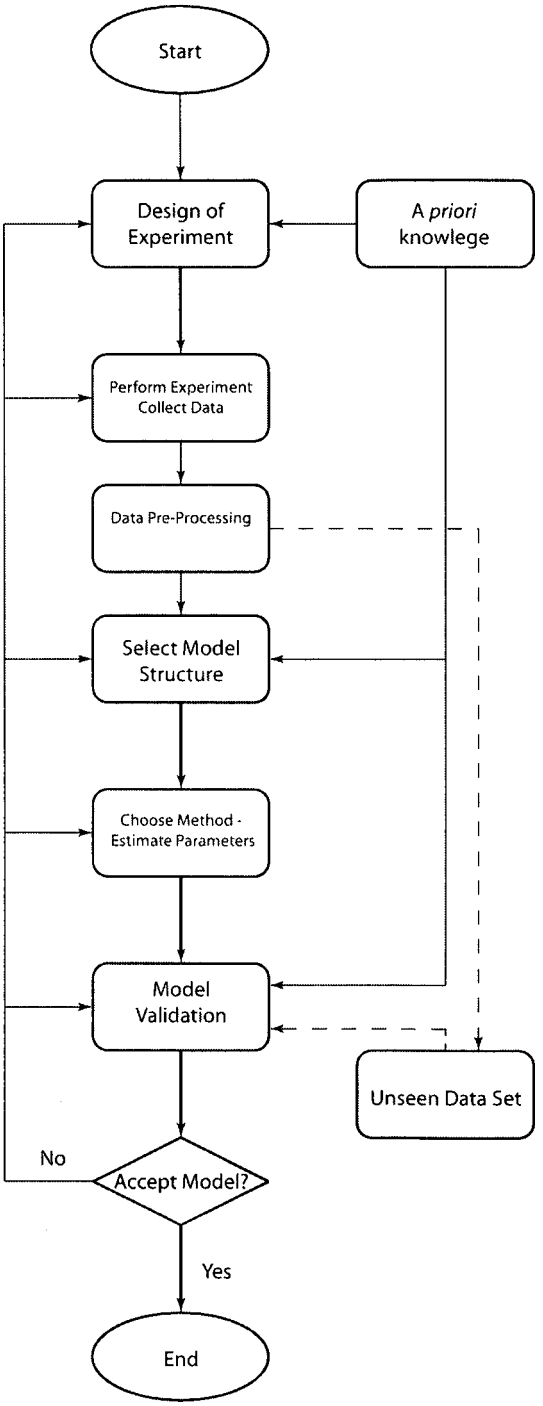

Figure 2.1: Flow chart illustrating the system identification process [8, 69, 101]

System identification is a broad and detailed topic and only an overview is presented here,

for more information the reader is directed to [69, 101] and references therein. Commercial software is available for many of the identification techniques, including linear parametric models [70], artificial neutral networks (ANN) [31] and genetic algorithms (GA) [73].

A schematic of a typical identification process is given in figure 2.1. The process can be highly iterative, particularly if no *a priori* information regarding the system response is available. The main steps can be summarised as follows:

Design of Experiment

Black box modelling requires the system to be excited with a sufficiently rich frequency spectrum to excite all the frequencies of interest. Some prior knowledge of the system dynamics is clearly helpful in the design of the test signals. The frequency content of the signal is obviously vital to which dynamics can be excited. Pseudo-random binary sequences (PRBS) are often favoured in linear identification since they excite a wide band of frequencies and have a white noise autocorrelation. The magnitude of the signal determines which output range is excited. If the system is thought to contain nonlinear dynamics, a multi-level signal is required to pick up magnitude dependent nonlinearities.

The sampling frequency is a limitation to the frequencies which can be successfully captured. Only frequencies less than half the sampling rate can be successfully identified. It is generally suggested that the sampling frequency is around 10 times the system bandwidth where possible [68].

The design of the experiment is crucial to successful system identification. Without any prior understanding of the system this stage can require several iterations. General guidance for the design of experiments can be found in [8, 69].

Data Processing

Prior to the identification the data must be processed. Often data is collected at a high sample rate to first allow for low-pass, anti-alias filtering of the signal. The data can subsequently be down-sampled to an appropriate level. Two sets of data are required: one set for identification and a second *unseen* set for validation of the resulting model. When considering linear identification any trends (such as mean values) should be removed. Outliers in the data should also be avoided, ideally the dataset should show no anomalous events.

Identification Technique

There are a large range of identification techniques available for both linear and nonlinear systems, including parametric difference equations, ANN and GA. The choice of identification technique is application specific and should consider the computational demand of the technique, the resulting model structure and the suitability for purpose (such as simulation, stability assessment or controller design). For detailed information on parametric models the reader is directed to [69, 99]. A tutorial outlining ANN in system identification can be found in [98].

Structure Selection

One of the biggest challenges in system identification is model structure selection. Fundamentally the type and size of structure should be sufficient to satisfactorily represent the system dynamics, without being too complex such that it is either poorly suited for controller design or is over-parameterised. *A priori* information can greatly assist at this stage of the process. In the absence of a typical model structure a range of statistical based structure selection techniques can be applied to the problem [18, 20, 106]. However, this stage of the identification process frequently requires validation of the model using unseen data and is therefore invariably iterative.

Model Acceptance

Before any model can be accepted it must be validated against unseen data. Visual inspection of the validation data can immediately demonstrate whether the model fit is acceptable. Fit functions can assist in measuring any improvement between models. Provided the fit appears acceptable, analysis of the residuals[1] can highlight any weaknesses in the proposed model. The residuals should ideally display an autocorrelation of white noise and have no correlation with the inputs or outputs.

2.3 Controller Design Considerations

For any control problem the designer has to consider a range of requirements and constraints. In powertrain applications closed loop stability, robustness and transient performance constraints are almost always required if satisfactory performance is to be obtained. Other considerations include the controller complexity, for example when considering multivariable systems a number of options for the design approach and technique can be applied.

[1] Model residuals r are defined as the difference between the recorded output y_r and model output y_m.

The simplest approach to the multivariable problem is to disregard any cross channel interactions and assume the system behaves as independent single-input-single-output (SISO) loops. Provided the system has relatively small cross channel interactions this assumption can be effective for controller design and provides the designer with the largest range of design options. Another approach to multivariable systems is to consider decentralised control, whereby the cross channel interactions are considered in the design process, however, the resulting controllers are implemented on their respective SISO loops. To improve the performance and validity of decentralised SISO control the plant can be augmented with decouplers. These are basic feedforward compensators which maximise the diagonal dominance at the frequencies where strong cross coupling is observed.

For systems with relatively large degrees of cross channel dynamics a multivariable controller is often essential if high performance is to be realised. In these cases the designer can either choose to apply SISO controllers to each loop in the system, the so-called 'loop at a time' approach or design the controller by consideration of the system's singular values. The loop at a time approaches are based on SISO design techniques and accordingly SISO analysis tools can be readily utilised. For example robustness considerations such as gain and phase margins can be computed for a particular loop by opening the loop under consideration with the other loops closed [78]. A common design approach for this methodology is 'sequential loop design', where each controller is designed independently and then the loops closed. For plant models with very strong cross channel interactions this approach can result in systems with very low robustness even through each loop may have been designed with significant robustness [100]. Moreover, for systems which are stable the performance is often poor as loops can often be observed to 'fight' each other.

The problems associated with sequential loop designs highlight the reasons singular values are more suited for multivariable designs. Specifically, the maximum singular values of particular closed-loop transfer functions must be bounded in a prescribed manner to ensure the desired system properties including robustness and transient performance properties are realised.

2.4 Low Order Controller Approaches

Low order controllers are still favoured in many industrial applications. Frequently this is a constraint due to the software or hardware which implements the algorithm. In these cases there is also the requirement for the controller order to be fixed to meet these constraints. These restrictions are particularly true in automotive engine management systems (EMS) where strategies implement control through scheduled fixed order controllers with parameters stored in look-up tables.

There are a number of reasons why low order controllers are often preferred over higher order solutions: the software or hardware is less complex, resulting in less potential faults in hardware or 'bugs' in software; the computational requirement for the system is also less. Often these requirements are driven by the cost of the system which implements the control, however even when cost and available electronics permit higher order control, PID type controllers are often favoured due to their transparency, where parameters offer some physical interpretation, therefore making tuning simpler and more intuitive [81]. The EMS computational requirement is minimised when implementing low order controllers and furthermore, the memory usage is significantly lower since fewer coefficients are stored in look-up tables.

Two basic methodologies can be applied to the design of low order controllers: a *direct* design approach whereby the controller is designed to meet the constraint on the controller; and an *indirect* approach where order reduction is applied in the design process. Order reduction can be applied to the plant prior to controller design and/or to the controller [5]. A schematic outlining these approaches to low order controller design is given in figure 2.2. To

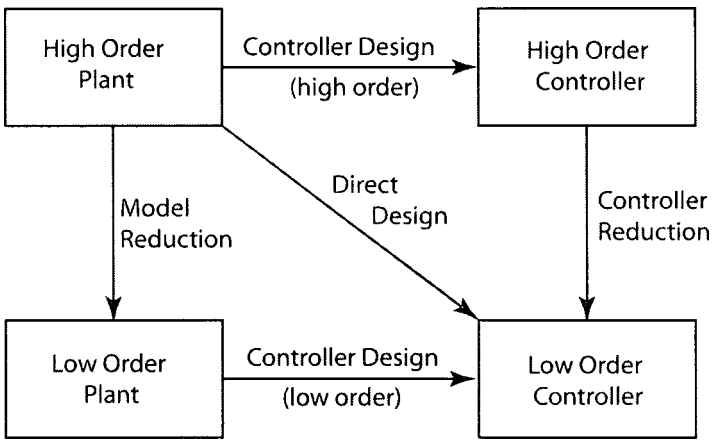

Figure 2.2: Approaches to low order controller design [5]

reduce plant or controller order a range of optimisation techniques can be applied. In general these approaches are based on minimising a cost function between the reduced and full order transfer functions $M_r(s)$ and $M(s)$ respectively. The different reduction algorithms generally only vary in the criteria used to evaluated how *close* the two structures are relative to each other [115]. In general the reduction is formulated in terms of a chosen norm, typically the Hankel or the L_∞ norm

$$||M(s) - M_r(s)||_\infty$$

An extension to many of the order reduction algorithms is the introduction of frequency based weightings. This requires the selection of weighting functions which focus the fit of the reduced structure over specific frequency ranges. The frequency weighted problem is

formulated as

$$||W_o(s)(M(s) - M_r(s))W_i(s)||_\infty \tag{2.1}$$

where W_o and W_i are transfer functions representing the output and input frequency weights respectively. The criteria for selecting the weighting functions is problem specific, for example when reducing a plant model the open loop properties should be maintained. Controller reduction generally requires the closed loop properties such as stability, robustness and bandwidth requirements to be well approximated. As with many frequency weights, the selection of input and output weighting functions requires experience to provide the required fit. The frequency ranges chosen are often dependent on the final order of the reduced structure. Guidelines for the selection of weighting choices can be found in [81, 108].

2.5 Linear Robust Feedback Control

A typical unity negative feedback system is depicted in figure 2.3. G and K denote the plant model and controller respectively. The aim of the controller is to keep the output y at the desired reference value r. The difference between the output and reference value gives an error signal e which is fed into the controller. The output of the controller u is used to compensate for the error. Feedback controllers are necessary due to uncertainty in plant modelling and for

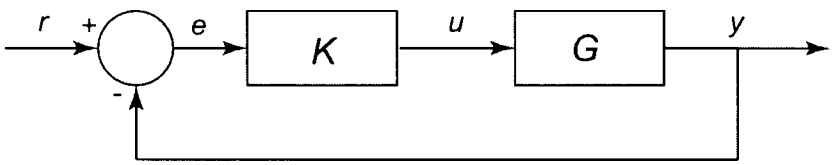

Figure 2.3: Unity negative feedback system

disturbance rejection. For a simple tracking problem a feedforward controller would be the obvious solution provided an exact plant model could be assumed. In reality a *perfect* model is rarely realisable due to modelling difficulties and external disturbances. In automotive engines manufacturing variations and different wear rates can result in large model uncertainties; furthermore environmental conditions are continually changing which act as disturbances to the system. Accordingly any control system must be *robust* to this variation and at the same time offer suitable performance within this envelope of uncertainty. In optimal control this is known as the robust-performance problem.

Additional robustness is required when a linear control law is applied to a nonlinear system. In practice most system will have some nonlinear behaviour. These nonlinearities can often be small enough to be considered as model uncertainty and therefore require additional robustness margins. In cases when the nonlinearities are more severe, compensators which linearise the plant can first be applied, followed by linear techniques. Nonlinear feedback

control is an expanding field which aims to deal with the nonlinearities directly, although in practical industrial application linear controllers scheduled over local linearised operating regions are often favoured due to their low order structures and better understood linear design and analysis methods.

This section describes four of the popular linear robust controller design techniques: loop shaping; optimal and suboptimal algebraic Riccati; Quantitative Feedback Theory (QFT); and, Parameter Space (PS). The merits of each method are considered particularly in terms of suitability for automotive feedback control.

2.5.1 Sensitivity Functions

Perhaps the most popular field covered in the literature with regard to feedback control is $\mathcal{H}_\infty$ theory. Conceptually $\mathcal{H}_\infty$ control is concerned with bounding the values of a given closed-loop transfer function of interest. Consider a closed-loop transfer function, often referred to as a *sensitivity function* $F(s)$, where the $\mathcal{H}_\infty$ norm is concerned with bounding the peak of the frequency response across all frequencies. It is typical to apply a frequency weighting function $W(s)$ to the transmission of interest and constrain the maximum peak of the weighted sensitivity function such that

$$||W(s)F(s)||_\infty \leq 1, \quad \forall\, \omega > 0 \tag{2.2}$$

Consider the feedback system given in figure 2.4, where $K(s)$ and $G(s)$ are transfer functions representing the controller and plant respectively. In total there are eight possible closed-loop input-output transmissions, six of which are unique for the designer to consider. Each of these unique transmissions are known as specific sensitivity functions. As the name suggests each relationship is a measure of the system sensitivity to a particular error. One or more of these transmissions can be shaped during a design by suitable weighting function which affects how the resulting controller will behave. The number and type of weighting functions is specific to the type and complexity of problem.

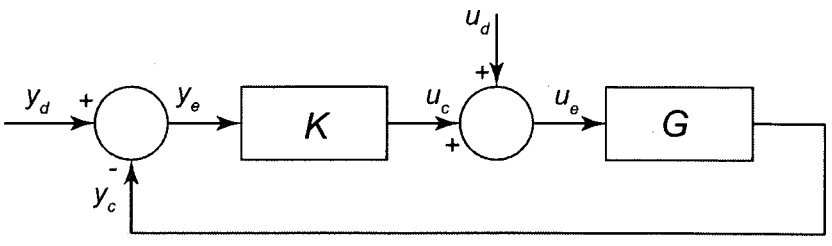

Figure 2.4: SISO unity negative gain feedback configuration

Primary Sensitivity

For the system depicted in figure 2.4, consider the transfer function y_d to y_e with the remaining inputs assumed to be zero. The closed loop system for this relationship is given by

$$y_e(s) = \frac{1}{1 + G(s)K(s)} y_d \tag{2.3}$$

This transmission is the primary sensitivity function $S(s)$ which for the multivariable case is defined as

$$S(s) = [I + G(s)K(s)]^{-1}$$

The shape of the primary sensitivity function is generally considered to add the desired transient performance. The transmission between the command and output makes this sensitivity necessary when designing for regulation and tracking control. This path can also be used for designs to reject disturbances on the output since this transmission shares the same closed-loop transfer function. The *sensitivity* of the system to the tracking error y_e is selected by the designer with consideration of the plant dynamics and system requirements. For example, a system prone to high frequency noise requires the gain of the sensitivity function at these frequencies to be high to prevent the system responding excessively to noise. Similarly, good low frequency disturbance rejection and tracking requires the primary sensitivity to have low gains at low frequencies.

Complementary Sensitivity

Robustness, particularly to high frequency uncertainty is often added into controller design by considering the complementary sensitivity function. With reference to figure 2.4 this is the transmission from y_d to y_c. The complementary sensitivity function T is defined as

$$T(s) = G(s)K(s)[I + G(s)K(s)]^{-1} = [I + G(s)K(s)]^{-1}G(s)K(s)$$

System performance and robustness can generally be translated into the primary and complementary sensitivity functions. It is noted however, that $S(s) + T(s) = I$ thereby implying that these two function are often a trade-off. The design problem is one of selecting appropriate bounds on these functions to ensure the system has the desired robustness and transient properties. These bounds are specified in the design process as weighting functions. A closed loop block diagram illustrating the weighted output is presented in figure 2.5. With

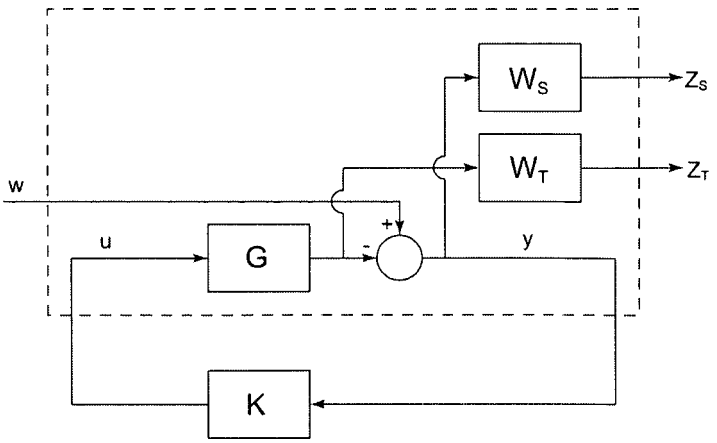

Figure 2.5: Feedback system with weighting functions

reference to this figure the following left hand[2] weighted outputs Z are obtained

$$\begin{aligned} Z_S(s) &= W_S(s)S(s) \\ Z_T(s) &= W_T(s)T(s) \end{aligned}$$

With reference to equation 2.2 the objective is to design the controller such that the condition is satisfied for each sensitivity used in the design. Good controller performance in the broad sense of meeting criteria such as robustness constraints, time response requirements or control effort limits requires careful selection of weighting functions. One of the greatest challenges when designing a controller is to ensure these requirements are adequately detailed in frequency based weighting functions. For example good tracking performance requires that:

- $||S(j\omega)||$ is small for small ω to ensure zero steady state error.
- $||T(j\omega)||$ is small for large ω such that the effect of high frequency noise is attenuated.
- $||T(j\omega)||$ is unity (0 dB) for small ω such that the low-frequency characteristics of the reference input are unaffected.

Figures 2.6 and 2.7 show typical frequency weighting functions bounding the primary and complementary sensitivity functions respectively.

2.5.2 Loop Shaping

As the name suggests loop shaping is a scheme for shaping the open loop system $L = GK$ by tuning the controller K. Whereas many $\mathcal{H}_\infty$ techniques create controllers to meet the

[2]Right hand weights can be applied in addition or as an alternative to the left hand weights depicted in figure 2.5. For clarity only left hand weights are considered in the sequel.

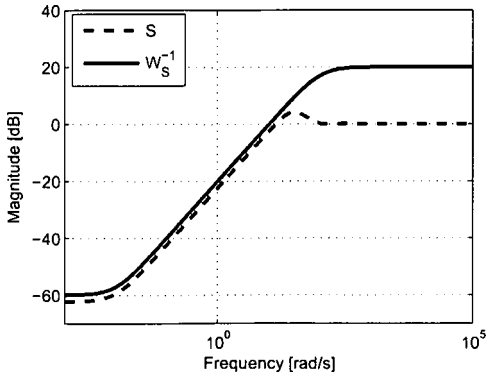

Figure 2.6: Typical weighting shape W_S

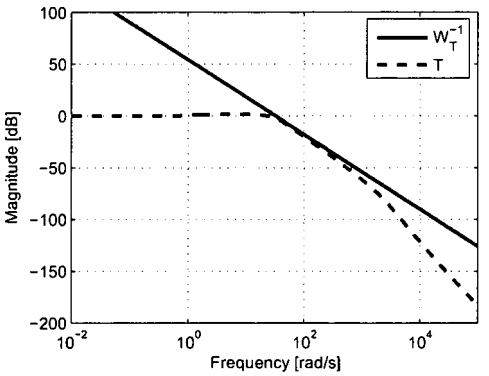

Figure 2.7: Typical weighting shape W_T

closed loop shapes S and T, loop-shaping is concerned with the open loop. Many of the constraints for the desired closed loop shapes can readily be translated into similar open loop requirements. For a SISO system the typical requirements of the loop function are:

- $|L(j\omega)| > 1$ (high loop gain) at low frequencies.
- $|L(j\omega)| < 1$ (low loop gain) at high frequencies.
- $L(j\omega)$ is a suitable distance from the critical point (particularly at frequencies close to the crossover frequency).
- $L(j\omega)$ has sufficiently large crossover frequency.
- $L(j\omega)$ satisfies the Nyquist stability criterion.

Further details of the loop shape requirements for multivariable systems, given in terms of the open loop singular values can be found in [74].

A range of techniques based on shaping the open loop are available for controller synthesis. The most simple techniques aim to achieve the required loop shape by sequentially adding proportional (P), integral (I) and derivative (D) elements to the controller. PS approaches are graphical techniques for obtaining low order controllers for SISO systems. QFT is an alternative technique for graphically shaping the loop. Higher order, normalized-coprime-factor control synthesis theory can be used the obtain the desired loop shapes automatically and are suited to both SISO and multiple-input-multiple-output (MIMO) systems. Commercial software for computing the controller to give the desired loop shape [10] make this technique attractive. However, for complex problems specifying the correct loop shape requires a great deal of experience. Furthermore, complex loop shapes or high order plant models can result in high order controllers.

More recently a $\mathcal{H}_\infty$ loop shaping procedure was developed by McFarlane and Glover [74]. In this technique the loop shape is defined using a precompensator W_1 and/or postcompensator W_2 to obtain the desired open-loop shape (in terms of open-loop singular values). These shaping functions W_1 and W_2 are combined with the plant to form a shaped plant $G_S = W_2 G W_1$. The next stage in the design finds the optimal robust stability margin γ from

$$\gamma_{opt} = \epsilon_{opt}^{-1} \equiv \inf_{K stabilizing} \left\| \begin{bmatrix} K_\infty \\ I \end{bmatrix} (I - G_S K_\infty)^{-1} G_S I \right\|_\infty \tag{2.4}$$

The designer selects a value $\epsilon \leq \epsilon_{opt}$ and synthesises the controller K_∞. The resulting feedback controller K is constructed by combining the controller with the shaping functions using

$$K = W_1 K_\infty W_2 \tag{2.5}$$

If satisfactory robustness, performance or time response of the closed-loop system is not achieved reiterations with alternative shaping functions are required. It is the ease of formulating the open-loop specifications which makes loop-shaping techniques particularly attractive.

A recent extension to the $\mathcal{H}_\infty$ loop shaping taking advantage of the technique for fixed PID structure controllers was presented in [41]. The K_∞ controller of equation 2.4 is replaced by a PID controller combined with the postcompenstor W_2. Accordingly, the K_∞ controller has the fixed structure $K_\infty = W_1^{-1} K_{PID}$ and the resulting feedback controller is K_{PID} in series with W_2 which acts as a low pass filter. The solution to K_{PID} (or any other fixed structure controller) is obtained by a linear matrix inequality (LMI) optimisation.

2.5.3 Algebraic $\mathcal{H}_\infty$ Theory

$\mathcal{H}_\infty$ feedback control is a frequency domain approach for the design of robust control systems. $\mathcal{H}_\infty$ control has received a considerable amount of attention since the control problem was first formulated by Zames [112] in the 1980s and for a detailed background to the topic the reader is directed to [36, 115, 63]. A number of commercially available software packages can be utilised to synthesise the controllers based on solving two Riccati equations.

The $\mathcal{H}_\infty$ norm for positive stable systems is given by the largest peak of the maximum singular value from the frequency response [100]

$$||M(s)||_\infty \equiv \sup_\omega (M(j\omega))$$

$\mathcal{H}_\infty$ controller design methods are based on limiting the peak of this maximum value for a particular transfer function such that it remains below a prescribed level.

With reference to figure 2.5 the system is configured into a block problem with two 'inputs': the disturbance w and the control input(s) u. The two 'outputs' are the weighted

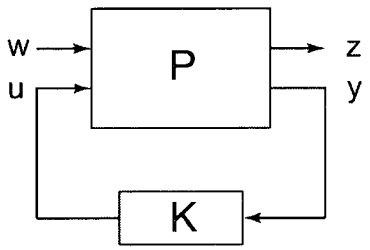

Figure 2.8: Block formulation

sensitivity functions z and the system output y. The block diagram for this formulation is given in figure 2.8 where the resulting augmented system P is obtained for controller synthesis. The augmented system is therefore written as

$$\begin{bmatrix} z \\ y \end{bmatrix} = \left[\begin{array}{c:c} P_{11} & P_{12} \\ \hdashline P_{21} & P_{22} \end{array}\right] \begin{bmatrix} w \\ u \end{bmatrix}$$

As an example, the augmented system for the system shown in figure 2.5 is

$$P = \left[\begin{array}{c:c} W_S & -W_S G \\ \hdashline 0 & -W_T G \\ \hdashline 1 & -G \end{array}\right]$$

The closed loop transfer function from w to z for the system P is obtained by a lower fractional transformation (LFT) as

$$\mathcal{F}_l(P, K) = P_{11} + P_{12}K(I - P_{22}K)^{-1}P_{21}$$

The controller is designed such that the worst-case output z due to an input w is maintained below a set threshold. In other words, the aim of $\mathcal{H}_\infty$ controller synthesis is to find a controller K such that the $\mathcal{H}_\infty$ norm of $\mathcal{F}_l(P, K)$ is bounded by a scalar γ, that is

$$||\mathcal{F}_l(P, K)||_\infty < \gamma$$

and that the resulting system is stable. The problem of obtaining K subject to γ being at a pre-determined level is called the *sub-optimal* $\mathcal{H}_\infty$ problem.

Nominal Performance

Nominal performance conventionally refers to achieving a specified time response performance level for the nominal plant, that is for a plant where no uncertainty in the model is assumed. The performance requirement is determined by the choice of weighting function W_S. The primary sensitivity function S must then be bounded, such that

$$||W_S(\omega)S(j\omega)||_\infty \leq 1$$

where the weighting function is a positive real function of frequency.

Robust Stability

For a set of plant models or a model with a prescribed level of uncertainty, a controller which is stable within this uncertainty is said to achieve robust stability. However, robust stability does not give any guarantees on the system performance for models within this spread of uncertainty. For robust stability an appropriate weighting function describing the uncertainty is required. The weighted complementary sensitivity function T must accordingly be bounded, such that

$$||W_T(\omega)T(j\omega)||_\infty \leq 1$$

2.5.4 Mixed Sensitivity Problem

In general it is necessary to achieve a certain degree of performance in the presence of plant uncertainty and this can be achieved by a mixed sensitivity approach. The two requirements are then generally combined into a single $\mathcal{H}_\infty$ norm cost function forming the so-called $\mathcal{H}_\infty$ standard problem [28]

$$\left|\left|\begin{matrix} W_S S \\ W_T T \end{matrix}\right|\right|_\infty \leq 1 \tag{2.6}$$

An important alternative to the mixed sensitivity formulation is the *robust performance* problem. This specification requires that the specified performance targets are obtained for all plant models which are described by the system uncertainty. The robust performance requirement is

$$|||W_S S| + |W_T T|||_\infty \leq 1 \tag{2.7}$$

A two-disc graphical interpretation of this requirement for SISO systems is shown in figure 2.9 [16, 35]. When solving the robust performance using algebraic Riccati techniques an approximation to the two discs is required since an exact solution cannot be obtained. A sufficient (but not necessary) condition to meet inequality 2.7 is for each sensitivity to be bounded as [35]

$$||W_S S|^2 + |W_T T|^2||_\infty \leq \frac{1}{2}$$

which is satisfied using the useful yet conservative inequality

$$\left|\left|\begin{matrix} W_S S \\ W_T T \end{matrix}\right|\right|_\infty \leq \frac{1}{\sqrt{2}}$$

The obvious advantage to the algebraic Riccati techniques is the extensive, established, numerically robust software which enables rapid controller synthesis. Also non-square multivariable problems can readily be solved for any number of inputs and outputs. A common difficulty with this approach in the synthesis of a controller to meet particular time domain

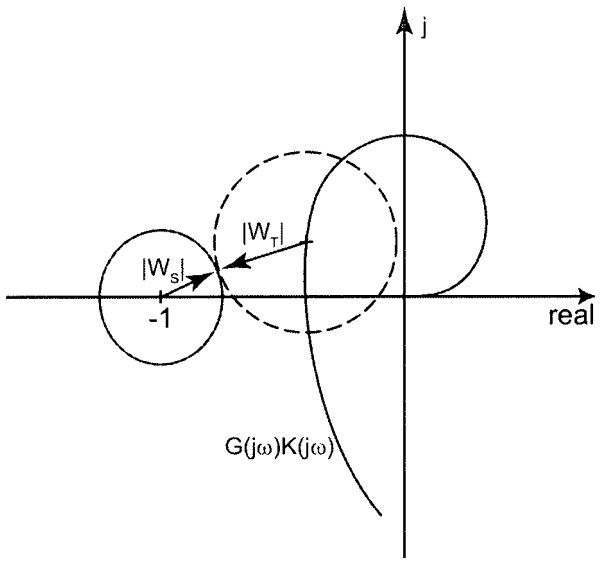

Figure 2.9: Two disc representation of the robust performance requirements

criteria is the selection of weighting functions. This problem is compounded for multivariable systems, particular those with a high degree of interaction. In algebraic techniques the only tuning mechanisms the designer has influence over is in the selection of weights. Whilst general guidelines are available for choosing weights, it is nevertheless well acknowledged that designs also require a high level of experience [100]. Furthermore, for highly coupled systems non-diagonal weights are required, however the design guidelines for these are not well established and are less clear.

Controllers which cannot achieve the specified weighting choices or which do not meet a satisfactory level of performance require the weighting choices to be reconsidered. This can and usually does result in the design process becoming iterative, particularly for mixed sensitivity designs since it is not always clear which of the weightings pose the constraints on the problem.

Another issue with standard algebraic solutions is the controller order. The controller order is determined by the sum of the order of the weights and the plant model. Therefore, even relatively low order models can result in high order controllers if a mixed sensitivity design is necessary. Subsequently it is often necessary to consider controller reduction algorithms which can result in performance below the required levels.

Algebraic techniques require the plant and weighting functions to be proper, real, rational functions which therefore imposes limits on the shapes of weighting functions which can be applied. For example, complementary sensitivity functions can be used to represent the system uncertainty. This uncertainty could have been obtained experimentally as a spread in the frequency response of the system. To make use of this information the designer is faced

with the task of finding an appropriate weighting which is a real, rational approximation of this uncertainty. Furthermore the designer must be conscious of the order of the weighting function as these affect the order of the controller. Another limitation of the technique is for systems with pure time delays, since these can not be handled directly and therefore, it is necessary to use rational transfer functions such as Padé approximations.

With reference to powertrain control, $\mathcal{H}_\infty$ controllers have been demonstrated to provide very high performance solutions. The main criticism of this technique for powertrain applications is that the controller order cannot easily be constrained to the low orders required for implementation in a production PCM.

$\mathcal{H}_\infty$ Optimal Control

An optimal $\mathcal{H}_\infty$ controller is one which minimises the $\mathcal{H}_\infty$ norm by obtaining a controller which achieves the lowest possible bound of the weighted sensitivity. The weighted sensitivity problem with a scalar variable γ can be written as

$$||W(s)F(s)||_\infty \leq \gamma, \quad \forall\, \omega > 0$$

The procedure called *γ-iteration* is that of obtaining the lowest γ using a binary search, generally this is found to quickly converge to the optimal value.

2.5.5 Quantitative Feedback Theory

The early origins of QFT date to the 1950s. Horowitz originally developed the idea to create a design approach that engineers could readily understand and apply [51]. The technique is a practical design method for designing control systems by quantitatively mapping the design specifications to constraints on the loop transmission. QFT is a frequency domain approach to controller design based on manipulating controller parameters in the Nichols plane.

A distinctive feature of QFT is the unique manner in which it handles plant uncertainty. The underlying philosophy of feedback control is to deal with uncertainties, whether these be inherent in the plant model or disturbances. One particular merit of QFT is the ability to work directly with either structured or unstructured uncertainty [52]. For example the uncertain plant P could have structured uncertainty represented by the plant set $\mathcal{P}$ arising due to uncertain parameters in the transfer function coefficients

$$\mathcal{P} = \left(P = \frac{k}{s+a}; \quad k \in [1, 10], \quad a \in [1, 4] \right) \tag{2.8}$$

Templates representing the spread of models due to the uncertainty are translated into the Nichols plane. For the system with uncertain coefficients given in equation 2.8 the set $\mathcal{P}$ is

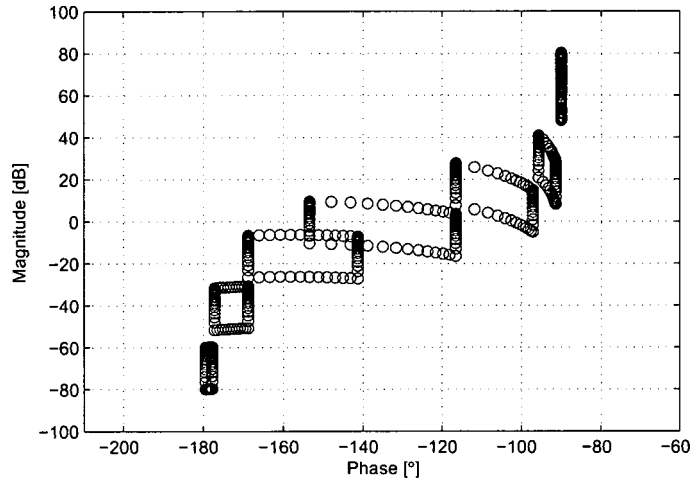

Figure 2.10: QFT templates in the Nichols plane

illustrated in figure 2.10 over several discrete frequencies in the range of interest. Alternatively the unstructured uncertainty could be obtained experimentally using a system identification approach over the range of operating points. At each frequency, variations in the models can be translated into discrete templates representing the uncertainty in the set of models $\mathcal{P}$. It is often convenient to represent this uncertainty or 'scatter' at each frequency as a disc which encompasses all the points, however, alternative shapes can readily be adopted in QFT. Figure 2.11 shows a typical set of plant models $G_i(j\omega)$ at a particular frequency in the complex plane, the nominal plant model G_0 can be assumed to lie at the centre of the template. Such uncertainty templates can readily be translated into the Nichols plane. The

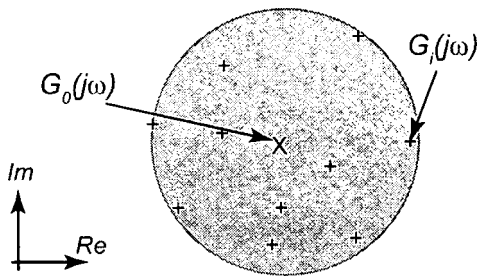

Figure 2.11: Unstructured uncertainty in the complex plane

basic design procedure [52] can be summerised as follows

1. Specify the desired closed-loop step response *envelope*. This model forms the upper and lower bounds on the closed loop step response.

2. Map the step response envelope into the equivalent frequency domain bounds.

3. Specify a disturbance rejection model in terms of the frequency domain.

4. Compute the necessary uncertainty templates for the plant $P(s)$ for a range of discrete frequencies.

5. Graphically display the regions meeting the specifications for shaping the nominal loop transmission L_0.

6. Interactively develop the compensator $K(s)$ until the loop transmission achieves the required specifications.

The loop shaping stage of the design must begin with a stable start controller. Often this is a simple PID type controller designed using classical methods. Higher order techniques can also be employed to obtain a more suitable start controller if the optimal QFT controller is to be obtained. The choice of start controller is often determined by restrictions on the resulting QFT controller. In either case the desired loop shape must ensure the nominal loop function satisfies the worst case QFT bounds, where the optimal QFT controller fits the optimal boundary and therefore requires higher orders. This stage of the design requires some degree of experience with the design technique.

The general approach to obtaining the desired loop shape is through the addition of poles or zeros in the controller until the QFT templates are avoided. Commercially available software packages [21, 53] create a Nichols chart environment to interactively shape the loop. Since in general only a small number of discrete frequencies are used in the generation of QFT templates the resulting controller must be analysed over a wider set of frequencies to ensure the design constraints are satisfied. Problematic frequencies can be plotted in any necessary subsequent re-designs.

QFT was originally intended to be an 'engineer friendly' solution to controller design because insights into design trade-offs between robustness and performance can be visualised. The interactive design process allows the designer some freedom on controller order. Early in the design process incompatible constraints can be detected and re-designed as appropriate. This ability to visually observe design constraints is a significant merit over non-graphical methods. One of the main advantages of QFT over techniques such as alegebraic $\mathcal{H}_\infty$ is the ability to handle parametric and and non-structured uncertainty directly. Furthermore, the technique can handle pure time delays non-conservatively.

QFT designs are undertaken with only a limited number of uncertainty templates. Accordingly, post design analysis often makes re-designs necessary. The generation of the templates themselves can be non-trivial and computationally demanding for complex systems with several uncertain parameters if a large number of QFT templates are designed. Whilst QFT can directly deal with parametric uncertainty, it is often very difficult to determine which parameters are uncertain and by what magnitude.

Some of the transparency and insight of the technique is lost when considering multivariable systems since the process of designing the loop shaping becomes significantly more complex and time consuming. Furthermore, multivariable designs become conservative and are realistically limited to systems with less than 3 inputs and 3 outputs [34]. There is still considerable research into developing systematic methodologies for multivariable plants. This has resulted in two district approaches [61]: non-sequential loop and sequential loop design methods. The limitations of each techniques are the requirement of a square plant model and in general only diagonal controllers can be designed.

2.5.6 Parameter Space Theory

Current linear algebraic $\mathcal{H}_\infty$ theory and associated software [11, 28, 115] provide powerful tools for systematically designing controllers for systems with multiple transient performance and stability robustness requirements. For many applications however, fixed low order, including PID, controllers are often preferred in industrial practice. Current PS methods allow the design of fixed low order controllers, but are limited in their ability to directly address multivariable problems.

PS methods offer a graphical way to design controllers. As the name suggests PS techniques are based on visually displaying a set of parameters which meet a given set of constraints. Assuming the constraint(s) can be achieved the design is then presented with an *admissible* region to select controller parameters. PS methods extend back at least to Niemark in the 1940s [79], [80] later followed by Mitrovic [76]. Early presentations were in [4, 84, 96, 104].

A large range of methodologies based in the PS have been developed. Early work focused on identifying stability regions and controller designs based on pole placement. As feedback theories have been developed PS techniques have been adapted to accommodate these, offering the usual PS benefits, namely transparency and insight. However, one area which has received very little attention in the PS is minimum variance (MV) design.

The PS approach based on Kharitonov's theorem to the robustness of relative (so-called γ) stability to transfer function parameters was presented by [2]. The work on PS design for gain and phase margin requirements was initiated in [30] and associated results presented in [26] and [27].

PS based PID and extended PID designs for relative stability in irrational systems, including the full treatment of the singular conditions was developed in [90] based on [95]. PS PID design for simultaneous bandwidth, gain and phase margin criteria as well as a treatment of the singular conditions was given in [92].

Besson and Shenton [15] developed a fixed order irrational SISO $\mathcal{H}_\infty$ PS method where

specifications for given weighting functions are mapped into a parameter plane and several specifications can be considered simultaneously by overlaying the regions. The method also allows higher order controllers to be designed by combining elemental 2nd order controllers. Similar results reported for PID controllers and square rational MIMO systems were developed independently and published in Japanese literature by Saeki [86] and have subsequently been developed, again for rational PID [88]. A PS frequency response method for irrational SISO robust performance design of fixed low order controllers, to non-conservatively achieve frequency response performance specifications with unstructured plant uncertainty was first reported in [16] and subsequently extended to irrational MISO problems [17]. A range of symbolic approaches to PS controller design is given in [3]. Detailed surveys of PS methods are presented in [44, 97].

Although sequential SISO design methods can be applied to many multivariable engineering applications, optimal robustness margins cannot then be obtained directly by the design process. However, one benefit of PS techniques is that multiple SISO loop margins can be superimposed and therefore can assist in sequential loop approaches. In the MIMO frequency response PS method reported by [87] a rational LFT formulation is given for the design of single element PID controllers.

Conditions to obtain rational MIMO PS boundaries are given by Muhler [77] in the form of equations in the determinant of the Hamiltonian matrices corresponding to the continuous $\mathcal{H}_\infty$ and $\mathcal{H}_2$ Riccati equations, for suggested use as a basis for symbolic computational methods. An important limitation in this and the other Riccati based formulations however, is that irrational systems such as systems with time delays are not directly addressed because the conditions are developed in terms of continuous finite state-space models only.

Frequency response based PS methods offer significant advantages over other controller design techniques. Non-parametric frequency response information such as output from identification or multiple model averaging processes can be used directly and rational plant approximations can be avoided. In application of the $\mathcal{H}_\infty$ approach weighting functions are instruments of the designer to be adapted during the design process. Frequency response PS methods provide good information to the designer on which weighting functions are close to constraint boundaries at which frequencies. Weighting functions for constraining both performance and uncertainty are also not limited to rational approximations. This is in distinction to Riccati $\mathcal{H}_\infty$ methods where both rational plant and weighting representations are required. The ability to map a number of single sensitivity constraints can also be of great advantage since it allows a designer to graphically observe which weights may be over-constrained [14]. The robust-performance mixed sensitivity approach used by many techniques often requires the conservative formulation

$$\left\| \begin{matrix} W_S S \\ W_T T \end{matrix} \right\|_\infty \leq 1$$

where W_S and W_T are frequency weights acting on the primary S and complementary T sensitivity functions respectively. Moreover these techniques do not present the designer with any insight into which sensitivities, weights or frequencies are problematic.

One of the disadvantages associated with PS methods for MIMO problems is that higher order controllers and systems with very large numbers of inputs and outputs may be difficult to synthesise. On the other hand to develop fixed low order controllers by existing Riccati $\mathcal{H}_\infty$ optimal control methods it is currently necessary to use order reduction techniques, which produce controllers that are in general then non-optimal for the chosen order. Another disadvantage of PS, particularly for multivariable systems is the number of iterations sometimes necessary, which can make the process time consuming. However, this iterative nature often gives a lot of insight into the design process and therefore changes to weightings or parameter choices can be made progressively. Furthermore, routines to automatically iterate through the parameter planes for sensitivity optimisation can readily be implemented if desired [86]. In contrast 'one-shot' algebraic techniques do not reveal to the designer which frequencies and/or weighting choices require modification for a design to be successful or improved upon. Furthermore, PS techniques are ideal for tuning time response criteria by the trial of gains within the admissible region. For problems where controller order is not a constraint alternative methods can be more attractive provided the designer has good *a priori* knowledge on the selection of weighting functions.

2.6 Robust Minimum Variance Control

The development of minimum variance (MV) control can be attributed to Åstrom [6] to deal with systems subject to stochastic disturbances. The framework originally intended for discrete, minimum phase systems creates a MV regulator which achieves the lowest possible output variance. At any time t, the control action $u(t)$ should minimise the output $y(t)$ based on the cost function

$$J = E[y^2(t+k)]$$

where E is the expectation function for the system with k delays. This work was later extended to include non-minimum phase systems [7].

The optimal MV regulator was intended only for zero mean disturbances and therefore could not reject non-zero mean disturbances or tracking to specific set-points. Subsequent developments included non-zero tracking regulation and de-tuned MV which limited the control effort [109]. Generalised minimum variance (GMV) allowed constraints additional to MV through the use of a more general cost function [29].

One of the problems associated with MV design techniques is that in general no guarantee

on robustness can be obtained. A common approach is to assess the robustness of the system after the design is complete and if necessary re-design with different constraints. One framework which aims to address these difficulties is $\mathcal{H}_2$ control. As opposed to minimising the maximum peak of a particular sensitivity function, as with $\mathcal{H}_\infty$ approaches, an alternative cost function based on the 2-norm of a sensitivity function $F(s)$ is considered

$$||F(s)||_2 \equiv \left(\frac{1}{2\pi}\int_{-\infty}^{\infty}|F(j\omega)|^2 d\omega\right)^{\frac{1}{2}}$$

The $\mathcal{H}_2$ norm is based on the area under the sensitivity function of interest, which can be considered analogous to energy. Therefore, minimising the $\mathcal{H}_2$ norm can be considered to minimise the noise transmission of the system in order to reject the disturbance [115]. As with $\mathcal{H}_\infty$ control, weighting functions are included in a typical design to ensure robustness and transient performance at the desired frequencies.

The links between $\mathcal{H}_2$ and MV are discussed in [105]. It can be demonstrated that the optimal $\mathcal{H}_2$ design closely approximates the MV regulator if the sensitivity functions are left un-weighted. One obvious solution to the design of low variance controllers with tracking, robustness and imposed limits on the amount of control action is therefore to consider $\mathcal{H}_2$ control. However, since the optimisation routines minimise the 2-norm the desired transient performance or robustness objectives are not necessarily guaranteed. To address this problem a number of mixed $\mathcal{H}_2/\mathcal{H}_\infty$ approaches have been developed which provide satisfactory variance characteristics with a degree of robustness [62].

Chapter 3

Experimental Setup

3.1 Introduction

The applications of the control techniques presented in this thesis are based on identified engine models and have been subsequently validated using the University of Liverpool engine and dynamometer facilities. Developing controllers to work on a physical system followed by validation of the performance can give a much greater insight into the problem and how to improve designs, where necessary. This chapter details the experimental setup that was used.

The original engine and dynamometer setup was designed for idle speed control work on a 1.6l Ford Zetec engine [91]. The specification of the engine is described in section 3.2. The engine is coupled to a low inertia DC dynamometer capable of moderate loading, detailed in section 3.3. An overview of the key engine sensors and actuators is given in section 3.3. The interfacing of these with the digital signal processing (DSP) unit, originally developed by Carroll [25], is also presented.

3.2 Engine Specification

The test engine used is a gasoline spark ignition (SI) 1.6l Ford Zetec. The engine has an inline configuration with four cylinders, where each cylinder has two inlet and two exhaust ports controlled by double overhead camshafts (DOHC). Fuel is injected sequentially into the inlet ports prior to the valves opening. Spark timing, fuel timing and duration can all be controlled from the standard engine management system (EMS) as fitted into a production vehicle. The specification for the engine is given in table 3.1 and a schematic of the crank domain timing events of the valves, fuelling and standard spark timings is given in figure 3.1.

The engine is of standard configuration other than control of exhaust gas recirculation (EGR) which is disabled from the EMS strategy. An electronically controlled valve from the

Table 3.1: Engine specifications: Zetec 1.6l

Cylinder bore	76.0 mm
Connecting rod length	136.2 mm
Compression ratio	10.3:1
Cubic displacement	1597 cm^3
Stroke length	88 mm
Maximum torque	138 Nm at 3500 rpm
Maximum power	67 kW ($\approx$ 90 PS $\approx$ 90 BHP)
Idle speed	880 rpm
Fuel	Unleaded RON 95 petrol

DSP unit allows EGR to be regulated, however for the applications in this thesis it has been set closed. EGR can be used at low-to-medium loads, where a small amount of exhaust gas is used to fill part of the cylinder volume with what is essentially an inert gas. This has the effect of reducing fuel consumption and also keeping combustion temperatures lower and therefore reducing NO_x production. Furthermore, any unburned hydrocarbons (HC) in the exhaust gas goes through a second combustion event to become oxidized. One of the problems associated with the introduction of EGR is a decrease in combustion stability which increases the cycle-to-cycle variation (CCV).

3.3 Experimental Configuration

3.3.1 Dynamometer

The dynamometer used for loading the engine is a low inertia DC electric motor, mainly suited to idle speed work. The dynamometer is used to provide or remove energy from the engine. Typically the dynamometer is used in torque control mode to apply a load against the engine. The inertia of the dynamometer is sufficiently low to replicate the dynamics of the flywheel and gearbox that are not mounted to the engine in this setup, and therefore presents a more realistic loading at idle or during de-clutched load transients.

3.3.2 Hardware/Software Interface

A schematic illustrating the hardware which interfaces with the engine for identification and control purposes is shown in figure 3.2. Excitation signals and measurements are made through a DSP unit attached to a standard desktop PC. The engine actuators, spark advance (SA) and dynamometer are controlled by the DSP unit interfaced this desktop PC. MATLAB 7.04, SIMULINK and Real-Time Workshop are used to generate models for implementing controllers or exciting the actuators. These models are then compiled and downloaded to

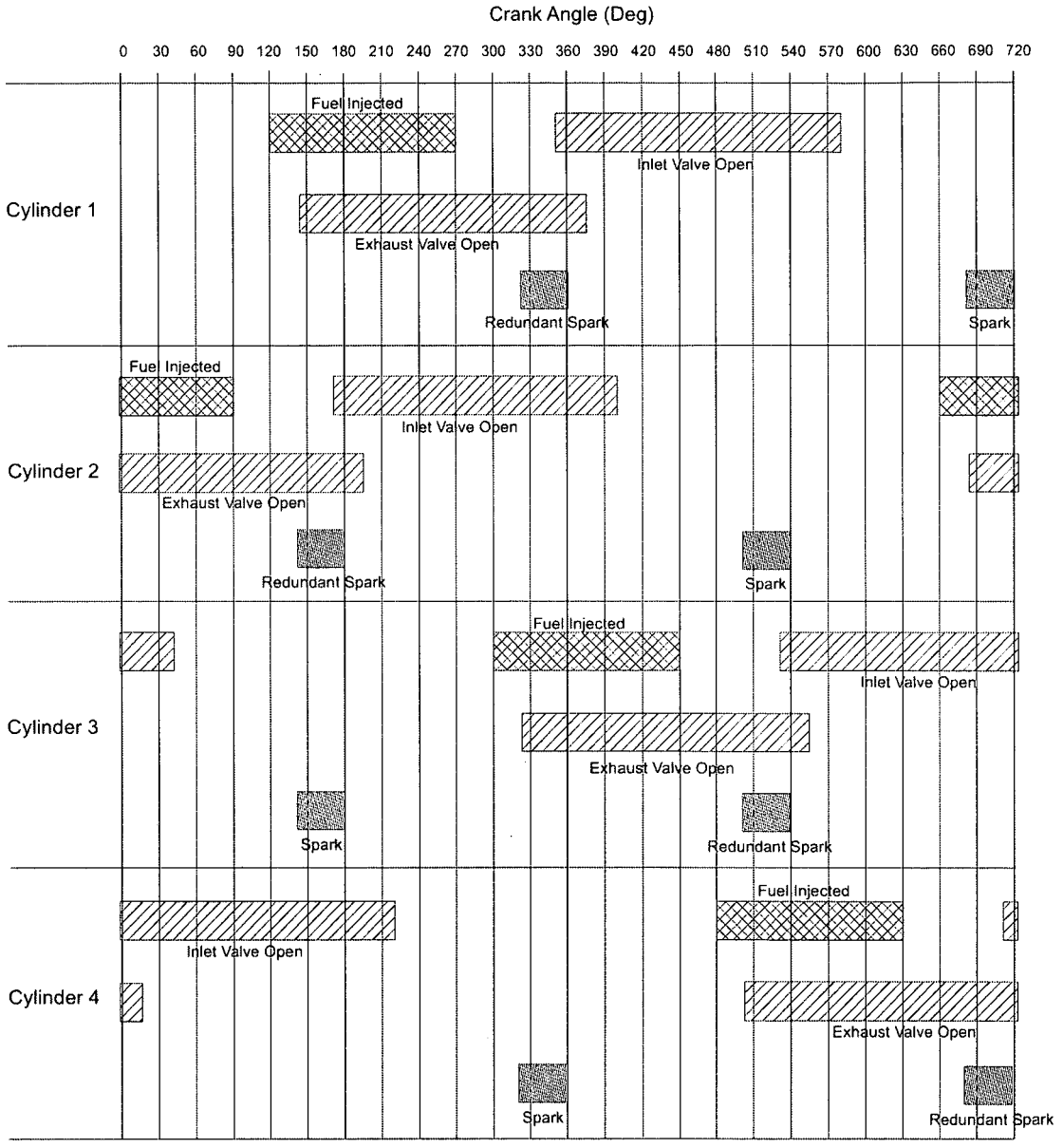

Figure 3.1: Valve, fuel and standard spark timings for the Zetec engine

Table 3.2: Card specifications in the dSpace rapid prototyping unit

Board	Function	Specification
DS1005	Processor Board	PowerPC 750GX running at 1 GHz
DS2003	Analogue Input Board	32 Channel ADC Board (16 bit)
DS4001	Digital IO	Timing and DIO
DS4002	Digital IO	DIO including PWM generation

the dSpace expansion box, which then runs tasks in real time and also acts as a multiplexer for the various inputs and outputs. A DS1005 real time interface card is responsible for processing the tasks in real time, which includes driving the digital outputs on DS4001 and DS4002 input-output (IO) cards and transferring data from these and a DS2003 analogue input card to the PC. A summary of the specifications of the cards in the dSpace expansion box is given in table 3.2. The online graphical interface and data capture software linked to dSpace is ControlDesk.

3.3.3 Key Instrumentation

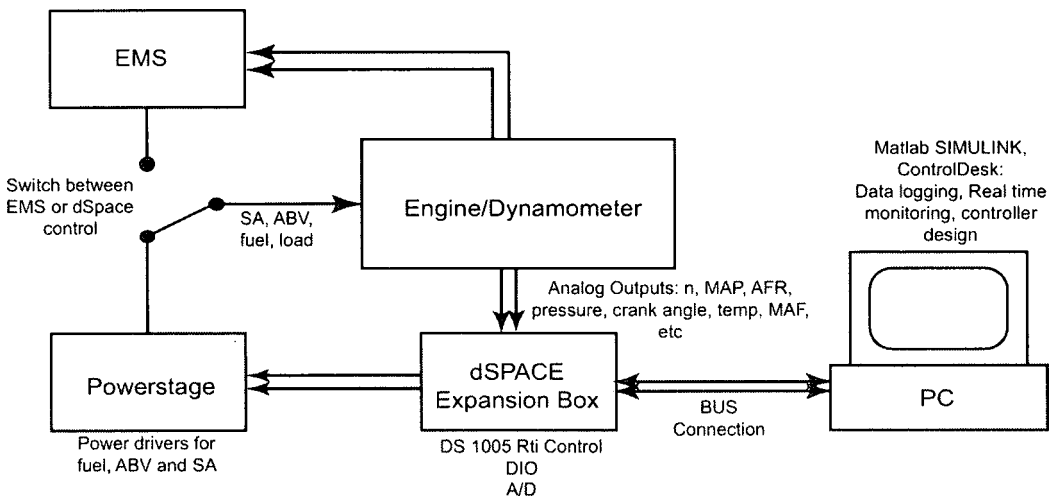

Figure 3.2: Hardware for identification and control

A schematic of the engine and key sensors are shown in figure 3.3. Many of the sensors in the setup are additional to the standard set fitted to the engine in a production vehicle. In general most sensors are sampled every degree when triggered by the angle encoder and subsequently downsampled accordingly. Data from the sensors are measured with a resolution of between 12 to 16 bits. The resolution is determined by the number of channels which are required and also the rate of capture due to limitations in the analogue to digital converter (ADC). The following sections outline the main sensors for control and identification used in the applications presented in the subsequent chapters.

Angle Encoder

An angle encoder mounted directly onto the crankshaft provides the main source of timing for much of the engine work. The encoder outputs two signals; one pulse every degree, and one pulse every 360° which also corresponds to top dead centre (TDC) for cylinder 1. The 1° pulses are transmitted to a hardware interrupt function on the DS4001 card which synchronises the timing between the engine and dSpace. The once per revolution pulse is also used to ensure no pulses are missed and continually checks and resets the crank angle in dSpace if any discrepancy is found.

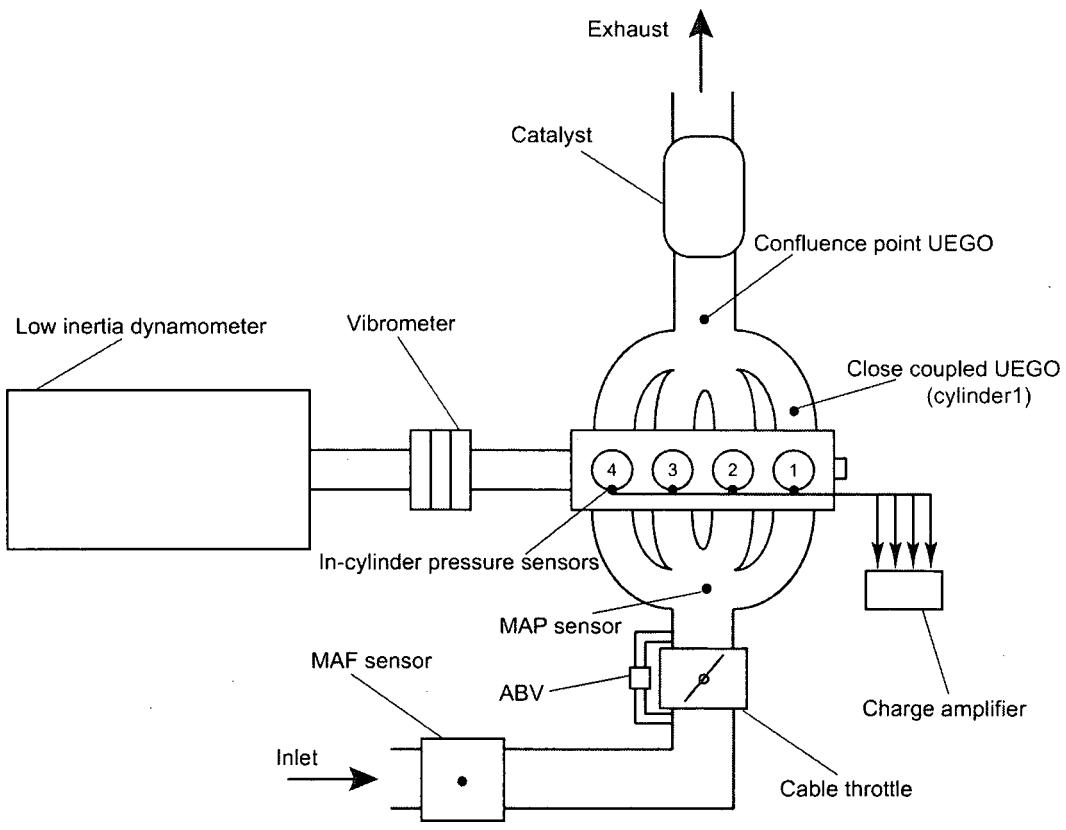

Figure 3.3: Schematic of the engine setup and key instrumentation

Pressure Sensors

Each of the cylinders are fitted with pressure sensors (Kistler 6123) screwed into fixing positions machined into the cylinder head. The sensors are linked to charge amplifiers and thereby give signals proportional to the cylinder pressure. These signals are used in conjunction with an algorithm for determining the peak pressure position (PPP) [25], although additional information such as the magnitude of the pressures could also be obtained.

MAP Sensor

A manifold absolute pressure (MAP) sensor is fitted onto one of the 'vacuum' hoses on the inlet manifold. This sensor or alternatively, a mass air flow (MAF) sensor, is one of the essential measurements needed for fuelling control. These measurements are used by many automotive manufacturers to give an indication of the mass of air entering the cylinders and the load applied to the engine.

Both the MAP and MAF sensors respond very quickly to changes in the air pressure or flow and are therefore potentially very information rich signals. The output of these sensors can clearly show individual valve opening events, and manifold filling and emptying. As a result, when considering event based fuelling identification and control, it was found that integrating these signals over 180° samples would give the most suitable values when used for information analogous to engine load. For other applications, such as systems with variable valve timing, alternative analysis of these signals may be more appropriate.

UEGO Sensors

Two universal exhaust gas oxygen (UEGO) sensors are fitted to the engine to allow monitoring of the air-to-fuel ratio (AFR). Also known as lambda or wideband sensors, these are heated devices that detect the presence of oxygen in the exhaust gas. These have a relatively large linear operating band and therefore, offer significant advantages over conventional production narrowband or heated exhaust gas oxygen (HEGO) sensors, which are reliant on switching or cyclic control. The disadvantage of the UEGO sensor relative to the HEGO sensor is their cost, which currently makes these unfeasible for installation in lower cost production vehicles. The voltage output from the UEGO sensor is proportional to the AFR, which for a gasoline port fuel injection (PFI) engine under normal stoichiometric conditions is the ratio of air mass to fuel mass and is typically 14.7:1. However, it is often useful to consider the ratio λ

$$\lambda = \frac{AFR_{\text{Measured}}}{AFR_{\text{Stoichiometric}}}$$

which provides the ratio of the measured AFR relative to the desired AFR which would give stoichiometric, thereby creating a normalised reading irrespective of fuel type or octane number.

In the setup, one of the UEGO sensors is mounted at the confluence point on the exhaust shortly after the manifold. This is the typical region for mounting an oxygen sensor on a production vehicle since CCV is smoothed out due to the mixing of the four cylinders. The second UEGO is fitted directly to the runner of the manifold for cylinder 1. This is mounted within 100 mm of the exhaust port to pick up the AFR for only this cylinder thereby allowing

individual cylinder control. Furthermore, the transport delay of the gases from the exhaust valve to the sensor are then minimised by this closer location.

Engine Speed

A tachometer attached to the vibrometer torque transducer (Torquemaster TM112), coupled between the engine and dynamometer is used for measuring engine speed. There are a number of alternative ways to measure the engine speed in the setup, including a tachometer coupled to the end of the dynamometer shaft, however, this can be less accurate during transient loads due to twist in the shafts. A second alternative is to use the angle encoder that is attached to the crankshaft which can be input to a frequency counter (available in dSpace), however this method can significantly increase the computational demand on the DSP system.

3.3.4 Engine Inputs

Authority over the SA, air bleed valve (ABV), fuel pulse width and injection angle can be controlled from either the EMS or can be bypassed and controlled independently using ControlDesk and dSpace. This setup allows the standard EMS strategies to control the inputs which are not under consideration, whilst the dSpace controls the remaining inputs which bypass the EMS. For example, when considering the effects of SA on the PPP, the effects of AFR can be deemed negligible (assuming the AFR is maintained close to a set-point) and therefore, it is advantageous to leave the fuelling under the control of the EMS. Alternatively, full control of the engine actuators can be achieved through dSpace attached to a bespoke powerstage unit if desired.

Spark Advance

The SA whilst not strictly an actuator can be controlled from dSpace. The engine runs on a redundant spark system whereby two cylinders spark simultaneously. This ignites the mixture in one cylinder and is paired with the cylinder which is 360° out of phase on its exhaust stroke. The paired cylinders and their appropriate ignition windows are shown in figure 3.1. A signal to trigger the spark is sent 3 ms before the desired spark event to allow the coil to charge for this period, after which time the ignition event occurs. This approach is typical of a production EMS, however, it does suffer from the inherent limitations due to the 3 ms dwell time that is estimated from engine speed, which can be subject to fluctuations over this period. Moreover, in this setup the interrupt signal can only be generated to the nearest degree since this is the base rate of the model, which effectively limits the resolution of the SA to 1°.

Air Bleed Valve

The ABV is used to regulate the air flow into the engine. The engine is fitted with a cable operated throttle and therefore is fitted with an ABV for the automatic regulation of air, typically at idling conditions. This also has the effect of smoothing air transients caused by any sudden changes in throttle angle. Although the throttle is not controlled electronically, the ABV has a relatively large degree of authority under low-to-medium loads. The amount of air that bypasses the throttle is defined by a pulse width modulated (PWM) signal operating at a frequency of approximately 300 Hz. The ABV can not only be considered equivalent to an electronic throttle but also a throttle position sensor, albeit with a lower range.

Fuel Injectors

Four sequentially operated fuel injectors are attached to the engine. Fuel is injected onto the inlet ports of the cylinders prior to the valves opening. This creates a pool of fuel in the manifold, some of which evaporates and mixes with the air due to the heat of the engine and is then drawn into the cylinders when the valves open. As with all PFI engines, not all of the fuel injected for a particular event will be drawn into the cylinder since the engine effectively fuels from the puddle developed in the inlet manifold runners. Accordingly, fuelling strategies must take account of these fuel puddle dynamics.

Assuming only one injection event occurs every 720° for each cylinder during normal operation, two variables that can controlled are: injection-start timing relative to the crank angle and injection pulse width. Since AFR control in PFI engines relies on fuel puddle dynamics, the injection start angle is less critical for control purposes. Therefore, the AFR application in the preceding chapters uses an injection start angle which is fixed to match that of a production EMS strategy. The engine management fuel injection window timings are shown in figure 3.1.

The second variable available for control is the fuel pulse width, which controls the length of time the injector stays open from the injection start angle. Due to the dynamics of the injectors the mass of fuel injected into the engine is not proportional to the pulse width.

3.3.5 Conclusions

A standard 1.6l Ford Zetec with PFI is coupled to a low inertia DC dynamometer for loading the engine. A DSP unit connected to a desktop PC allows authority over the fuel pulse width, fuel timing, SA and ABV. The ABV can be considered to be analogous to an electronic throttle only with a smaller range of authority. EGR is disabled for the experimental work

covered in this thesis. For many engine tests is it advantageous to leave the EMS to control some of the actuators such as the fuel injectors. Sampling is in general carried out every degree in synchronisation with the angle encoder. The resolution at which the sensors are sampled can be adjusted as necessary. In general important variables are recorded with 12-16 bit resolution.

Chapter 4

Parameter Space Constrained-Variance Control

4.1 Introduction

Many powertrain processes are subject to persistent noise disturbances. Controller design for such processes requires consideration of the output variance for satisfactory performance requirements to be realised. Maintaining the peak pressure position (PPP) of the cylinder at an empirically determined set-point can maximise the torque output [48]. The spark advance (SA) primarily governs this position, however, due to the chaotic nature of combustion a significant amount of variance in the output is observed. Robust control techniques can readily be applied to such processes to introduce properties such as tracking and disturbance rejection, however, in general these can excite the output variance leading to poor steady-state performance. Accordingly, designs which aim to suppress or *minimise* this variance are particularly useful for many powertrain processes.

This chapter presents a novel closed-form single-input-single-output (SISO) parameter space (PS) approach to designing fixed order, two term controllers such as PI or PD which is readily implementable as a fast and robust numerical algorithm for interactive design. The technique is based on mapping loci of constant variance for continuous and discrete rational systems. White noise coloured by a rational filter is assumed to be the output disturbance to a rational plant. PS mappings are developed from the mean-squared value, evaluated from the spectral density function and Leverrier's algorithm to produce loci for a given closed loop output variance. These loci can be used either on their own or superimposed with other requirements such as sensitivity functions or gain and phase margin boundaries in the parameter plane thus creating a robust constrained-variance PS method. Minimum variance subject to additional design constraints can then be obtained by iteratively reducing the variance level until the admissible parameter region is exhausted.

A design example for the regulation of engine speed at idle demonstrates a mixed constraint design. The technique is successfully applied and experimentally validated for the regulation of the peak pressure position (PPP), which illustrates the effectiveness and simplicity of the technique.

4.1.1 Minimum Variance Control

The minimum variance (MV) controller was first developed by Åstrom [6] for discrete linear time-invariant (LTI) systems subject to stochastic disturbances. This work was later extended to include non-minimum phase systems [7]. These basic MV designs acted only as regulators. A successful variant of the MV regulator is the detuned MV controller, where the resulting output variance is traded-off with the control action to prevent excessive control signals [109]. For the many applications requiring tracking whilst retaining MV-type disturbance rejection, an integrator was incorporated in several subsequent developments. Generalised minimum variance (GMV) allowed constraints additional to MV through the use of a more general cost function [29].

MV type controllers are of significant importance for many industrial applications such as gust suppression acting on aircraft [75] and regulation in active automotive suspension systems [109]. Controllers intended to minimise the output variance are often a compromise between the tracking performance and the disturbance rejection. Fixed low order PID type controllers are often required to realise such control in industrial practice for implementation and tuning purposes. Grimble [42] presented an approximate discrete frequency recursive approach to linear-quadratic-Gaussian (LQG) optimisation for design of continuous-time, restricted (fixed) structure controllers such as PID and described a conservative cost function method for also achieving gain and phase margin specifications [43].

In other control problems PS methods have been found to be particularly useful for low-order design and for multi-objective designs, where constraints such as gain and phase margin and $\mathcal{H}_\infty$ bounds on sensitivity functions can be superimposed onto parameter planes. However, despite the range of techniques developed for robust PS controller design, little work has been published relating to constrained variance or minimum variance. A PS approach for constraints on the $\mathcal{H}_2$ norm has been suggested in [3] and [77]. The proposed method is not based on a closed-form solution but on the somewhat demanding use of computer algebra to solve the associated Hamiltonion equations to produce the parameter boundaries.

4.2 Closed Loop Variance - Continuous Systems

This section describes how loci defining controller gains to give a fixed closed-loop output variance for system subject to persistent noise disturbances can be generated. First the problem is defined and the definite integral describing how the output variance is calculated is given. The following subsection describes how the coefficients of the closed loop transfer function determine this variance and how these can be computed for any known rational system. The results are then extended to allow loci of unknown controller coefficients to be computed for any fixed output variance. Specific matrix forms are given for PI and PD controllers and the section is summarised with an algorithm for generating the parameter plane loci. An idle speed example is used to demonstrate the technique.

The approach is based on computing output variance loci for a closed loop plant model for the assumed Gaussian disturbance rational plant and colouring filter. For simplicity an auto regressive moving average with exogenous input (ARMAX) plant model is assumed. The system under consideration here is the negative unity feedback control configuration of figure 4.1, where the transfer function $G_b(s) = \frac{b(s)}{a(s)}$ represents the plant which is assumed to consist of two polynomials $b(s) = b_l s^l + b_{l-1} s^{l-1} + \ldots + b_1 s + b_0$ and $a(s) = a_n s^n + a_{n-1} s^{n-1} + \ldots + a_1 s + a_0$ where $l \leq n$ and where the coefficients a_i for $i = 0, 1, 2 \ldots, l$ and b_j for $j = 0, 1, 2, \ldots, n$ are real and there are no unstable pole cancellations. The colouring filter of the noise process

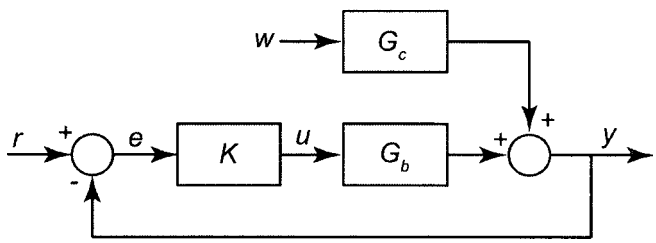

Figure 4.1: Closed loop system with coloured noise disturbance

is assumed stable and subject to a unit variance white noise input and is described by the rational transfer function $G_c(s) = \frac{c(s)}{a(s)}$ with $c(s) = c_m s^m + c_{m-1} c^{m-1} + \ldots + c_1 s + c_0$ where $m \leq n$.

The closed loop transfer function from the disturbance w to the output error y with Laplace transforms $\hat{w}$ and $\hat{y}$ is accordingly given by

$$\frac{\hat{y}}{\hat{w}}(s) = \frac{G_c}{1 + KG_b} = \frac{e(s)}{d(s)} \tag{4.1}$$

where $e(s)$ and $d(s)$ are associated numerator and denominator polynomials. With w representing a white noise zero mean process of power per unit bandwidth W, ie $(\Phi_{ww}(\omega) = W)$,

the variance of the zero mean process is given by

$$\overline{y^2(t)} = \frac{1}{2\pi}\int_{-\infty}^{+\infty}\left|\frac{\hat{y}}{\hat{w}}(j\omega)\right|^2 \Phi_{ww}(\omega)d\omega$$

The variance per unit white noise $\sigma^2 = \frac{\overline{e^2(t)}}{W}$ can therefore be written as

$$\sigma^2 = \frac{1}{2\pi}\int_{-\infty}^{+\infty}\frac{|G_c(s)|^2}{|1+K(s)G_b(s)|^2}d\omega \tag{4.2}$$

which can be computed from the definite integral

$$\sigma^2 = \frac{1}{2\pi j}\int_{-j\infty}^{+j\infty}\frac{e(s)e(-s)}{d(s)d(-s)}ds \tag{4.3}$$

where $e(s) = \sum_{k=0}^{n-1} e_k s^k$ and $d(s) = \sum_{k=0}^{n} d_k s^k$. Solutions to the definite integral in equation 4.3 are presented in [38] in the form of standard tables based on the numerator and denominator coefficients $e(s)$ and $d(s)$. The closed-form expressions for the integrals significantly increase in complexity with increasing system order and so the tables are given only up to order eight. In contrast the subsequent section describes how loci for two term PI and PD controllers can be generated for any order system, subject to the controlled closed loop system being strictly proper.

4.2.1 Evaluation of the Mean-Square Definite Integral

Following the basic approach in [38], consider the integrand of equation 4.3 which can be expressed as the sum of two rational functions

$$\frac{e(s)e(-s)}{d(s)d(-s)} = \frac{f(s)}{d(s)} + \frac{g(s)}{d(-s)} \tag{4.4}$$

where $f(s) = \sum_{i=0}^{n-1} f_i s^i$ and $g(s) = \sum_{i=0}^{n-1} g_i s^i$ are of degree $n-1$. Now since $e(s)e(-s)$ is an even function of s it follows that $g(s) = f(-s)$. Accordingly the integrand in 4.3 becomes

$$\sigma^2 = \frac{1}{\pi j}\int_{-j\infty}^{+j\infty}\frac{f(s)}{d(s)}ds$$

This is seen to be twice the inverse Laplace transform of $f(s)/d(s)$ evaluated at $t = 0$ so from the initial-value theorem the value of the integral is

$$\sigma^2 = \frac{f_{n-1}}{d_n} \tag{4.5}$$

It can been seen that for any given system the coefficients f_{n-1} and d_n of equation 4.4 determine the variance at the output. These coefficients can be found by expansion and comparison of the coefficients as follows: From equation 4.4 and by virtue of $g(s) = f(-s)$ then we get

$$\frac{e(s)e(-s)}{d(s)d(-s)} = \frac{f(s)}{d(s)} + \frac{f(-s)}{d(-s)}$$

which can be written as

$$e(s)e(-s) = f(s)d(-s) + f(-s)d(s) \tag{4.6}$$

The left hand side of equation 4.6 can be expressed as

$$e(s)e(-s) = \sum_{i,k=0}^{n-1} (-1)^k e_i e_k s^{i+k}$$

which may be written

$$e(s)e(-s) = \sum_{m=0}^{2n-2} 2E_m s^m \tag{4.7}$$

where

$$\begin{aligned} E_m &= \frac{1}{2}\sum_{k=0}^{m}(-1)^k e_k e_{m-k} \text{ for } 0 \le m \le n-1 \\ &= \frac{1}{2}\sum_{k=m-n+1}^{n-1}(-1)^k e_k e_{m-k} \text{ for } n \le m \le 2n-2 \end{aligned}$$

Similarly, the right hand side of equation 4.6 can be expressed as

$$f(s)d(-s) = \sum_{i=0}^{n-1}\sum_{k=0}^{n}(-1)^k f_i d_k s^{i+k}$$

which may be written

$$f(s)d(-s) = \sum_{m=0}^{2n-1} Y_m s^m \tag{4.8}$$

where

$$\begin{aligned} Y_m &= \sum_{i=0}^{m}(-1)^{m-i} f_i d_{m-i} \text{ for } 0 \le m \le n-1 \\ &= \sum_{i=m-n}^{n-1}(-1)^{m-i} f_i d_{m-i} \text{ for } n \le m \le 2n-1 \end{aligned} \tag{4.9}$$

Substitution of equations 4.8 and 4.7 into equation 4.6 gives

$$\sum_{m=0}^{2n-2} E_m s^m = \sum_{m=0}^{2n-1} \frac{1+(-1)^m}{2} Y_m s^m \tag{4.10}$$

Since coefficients of odd powers are zero, equation 4.10 results in

$$E_m = Y_m, (m = 0, 2, 4, \ldots, 2n-2)$$

By virtue of equation 4.9 this results in the n equations

$$\begin{aligned} \sum_{i=0}^{m}(-1)^i f_i d_{m-i} &= E_m \text{ for } 0 \le m \le n-1 \\ \sum_{i=m-n}^{n-1}(-1)^i f_i d_{m-i} &= E_m \text{ for } n \le m \le 2n-1 \end{aligned} \tag{4.11}$$

in the n terms $(-1)^i f_i, (i = 0, 1, 2, \ldots, n-1)$ as in [38]. In matrix form equation 4.11 is

$$DF = E \tag{4.12}$$

where E is a vector of scalar coefficients readily computed from the closed loop numerator coefficients using equation 4.7 and has the form

$$E = \begin{bmatrix} E_0 \\ E_2 \\ \cdot \\ \cdot \\ \cdot \\ E_{2n-2} \end{bmatrix}$$

F is a vector of scalar unknowns of the form

$$F = \begin{bmatrix} f_0 \\ -f_1 \\ \cdot \\ \cdot \\ \cdot \\ (-1)^{n-1} f_{n-1} \end{bmatrix}$$

and D is a matrix of the closed loop denominator coefficients d, which for odd n is of the form

$$D = \begin{bmatrix} d_0 & 0 & 0 & \ldots & 0 \\ d_2 & d_1 & d_0 & \ldots & 0 \\ \vdots & & & & \vdots \\ d_{n-1} & d_{n-2} & d_{n-3} & \ldots & d_0 \\ 0 & d_n & d_{n-1} & \ldots & d_2 \\ \vdots & & & & \vdots \\ 0 & 0 & 0 & \ldots & d_{n-1} \end{bmatrix}$$

and for even n, is of the form

$$D = \begin{bmatrix} d_0 & 0 & 0 & \ldots & 0 \\ d_2 & d_1 & d_0 & \ldots & 0 \\ \vdots & & & & \vdots \\ d_n & d_{n-1} & d_{n-2} & \ldots & d_0 \\ 0 & 0 & d_n & \ldots & d_2 \\ \vdots & & & & \vdots \\ 0 & 0 & 0 & \ldots & d_{n-2} \end{bmatrix}$$

Solving the matrix equation $F = D^{-1}E$ and taking the coefficient f_{n-1} from F allows a solution for the output variance by subsequent substitution into equation 4.5.

4.2.2 Loci of Fixed Variance

In this section loci of fixed variance are generated for closed loop systems with unknown controller parameters. Using the results of the previous section we wish to relate the closed loop variance (as expressed by the ratio of closed loop coefficients of equation 4.5) to the controller parameters that will give a desired output variance. It is assumed the controller is proper and has a fixed denominator. Therefore, the closed-loop system for a two term controller takes the form

$$\frac{e(s)}{d(s)} = \frac{e(s)}{d_0(s) + k_1 d_1(s) + k_2 d_2(s)} \tag{4.13}$$

The elements of matrix E in equation 4.12 are directly computable from the closed loop numerator $e(s)$. The matrix of denominator coefficients, D is now a function of the controller K. For a two term controller D can be written

$$D(k) = D_0 + k_1 D_1 + k_2 D_2$$

Expressing the two controller parameters in polar coordinates, $k_1 = k\cos(\theta)$ and $k_2 = k\sin(\theta)$, we can write equation 4.12 as

$$\left[D_0 + k\left[\cos(\theta)D_1 + \sin(\theta)D_2\right]\right] F = E \tag{4.14}$$

Since $[\cos(\theta)D_1 + \sin(\theta)D_2]$ has singular solutions only at a small number of isolated points of θ a solution $F(k)$ for F in terms of k_1 and k_2 can be obtained for almost any given θ as a numerical inverse from [1]

$$F(k) = [kI + [\cos(\theta)D_1 + \sin(\theta)D_2]^{-1}D_0]^{-1}[\cos(\theta)D_1 + \sin(\theta)D_2]^{-1}E$$

Denoting $\bar{D} = -[\cos(\theta)D_1 + \sin(\theta)D_2]^{-1}D_0$ and $\bar{E} = [\cos(\theta)D_1 + \sin(\theta)D_2]^{-1}E$ this can be written

$$F(k) = [kI - \bar{D}(k)]^{-1}\bar{E} \tag{4.15}$$

which has the form of the matrix equation 4.12. The inverse of the characteristic matrix $[kI - \bar{D}(k)]$ [89] can then be obtained in the form

$$[kI - \bar{D}(k)]^{-1} = \frac{X(k)}{x(k)} \tag{4.16}$$

where by expansion

$$X = [k^{n-1}I_n + k^{n-2}X_1 + k^{n-3}X_3 + \ldots + k^0 X_{n-1}]$$

and

$$x(k) = k^n + x_1 k^{n-1} + \ldots + x_n$$

[1] A solution $F(k)$ for F in terms of k_1 and k_2 could alternatively be obtained by polynomial matrix inverse methods.

. X_i and x_i can be computed by Leverrier's algorithm [89]

$$x_1 = -tr(\bar{D}), \quad X_1 = \bar{D} + x_1 I_n$$

$$x_k = -\frac{1}{k} tr(\bar{D} X_{k-1}), \quad k = 2, 3, \ldots, n$$

$$X_k = \bar{D} X_{k-1} + x_k I_n, \quad k = 2, 3, \ldots, n-1$$

From equation 4.5 a solution to k for a specified constant variance σ^2 is determined from the roots of the scalar polynomial in k

$$\sigma^2 d_n(k) x(k) - f_{n-1}(k) = 0 \tag{4.17}$$

Substituting equation 4.16 into 4.15 and expanding yields

$$F(k) = \frac{1}{x(k)} [k^{n-1} I_n + k^{n-2} X_1 + k^{n-3} X_2 \ldots, + k^0 X_{n-1}] \bar{E}$$

Since the variance is determined by the highest coefficient of F (f_{n-1}), we now let ϵ be the $n \times 1$ vector containing all zeros except for the nth element which is $(-1)^{n-1}$, that is

$$\epsilon^T = \begin{bmatrix} 0 & 0 & . & . & . & (-1)^{n-1} \end{bmatrix}$$

so the scalar polynomial in k, $f_{n-1}(k)$ is obtained from the vector of rationals $F(k)$ by $f_{n-1}(k) = \epsilon^T F(k) x(k)$. Thus we obtain the coefficients of $f_{n-1}(k)$ from

$$f_{n-1}(k) = \bar{F}_0 k^0 + \bar{F}_1 k^1, \ldots, + \bar{F}_n k^{n-1} \tag{4.18}$$

where

$$\bar{F}_0 = \epsilon^T X_{n-1} \bar{E}, \quad \bar{F}_1 = \epsilon^T X_{n-2} \bar{E}, \quad \ldots \quad , \bar{F}_n = \epsilon^T I_n \bar{E}$$

Thus for any plant and two-term controller a polynomial in k of the form of equation 4.17 exists. Discretising the controller gains for $\theta \in [0; 2\pi)$ such that

$$K = k_1 + k_2 s = k \left(\cos(\theta) + s \sin(\theta) \right) \tag{4.19}$$

allows the roots of the resulting polynomial of equation 4.17 to be obtained for each θ in the polar plane for any specified variance σ^2. The roots of k can then be translated into the controller gains k_1 and k_2 and subsequently mapped into the chosen parameter plane. The following subsections describe the formation of the denominator coefficient matrix D for PI and PD controller structures.

PI Controller

The matrices D_0, D_1 and D_2 for a proportional-integral controller, $K = \frac{k_p s + k_i}{s}$ are readily computed for a closed loop system defined by equation 4.1. For a PI controller the closed loop transfer function is given by

$$\frac{\hat{y}}{\hat{w}}(s) = \frac{G_c}{1 + \frac{k_p s + k_i}{s} G_b}$$

For an ARMAX structure this simplifies to the rational representation

$$\frac{\hat{y}}{\hat{w}}(s) = \frac{sc(s)}{sa(s) + (k_p s + k_i)b(s)} = \frac{e(s)}{d(s)}$$

Let $k_1 = k_p$ and $k_2 = k_i$; matrix D can therefore be written as

$$D = k_1 D_1 + k_2 D_2 + D_0$$

where for odd powers of n

$$D_1 = \begin{bmatrix} 0 & 0 & 0 & \dots & 0 \\ b_1 & b_0 & 0 & \dots & 0 \\ \vdots & & & & \vdots \\ b_{n-2} & b_{n-3} & b_{n-4} & \dots & 0 \\ 0 & b_{n-1} & b_{n-2} & \dots & b_1 \\ \vdots & & & & \vdots \\ 0 & 0 & 0 & \dots & b_{n-2} \end{bmatrix}$$

$$D_2 = \begin{bmatrix} b_0 & 0 & 0 & \dots & 0 \\ b_2 & b_1 & b_0 & \dots & 0 \\ \vdots & & & & \vdots \\ b_{n-1} & b_{n-2} & b_{n-3} & \dots & b_0 \\ 0 & b_n & b_{n-1} & \dots & b_2 \\ \vdots & & & & \vdots \\ 0 & 0 & 0 & \dots & b_{n-1} \end{bmatrix}$$

$$D_0 = \begin{bmatrix} 0 & 0 & 0 & \dots & 0 \\ a_1 & a_0 & 0 & \dots & 0 \\ \vdots & & & & \vdots \\ a_{n-2} & a_{n-3} & a_{n-4} & \dots & 0 \\ 0 & a_{n-1} & a_{n-2} & \dots & a_1 \\ \vdots & & & & \vdots \\ 0 & 0 & 0 & \dots & a_{n-2} \end{bmatrix}$$

and for even powers of n the matrices are given as

$$D_1 = \begin{bmatrix} 0 & 0 & 0 & \dots & 0 \\ b_1 & b_0 & 0 & \dots & 0 \\ \vdots & & & & \vdots \\ b_{n-1} & b_{n-2} & b_{n-3} & \dots & b_0 \\ 0 & 0 & b_{n-1} & \dots & b_2 \\ \vdots & & & & \vdots \\ 0 & 0 & 0 & \dots & b_{n-2} \end{bmatrix}$$

$$D_2 = \begin{bmatrix} b_0 & 0 & 0 & \dots & 0 \\ b_2 & b_1 & b_0 & \dots & 0 \\ \vdots & & & & \vdots \\ b_n & b_{n-1} & b_{n-2} & \dots & b_1 \\ 0 & 0 & b_n & \dots & b_3 \\ \vdots & & & & \vdots \\ 0 & 0 & 0 & \dots & b_{n-1} \end{bmatrix}$$

$$D_0 = \begin{bmatrix} 0 & 0 & 0 & \dots & 0 \\ a_1 & a_0 & 0 & \dots & 0 \\ \vdots & & & & \vdots \\ a_{n-1} & a_{n-2} & a_{n-3} & \dots & a_0 \\ 0 & 0 & a_{n-1} & \dots & a_2 \\ \vdots & & & & \vdots \\ 0 & 0 & 0 & \dots & a_{n-2} \end{bmatrix}$$

PD Controller

Constant variance loci determining the gains of a proportional-derivative controller, $K = k_d s + k_p$ for an ARMAX structure are governed by the closed loop transfer function

$$\frac{\hat{y}}{\hat{w}}(s) = \frac{c(s)}{a(s) + (k_d s + k_p) b(s)} = \frac{e(s)}{d(s)}$$

With $k_1 = k_d$ and $k_2 = k_p$ in equation 4.14, matrix D can therefore be written as

$$D = k_1 D_1 + k_2 D_2 + D_0$$

where for odd powers of n

$$D_1 = \begin{bmatrix} 0 & 0 & 0 & \dots & 0 \\ b_1 & b_0 & 0 & \dots & 0 \\ \vdots & & & & \vdots \\ b_{n-2} & b_{n-3} & b_{n-4} & \dots & 0 \\ 0 & b_{n-1} & b_{n-2} & \dots & b_1 \\ \vdots & & & & \vdots \\ 0 & 0 & 0 & \dots & b_{n-2} \end{bmatrix}$$

$$D_2 = \begin{bmatrix} b_0 & 0 & 0 & \dots & 0 \\ b_2 & b_1 & bB_0 & \dots & 0 \\ \vdots & & & & \vdots \\ b_{n-1} & b_{n-2} & b_{n-3} & \dots & b_0 \\ 0 & b_n & b_{n-1} & \dots & b_2 \\ \vdots & & & & \vdots \\ 0 & 0 & 0 & \dots & b_{n-1} \end{bmatrix}$$

$$D_0 = \begin{bmatrix} a_0 & 0 & 0 & \dots & 0 \\ a_2 & a_1 & a_0 & \dots & 0 \\ \vdots & & & & \vdots \\ a_{n-1} & a_{n-2} & a_{n-3} & \dots & a_0 \\ 0 & a_n & a_{n-1} & \dots & a_2 \\ \vdots & & & & \vdots \\ 0 & 0 & 0 & \dots & a_{n-1} \end{bmatrix}$$

Similarly for even powers of n

$$D_1 = \begin{bmatrix} 0 & 0 & 0 & \dots & 0 \\ b_1 & b_0 & 0 & \dots & 0 \\ \vdots & & & & \vdots \\ b_{n-1} & b_{n-2} & b_{n-3} & \dots & b_0 \\ 0 & 0 & b_{n-1} & \dots & b_2 \\ \vdots & & & & \vdots \\ 0 & 0 & 0 & \dots & b_{n-2} \end{bmatrix}$$

$$D_2 = \begin{bmatrix} b_0 & 0 & 0 & \dots & 0 \\ b_2 & b_1 & b_0 & \dots & 0 \\ \vdots & & & & \vdots \\ b_n & b_{n-1} & b_{n-2} & \dots & b_1 \\ 0 & 0 & b_n & \dots & b_3 \\ \vdots & & & & \vdots \\ 0 & 0 & 0 & \dots & b_{n-1} \end{bmatrix}$$

$$D_0 = \begin{bmatrix} a_0 & 0 & 0 & \dots & 0 \\ a_2 & a_1 & a_0 & \dots & 0 \\ \vdots & & & & \vdots \\ a_n & a_{n-1} & a_{n-2} & \dots & a_1 \\ 0 & 0 & a_n & \dots & a_3 \\ \vdots & & & & \vdots \\ 0 & 0 & 0 & \dots & a_{n-1} \end{bmatrix}$$

4.2.3 Computational algorithm

The algorithm for generating the PS loci can be summerised as follows:

1. Determine appropriate controller structure such as PI and PD.
2. Choose a desired closed-loop output variance σ^2.
3. Express the closed-loop system with unknown controller parameters in the form $\frac{e(s)}{D_0+k_1D_1+k_2D_2}$.
4. Generate the vector of numerator coefficients E using equations 4.7 and 4.12.

5. Generate the denominator based coefficient matrices D_0, D_1 and D_2 as defined for the particular controller structure.
6. Choose a value of θ in the polar plane.
7. Compute $\bar{E}$ and $\bar{D}$ in the form of equation 4.15 using the results from steps (3) and (4).
8. Compute the inverse characteristic matrix of equation 4.15 using Leverrier's algorithm. If the solution is singular discard the result and return to step (5).
9. Compute the coefficient f_{n-1} from equation 4.18.
10. For the chosen output variance σ^2 calculate the roots of the polynomial in equation 4.17.
11. Map the roots of the previous step into controller gains as per equation 4.19.
12. Return to step (5) and repeat for several discrete values of $\theta \in [0; 2\pi)$

4.2.4 Idle Speed Controller Design Example

The idle speed problem is that of regulating the engine speed about a set-point despite torque loads applied to the engine. This requires a degree of robustness since load and speed operating conditions can vary considerably. Furthermore environmental effects such as temperature and humidity can add a large degree of model uncertainty.

The following example for idle speed control in a gasoline IC engine demonstrates the benefit of constraining the output variance. Robustness, tracking and disturbance rejection are also necessary and therefore a non-conservative multi-objective design is demonstrated. The output variance for the idle speed problem is significant due, in part to crank pulsing and also the chaotic nature of combustion. Accordingly, the main objective for the idle speed problem is to satisfactorily reject disturbances, however in order to obtain good driver perception of the engine smoothness and a low noise vehicle-harshness (NVH) rating, it is advantageous to also consider the output variance.

A time delay of several engine cycles exists between control input and response for the idle speed problem. The proposed technique cannot be used directly for systems with pure time delays, however it is common practice to approximate time delays with Padè approximations. For simplicity of demonstrating the control technique the time delay was neglected by shifting the input data prior to identification. The resulting continuous ARMAX model of an engine at idle without time delay was obtained as

$$G_b = \frac{-541s + 2.098 \times 10^4}{s^2 + 3.571s + 7.64}$$

with the noise channel dynamics

$$G_c = \frac{18.5s + 132.2}{s^2 + 3.571s + 7.64}$$

For good tracking and disturbance rejection a PI controller is a suitable structure, since the integral action ensures zero steady-state error. This can also be used to track various reference set-points such as fast idle during start-up, where the idle speed is elevated to ensure the engine remains smooth and to accelerate the time to light-off (heating) of the three way catalytic converter. The closed loop transfer function is order 3 ($n = 3$), and thus the associated D matrices given in section 4.2.2 are

$$D_1 = \begin{bmatrix} 0 & 0 & 0 \\ b_1 & b_0 & 0 \\ 0 & 0 & b_1 \end{bmatrix}, \quad D_2 = \begin{bmatrix} b_0 & 0 & 0 \\ 0 & b_1 & b_0 \\ 0 & 0 & 0 \end{bmatrix}, \quad D_0 = \begin{bmatrix} 0 & 0 & 0 \\ a_1 & a_0 & 0 \\ 0 & a_2 & a_1 \end{bmatrix}$$

Matrix E of equation 4.2.1 is readily obtained from the numerator coefficients using equation 4.11 to give

$$E = \begin{bmatrix} 0 \\ -c_0^2 \\ c_1^2 \end{bmatrix}$$

For this design a variance loci of 240 rpm^2 were used. This corresponds to two-thirds of the open loop variance (367 rpm^2) and was used to produce a significant reduction in output variance, without adding excessive constraints on the system in order to satisfactorily meet the disturbance rejection criteria.

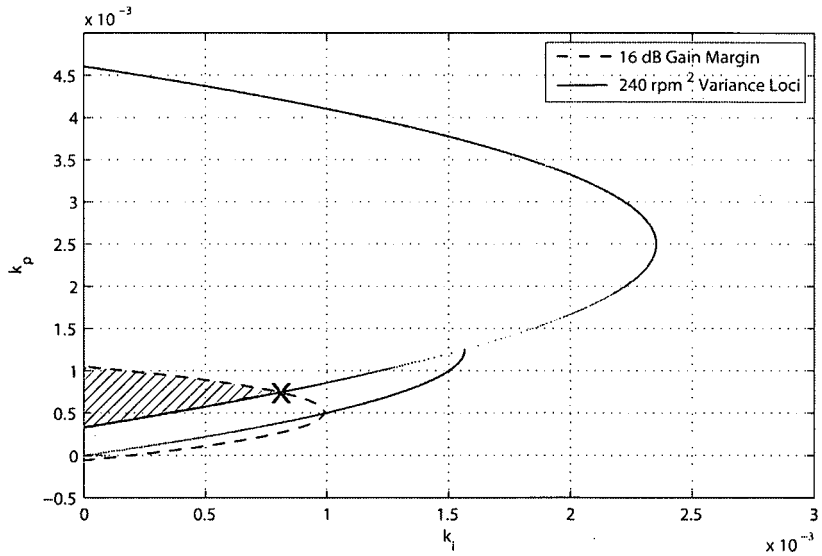

Figure 4.2: k_i, k_p parameter plane with 16 dB GM and 240 rpm^2 variance loci

Robustness was introduced into the design by superimposing a gain margin locus. It is a particular merit of the PS method that it allows several, often conflicting requirements

to be mapped onto the same plane without unnecessary conservatism. Superimposing the specifications reveals to the designer which region(s) meet all the constraints simultaneously. To ensure sufficient robustness a gain margin (GM) of 16 dB was selected; a typical level used for the idle speed problem. Figure 4.2 shows the resulting parameter plane, where the admissible region meeting both specifications is hatched. In order to have sufficient tracking the maximum permitted integral gain was selected from the admissible region as indicated by the marker.

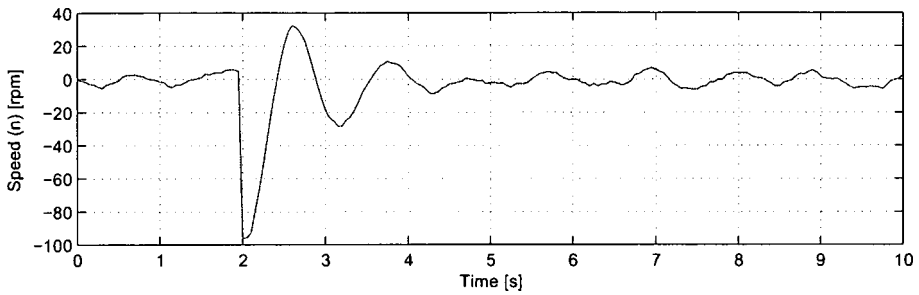

Figure 4.3: Time response of the speed to a disturbance of 100 rpm at $t = 2s$

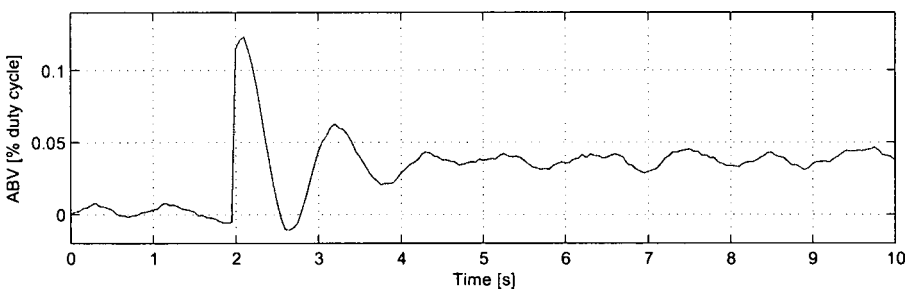

Figure 4.4: ABV control effort response to step disturbance at $t = 2s$

A typical step response of the simulated closed loop system with noise dynamics is presented in figure 4.3. The system shows a 30% overshoot and 5% settling time in under 3 seconds. The control action in response to the coloured noise and step disturbance is displayed in figure 4.4

Bode and Nyquist plots of the controlled open loop system are displayed in figure 4.5 and figure 4.6 respectively.

4.3 Loci of Constrained-Variance - Discrete Systems

The closed loop system of figure 4.7 is assumed to be determined by a proper rational plant transfer function $G_b(z) = \frac{b(z)}{a(z)}$ and rational noise transfer function $G_c(z) = \frac{c(z)}{a(z)}$, where $a(z) = \sum_{k=0}^{m} a_k z^k$ is a common denominator polynomial of degree m and the plant and noise

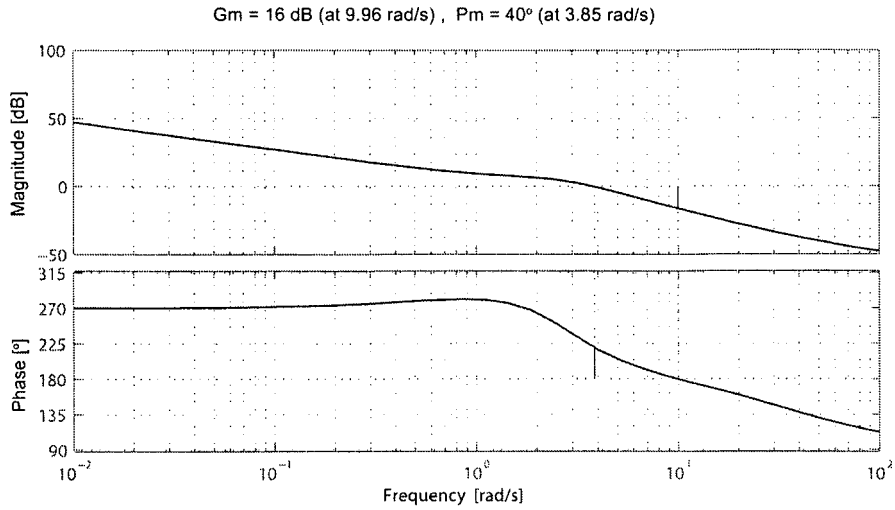

Figure 4.5: Bode plot indicating the margins for controlled open loop idle speed system

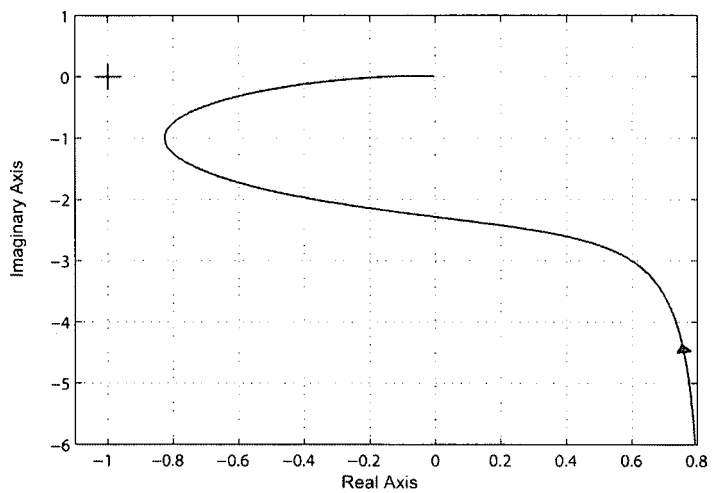

Figure 4.6: Nyquist plot demonstrating the robustness of idle speed system

numerator polynomials are each taken to be of degree $\leq m$ and m respectively given by $b(z) = \sum_{k=0}^{m} b_k z^k$ and $c(z) = \sum_{k=0}^{m} c_k z^k$. It is assumed that there are no unstable pole-zero cancellations. For the assumed PID or PI controller transfer function $K(z)$ the closed loop transfer function from the disturbance w to the output error y_e with z-transforms $\hat{w}$ and $\hat{y}_e$ is then rational and given by

$$\frac{\hat{y}_e}{\hat{w}}(z) = G(z) = \frac{G_c(z)}{1 + K(z)G_b(z)} = \frac{e(z)}{d(z)} \tag{4.20}$$

where $e(z) = \sum_{k=0}^{n} e_k z^k$ and $d(z) = \sum_{k=0}^{n} d_k z^k$ are the associated closed loop numerator and denominator polynomials.

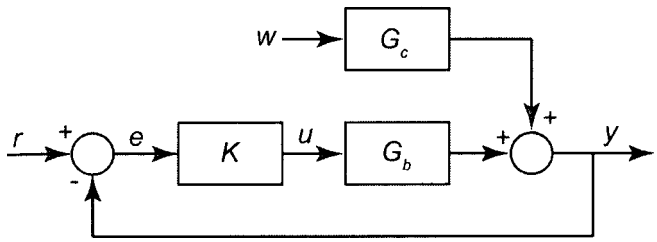

Figure 4.7: Closed loop system with coloured noise disturbance

The mean square value of a system $\phi_{rr}(nT)$ expressed as a function of the input white noise zero mean process power Φ_{rr} is [67]

$$\phi_{rr}(nT) = \frac{1}{2\pi j} \oint_{c_1} \Phi_{rr}(z) z^{n-1} dz \tag{4.21}$$

where it is assumed the system is stable and c_1 denotes a contour on the unit circle. Defining the variance per unit white noise $\sigma^2 = \frac{\phi_{rr}}{\Phi_{rr}}$ and evaluating equation 4.21 at $n = 0$ gives

$$\sigma^2 = \frac{1}{2\pi j} \oint_{c_1} |G(z)|^2 \frac{dz}{z} \tag{4.22}$$

Substituting (4.20) into (4.22) gives

$$\sigma^2 = \frac{1}{2\pi j} \oint_{c_1} \frac{e(z)e(z^{-1})}{d(z)d(z^{-1})} \frac{dz}{z} \tag{4.23}$$

The integrand can be written as the sum of two fractions

$$\frac{e(z)e(z^{-1})}{d(z)d(z^{-1})} = \frac{f(z)}{d(z)} + \frac{g(z)}{d(z^{-1})} \tag{4.24}$$

where $f(z) = \sum_{i=0}^{n} f_i z^i$ and $g(z) = \sum_{i=0}^{n} g_i z^i$ are of degree n. Since $|G(z)|^2 = |G(z^{-1})|^2 = G(z)G(z^{-1})$ it follows that the residues of any pole of $G(z)G(z^{-1})$ at z_i are the residues of its corresponding pole at z_i^{-1} and therefore that $g(z) = f(z^{-1})$. The integral of (4.23) then becomes

$$\sigma^2 = \frac{1}{2\pi j} \oint_{c_1} \frac{f(z)}{d(z)} + \frac{f(z^{-1})}{d(z^{-1})} \frac{dz}{z}$$

and thus

$$\sigma^2 = \frac{1}{\pi j} \oint_{c_1} \frac{f(z)}{d(z)} \frac{dz}{z} \tag{4.25}$$

Now any z-transform pair (x, X) is subject to the the inverse z-transform relation

$$x[n] = \frac{1}{2\pi j} \oint_{c_1} X(z) z^{n-1} dz \;\; ; \;\; n = 0, 1, \ldots \tag{4.26}$$

Setting $X(z) = \frac{2f(z)}{d(z)}$, then equation 4.26 for $n = 0$ gives $x[0] = \sigma^2$. From the initial value theorem,

$$x[0] = \lim_{z \to \infty} X(z)$$

and we thereby obtain

$$\sigma^2 = \frac{2f_n}{d_n} \tag{4.27}$$

and to determine the variance of a given system it is necessary to compute the coefficients of f_n and d_n. From equation 4.24 we get

$$f(z)d(-z) + f(-z)d(z) = e(z)e(-z) \tag{4.28}$$

The left hand side of equation 4.28 can be obtained from

$$\begin{aligned} f(z)d(z^{-1}) + f(z^{-1})d(z) &= \sum_{i=0}^{n}\sum_{k=0}^{n} f_i d_k z^{i-k} \\ &+ \sum_{i=0}^{n}\sum_{k=0}^{n} f_i d_k z^{k-i} \end{aligned} \tag{4.29}$$

similarly the right hand side of equation 4.28 is given by

$$e(z)e(z^{-1}) = \sum_{i=0}^{n}\sum_{k=0}^{n} e_i e_k z^{i-k} \tag{4.30}$$

Expansion of equations 4.29 and 4.30 and comparison of the coefficients of the different powers of z results in $n+1$ simultaneous equations.

Writing equation 4.28 in matrix form now readily gives the coefficients f_i by the solution of $F = [f_0, f_1, \ldots, f_n]^T$ in

$$DF = E \tag{4.31}$$

where C is obtained from

$$E = \begin{bmatrix} E_0 & E_1 & \ldots & E_n \end{bmatrix}^T \;\; ; \;\; E_k = \sum_{i=0}^{n-k} e_i e_{i+k} \tag{4.32}$$

and the D takes the form

$$D = \begin{bmatrix} d_0 & d_1 & d_2 & \ldots & d_n \\ d_1 & d_2 & \ldots & d_n & 0 \\ d_2 & \ldots & d_n & 0 & 0 \\ \vdots & & & & \vdots \\ d_n & 0 & 0 & 0 & 0 \end{bmatrix} + \begin{bmatrix} d_0 & d_1 & d_2 & \ldots & d_n \\ 0 & d_0 & d_1 & \ldots & d_{n-1} \\ 0 & 0 & d_0 & \ldots & d_{n-2} \\ \vdots & & & & \vdots \\ 0 & 0 & 0 & 0 & d_0 \end{bmatrix} \tag{4.33}$$

It follows that the output variance can be directly computed from the coefficients of the system.

4.4 Loci of Fixed Variance

For controller design and the associated parameter plane mappings consider the two controller-numerator parameters which will result in the closed-loop form

$$\frac{e(z)}{d(z)} = \frac{e(z)}{d_0(z) + k_1 d_1(z) + k_2 d_2(z)} \tag{4.34}$$

The parameters of such a controller are required to result in an output variance constrained at a pre-determined magnitude using the results of the previous section.

The numerator coefficients matrix C of equation 4.32 for the system of 4.34 is independent of parameters k_1, k_2 and can therefore readily be determined using the closed loop numerator coefficients. The matrix of closed-loop denominator coefficients D of equation 4.33 for the system of 4.34, on the other hand, is a function of the numerator parameters k_1, k_2 of the controller. For the two term controller D can be written

$$D = D_0 + k_1 D_1 + k_2 D_2 \tag{4.35}$$

Expressing the two controller parameters in polar coordinates, $k_1 = k\cos(\theta)$ and $k_2 = k\sin(\theta)$, we can write equation 4.31 as

$$\left[k\left[\cos(\theta)D_1 + \sin(\theta)D_2\right] + D_0\right]F = E$$

Since $[\cos(\theta)D_1 + \sin(\theta)D_2]$ at worst has singular solutions only at isolated points of θ a solution $F(k)$ for F in terms of k_1 and k_2 can be obtained for almost any given θ as a numerical inverse from[2]

$$F(k) = [kI + [\cos(\theta)D_1 + \sin(\theta)D_2]^{-1}D_0]^{-1}[\cos(\theta)D_1 + \sin(\theta)D_2]^{-1}E$$

Denoting $\bar{D} = -[\cos(\theta)D_1 + \sin(\theta)D_2]^{-1}D_0$ and $\bar{E} = [\cos(\theta)D_1 + \sin(\theta)D_2]^{-1}E$ this can be written

$$F(k) = [kI - \bar{D}]^{-1}\bar{E}$$

The inverse of the characteristic matrix $[kI - \bar{D}]$ can then be obtained in the form

$$[kI - \bar{D}]^{-1} = \frac{X(k)}{x(k)}$$

which for X of dimension $n \times n$, can by expansion be written as

$$\frac{X(k)}{x(k)} = \frac{1}{x(k)}[k^{n-1}I_n + k^{n-2}X_1 + k^{n-3}X_3 \ldots, +k^0 X_{n-1}]$$

[2] A solution $F(k)$ for F in terms of k_1 and k_2 could alternatively be obtained by polynomial matrix inverse methods.

where $x(k)$ is $k^n + x_1 k^{n-1} + \ldots + x_n$ and X_i and x_i can be computed by Leverrier's algorithm [89]

$$x_1 = -tr(\bar{D}), \quad X_1 = \bar{D} + x_1 I_n$$
$$x_k = -\frac{1}{k} tr(\bar{D} X_{k-1}), \quad k = 2, 3, \ldots, n$$
$$X_k = \bar{D} X_{k-1} + x_k I_n, \quad k = 2, 3, \ldots, n-1$$

From equation 4.27, the unknown controller parameter values at boundaries of constant variance σ^2, are determined by the roots of the polynomial equation in k

$$\tfrac{1}{2}\sigma^2 d_n(k) x(k) - f_n(k) = 0 \tag{4.36}$$

Given

$$F(k) = \frac{1}{x(k)} \quad [k^{n-1} I_n + k^{n-2} X_1 + \ldots + k^0 X_{n-1}]\bar{E}$$

let ϵ be a $n \times 1$ vector containing all zeros except for the n^{th} element which is 1, that is

$$\epsilon = \begin{bmatrix} 0 & 0 & \ldots & 1 \end{bmatrix}^T$$

then the scalar polynomial in k, $f_n(k)$, is obtained from the vector of rationals $F(k)$ by $f_n(k) = \epsilon^T F(k) x(k)$.

Thus the coefficients of $f_n(k) = \bar{F}_0 k^0 + \bar{F}_1 k^1 + \ldots + \bar{F}_n k^{n-1}$ are obtained from

$$\bar{F}_0 = \epsilon^T X_{n-1} \bar{E}, \quad \bar{F}_1 = \epsilon^T X_{n-2} \bar{E}, \quad \ldots \quad \bar{F}_n = \epsilon^T I_n \bar{E}$$

It follows that for any plant and two-term controller a polynomial in k of the form of equation 4.36 exists. Discretising the controller gains for $\theta \in [0; 2\pi)$ such that

$$K = k_1 + k_2 z = k\left(\cos(\theta) + z\sin(\theta)\right) \tag{4.37}$$

allows the roots of the resulting polynomial of equation 4.36 to be obtained for each θ for any specified variance σ^2. The roots of k can then be translated into the controller gains k_1 and k_2 and subsequently mapped into the chosen parameter plane.

4.4.1 Closed-Loop Structure

We will consider parameter plane mappings for two parameters at a time in the form two term controllers. With one fixed gain k_0 and two unknown gains k_1, k_2 in the controller numerator $p(z) = k_0 p_0(z) + k_1 p_1(z) + k_2 p_2(z)$, in equation 4.34 takes the form

$$\frac{e(z)}{d(z)} = \frac{q(z)c(z)}{q(z)a(z) + k_0 p_0(z)b(z) + k_1 p_1(z)b(z) + k_2 p_2(z)b(z)} \tag{4.38}$$

so that $d_0(z) = q(z)a(z) + k_0 p_0(z)b(z)$, $d_1(z) = p_1(z)b(z)$ and $d_2(z) = p_2(z)b(z)$.

4.4.2 PI Controller Gains

For a PI controller transfer function

$$K(z) = k_p + \frac{k_i z}{z-1} = \frac{k_p(z-1) + k_i z}{z-1} = \frac{(k_p + k_i)z - k_p}{z-1}$$

the closed loop transfer function given in equation 4.20 can be expressed in the proper rational form of equation 4.34 by setting

$$q(z) = z - 1$$

$$p(z) = (k_p + k_i)z - k_p$$

To map the PI gains $(k_1, k_2) = (k_p, k_i)$

$$p_0(z) = 0; p_1(z) = z - 1; p_2(z) = z$$

In this case

$$\begin{aligned} e(z) &= -c_0 + (c_0 - c_1)z + (c_1 - c_2)z^2 + \ldots + c_m z^m \\ d_0(z) &= -a_0 + (a_0 - a_1)z + (a_1 - a_2)z^2 + \ldots + a_m z^m \\ d_1(z) &= -b_0 + (b_0 - b_1)z + (b_1 - b_2)z^2 + \ldots + b_m z^m \\ d_2(z) &= b_0 + b_1 z + b_2 z^2 + \ldots + b_m z^{m-1} \end{aligned}$$

and therefore the $m+2 \times 1$ matrix C, and $m+2 \times m+2$ matrices D_0, D_1 and D_2 of equation 4.35 can also be readily generated for this case by means of equations 4.39, 4.40 and 4.41. The matrix of numerator parameters $A = [f_0, f_1, \ldots, f_n]^T \;;\; n = m+1$ may thus be determined by solution of equation 4.31. The roots of k follow from equation 4.36 and can be translated into controller coefficients k_1 and k_2 from equation 4.37.

$$D_0 = \begin{bmatrix} -a_0 & a_0 - a_1 & a_1 - a_2 & \ldots & a_m \\ 0 & -a_0 & a_0 - a_1 & \ldots & a_1 - a_m \\ 0 & 0 & -a_0 & \ldots & a_0 - a_{m-1} \\ \vdots & \vdots & \vdots & \ddots & \vdots \\ 0 & 0 & 0 & \ldots & -a_0 \end{bmatrix} + \begin{bmatrix} -a_0 & a_0 - a_1 & a_1 - a_2 & \ldots & a_m \\ \vdots & \vdots & \vdots & \ddots & \vdots \\ a_{m-2} - a_{m-1} & a_{m-1} - a_m & a_m & \ldots & 0 \\ a_{m-1} - a_m & a_m & 0 & \ldots & 0 \\ a_m & 0 & 0 & \ldots & 0 \end{bmatrix} \quad (4.39)$$

$$D_1 = \begin{bmatrix} -b_0 & b_0 - b_1 & b_1 - b_2 & \dots & b_m \\ 0 & -b_0 & b_0 - b_1 & \dots & b_1 - b_m \\ 0 & 0 & -b_0 & \dots & b_0 - b_{m-1} \\ \vdots & \vdots & \vdots & \ddots & \vdots \\ 0 & 0 & 0 & \dots & -b_0 \end{bmatrix} + \begin{bmatrix} -b_0 & b_0 - b_1 & b_1 - b_2 & \dots & b_m \\ \vdots & \vdots & \vdots & \ddots & \vdots \\ b_{m-2} - b_{m-1} & b_{m-1} - b_m & b_m & \dots & 0 \\ b_{m-1} - b_m & b_m & 0 & \dots & 0 \\ b_m & 0 & 0 & \dots & 0 \end{bmatrix} \tag{4.40}$$

$$D_2 = \begin{bmatrix} b_0 & b_1 & b_2 & \dots & b_m & 0 \\ 0 & b_0 & b_1 & \dots & b_{m-1} & b_m \\ 0 & 0 & b_0 & \dots & b_{m-2} & b_{m-1} \\ \vdots & \vdots & \vdots & \ddots & \vdots & \vdots \\ 0 & 0 & 0 & \dots & b_0 & b_1 \\ 0 & 0 & \dots & 0 & 0 & b_0 \end{bmatrix} + \begin{bmatrix} b_0 & b_1 & \dots & b_m & 0 \\ \vdots & \vdots & \ddots & \vdots & \vdots \\ b_{m-1} & b_m & \dots & 0 & 0 \\ b_m & 0 & \dots & 0 & 0 \\ 0 & 0 & \dots & 0 & 0 \end{bmatrix} \tag{4.41}$$

4.4.3 PID Controller Gains

For a PID controller transfer function

$$\begin{aligned} K(z) &= k_p + \frac{k_i z}{z-1} + \frac{k_d(z-1)}{T_d z} = \frac{k_d/T_d(z-1)^2 + k_p z(z-1) + k_i z(z-1)}{z(z-1)} \\ &= \frac{(k_d/T_d + k_p + k_i)z^2 - (k_p + 2k_d/T_d)z + k_d/T_d}{z(z-1)} \end{aligned}$$

the closed loop transfer function given in equation 4.20 can be expressed in the proper rational form of equation 4.34 by setting

$$q(z) = z(z-1)$$

$$p(z) = (k_d/T_d + k_p + k_i)z^2 - (k_p + 2k_d/T_d)z + k_d/T_d$$

$$p(z) = k_d/T_d(z^2 - 2z + 1) + k_p z(z-1) + k_i z^2$$

Mapping PD parameters of PID

To map the PD gains $(k_1, k_2) = (k_d, k_p)$ with fixed k_i

$$p_0(z) = k_i z^2; p_1(z) = (z^2 - 2z + 1); p_2(z) = z(z-1)$$

In this PD case

$$\begin{aligned}
e(z) &= 0 - c_0 z + (c_0 - c_1)z^2 + (c_1 - c_2)z^3 + \ldots + c_n z^{m+1} \\
d_0(z) &= 0 - a_0 z + (a_0 - a_1)z^2 + (a_1 - a_2)z^3 + \ldots + a_n z^{m+1} \\
&+ k_i(-b_0 z^2 + (b_0 - b_1)z^3 + (b_1 - b_2)z^4 + \ldots + b_n z^{m+2}) \\
d_1(z) &= b_0 z^2 + b_1 z^3 + b_2 z^4 + \ldots + b_n z^{m+2} + 0 - 2b_0 z - 2b_1 z^2 - 2b_2 z^3 + \ldots - 2b_n z^{m+1} \\
&+ b_0 + b_1 z + b_2 z^2 + \ldots + b_n z^m \\
d_2(z) &= +0 - b_0 z + (b_0 - b_1)z^2 + (b_1 - b_2)z^3 + \ldots + b_n z^{m+1}
\end{aligned}$$

Now for any $m+1 \times 1$ matrix of parameters $b = [b_0, b_1, \ldots, b_m]^T$ denote the $m+3 \times m+3$ matrices $D[b]_2$, $D[b]_1$ and $D[b]_0$ by

$$D[b]_0 = \begin{bmatrix} b_0 & b_1 & b_2 & \ldots & b_m & 0 & 0 \\ 0 & b_0 & b_1 & \ldots & b_{m-1} & b_m & 0 \\ 0 & 0 & b_0 & \ldots & b_{m-2} & b_{m-1} & b_m \\ \vdots & \vdots & \vdots & \ddots & \vdots & \vdots & \vdots \\ 0 & 0 & 0 & \ldots & b_0 & b_1 & b_2 \\ 0 & 0 & 0 & \ldots & 0 & b_0 & b_1 \\ 0 & 0 & 0 & \ldots & 0 & 0 & b_0 \end{bmatrix} + \begin{bmatrix} b_0 & b_1 & \ldots & b_m & 0 & 0 \\ \vdots & \vdots & \ddots & \vdots & \vdots & \vdots \\ b_{m-1} & b_m & \ldots & 0 & 0 & 0 \\ b_m & 0 & \ldots & 0 & 0 & 0 \\ 0 & 0 & \ldots & 0 & 0 & 0 \\ 0 & 0 & \ldots & 0 & 0 & 0 \end{bmatrix}$$

$$D[b]_1 = \begin{bmatrix} 0 & b_0 & b_1 & b_2 & \ldots & b_m \\ 0 & 0 & b_0 & b_1 & \ldots & b_{m-1} \\ 0 & 0 & 0 & b_0 & \ldots & b_{m-2} \\ \vdots & \vdots & \vdots & \vdots & \ddots & \vdots \\ 0 & 0 & 0 & 0 & \ldots & b_0 \\ 0 & 0 & 0 & 0 & \ldots & 0 \end{bmatrix} + \begin{bmatrix} 0 & b_0 & b_1 & \ldots & b_m & 0 \\ \vdots & \vdots & \vdots & \ddots & \vdots & \vdots \\ b_{m-2} & b_{m-1} & b_m & \ldots & 0 & 0 \\ b_{m-1} & b_m & 0 & \ldots & 0 & 0 \\ b_m & 0 & 0 & \ldots & 0 & 0 \\ 0 & 0 & 0 & \ldots & 0 & 0 \end{bmatrix}$$

$$D[b]_2 = \begin{bmatrix} 0 & 0 & b_0 & b_1 & b_2 & \ldots & b_m \\ 0 & 0 & 0 & b_0 & b_1 & \ldots & b_{m-1} \\ 0 & 0 & 0 & 0 & b_0 & \ldots & b_{m-2} \\ \vdots & \vdots & \vdots & \vdots & \vdots & \ddots & \vdots \\ 0 & 0 & 0 & 0 & 0 & \ldots & b_0 \\ 0 & 0 & 0 & 0 & 0 & \ldots & 0 \\ 0 & 0 & 0 & 0 & 0 & \ldots & 0 \end{bmatrix} + \begin{bmatrix} 0 & 0 & b_0 & b_1 & \ldots & b_m \\ \vdots & \vdots & \vdots & \vdots & \ddots & \vdots \\ b_{m-2} & b_{m-2} & b_{m-1} & b_m & \ldots & 0 \\ b_{m-2} & b_{m-1} & b_m & 0 & \ldots & 0 \\ b_{m-1} & b_m & 0 & 0 & \ldots & 0 \\ b_m & 0 & 0 & 0 & \ldots & 0 \end{bmatrix}$$

For $m+1 \times 1$ matrix of parameters $a = [a_0, a_1, \ldots, a_m]^T$ define $m+3 \times m+3$ matrices $D[a]_2$, $D[a]_1$ and $D[a]_0$ in a similar way, and define similar matrices $D[c]_2$, $D[c]_1$ and $D[c]_0$ for the $m+1 \times 1$ matrix of parameters $c = [c_0, c_1, \ldots, c_m]^T$.

Then for the PD mapping we have $D = D_0 + k_1 D_1 + k_2 D_2$ where $D_0 = D[a]_2 - D[a]_1 + k_i D[b]_2$, $D_1 = D[b]_2 - 2D[b]_1 + D[b]_0$ and $D_2 = D[b]_2 - D[b]_1$

With the matrices C, D_0, D_1 and D_2 thus generated, the matrix of numerator parameters $A = [f_0, f_1, \ldots, f_n]^T$ can be determined by solution of equation 4.31. The roots of k follow from equation 4.36 which can be translated into controller coefficients k_1 and k_2 from equation 4.37.

Mapping PI parameters of PID

To map the PI gains $(k_1, k_2) = (k_p, k_i)$ with fixed k_d

$$p_0(z) = \frac{k_d}{T_d}(z^2 - 2z + 1); p_1(z) = z(z-1); p_2(z) = z^2$$

In this PI case

$$\begin{aligned}
e(z) &= 0 - c_0 z + (c_0 - c_1)z^2 + (c_1 - c_2)z^3 + \ldots + c_n z^{m+1} \\
d_0(z) &= 0 - a_0 z + (a_0 - a_1)z^2 + (a_1 - a_2)z^3 + \ldots + a_n z^{m+1} \\
&+ k_d/T_d(b_0 z^2 + b_1 z^3 + b_2 z^4 + \ldots + b_n z^{m+2} \\
&+ 0 - 2b_0 z - 2b_1 z^2 - 2b_2 z^3 + \ldots - 2b_n z^{m+1} \\
&+ b_0 + b_1 z + b_2 z^2 + \ldots + b_n z^m) \\
d_1(z) &= 0 - b_0 z + (b_0 - b_1)z^2 + (b_1 - b_2)z^3 + \ldots + b_n z^{m+1} \\
d_2(z) &= 0 + 0z + b_0 z^2 + b_1 z^3 + \ldots + b_n z^{m+2}
\end{aligned}$$

Then for the PI mapping we have $D = D_0 + k_1 D_1 + k_2 D_2$ where $D_0 = D[a]_2 - D[a]_1 + k_d/T_d(D[b]_2 - 2D[b]_1 + D[b]_0)$, $D_1 = D[b]_2 - D[b]_1$ and $D_2 = D[b]_2$.

The matrix of numerator parameters $F = [f_0, f_1, \ldots, f_n]^T$ may thus again be determined by solution of equation 4.31. The roots of k follow from equation 4.36 and can again be translated into controller coefficients k_1 and k_2 from equation 4.37.

4.4.4 Design Example

The technique is illustrated for the discrete-time system given in [109]

$$y(t) = 0.32y(t-1) + 2u(t-2) + e(t) + 0.5e(t-1) \tag{4.42}$$

where the variance of noise entering the colouring filter is given as $\sigma_w^2 = 2$.

The achievable reduction in the output variance is limited by the order of the controller. The MV controller for a particular problem can be found by solving the polynomial Diophantine equation for F and G to satisfy [109]

$$E = AF + z^{-k}G \tag{4.43}$$

where E and A are numerator and denominator polynomials of the noise model G_c and F and G are defined as

$$\begin{aligned}
F &= 1 + f_1 z^{-1} + \ldots + f_{k-1} z^{-(k-1)} \\
G &= g_0 + g_1 z^{-1} + \ldots + g_{n_g} z^{-n_g}
\end{aligned}$$

where $n_g = \max(n_a - 1, n_c - k)$ and k is the number of discrete time delays in the plant G_b. Assuming negative feedback the MV regulator is

$$K_{MV} = \frac{G}{BF}$$

where B is the numerator polynomial of the plant model G_b. The output variance is equal to

$$\sigma_y^2 = (1 + f_1^2 + \ldots + f_{k-1}^2)\sigma_w^2 \tag{4.44}$$

The second order problem considered here has a delay of two ($k = 2$) and therefore we obtain the polynomials

$$\begin{aligned} F &= 1 + f_1 z^{-1} \\ G &= g_0 \end{aligned}$$

which with reference to equation 4.43 results in the Diophantine equation

$$(1 + 0.5z^{-1}) = (1 - 0.32z^{-1})(1 + f_1 z^{-1} + z^{-2} g_0)$$

leading to $f_1 = 0.82,\ g_0 = 0.2624$, resulting in the MV regulator

$$K_{MV} = \frac{0.2624z}{2(z + 0.82)}$$

From equation 4.44 the resulting closed loop output variance is 3.34. To incorporate a non-zero tracking requirement in the system it is possible to augment the plant with an integrator $\frac{z}{z-1}$ before designing the feedback controller, for which the combined controller and integrator K_{IMV} is then

$$K_{IMV} = \frac{2.0824z - 0.5824}{2z + 3.64} \frac{z}{z - 1}$$

with an output variance of 9.97. The time response of the two controllers is displayed in figure 4.8 subject to a step demand in the reference signal r from 0 to 100 applied at 1s. It can be seen that the controller with non-zero regulation produces a very undesirable overshoot, which may readily result in excessive control action. To demonstrate the parameter space approach a PI controller is designed with the output variance constrained to 5.0 with an aim to achieve improved tracking performance whilst obtaining lower output variance, closer to the theoretical minimum.

Rewriting the system in equation 4.42 in terms of G_b and G_c with a unit variance input gives

$$\begin{aligned} G_b &= \frac{2}{z^2 - 0.32z} = \frac{b_0}{a_2 z^2 + a_1 z + a_0} \\ G_c &= \frac{\sqrt{2}z^2 + 0.5\sqrt{2}z}{z^2 - 0.32z} = \frac{c_2 z^2 + c_1 z + c_0}{a_2 z^2 + a_1 z + a_0} \end{aligned}$$

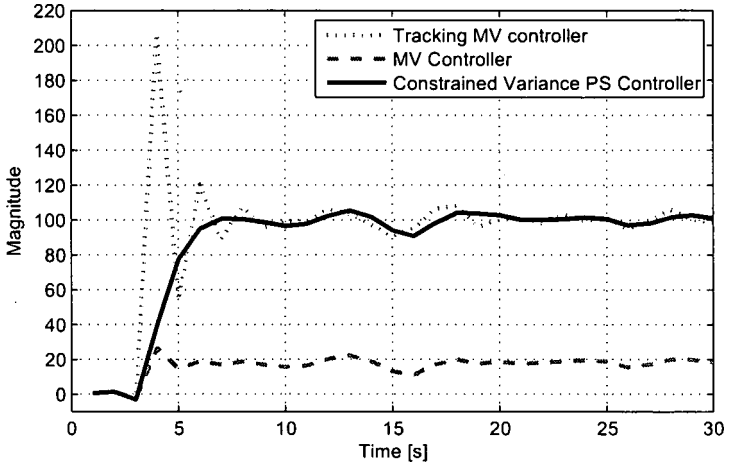

Figure 4.8: Controller response to step demand change from 0 to 100 at 1s

From section 4.4.2 we derive the matrices D_0, D_1 and D_2

$$D_0 = \begin{bmatrix} 0 & 0.32 & -1.32 & 1 \\ 0 & 0 & 0.32 & -1.32 \\ 0 & 0 & 0 & 0.32 \\ 0 & 0 & 0 & 0 \end{bmatrix} + \begin{bmatrix} 0 & 0.32 & -1.32 & 1 \\ 0.32 & -1.32 & 1 & 0 \\ -1.32 & 1 & 0 & 0 \\ 1 & 0 & 0 & 0 \end{bmatrix}$$

$$= \begin{bmatrix} 0 & 0.64 & -2.64 & 2 \\ 0.32 & -1.32 & 1.32 & -1.32 \\ -1.32 & 1 & 0 & 0.32 \\ 1 & 0 & 0 & 0 \end{bmatrix}$$

$$D_1 = \begin{bmatrix} -2 & 2 & 0 & 0 \\ 0 & -2 & 2 & 0 \\ 0 & 0 & -2 & 2 \\ 0 & 0 & 0 & -2 \end{bmatrix} + \begin{bmatrix} -2 & 2 & 0 & 0 \\ 2 & 0 & 0 & 0 \\ 0 & 0 & 0 & 0 \\ 0 & 0 & 0 & 0 \end{bmatrix}$$

$$= \begin{bmatrix} -4 & 4 & 0 & 0 \\ 2 & -2 & 2 & 0 \\ 0 & 0 & -2 & 2 \\ 0 & 0 & 0 & -2 \end{bmatrix}$$

$$D_2 = \begin{bmatrix} 2 & 0 & 0 & 0 \\ 0 & 2 & 0 & 0 \\ 0 & 0 & 2 & 0 \\ 0 & 0 & 0 & 2 \end{bmatrix} + \begin{bmatrix} 2 & 0 & 0 & 0 \\ 0 & 0 & 0 & 0 \\ 0 & 0 & 0 & 0 \\ 0 & 0 & 0 & 0 \end{bmatrix}$$

$$= \begin{bmatrix} 4 & 0 & 0 & 0 \\ 0 & 2 & 0 & 0 \\ 0 & 0 & 2 & 0 \\ 0 & 0 & 0 & 2 \end{bmatrix}$$

From Leverrier's algorithm and with reference to equation 4.36 results a polynominal in k with four roots ($n+1$, where n is the degree of the controlled closed loop system). One

thousand discrete points for $\theta \in [0; 2\pi)$ were used for the design. From the parameter plane with all $n+1$ loci it is quickly revealed to the designer which are useful for a controller design. The resulting parameter plane showing stable controller gains ($k_i > 0$) is presented in figure 4.9.

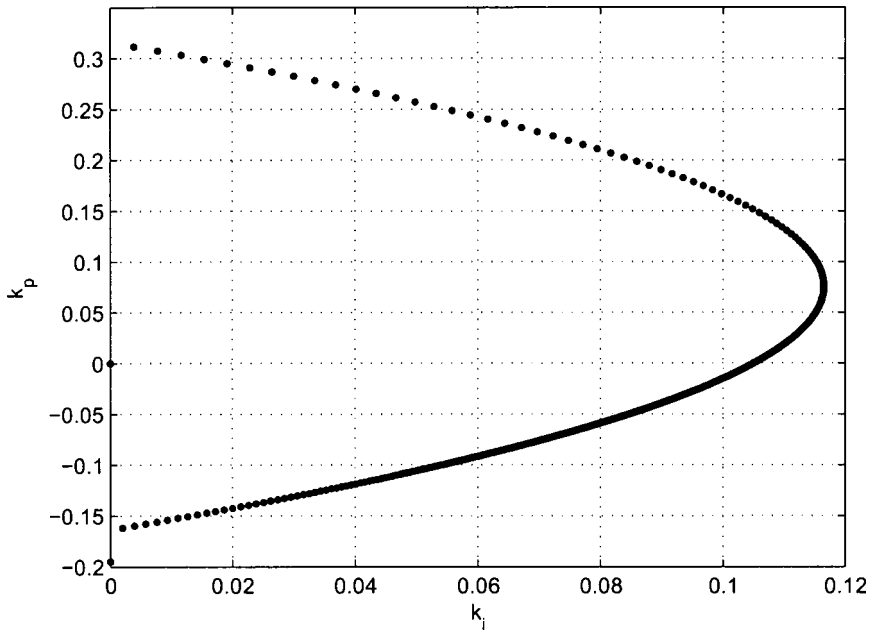

Figure 4.9: k_i, k_p parameter plane with variance constrained to 5.0

For good tracking performance the maximum permitted integral gain is selected, i.e $k_i = 0.1165$ and $k_p = 0.0763$ resulting in the parameter space controller

$$K_{PS} = \frac{0.1928z - 0.0763}{z - 1}$$

The time response of the parameter space controller compares favourably against the alternative integral-MV controller as can be seen in figure 4.8. The two tracking controllers show similar settling times, however the parameter space design reveals no overshoot. Several variance loci can also be superimposed onto the parameter plane to provide a graphical set of suitable controllers, thus creating an admissible region which provides transparency between the trade-off in improvements in time response against increases in output variance.

A comparison is made here in terms of tracking performance and output variance. However, one benefit of parameter space techniques is the ability to non-conservatively add additional requirements, which can be superimposed to further constrain the admissible area. For example gain and phase margins or multiple $\mathcal{H}_\infty$ sensitivity functions can also be included into the design to provide a robust minimum-variance technique for low order controllers.

4.5 Cylinder Balancing using MV PPP Control

The timing of the spark advance (SA) largely determines the release of energy and therefore the shape and position of pressure curve relative to the crank angle. It is well understood that there exists for each engine type, a fixed peak pressure position (PPP) to give maximum best torque (MBT) . Optimal engine efficiency for any given engine configuration can be obtained by controlling the combustion such that the PPP coincides with this best position. For the engine under consideration here this angle is approximately 16° after top dead centre (TDC) [48].

Various studies have demonstrated the advantages of using feedback for the control of PPP (and therefore MBT), rather than relying on static SA maps stored in engine management system (EMS) [25, 71, 85]. Mechanical wear of components over time and varying environmental conditions makes a strong case for feedback control. Moreover, allowing each cylinder to be controlled independently provides the opportunity for increased engine efficiency since MBT can be obtained from each cylinder if the PPP is regulated to the optimum position. Furthermore, balancing each cylinder ensures no unnecessary roughness which provides improved component life and driver perception of performance.

Due to the chaotic nature of combustion, the regulation of the PPP requires control laws which consider the closed loop variance. $\mathcal{H}_2$ and MV control laws have been successfully demonstrated in [105] and [107].

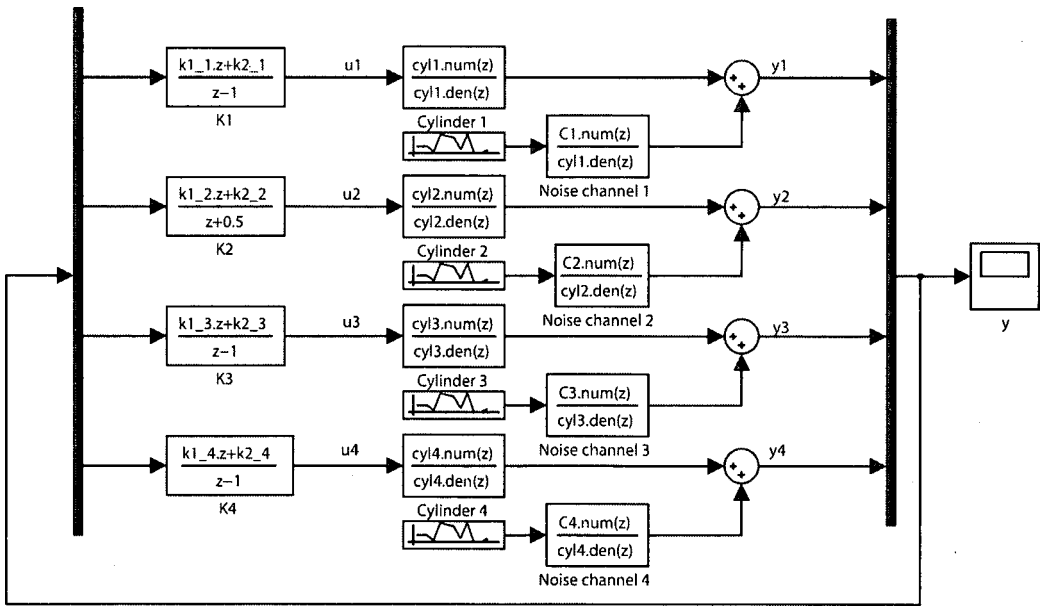

Figure 4.10: SA-PPP Block diagram

For a n cylinder engine it is proposed that n SISO feedback controllers can be used to provide good feedback control of the PPP response since inter-cylinder dependency is very small [105]. In the following sections the cross channel interaction is considered. SISO parameter space MV feedback is subsequently applied using a PI controller. The corresponding system configuration is depicted in figure 4.10, for the four-cylinder engine used in this application. The system outputs (PPP) are denoted y_i, with inputs (SA) u_i controlled by SISO PI controllers on cylinders $i = 1, \ldots, 4$.

4.5.1 ARMAX Identification

The engine under consideration here is a $1.6l$ port fuel injection Ford Zetec. During the identification the air entering the engine was regulated by a fixed air bleed valve (ABV) of 0.56 duty cycle and a medium load was applied to the engine via a low inertia dynamometer. The SA was perturbed using a random number in integer values between 20-30° where this level was held for a minimum of 2-5 combustion events for each cylinder. Different random number sequences were used in the generation of the 4 spark inputs to ensure the input signals were uncorrelated in order to assess the degree of cross channel interaction. The fuelling was left under the control of the EMS.

The output y (PPP) was calculated relative to TDC of each cylinder at 0°, 180°, 360°, 540° corresponding to cylinders 4, 2, 1, 3 respectively. To assess the degree of interaction between cylinders, a multivariable auto-regressive moving average (ARMA) model was identified.

Multivariable Bode plots suggest the system has relatively insignificant off diagonal dynamics [105]. This diagonal dominance was further tested by evaluating the relative gain array (RGA) for the multivariable plant model. The RGA of a non-singular square matrix G is defined as [100]

$$\text{RGA}(G(\omega)) = \Lambda(G(\omega)) \triangleq G(\omega) \times (G(\omega)^{-1})^T \tag{4.45}$$

The RGA for the multivariable structure was calculated at $\omega = 0$ to be

$$\Lambda(G(0)) = \begin{bmatrix} 1.0053 & 0.001470 & 0.0004923 & 0.004328 \\ 0.0013885 & 1.0016 & 0.0005228 & 0.000756 \\ 0.0004908 & 0.000504 & 0.99824 & 0.000764 \\ 0.0044085 & 0.000655 & 0.000743 & 1.0043 \end{bmatrix} \tag{4.46}$$

The diagonal dominance can be measured by the quantity

$$\text{RGA-number} = ||\Lambda(G) - I||_{sum} \tag{4.47}$$

The RGA-number at $\omega = 0$ was computed as 0.03, similarly low values were computed up to the sampling frequency. This value indicates the problem is strongly suited to decentralised control, which can be observed from the RGA approximating a unit matrix. Accordingly, it is assumed the system effectively behaves as 4 separate SISO loops.

Identification data was split into 4 sets of data each sampling the SA and PPP once every 720°. The data was sampled for each cylinder at top dead centre (TDC) position after the spark event for that particular cylinder to ensure all the datasets displayed the same model structure. Figure 4.11 shows a typical input-output dataset used for the identification; the figure showning data for cylinder 1.

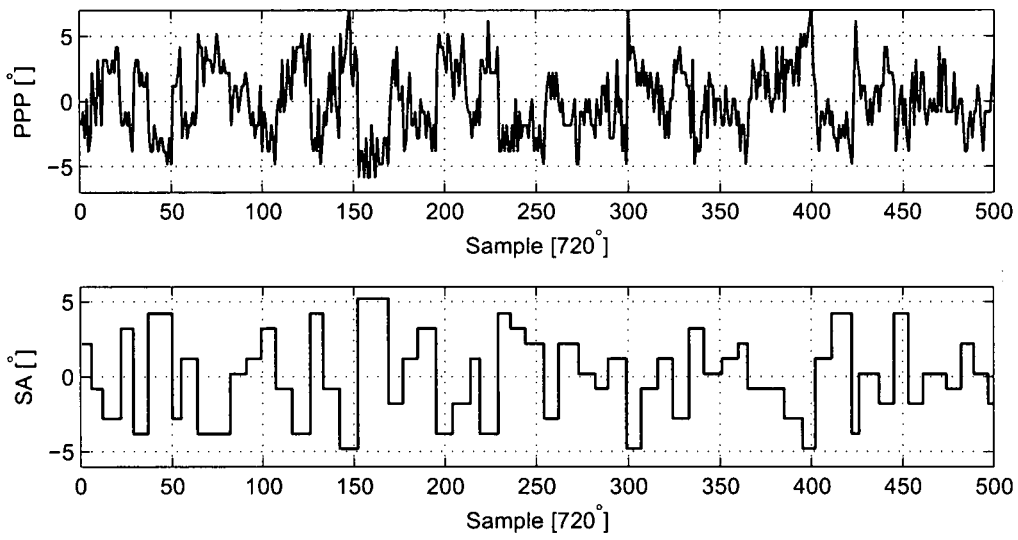

Figure 4.11: Input-output data for identification of SA-PPP for cylinder 1

The SA-PPP relationship has been demonstrated to be a highly linear process over a given spot point [105], with a significant amount of process noise and stochastic noise due to combustion variability [25]. Accordingly mean value SISO ARMAX models were identified using the Matlab System Identification Toolbox [70] for each cylinder

$$a(z)y(t) = b(z)u(t) + c(z)e(t)$$

where the structure selection for the identification was based on both *a priori* information of the system behavior and statistical analysis using validation data. Fit quality, whiteness of residuals and the Akaike's Information Criterion (AIC) were used for the main assessment.

The resulting structure that was found to satisfactorily explain the dynamics was

$$\begin{aligned} a(z) &= a_2 z^2 + a_1 z + a_0 \\ b(z) &= b_1 z + b_0 \\ c(z) &= c_2 z^2 + c_1 z + c_0 \end{aligned}$$

Coefficients for the 4 identified models are presented in table 4.1

Table 4.1: ARMAX coefficients

	a_2	a_1	a_0	b_1	b_0	c_2	c_1	c_0
Cylinder 1	1	-0.8424	-0.0571	0.8122	-0.7246	1	-0.7528	-0.1159
Cylinder 2	1	-0.7116	-0.0609	-0.8527	0.6500	1	-0.6936	-0.0465
Cylinder 3	1	-0.0656	0.1017	-0.0011	-0.8387	1	-0.1094	0.1595
Cylinder 4	1	-0.8645	0.3364	0.1467	-0.5043	1	-0.9121	0.3660

4.5.2 Controller Design

Regulation of the PPP when subject to noise due to the stochastic nature of combustion and step disturbances requires controllers than can track to a desired set point and adequately reject noise. Therefore to ensure tracking and disturbance rejection, a PI type controller is developed. With reference to section 4.2.2 the relationship between the noise and error to be controlled for the closed loop system with a PI feedback controller is

$$\frac{e(z)}{d(z)} = \frac{c_2 z^2 + c_1 z + c_0}{a_2 z^2 + a_1 z + a_0 - \left(\frac{(k_p+k_i)z-k_p}{z-1}\right)(b_1 z + b_0)}$$

which can be written as

$$\frac{e(z)}{d(z)} = \frac{q(z)c(z)}{q(z)a(z) + k_0 p_0(z)b(z) + k_1 p_1(z) + k_2 p_2(z)b(z)}$$

For a PI controller (see section 4.4.2) $q(z) = z - 1$, $p_0(z) = 0$, $p_1(z) = z + 1$ and $p_2(z) = z$. The corresponding matrices of denominator coefficients are

$$D_1 = \begin{bmatrix} 0 & 2b_1 & 2b_0 & 0 \\ b_1 & -b_0 & b_1 & b_0 \\ b_0 & 0 & 0 & 0 \\ 0 & 0 & 0 & 0 \end{bmatrix}$$

$$D_2 = \begin{bmatrix} 0 & 0 & 2b_1 & 2b_0 \\ 0 & b_1 & b_0 & b_1 \\ b_1 & b_0 & 0 & 0 \\ b_0 & 0 & 0 & 0 \end{bmatrix}$$

$$D_0 = \begin{bmatrix} 2a_2 & 2(a_1 - a_2) & 2(a_0 - a_1) & -2a_0 \\ a_1 - a_2 & a_0 - a_1 + a_2 & a_1 - a_2 - a_0 & a_0 - a_1 \\ a_0 - a_1 & -a_0 & a_2 & a_1 - a_2 \\ -a_0 & 0 & 0 & a_2 \end{bmatrix}$$

For the problem posed here the output variance is least when the system is open loop since the plant model contains only one time delay ($k = 1$). Therefore, adding a feedback loop to this system cannot aim to reduce the output variance, however it is desirable to add tracking by means of a PI controller if the PPP is to be regulated to 16°. Accordingly, to ensure the controlled system did not excessively increase the output variance but also demonstrated a good degree of tracking and disturbance rejection, a variance bound of 10% greater than the simulated output variance was used for the generation of the controller bounds. The control bounds for the stable region in the parameter plane for each cylinder is presented in figure 4.12.

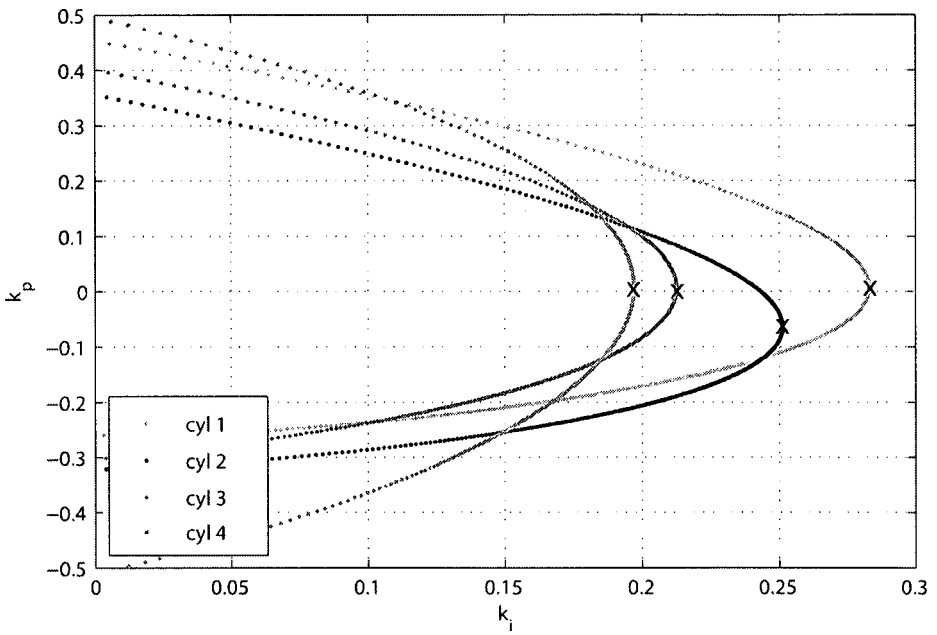

Figure 4.12: Controller bounds corresponding to $\sigma^2 = 1.1$

Examination of figure 4.12 highlights relatively large variations in controller bounds due to cylinder-to-cylinder model variations. For each cylinder the maximum integral gain was selected to ensure the greatest degree of tracking and disturbance rejection as indicated by the markers.

4.5.3 Control Results

The four SISO PI controllers were simultaneously tested on the engine and critically assessed for performance and robustness. Since the controllers were designed to behave like a set of de-tuned MV controllers the system was analysed for closed loop variance relative to open loop performance and also for tracking and disturbance rejection.

To assess the open loop variance it was necessary to manually tune the open loop SA for each cylinder until the PPP for that cylinder was approximately at 16°. Accordingly during this test the SA was set to 29°, 28°, 27° and 31° for cylinders 1 to 4 respectively. This result immediately demonstrates the potential benefit from cylinder balancing at it was necessary to tune each SA differently. The variance was recorded over 500 samples for the open and closed loop system and the results summarised in table 4.2

Table 4.2: Comparison of open and closed loop performance

	σ^2_{OL}	σ^2_{CL}	$\overline{x}_{OL}$	$\overline{x}_{CL}$
Cylinder 1	2.91	3.20	15.69	16.00
Cylinder 2	3.59	3.40	16.41	16.04
Cylinder 3	3.67	2.96	16.32	16.00
Cylinder 4	3.42	3.51	16.93	16.00

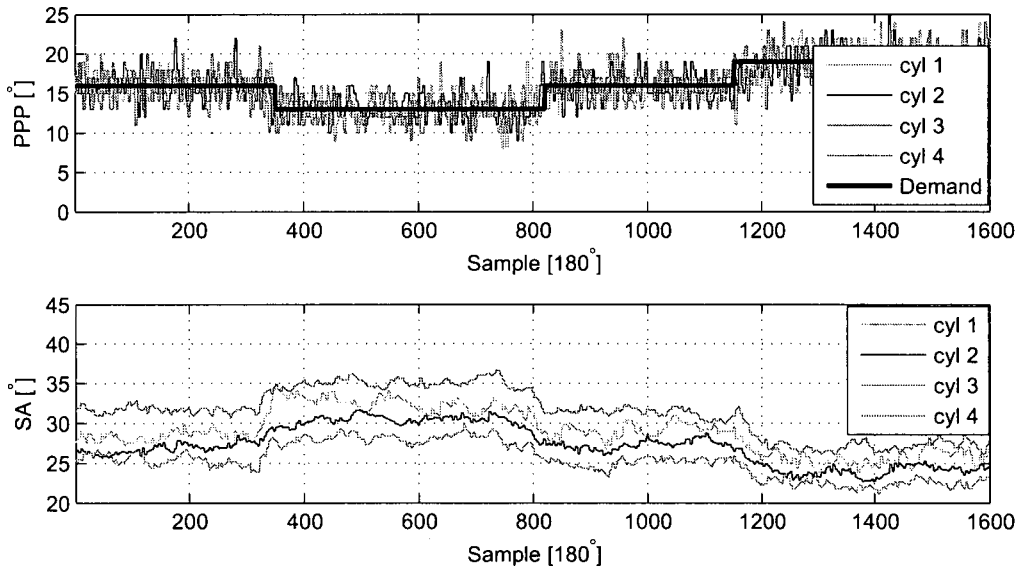

Figure 4.13: PPP response to step demands

It can be seen that the variance in the PPP measurement was increased as a consequence of closed loop control. Since the theoretical variance could not be reduced for this problem the design was intended to allow an increase in variance of 10% to ensure adequate tracking could be included. Cylinders 1 and 4 show a small increase in variance whereas cylinder 2 and 3 reveal a decrease. This reduction is likely to be due to the difficulty in obtaining accurate plant and noise models, where it can be seen that the open and closed loop variance is significantly higher than the coloured noise filter would suggest, however the design objective of adding tracking without excessive increases in output variance was successful[3]. The closed

[3]It should also be noted that the resolution in the measurement of PPP and timing of the SA is restricted to 1°.

loop mean PPP was found to track exactly to 16° indicating strong integral gains.

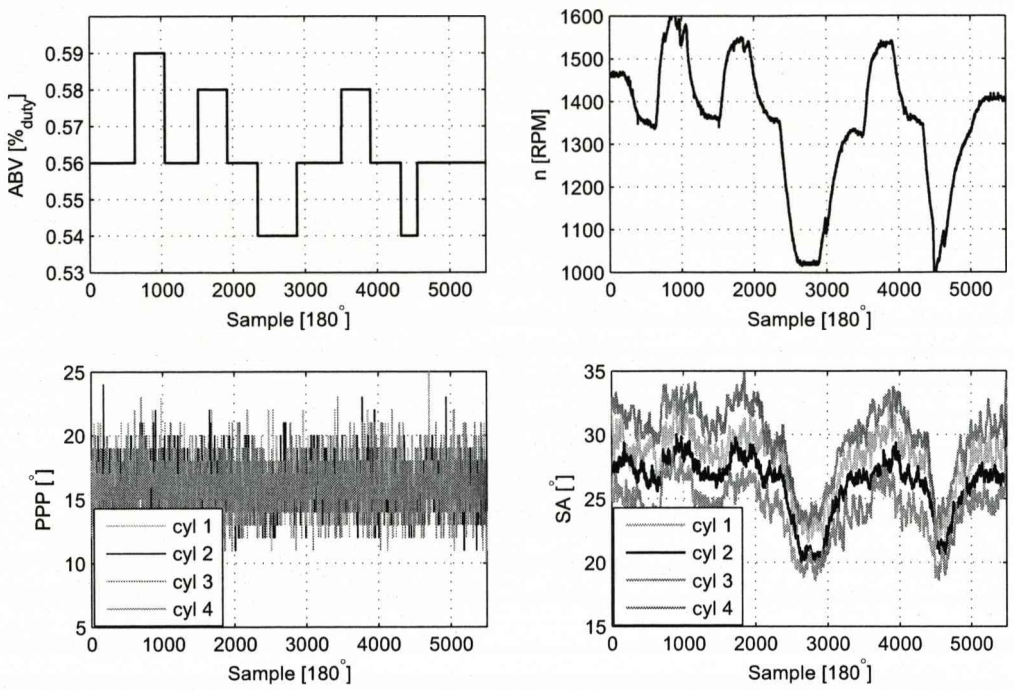

Figure 4.14: Speed n, SA and PPP response to ABV steps with closed loop control

To further assess the tracking performance several step demands in PPP were trialled and the results are displayed in figure 4.13. Such step changes in demand could be required if the presence of engine knock was detected or during start-up for example. The SA control action during the step changes can be seen in figure 4.13. Examination reveals that no overshoot is observed and that settling is relatively fast, around 20 engine events (180°) corresponding to approximately 0.55s at the nominal engine speed. Additionally the controller demonstrated significant robustness to changes in load and speed conditions. A section of data showing step changes to the ABV to perturb the engine speed is shown in figure 4.14. Large changes in the SA are observed to ensure the PPP tracks to the set-point however no significant deviation in PPP can be detected.

Nyquist loci for the four cylinders are shown in figure 4.15. The corresponding gain, delay and phase margins are presented in table 4.3.

4.6 Conclusions

A novel minimum and constrained-variance parameter space controller design technique has been developed for both discrete and continuous systems. Use is made of the mean squared

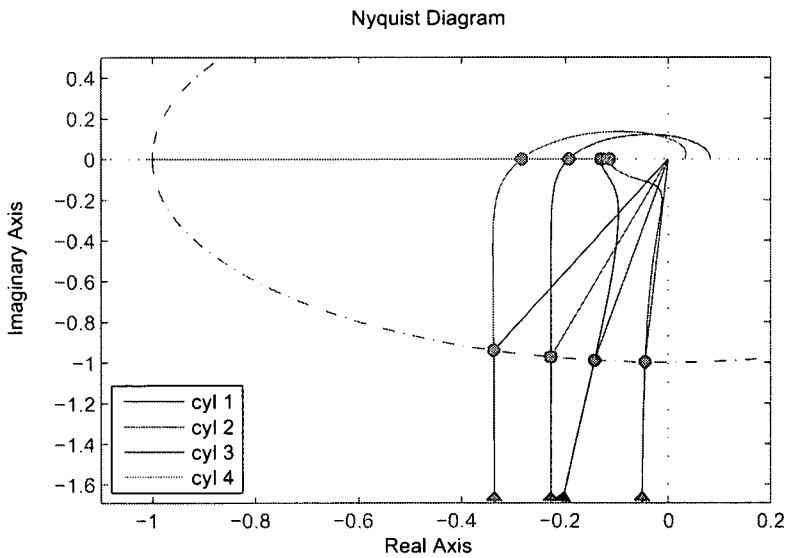

Figure 4.15: Nyquist loci for cylinders 1 - 4

Table 4.3: Comparison of closed loop stability margins and corresponding frequencies

	Gain Margin [dB]	Delay Margin [delays]	Phase Margin [°]
Cylinder 1	17.7 (26.6 rad/s)	6.45 (1.87 rad/s)	81.8 (1.87 rad/s)
Cylinder 2	18.8 (26.6 rad/s)	13.5 (0.96 rad/s)	87.4 (0.96 rad/s)
Cylinder 3	14.3 (9.23 rad/s)	7.73 (1.47 rad/s)	76.8 (1.47 rad/s)
Cylinder 4	10.9 (5.34 rad/s)	8.06 (1.29 rad/s)	70.2 (1.29 rad/s)

value, evaluated from the spectral density function and Leverrier's algorithm to compute loci for a given closed loop output variance, provided the closed-loop system is rational and strictly proper. Loci of constant variance can thus be readily computed and mapped into parameter planes for rational two term controllers.

The usual advantages of parameter space techniques apply where other design criteria may be superimposed allowing multiple objectives to be achieved non-conservatively. Furthermore, the designer is presented with graphical sets of controller parameters and can accordingly tune for time response if desired. An idle speed problem demonstrated this merit.

A discrete example was used to compare a MV design, a tracking MV design and the parameter space technique. The parameter space technique was demonstrated to have improved tracking properties over both algebraic MV designs. Moreover, this was achieved with a significantly lower output variance than the MV controller with tracking.

An experimental implementation of a design for controlling the PPP from the SA demonstrated the merits of the technique for designing low order controllers. SISO constrained-variance controllers were designed and implemented on all four cylinders of the University of Liverpool engine and low inertia dynamometer. The experimental validation showed the advantages of using closed loop control for the problem in terms of the potential increases in engine efficiency from cylinder balancing and accurate tracking without excessively exciting the noise dynamics.

Chapter 5

Multivariable Parameter Space Control

5.1 Introduction

The IC engine is a highly coupled multivariable system. The interactions between the several inputs and measured output are numerous and complex. For example, the air-to-fuel ratio (AFR) is affected most severely by the air and fuel inputs, but is also influenced by the spark advance (SA) and exhaust gas recirculation (EGR). For simplicity, the AFR control problem on the SI engine has historically been treated as a single-input-single-output (SISO) problem, where fuel is the input. In general under driving conditions throttle is operated by the driver and therefore the air path can only be considered as a disturbance. However, under idle conditions the EMS has control over both the fuel and air channels and therefore, it is sensible to make use of these strong interactions. Similarly, most production EMS strategies primarily regulate the idle speed using the air path, however the fuel channel can also affect the engine speed.

It is the strong coupling and interactions in systems which make multivariable control an attractive option. Whilst SISO control algorithms and analysis can be quicker and simpler to implement, the resulting system can display poor transient performance and/or low robustness. These problems associated with SISO and sequential loop designs have led to multivariable designs being based on singular values. Such designs can then maximise the system's transient performance and robustness properties without the risk of loops 'fighting' each other. Better results should generally then be achievable in a multiple-input-multiple-output (MIMO) problem by using explicit MIMO techniques that directly address these issues.

Recently, MIMO parameter space (PS) results, suitable for developing in computer algebra systems, have been presented by [77]. Conditions to obtain parameter space boundaries are

given in the form of equations in the determinant of the Hamilitionian matrices corresponding to the continuous $\mathcal{H}_\infty$ and $\mathcal{H}_2$ Riccati equations, and should thereby lead to symbolic PS methods for rational continuous systems. An important limitation is that irrational systems are not directly addressed as the conditions are developed in terms of continuous state-space models only.

Frequency-response PS methods offer significant advantages over other controller design techniques, since the frequency response of the plant found from non-parametric identification can be used directly and as such irrational systems including systems with multiple pure time delays can be handled directly, without the need for rational approximations. This is in distinction to Riccati $\mathcal{H}_\infty$ methods where rational representations are required. Furthermore, the frequency response approach is treated uniformly for continuous or discrete systems. Another important merit of the these non-parametric frequency response methods over Riccati based techniques is that weighting functions do not need to be rational or indeed proper. A disadvantage of PS methods is that higher order controllers and controllers with very large numbers of inputs and outputs may be difficult to find, although the PS methods are useful in refining higher order controllers obtained by other methods.

This chapter details the development of a PS technique for square multivariable systems based on $\mathcal{H}_\infty$ constraints. Stability and sensitivity constraints are defined in section 5.2. The technique is based on iteratively tuning fixed, second order controllers elements. Inspection of the singular values for a closed loop transfer function leads to determinant equations with complex plane solutions which are presented in section 5.2.5. The mapping equations for these complex solutions into the various parameter planes are given in section 5.3. Section 5.4 lists the computational algorithm and presents a suggested design procedure for the technique. In section 5.5 an idle speed problem for a natural gas engine demonstrates the PS technique, where the design objectives are primarily time domain criteria. Two alternative MIMO techniques are also detailed for comparative purposes. Some conclusions for the technique and application are given in section 5.6.

5.2 Calculating Admissible Parameter Space Regions

Regions in the PS which meet weighted sensitivity functions for MIMO systems can be computed by considering two controller gains at a time and keeping the remaining gains fixed. One elemental controller (of a matrix of controller transfer functions) is considered at a time and the remaining elements are fixed. Accordingly, SISO PS techniques can be extended into a MIMO controller design scheme.

The following method relies only on the non-parametric frequency response of the system

and therefore both discrete and continuous systems can be handled uniformly. The resulting complex loci defining admissible regions can then be mapped into either discrete or continuous controller planes.[1]

Let the plant G be characterised by an $n \times n$ non-parametric continuous frequency response matrix $G(j\omega) = [g_{i,j}(j\omega)]$ and the controller to be designed be characterised by the $n \times n$ transfer function matrix $K(s) = [k_{i,j}(s)]$ comprising of elemental second order continuous controllers [15] of the form

$$k_{i,j}(s) = \frac{b_{2_{ij}} s^2 + b_{1_{ij}} s + b_{0_{ij}}}{a_{2_{ij}} s^2 + a_{1_{ij}} s + a_{0_{ij}}} \tag{5.1}$$

where $b_2, b_1, b_0, a_2, a_1, a_0 \in \mathbb{R}$ are the gains of the transfer function.

Parameter space methods are used to graphically display regions meeting stability and/or performance requirements. Consider a sensitivity function F which is weighted by the function W subject to the H_∞ norm constraint

$$||W(j\omega)F(j\omega)|| < 1, \quad \forall\, \omega \in [0; +\infty)$$

At any particular frequency the sensitivity function is a function of the plant and controller gains and the boundary condition can be assessed from the maximum singular value, that is

$$\overline{\sigma}[W(j\omega)F(j\omega)] = 1$$

A location matrix E is used to selected one element of the controller matrix whilst keeping the remaining element gains fixed K_0, that is

$$K(j\omega) = K_0(j\omega) + k(j\omega)E$$

Accordingly the unknown complex controller gain k is a function of

$$k = f(G, K_0, E, W)$$

In the sequel, regions meeting stability and sensitivity requirements are developed for multivariable systems. These solutions are shown to have complex circular solutions. The mapping equations for these solutions are given to allow two gains of the controller structure shown in equation 5.1 to be plotted into parameter planes.

5.2.1 Nominal Stability Equations

The most fundamental requirement of the controller is to ensure the closed loop system is stable for the nominal system. Nominal stability for a multivariable system can be assessed from the generalised Nyquist criterion which states [100]: "The closed loop system with loop transfer function $L(s)$ and negative feedback is stable if the Nyquist plot of $|I + L(s)|$

[1] For clarity the equations in the sequel are derived for the continuous case.

1. makes P_{ol} anti-clockwise encirclements of the origin, and

2. does not pass through the origin."

This condition can be tested by considering the inequality

$$|(I + G(j\omega)K(j\omega))| \neq 0 \tag{5.2}$$

for $\forall\ \omega \in [0, \infty)$. In practice it is necessary to only analyse a finite set Ω comprising N_f frequencies of the form $\Omega = \{\omega_1, \omega_2, \ldots \omega_{N_f}\}$, the number and range of particular frequencies chosen depending upon the application dynamics. In the sequel we consider the parameter space boundary for one particular frequency. A complete solution is obtained by superimposing a set of frequencies. Therefore for simplicity we drop reference to the arbitrary frequency point ω under consideration. Since singular values are always positive and real, equation 5.2 is equivalent to

$$\underline{\sigma}(I + GK) > 0$$

by the continuity of the eigenvalues as a function of the matrix parameters, PS stability boundaries can also be obtained from the eigenvalue equality[2]

$$\underline{\lambda}(I + GK + K^*G^* + GKK^*G^*) > 0 \tag{5.3}$$

From inequality (5.3), the boundary conditions defining the two possible sets is obtained from solutions to

$$|I + GK + K^*G^* + GKK^*G^*| = 0$$

which by pre and post multiplying by G^{-1} and G^{*-1} respectively gives

$$|G^{-1}G^{*-1} + KG^{*-1} + G^{-1}K^* + KK^*| = 0 \tag{5.4}$$

Now we consider the parameter plane for one element of the controller matrix and keep the other controller elements fixed. Accordingly we make the substitution $K = kE + K_0$ where k a complex unknown gain at each frequency located by the matrix $E = \delta_{i,j}$ and K_0 a matrix of fixed complex gains at each frequency. From equation 5.4 we get

$$\begin{array}{l} |\ G^{-1}G^{*-1} + K_0G^{*-1} + G^{-1}K_0^* + K_0K_0^* \\ +kE(G^{*-1} + K_0^*) \\ +k^*(G^{-1} + K_0)E^* \\ +kk^*EE^*| = 0 \end{array} \tag{5.5}$$

which is a determinant equation of the form

$$|A + kB + k^*C + kk^*D| = 0 \tag{5.6}$$

[2] * denotes the complex conjugate

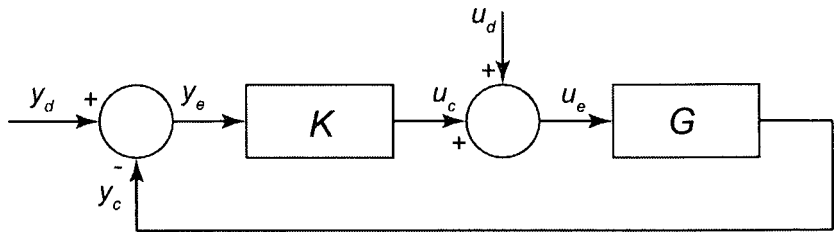

Figure 5.1: Unity negative gain feedback configuration

where the component matrices are

$$\begin{aligned} A &= G^{-1}G^{*-1} + G^{-1}K_0^* + K_0G^{*-1} + K_0K_0^* \\ B &= E(G^{*-1} + K_0^*) \\ C &= (G^{-1} + K_0)E^* \\ D &= EE^* \end{aligned}$$

5.2.2 Primary Sensitivity

With reference to figure 5.1 consider the transmission from the reference signal y_d to the error signal y_e. The relation from the reference signal to the error signal is known as the *primary sensitivity* function S. Assuming $u_d = 0$, the primary sensitivity function is derived from

$$y_c = GKy_e \; ; \quad y_e = y_d - y_c \; \Rightarrow y_e(I + GK) = y_d$$

in matrix form

$$S = \frac{y_e}{y_d} = [I + GK]^{-1}$$

Constrains on the primary sensitivity function are given in terms of frequency domain weights. The generation of the complex controller bounds to meet the weighting imposed for nominal time response performance requirements are associated with the primary sensitivity function, shaped by a left weighting function W_S such that

$$||W_S(j\omega)S(j\omega)||_\infty \leq 1, \quad \forall\, \omega \in [0; +\infty)$$

The controller regions that meet this maximum singular value inequality on the primary sensitivity function S are determined by the singular value inequality on the weighting function W_S given by

$$\overline{\sigma}[W_S(j\omega)S(j\omega)] < 1$$

the boundaries of which, by continuity, can be determined by solution of the boundary condition

$$\underline{\sigma}[S(j\omega)^{-1}W_S(j\omega)^{-1}] = 1$$

Dropping the reference to the arbitrary frequency, the boundaries are obtained from the solution to

$$\underline{\lambda}(W_S^{-1}W_S^{*-1} + GKW_S^{-1}W_S^{*-1} + W_S^{-1}W_S^{*-1}K^*G^* + GKW_S^{-1}W_S^{*-1}K^*G^*) = 1$$

the solutions to which equality are also solutions to

$$|W_S^{-1}W_S^{*-1} + GKW^{-1}W_S^{*-1} + W_S^{-1}W_S^{*-1}K^*G^* + GKW_S^{-1}W_S^{*-1}K^*G^* - I| = 0 \qquad (5.7)$$

Now let $K = kE + K_0$. Equation 5.7 may then be rewritten as

$$\begin{aligned}
&| W_S^{-1}W_S^{*-1} + GK_0W_S^{-1}W_S^{*-1} - I + GK_0W_S^{-1}W_S^{*-1}K_0^*G^* + W_S^{-1}W_S^{*-1}K_0^*G^* \\
&+k(GEW_S^{-1}W_S^{*-1} + GEW_S^{-1}W_S^{*-1}K_0^*G^*) \\
&+k^*(W_S^{-1}W_S^{*-1}E^*G^* + GK_0W^{-1}W_S^{*-1}E^*G^*) \\
&+kk^*GEW_S^{-1}W_S^{*-1}E^*G^* \ | = 0
\end{aligned}$$

which by pre and post multiplication by G^{-1} and G^{*-1} gives

$$\begin{aligned}
&| G^{-1}W_S^{*-1}W_S^{-1}G^{*-1} + K_0W_S^{-1}W_S^{*-1}K_0^* + G^{-1}W_S^{-1}W_S^{*-1}K_0^* - G^{-1}G^{*-1} \\
&+K_0W_S^{-1}W_S^{*-1}G^{*-1} \\
&+ kEW_S^{-1}W_S^{*-1}(G^{*-1} + K_0^*) \\
&+ k^*(G^{-1} + K_0)W_S^{-1}W_S^{*-1}E^* \\
&+ kk^*EW_S^{-1}W_S^{*-1}E^*| = 0
\end{aligned} \qquad (5.8)$$

With reference to equation 5.6 the derived matrices for the weighted primary sensitivity function are

$$\begin{aligned}
A &= G^{-1}W_S^{*-1}W_S^{-1}G^{*-1} - G^{-1}G^{*-1} + K_0W_S^{-1}W_S^{*-1}K_0^* + G^{-1}W_S^{-1}W_S^{*-1}K_0^* \\
&\quad +K_0W_S^{-1}W_S^{*-1}G^{*-1} \\
B &= EW_S^{-1}W_S^{*-1}(G^{*-1} + K_0^*) \\
C &= (G^{-1} + K_0)W_S^{-1}W_S^{*-1}E^* \\
D &= EW_S^{-1}W_S^{*-1}E^*
\end{aligned}$$

5.2.3 Complementary Sensitivity

With reference to figure 5.1 consider the transmission from the reference signal y_d to the output signal y_c. The relationship from the reference signal to the output signal is termed the *complementary sensitivity* function T. The transfer function of this transmission, assuming $u_d = 0$ is derived from

$$y_c = GKy_e \ ; \quad y_e = y_d - y_c \ \Rightarrow y_c(I + GK) = (GK)y_d$$

hence in matrix form

$$T = \frac{y_c}{y_d} = GK[I + GK]^{-1}$$

Design based on satisfying inequalities on the complementary sensitivity function can be handled in a similar way to the primary sensitivity case. Regions satisfying the norm constraint can be written as

$$\overline{\sigma}(W_T(\omega)G(j\omega)K(j\omega)\left[I+G(j\omega)K(j\omega)\right]^{-1}) < 1$$

or equally by considering the minimum singular value

$$\underline{\sigma}(\left[I+(G(j\omega)K(j\omega))^{-1}\right]W_T(\omega)^{-1}) > 1$$

Again dropping the reference to the arbitrary frequency point ω under consideration, it follows that the boundary condition can be found by solution of the eigenvalue equality

$$\begin{aligned}&\underline{\lambda}(W_T^{-1}W_T^{*-1}+W_T^{-1}W_T^{*-1}G^{*-1}K^{*-1}+K^{-1}G^{-1}W_T^{-1}W_T^{*-1}\\&+K^{-1}G^{-1}W_T^{-1}W_T^{*-1}G^{*-1}K^{*-1})=1\end{aligned}$$

which is solved from the determinant

$$\begin{aligned}&|\,W_T^{-1}W_T^{*-1}+W_T^{-1}W_T^{*-1}G^{*-1}K^{*-1}+K^{-1}G^{-1}W_T^{-1}W_T^{*-1}\\&+K^{-1}G^{-1}W_T^{-1}W_T^{*-1}G^{*-1}K^{*-1}-I|=0\end{aligned} \tag{5.9}$$

For the purpose of controller design to meet simultaneous specifications on different sensitivity function types it is necessary to consistently work with either K or K^{-1}. This then allows super-position of the different sensitivities in the same parameter space. Accordingly we choose here to determine complex controller bounds for elements of K. Therefore we pre and post multiply equation 5.9 by K and K^* respectively as is necessary to ensure the solutions can be mapped onto the parameter planes with other sensitivity functions solved for K.

$$\begin{aligned}&|\,KW_T^{-1}W_T^{*-1}K^*-KK^*+KW_T^{-1}W_T^{*-1}G^{*-1}+G^{-1}W_T^{*-1}W_T^{-1}K^*\\&+G^{-1}W_T^{-1}W_T^{*-1}G^{*-1}|=0\end{aligned} \tag{5.10}$$

Again letting $K = kE + K_0$, equation 5.10 may then be rewritten as

$$\begin{aligned}&|\,K_0W_T^{-1}W_T^{*-1}K_0^*-K_0K_0^*+K_0W_T^{-1}W_T^{*-1}G^{*-1}+G^{-1}W_T^{-1}W_T^{*-1}K_0^*\\&+G^{-1}W_T^{-1}W_T^{*-1}G^{*-1}\\&+kE(W_T^{-1}W_T^{*-1}G^{*-1}+W_T^{-1}W_T^{*-1}K_0^*-K_0^*)\\&+k^*(G^{-1}W_T^{-1}W_T^{*-1}+K_0W_T^{-1}W_T^{*-1}-K_0)E^*\\&+kk^*EW_T^{-1}W_T^{*-1}E^*-EE^*|=0\end{aligned} \tag{5.11}$$

This may be expressed in the form of equation 5.6 by setting the derived matrices for the weighted complementary sensitivity function as $A = K_0W_T^{-1}W_T^{*-1}K_0^* - K_0K_0^* + K_0W_T^{-1}W_T^{*-1}G^{*-1}+G^{-1}W_T^{-1}K_0^*+G^{-1}W_T^{-1}W_T^{*-1}G^{*-1}$, $B = E(W_T^{*-1}G^{*-1}+W_T^{-1}W_T^{*-1}K_0^*-K_0^*)$, $C = (G^{-1}W_T^{-1}+KW_T^{-1}W_T^{*-1}-K_0)E^*$, $D = EW_T^{-1}W_T^{*-1}E^*-EE^*$.

5.2.4 Control Effort Sensitivity

With reference to figure 5.1 consider the transmission from the reference signal y_d to the control signal u_e. The relationship from the reference signal to the control input to the plant is known as the *control effort sensitivity* function U. The transfer function of the relationship, assuming $u_d = 0$ is derived from

$$u_e = Ky_e \; ; \quad y_e = y_d - y_c \; ; \quad y_c = u_e G \Rightarrow u_e(I + GK) = Ky_d$$

which in matrix form can be written as

$$U = \frac{u_e}{y_d} = K[I + GK]^{-1}$$

The aim of the multivariable parameter space for the control effort sensitivity is to graphically determine the controller regions that meet the specification set by the frequency domain weighting function W_U such that

$$||U(j\omega)|| \leq |W_U^{-1}(\omega)|$$

Constraints on the control effort sensitivity function have the form

$$\overline{\sigma}(W_U(\omega)K(j\omega)\left[I + G(j\omega)K(j\omega)\right]^{-1}) < 1$$

which can be mapped to complex bounds on the elements of the controller and thereby to the controller parameter space array by solution of

$$\underline{\sigma}(\left[K(j\omega)^{-1} + G(j\omega)\right] W_U(\omega)^{-1}) = 1$$

that is of

$$\underline{\sigma}(K(j\omega)^{-1}W_U(\omega)^{-1} + G(j\omega)W_U(\omega)^{-1}) = 1$$

for $\forall\, \omega \in \Omega$. Again dropping reference to the arbitrary frequency point ω under consideration we can write the above equality most conveniently in this case as

$$\underline{\lambda}(K^{-1}W_U^{-1}W_U^{*-1}K^{*-1} + K^{-1}W_U^{-1}W_U^{*-1}G^* + GW_U^{-1}W_U^{*-1}K^{*-1} + GW_U^{-1}W_U^{*-1}G^*) = 1$$

The equation above may be tested by

$$|K^{-1}W_U^{-1}W_U^{*-1}K^{*-1} - I + K^{-1}W_U^{-1}W_U^{*-1}G^* + GW_U^{-1}W_U^{*-1}K^{*-1} + GW_U^{-1}W_U^{*-1}G^*| = 0$$

which by pre and post multiplication by K and K^* respectively is equivalent to

$$|W_U^{-1}W_U^{*-1} - KK^* + W_U^{-1}W_U^{*-1}G^*K^* + KGW_U^{-1}W_U^{*-1} + KGW_U^{-1}W_U^{*-1}G^*K^*| = 0 \quad (5.12)$$

Again suppose $K = kE + K_0$ with k a complex unknown gain located by the matrix E and to be determined at a particular frequency and K_0 a matrix of fixed complex gains at that frequency. Equation 5.12 may then be rewritten as

$$\begin{aligned} &| W_U^{-1}W_U^{*-1} + W_U^{-1}W_U^{*-1}G^*K_0 + K_0GW_U^{-1}W_U^{*-1}G^*K_0^* \\ &+K_0GW_U^{-1}W_U^{*-1} - K_0K_0^* \\ &+ kE(GW_U^{-1}W_U^{*-1}G^*K_0^* + GW_U^{-1}W_U^{*-1} - K_0^*) \\ &+ k^*(W_U^{-1}W_U^{*-1}G^* + K_0GW_U^{-1}W_U^{*-1}G^* - K_0)E^* \\ &+ kk^*(EGW_U^{-1}W_U^{*-1}G^*E^* - EE^*)| = 0 \end{aligned} \tag{5.13}$$

Identifying this with the form of equation 5.6 yields the matrices $A = W_U^{-1}W_U^{*-1} - K_0K_0^* + W_U^{-1}W_U^{*-1}G^*K_0 + K_0GW_u^{-1}W_U^{*-1}G^*K_0^* + K_0GW_U^{-1}W_U^{*-1}$, $B = E(GW_U^{-1}W_U^{*-1}G^*K_0^* - K_0^* + GW_U^{-1}W_U^{*-1})$, $C = (W_U^{-1}W_U^{*-1}G^* + K_0GW_U^{-1}W_U^{*-1}G^* - K_0)E^*$, $D = EGW_U^{-1}W_U^{*-1}G^*E^* - EE^*$.

5.2.5 Complex Controller Bounds

The controller bounds are found by solving the determinant equations 5.5, 5.8, 5.11 and 5.13. Accordingly, we consider solutions of equations in the general format of equation 5.6. Without loss of generality consider the case of finding the complex gains for an element in the first row of the controller, that is $E = [\delta_{1j}]$. The coefficient matrices of equation 5.6 can then be partitioned as

$$A = \begin{bmatrix} a_{11} & a_{21}^* \\ a_{21} & A_{22} \end{bmatrix}, \quad B = \begin{bmatrix} b_{11} & b_{12} \\ 0_{21} & 0_{22} \end{bmatrix}, \quad C = \begin{bmatrix} c_{11} & 0_{12} \\ c_{21} & 0_{22} \end{bmatrix}, \quad D = \begin{bmatrix} d_{11} & 0_{12} \\ 0_{21} & 0_{22} \end{bmatrix}.$$

which with reference to the determinant given in equation 5.6 becomes

$$\begin{vmatrix} a_{11} + kb_{11} + k^*c_{11} + kk^*d_{11} & a_{21}^* + kb_{12}^* \\ a_{21} + k^*c_{21} & A_{22} \end{vmatrix} = 0 \tag{5.14}$$

It is noted that due to the presence of the $G^{-1}G^{*-1}$ terms in the expressions for the matrix A, a small perturbation in any K_0 can always yield $|A_{22}| \neq 0$ in both the nominal stability and sensitivity function cases. It can therefore be concluded that the occurrence of such a singularity should almost always not arise. Thus, assuming $|A_{22}| \neq 0$ equation 5.14 is equivalent to

$$a_{11} + kb_{11} + k^*c_{11} + kk^* - (a_{21}^* + kb_{21}^*)A_{22}^{-1}(a_{21} + k^*c_{21}) = 0$$

which may conveniently be written

$$a + kb + k^*c + kk^*d = 0 \tag{5.15}$$

where a and d are real

$$\begin{aligned} a &= a_{11} - a_{21}^*A_{22}^{-1}a_{21}, \\ d &= d_{11} - b_{21}^*A_{22}^{-1}c_{21}. \end{aligned}$$

and b and c are complex

$$\begin{aligned} b &\equiv b_R + jb_I = b_{11} - b_{21}^* A_{22}^{-1} a_{21}, \\ c &\equiv c_R + jc_I = c_{11} - a_{21}^* A_{22}^{-1} c_{21}. \end{aligned}$$

Equation 5.15 is thereby equivalent to

$$a + k_R b_R - k_I b_I + k_R c_R + k_I c_I + (k_R^2 + k_I^2)d + j(k_R b_I + k_I b_R + k_R c_I - k_I c_R) = 0$$

which since $b_{21} = c_{21}$ and $b_{11} = \bar{c}_{11}$, that is $b = \bar{c}$ (and thus $b_R = c_R$ and $b_I = -c_I$), reduces to the real equation

$$a + 2k_R b_R - 2k_I b_I + (k_R^2 + k_I^2)d = 0 \tag{5.16}$$

which is the equation of a conic section defining the complex controller bounds k_R and k_I for the chosen elemental controller determined by the chosen location matrix E.

5.3 Mapping Solutions into Parameter Planes

The conic equation given in equation 5.16 has a circular solution since both k_R^2 and k_I^2 share the same coefficient d. The solutions to such conics constitute the complex controller boundaries and are readily determined. These may conveniently be determined by trigonometric parameterisation over a range of discrete points $\theta \in [0, 2\pi)$.

The circular results obtained at each of the discrete frequencies $\omega \in \Omega$ can be mapped into parameter planes of interest. The mapped solutions are elliptical, each of which divides the plane into two regions, one of which contains the solution. Besson and Shenton [15] have shown that if any point in such a conic section is a solution, then all the points in the section are also solutions. The centre of the conic can thus be tested to check which side of the boundary the solution lies. The graphical convention used by [15] will be adopted here whereby dotted lines represent a boundary whose *insides* are solutions whereas solid lines represent a boundary whose *outsides* are solutions. A range of frequencies of interest can then be superimposed onto a single parameter plane to give admissible regions satisfying all frequencies.

5.3.1 Continuous Controller Mapping

Consider the continuous controller element with the structure defined in equation 5.1. The complex controller bounds defined in equation 5.16 can now be mapped into convenient parameter planes by equating the complex gains to the controller element defined in equation

5.1. Making the substitution $s = j\omega$ the real and imaginary parts of the elementary controller are obtained as

$$k_R = \frac{(b_0 - b_2\omega^2)(a_0 - \omega^2) + (a_1 b_1 \omega^2)}{(a_0 - \omega^2)^2 + a_1^2\omega^2} \tag{5.17}$$

and

$$k_I = \frac{b_1\omega(a_0 - \omega^2) - a_1\omega(b_0 - b_2\omega^2)}{(a_0 - \omega^2)^2 + a_1^2\omega^2} \tag{5.18}$$

Now by choosing one controller coefficient with an odd power of s and one with an even power of s the mapping transformations are readily obtained. For example, suppose b_0 and b_1 are to be tuned and therefore a_2, a_1, a_0, b_2 are fixed for this iteration. Then for any value for θ

$$k_R + jk_I = \frac{-b_2\omega^2 + jb_1\omega + b_0}{-a_2\omega^2 + ja_1\omega + a_0}$$

and therefore solutions are readily obtained from

$$(k_R + jk_I)(-a_2\omega^2 + ja_1\omega + a_0) + b_2\omega^2 = K_R + jK_I = jb_1\omega + b_0$$

Finally a change of axes is required to give the solution

$$\begin{bmatrix} b_0 \\ b_1 \end{bmatrix} = \begin{bmatrix} 1 & 0 \\ 0 & \omega^{-1} \end{bmatrix} \begin{bmatrix} K_R \\ K_I \end{bmatrix} \tag{5.19}$$

Other particularly useful planes have been found to be (b_1, b_2) and (a_0, a_1). An example of the mapping from the complex circular solution to the parameter plane is given in figure 5.2, shown for a single frequency.

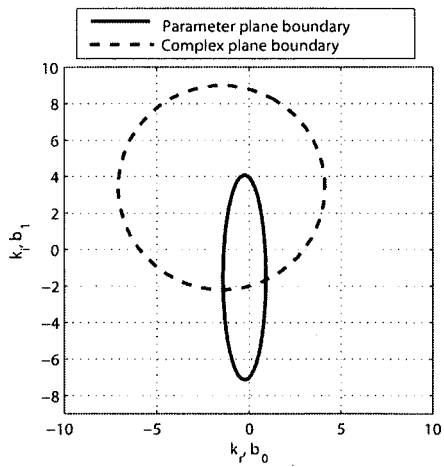

Figure 5.2: Parameter plane boundary mapped from the complex circular solution at one frequency

5.4 Controller design procedure

5.4.1 Computational algorithm

The following steps outlines one suggested algorithm for generating the parameter planes

1. Select desired sensitivity functions for the design.
2. Select weighting functions.
3. Select a particular controller element E and controller gains to generate the parameter plane.
4. Select frequency ω in the range of interest.
5. Obtain complex frequency response matrices for the chosen weighting functions W_i, plant G and fixed controller gains K_0.
6. Generate component matrices A, B, C, D of the generalised determinant equation 5.6 for each stability and sensitivity function of interest.
7. Partition the matrices as per equation 5.14.
8. Obtain the complex circular solution of equation 5.16 for each design constraint.
9. Map the complex solution into the parameter plane using mapping equations 5.17 and 5.18
10. Return to step (4) and repeat for a range of discrete ω in the range of interest.
11. From the completed parameter plane select suitable gains.
12. If required return to step (2) to tighten or relax weighting function(s).
13. Return to step (3) and repeat for all controller elements and gains until satisfactory controller is obtained.

5.4.2 Design Procedure

Once the region satisfying all the frequencies has been identified the designer is able to select a set of gains. An obvious approach adopted by both [14] and [88] is to use either a manual or numerical optimisation technique to maximise some multiplier, γ, acting on the weighting function. This optimisation approach involves selecting the gains at the centre of each admissible region. An example parameter plane is shown in figure 5.3 where the centre

of the admissible region corresponds to gains most suited to the chosen weighting functions. Once a pair of controller coefficients are selected these are then added to the fixed part of the controller, K_0. With the updated controller the designer can then either select a different element to tune or a different pair of controller gains. This stage of the design process requires the designer to navigate through various planes to select each of the possible controller gains. Most designs will require the designer to re-visit parameter planes periodically as the process can require several iterations.

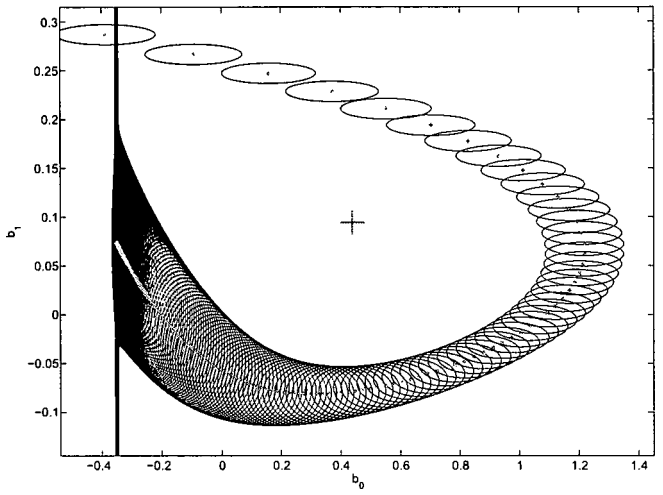

Figure 5.3: Parameter plane showing the bounded set for selection of controller gains

As an alternative to selecting gains towards the centre of the admissible region, the PS technique can present the designer with freedom to trial other suitable gains. Each parameter plane presents the designer with flexibility in the choice of controller coefficients, which can be particularly useful when considering other design criteria such as time response criteria. In this case the designer is steered towards a solution by the frequency domain weighting functions, however in each admissible region various gains can be trialled. This facilitates a technique for meeting necessary frequency constraints such as robustness and also tuning for improved time response. Furthermore, it is well acknowledged that 'optimal' weighting functions can be very difficult to decide upon for complex multivariable problems. It is one of the advantages of the PS technique that it allows this freedom to move away from the centre of the admissible region. In addition, problems with weighting choices and problematic frequencies are more transparent to the designer. In such cases the designer can either re-evaluate the weighting choices or select gains at alternative points within the admissible region.

A schematic outlining the typical design process and necessary iterations is given in figure 5.4. It can be seen that after the generation of each parameter plane the designer has the

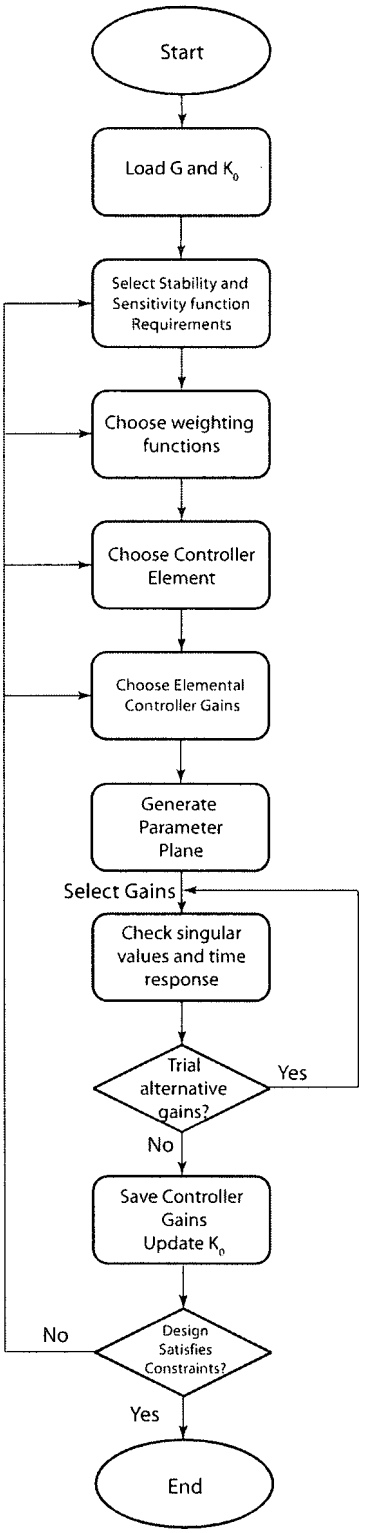

Figure 5.4: Flow chart illustrating the typical PS controller design process

freedom to try a range of controller gains within the admissible region. Once the designer has selected a set of gains the design may be complete or require subsequent iterations. The

parameter planes give the designer insight into the trade-offs and constraints and therefore, the designer is able to detect whether weighting choices are appropriate or if the design requires additional parameter plane iterations.

5.5 Natural Gas Engine Design Example

The idle speed problem remains an active problem in automotive control. The range of controller design approaches and the number of control channels used in each demonstrates the breadth of the problem. A survey of many of these controller techniques applied to the idle speed problem are documented in [54]. In the spark ignition (SI) engine the control engineer has three potential channels of actuation available. These are: the amount of air entering the engine, determined by the operation of the air bleed valve (ABV) or increasingly common an electronic throttle; the amount of spark advance (SA); and the amount of fuel injected into each cylinder. The aim of the idle speed controller is to maintain a low, near constant engine speed in the presence of torque disturbances. At the same time other factors such as fuel economy, AFR, emissions and the so called 'noise and vehicle-harshness' (NVH) must also be considered.

One of the difficulties in rejecting torque disturbances acting on the engine is due to the significant time delays in the system. The air entering the engine is the primary channel for the regulation of the engine speed. Significant time delays exist due to the transport delay from the actuator to the inlet manifold, where the manifold filling dynamics can also delay the air further. Finally, there is an induction to power stroke delay due to the discrete operating nature of the engine. Figure 5.5 gives a schematic of the air path in a natural gas SI engine from the intake to the exhaust, where it can be seen that the fastest effective actuator is the spark plug since this can affect the next combustion event. The fuel injectors can also be used for control, however in the port-injected engine these suffer from time lags and delays due to wall wetting dynamics and due to the induction to power stroke delay.

In production engines the idle speed control problem is conventionally considered to be a multiple-input-single-output (MISO) system, where the air flow and spark is used to regulate the speed using scheduled proportional-integral-derivative (PID) controllers to ensure zero steady-state error and reject disturbances [54]. During torque disturbances the SA is used to provide fast additional torque by advancing toward the optimal position for maximum best torque (MBT). The authority of the spark channel is relatively small but it is faster acting than the air channel. However, in order to achieve this additional torque input from the spark during load transients it is necessary to operate the spark at an operating point away from MBT during normal operation and accordingly, fuel consumption is increased as a consequence.

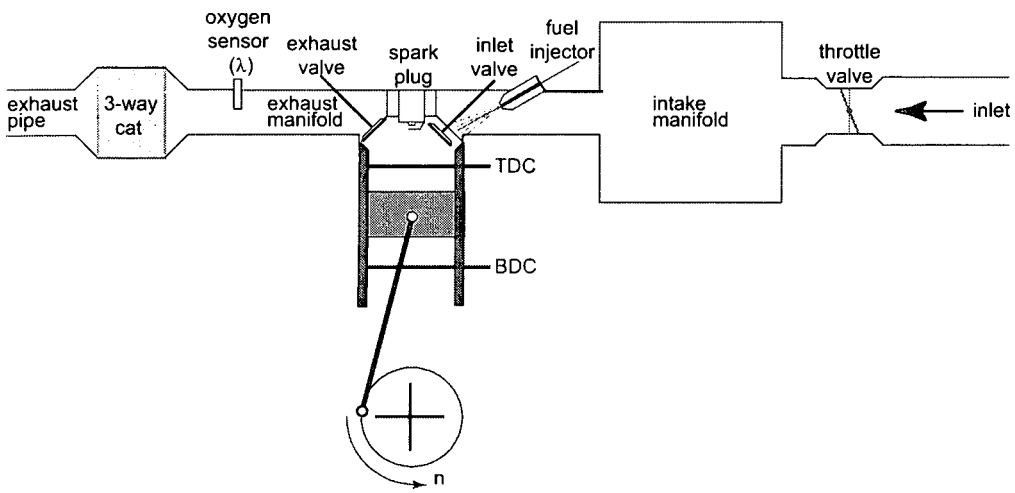

Figure 5.5: Engine schematic of a natural gas SI engine

When considering the idle speed problem one of the main constraints imposed on the engineer is the controller order. Typically, the idle speed controller in a commercial engine management system (EMS) is based upon PID-type controllers with scheduled gains implemented from look-up tables. Since such fixed, low-order controllers are required for implementation, techniques which produce higher order controllers must subsequently undergo order reduction methods.

Many analytical approaches to the idle speed problem have been suggested in the literature, where the design techniques are often applied a loop-at-a-time. Sequential loop designs can make achieving good transient performance difficult and the level of robustness cannot be guaranteed for multivariable systems without consideration of the system's singular values [33]. Recent applications of multivariable control techniques to the MISO idle control problem include algebraic Riccati [24],[110], $\mathcal{H}_\infty$ PS [17], quantitative feedback theory (QFT) [58], model predictive control (MPC) [72] and μ-synthesis [54]. Many of these techniques demonstrate improved performance over current production strategies implemented in the EMS, however excepting for the PS approach, they are also of high order.

More recently some research has investigated multivariable approaches to the idle problem. Conventionally at idle, fuelling control is implemented in a SISO control loop that is designed independently of the idle control loops. In fact, by incorporating fuelling as a control action, it is found that the idle control problem is quite naturally formulated as a MIMO problem. This provides additional actuation for the control of the engine speed and also has the advantage that the regulation of the air entering the engine can be considered with respect to the control of the AFR. A 3×3 formulation based on this approach is considered in [45] where the throttle angle, mass of fuel and SA are used to control engine speed, manifold absolute pressure (MAP) and AFR. The inclusion of fuel necessitates the requirement for a fast feedforward controller

on the fuel path and a high order $\mathcal{H}_\infty$ controller is used for feedback. A similar approach to the problem can be found in [40], where for a natural gas engine the throttle and fuel mass flow rate are chosen for the control of engine speed and AFR. The authors there also apply a novel multivariable PI tuning technique for disturbance rejection based on the discrete system, closed loop eigenvalues.

This remainder of this section investigates techniques for designing multivariable controllers for a natural gas SI engine idle-speed problem. The difficulties in designing multivariable controllers to meet time response criteria are addressed and simulation results from the PS method, algebraic $\mathcal{H}_\infty$ Riccati and a novel eigenvalue technique for the design of a MIMO controller are compared.

5.5.1 Natural Gas Engine Model

A published SI engine model engine is taken from [40], which is in discrete transfer function form based on a linearisation of a parameter identified model of a lean burn natural gas engine model. The control inputs are electronic throttle angle α ($\%_{max}$) and fuel mass-flow rate $\dot{m}$ (lbm/hr). The controlled outputs are engine speed n (rpm) and AFR L. A torque disturbances T (lbf) is assumed to act through the flywheel dynamics G_d on the speed output. The discrete transfer functions governing the plant and disturbance dynamics, based on a 0.1 s sample time are

$$\begin{aligned}
G_{11}(z) &= \frac{\delta n}{\delta \alpha} = \frac{2.56z^{-1} + 2.0z^{-2}}{1 - 1.486z^{-1} + 0.529z^{-2}} \\
G_{12}(z) &= \frac{\delta n}{\delta \dot{m}_{fi}} = \frac{-6.38z^{-1} - 3.04z^{-2} + 1.28z^{-3}}{1 - 1.486z^{-1} + 0.504z^{-2}} \\
G_{21}(z) &= \frac{\delta L}{\delta \alpha} = \frac{0.64}{z - 0.545} \\
G_{22}(z) &= \frac{\delta L}{\delta \dot{m}_{fi}} = \frac{-2.03}{z - 0.537}
\end{aligned}$$

where a maximum step disturbance of 3.7 ft.lbf (5 Nm) is assumed, corresponding to the load of a power-steering pump. The system with a negative feedback controller is depicted in figure 5.6. The relative gain array (RGA) can be used to assess the degree of cross channel interaction in the model. The RGA is defined in equation 4.45, where for a 2×2 matrix it can been observed that only one element is necessary to assess the degree of cross channel interaction.

$$\Lambda(G) = \begin{bmatrix} \lambda_{11} & \lambda_{12} \\ \lambda_{21} & \lambda_{22} \end{bmatrix} = \begin{bmatrix} \lambda_{11} & 1 - \lambda_{11} \\ 1 - \lambda_{11} & \lambda_{11} \end{bmatrix} \tag{5.20}$$

For this example the RGA reveals a considerable amount of cross channel interaction across all frequencies as can be seen in figure 5.7. Accordingly it is suggested a multivariable controller is necessary to provide maximum performance. The inclusion of the fuel channel extends

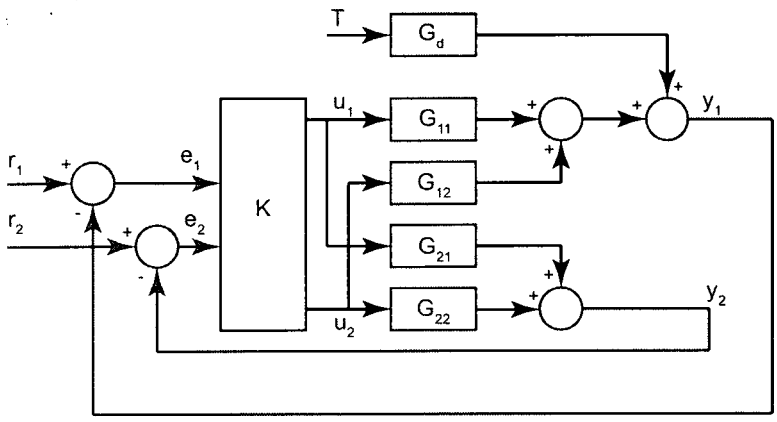

Figure 5.6: Block diagram of engine model with feedback loop

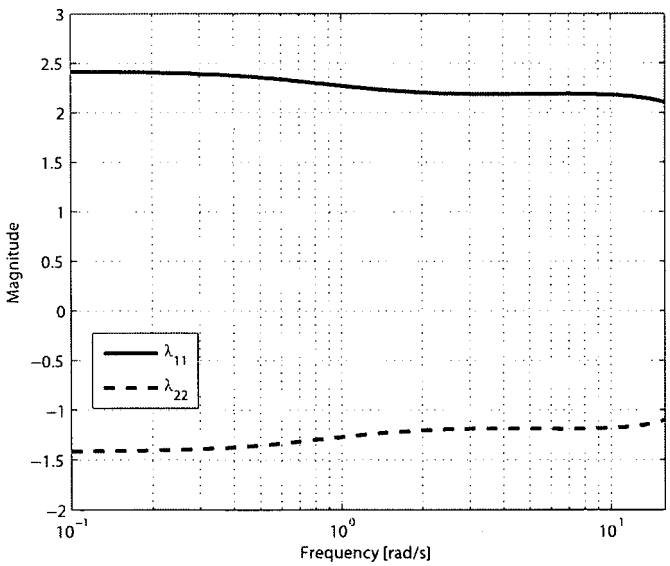

Figure 5.7: Frequency varying RGA

the problem of disturbance rejection to both the speed and AFR outputs. Including the air and fuel as inputs may then improve the speed of response for both channels. A separate SISO fuelling controller for the AFR would not respond as quickly to disturbances caused by the throttle or torque inputs and therefore the control of AFR can potentially be improved beyond that available in a SISO fuelling scheme. Furthermore, the fuel provides an additional control input for disturbance rejection on the speed channel since the spark is assumed to be set for MBT. Moreover, since the example is for a lean burn engine, changes in the demand for AFR are in fact less likely to have a detrimental impact on the regulation of the engine speed with MIMO control.

The problem as posed in [40] is a speed regulation problem in the presence of torque disturbances. A controller which utilises the plant interaction rather than decoupling the outputs is the suggested approach in this chapter to achieve maximum disturbance rejection. Fast settling times are also desirable, particularly on the AFR path if emission requirements are to be realised. Large authority on the fuel control effort is available at idle. In contrast the electronic throttle rate authority is relatively limited. For the benchmark example of this paper this is limited to 4% of maximum throttle angle per second.

5.5.2 Controller Design

For this study a parameter space tuned MIMO controller is designed. A multivariable PI controller design technique based on the discrete closed loop eigenvalues and specifically aimed at disturbance rejection is then considered. Finally a higher order algebraic Riccati design is also developed.

PS tuned PI

Recent parameter space developments have lead to a range techniques suitable for the design of multivariable controllers and the PS results presented here may be obtained by a variety of PS techniques including those described in [77] and [87] specifically for designing PID controllers.

Here we consider the design of 2×2 elemental controllers

$$K = \begin{bmatrix} K_{11} & K_{12} \\ K_{21} & K_{22} \end{bmatrix}$$

where for a continuous controller each element has the 2nd order structure

$$K_{ij} = k_p + \frac{k_i}{s} + \frac{k_d s}{1 + \tau s} \tag{5.21}$$

where k_p, k_i and k_d correspond to the proportional, integral and derivative gains respectively and τ is the time constant on the derivate gain.

One advantage of the PS technique is the freedom the designer has over the controller order. Multiple controller elements can be combined in order to create higher order controllers [17]. Conversely, specific parameters can be constrained to zero to achieve low order. For proper comparison with the discrete tuned eigenvalue designed controller, which is limited to PI, the same structure PS controller is considered here. Accordingly only PI planes were used in the design and the derivative gains set to zero.

Multiple sensitivity functions can be considered either in a conservative mixed sensitivity formulation or by several single sensitivities superimposed over each other on parameter planes. In the sequel we demonstrate that results for this particular application can be obtained by using merely one sensitivity function, by taking advantage of the interactive nature of the technique.

To achieve the AFR and engine speed set-point tracking and the torque disturbance rejection, it was necessary to use the primary sensitivity function to obtain the required transient performance. The nominal performance requirement for a multivariable system is dependent on the singular values of the primary sensitivity function

$$S = [I_n + G(j\omega)K(j\omega)]^{-1}$$

which is shaped by a weighting function W_S so that

$$||W_S(\omega)S(j\omega)||_\infty \leq 1, \quad \forall\, \omega \in [0; +\infty)$$

The primary sensitivity weighting function W_S was shaped for high gains at low frequencies. This has the effect of giving the design good tracking and disturbance rejection. A first order (non-proper) weighting function with a breakpoint at 5 rad/s was selected, however during the design the scalar γ acting on the weighting function was adjusted during the parameter plane iterations.

$$W_S = \gamma \frac{0.2s + 1}{s} I_2$$

PS controllers can be designed from any start point in the parameter plane, provided it is stable or can be stablised easily within a few iterations. This allows controllers designed using other methods to be re-tuned or complete controllers to be designed from the start, usually with the numerator coefficients set to zero. For proper comparison with the discrete tuned eigenvalue designed controller, which is limited to PI the same structure PS controller is considered here. Gangopadhyay [40] demonstrated that two PI SISO controllers designed

using a Ziegler-Nichols tuning method were inadequate for controlling this problem. However this 'basic' controller is an ideal starting condition and was therefore used as the start controller for the PS design. The Ziegler-Nichols start controller as presented in [40] is given as

$$K_{ZN}(s) = \begin{bmatrix} \frac{0.1s+0.2}{s} & 0 \\ 0 & \frac{-0.04s-0.5}{s} \end{bmatrix}$$

The first parameter plane iteration began on the off-diagonal element k_{12} with γ set to 0.1. The corresponding parameter plane is shown in figure 5.8 which indicates the admissible region, start point (X) and selected controller gains (+). Initially controller gains were selected

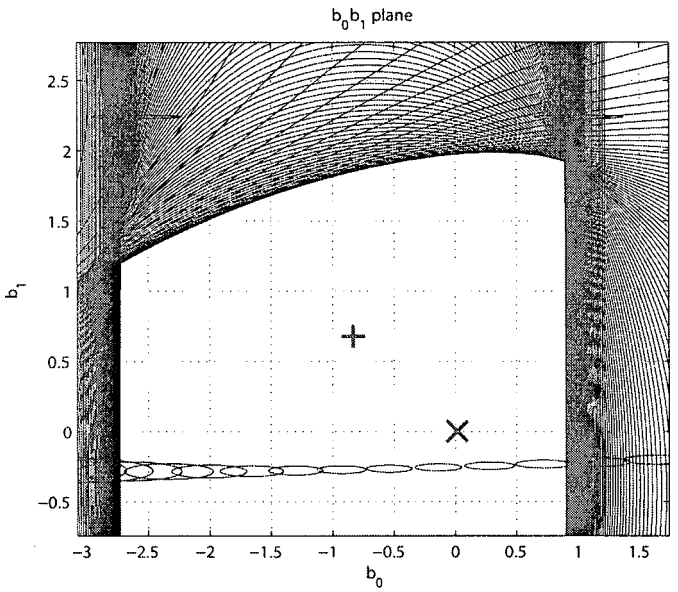

Figure 5.8: Parameter plane: 1st iteration k_{12}, $\gamma = 0.1$

at the centre of the admissible region and after each iteration γ was gradually increased. After four parameter plane iterations the oscillatory time response of the Ziegler-Nichols controller was significantly reduced. After eight parameter plane iterations, at which point γ had been increased to 0.7, no further increases were made since these resulted in control efforts above the throttle constraint. At this stage in the design the disturbance induced time responses were significantly improved, however it was necessary to monitor the control effort of the throttle to ensure it did not exceed the design constraints. A further four more iterations resulted in a tuned time response not exceeding the throttle constraint. An additional four iterations finely tuned the transient time responses to ensure best performance was obtained for the controller order. Figure 5.9 shows the final gains selected in the final (16th) iteration for the controller element k_{22}. The resulting parameter space controller is

$$K_{PS}(s) = \begin{bmatrix} \frac{0.1623s+0.812}{s} & \frac{-0.1649s-1.748}{s} \\ \frac{-0.0716s+0.2296}{s} & \frac{-0.2998s-1.148}{s} \end{bmatrix}$$

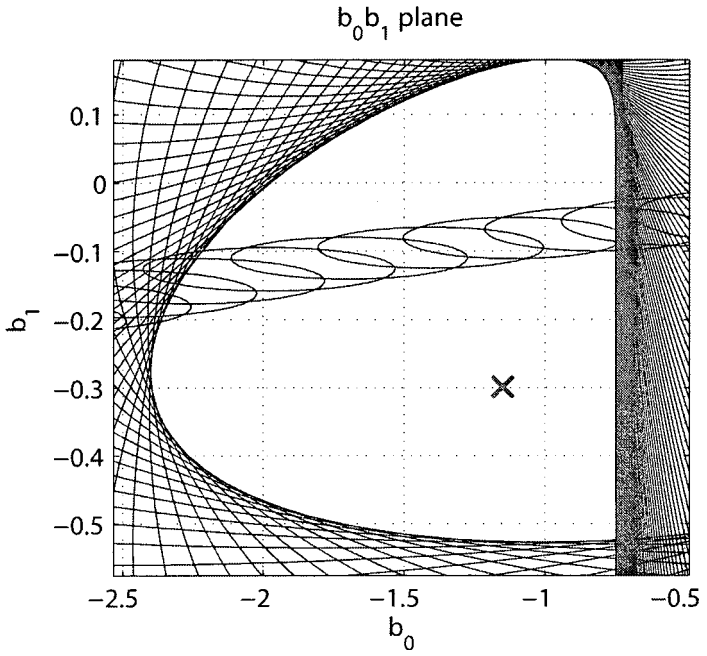

Figure 5.9: Final parameter plane (16th) iteration k_{22}, $\gamma = 0.7$

Additional sensitivity functions could have readily been included in the design, however for this problem it was found unnecessary. One of the benefits of the PS technique is the guidance the planes can provide in the selection of appropriate weighting functions. For designs with multiple sensitivity function constraints the designer can graphically determine which weighting choices are over constrained. Nevertheless, the use of additional sensitivity function constraints can be an added complication. It is of considerable benefit that the PS method can eliminate the need for the use of an additional control input sensitivity function constraint, by providing the ability to tune the time responses interactively within the admissible parameter plane region.

Eigenvalue tuned PI

A discrete controller design technique for designing a multivariable PI controller is detailed in [40]. Inspection of the closed loop eigenvalues is used as the basis for tuning controller gains. The proportional gains are tuned first for disturbance rejection. The integral gains are then tuned to provide decoupling of the closed loop plant at steady state. A Tustin bilinear approximation is used to give the continuous equivalent controller

$$K_{Eig}(s) = \begin{bmatrix} \frac{0.037s+0.119}{s} & \frac{0.02s-1.98}{s} \\ \frac{-0.106s-0.198}{s} & \frac{-0.064s-1.235}{s} \end{bmatrix}$$

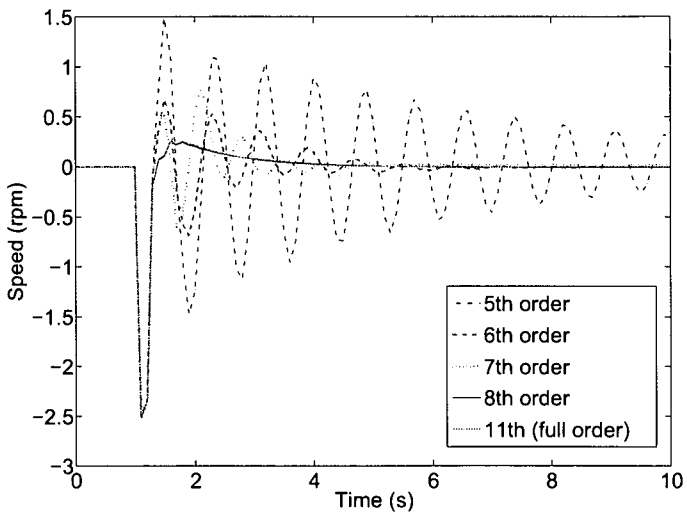

Figure 5.10: Time response for Riccati reduced order controllers

Algebraic Riccati Design

An higher order $\mathcal{H}_\infty$ feedback controller was designed using the DGKF two algebraic Riccati equations (ARE) method [36] as implemented in the Matlab Robust Control Toolbox [28]. The design was carried out in the continuous domain using bilinear Tustin approximation to convert to and from the discrete domain. Primary and control effort weighting functions were both necessary to provide the required robust disturbance rejection performance without excessive control action. Guidelines for shaping the weighting functions were taken from [28] and [100]. A second order primary sensitivity weighting function

$$W_S = \gamma \frac{s^2 + 50s + 500}{100s^2 + 30s + 0.1} I_2 \tag{5.22}$$

was required to achieve good disturbance rejection and tracking performance. A control effort sensitivity weighting of a constant gain at all frequencies, was used to bound the maximum gains. The separate constraints on the air and fuel flow were chosen to reflect the relatively tight authority on electronic-throttle rate and relatively wide degree of authority on the fuelling. Accordingly the selected matrix weighting function was

$$W_U = \begin{bmatrix} 0.5 & 0 \\ 0 & 0.005 \end{bmatrix} \tag{5.23}$$

The resulting continuous controller was 11th order, which can be reduced to an 8th order without significant loss in performance using a balanced model truncation on the normalized coprime factors, but further reduction leads to poor performance or instabilities. The speed of response to a torque disturbance step input can be seen for several of the reduced order controllers in figure 5.10. It can be seen that controllers with a 7th and lower order are much

more oscillatory in response. All of the order reduction techniques as implemented by the Matlab Robust Control were found to result in unstable 4th order and lower controllers. These techniques were: the balanced truncation via square-root method; the balanced truncation via Schur method; the balanced stochastic truncation via Schur method; the balanced truncation method for normalized coprime factors; and, the Hankel minimum degree approximation [28].

The continuous state space representation for the reduced 8th order controller was found to be

$$A_{ARE} = \begin{bmatrix} -1169 & -375.2 & -527.4 & -188.1 & -187.3 & 53.2 & 61.6 & -97.51 \\ -421.2 & -135.1 & -189.9 & -68.34 & -68.22 & 19.21 & 22.35 & -35.28 \\ -651.5 & -207.8 & -300.3 & -129.7 & -121.4 & 36.29 & 35.54 & -58.15 \\ 159.6 & 53.25 & 69.65 & -8.824 & -13.38 & 6.571 & -3.015 & -0.5885 \\ 307.4 & 99.85 & 154.1 & 45.26 & 20.54 & -5.402 & -3.398 & 5.509 \\ -112.7 & -36.47 & -52.97 & -10.41 & -4.918 & -0.02023 & 1.938 & -1.055 \\ -43.5 & -14.32 & -15.57 & 5.485 & -3.266 & -1.455 & -2.13 & 5.76 \\ 107.8 & 35.06 & 43.85 & -2.594 & 3.589 & 3.602 & 3.54 & -14.09 \end{bmatrix}$$

$$B_{ARE} = \begin{bmatrix} -33.4 & -58.96 \\ -11.57 & -21.13 \\ -20.19 & -27.93 \\ 0.03327 & 8.544 \\ 6.293 & 12.74 \\ -2.221 & -4.959 \\ -0.3288 & -2.208 \\ 1.6 & 5.135 \end{bmatrix}$$

$$C_{ARE} = \begin{bmatrix} 4.957 & 1.738 & -3.914 & -3.519 & -0.5099 & 0.6712 & -0.02125 & -0.1742 \\ 112.2 & 35.33 & 48.69 & 15.49 & 14.42 & -4.276 & -4.946 & 7.875 \end{bmatrix}$$

$$D_{ARE} = \begin{bmatrix} -0.00743 & -0.01657 \\ 2.778 & 5.283 \end{bmatrix}$$

5.5.3 Simulation Results

Each of the three controllers was converted to discrete form using a Tustin bilinear transformation and this was used in simulation. Time responses for the PS, Riccati and eigenvalue tuned PI controller were compared. Figures 5.9 and 5.12 show the output response of the three controllers to a step torque disturbance of 3.7 ft lbf (5 Nm). A small decrease in the maximum overshoot, significantly better settlings times and a much less oscillatory response were found from the Riccati and PS controllers.

The Riccati designed controllers display similar time response behavior to the PS design. The improvements in time response compared to the eigenvalue based design can be observed from the control action in figures 5.11 and 5.14. Both the Riccati and PS make maximum use of the throttle control action available, which also results in faster fuel input.

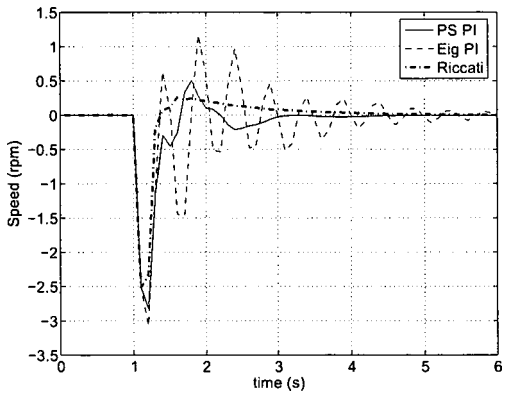

Figure 5.11: Speed response to a torque disturbance

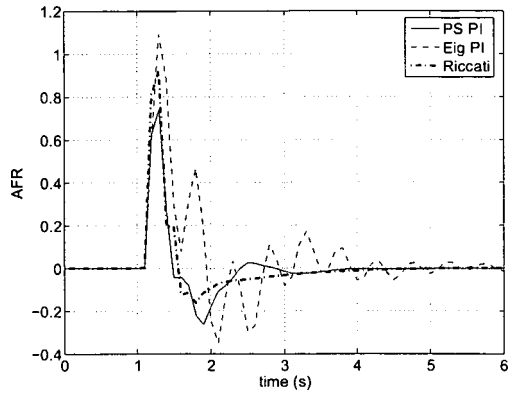

Figure 5.12: AFR response to a torque disturbance

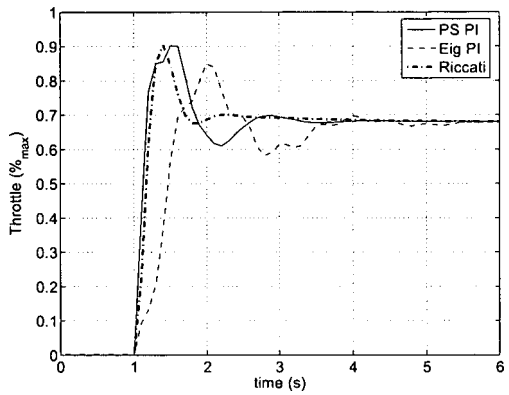

Figure 5.13: Throttle response due to a torque disturbance

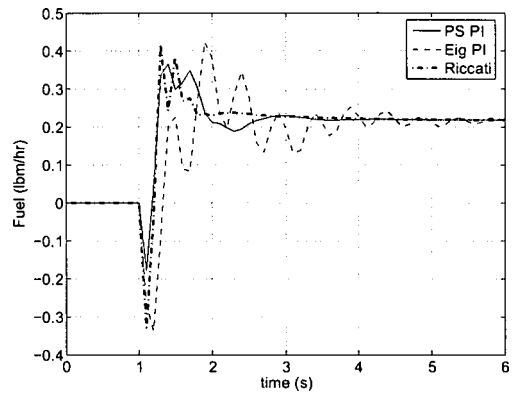

Figure 5.14: Fuel response due to a torque disturbance

During startup the tracking demand of the engine speed is often adjusted as the engine warms up. A step demand change to the speed command can be observed in figure 5.13 and the affect of this transient of the AFR channel can be seen in figure 5.16. It can again be seen that the PS and Riccati controllers are a significant improvement over the alternative PI design.

The maximum singular values of the primary sensitivity function are given in figure 5.17. No specific robustness constraint was included in the design specifications [40], however, it can be seen that the reduced 8th order Riccati controller has the greatest robustness. The PS technique was found to give similar robustness to the PI design based on the eigenvalue method, although marginally improved as can be observed from a lower absolute maximum singular value.

The disturbance rejection performance improvement of the PS design over the suggested eigenvalue designed PI controller is substantial for the same order controller and with similar levels of robustness. The Riccati design demonstrated very similar levels of performance

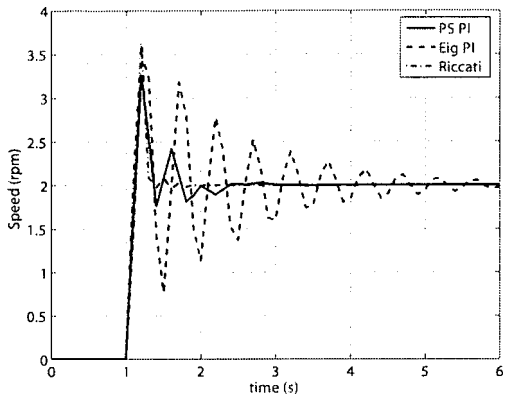

Figure 5.15: Speed response to a step demand

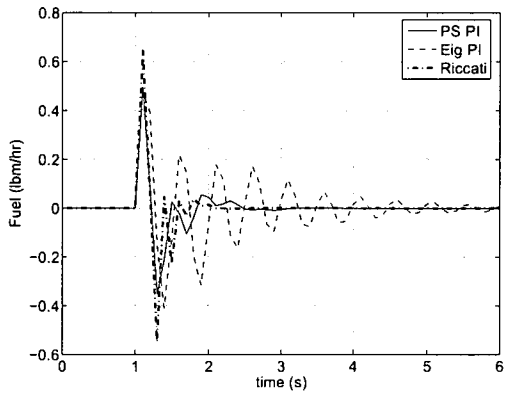

Figure 5.16: AFR response to a step demand change in speed

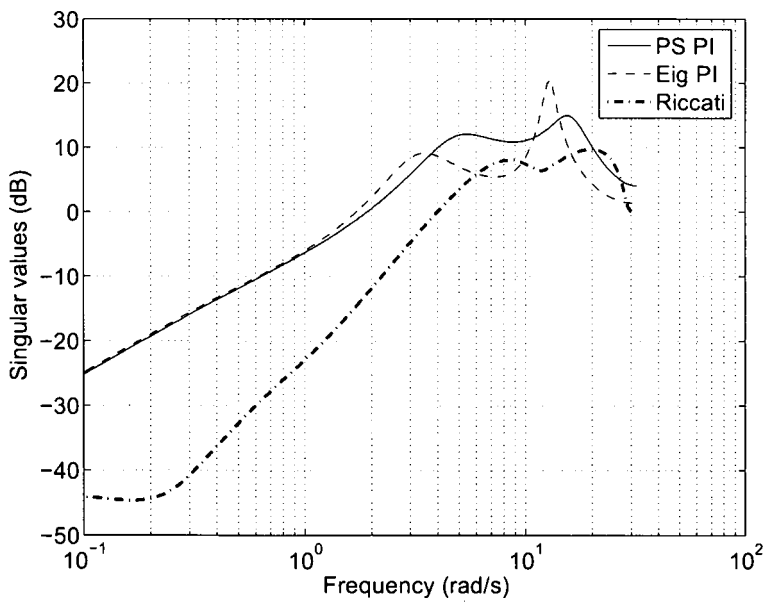

Figure 5.17: Primary sensitivity function of each controller

to the PS design, with the aforementioned benefit of additional robustness at the cost of a significantly higher order controller. It might be expected that it should be possible in any good design technique to easily sacrifice unnecessary robustness for increase in performance, however designer control over this trade-off in the Riccati design process was found to be more limited than in the PS technique due to the difficulties in choosing frequency domain weighting functions for time response criteria. Despite additional robustness, since the order of the Riccati design could not be reduced below 5th it could not be implemented in most current commercial EMS software. Furthermore, the selection of the weighting functions are much more difficult in the Riccati approach whereas the interactive PS methods allow for simpler weighting choices and more freedom to tune for time response.

5.6 Conclusions

The technique presented in this chapter allows for nominal performance and robust stability using MIMO $\mathcal{H}_\infty$ norm specifications on weighted sensitivity functions. The proposed method is uniformly adapted to producing controllers in continuous and discrete systems. The technique designs fixed, low order controllers through an interactive PS method for MIMO plants which are square and invertible in the input and output feedback channels. Regions satisfying the performance and stability constraints are superimposed graphically to give the designer insight in the design process.

The PS and Riccati methods were shown to give better time response performance for the same level of robust stability as an eigenvalue based PI tuning method.

A multivariable idle speed disturbance rejection example demonstrated that using the PS method to map just the primary sensitivity function to the parameter plane can yield large improvements over existing low order and reduced order controller design methods. The PS approach can yield performance close to a full order algebraic Riccati solution using a mixed primary and control sensitivity formulation. The PS and Riccati controller design techniques were shown to give better time response performance for the same level of robust stability as the eigenvalue PI tuning method.

When designing controllers the interactive nature of PS techniques allows the designer to select controller gains to meet time response criteria from a basic weighting function. This is in contrast to alternative techniques which require carefully selected weighting functions to achieve good time response. The PS method was shown to alleviate much of the difficulty in selecting the weighting functions since only a basic first order weighting function was required for the primary sensitivity.

Since production automotive EMS generally implement controllers through the use of low

order look-up tables, even the lowest order stable controller found using the $\mathcal{H}_\infty$ Riccati design techniques with order reduction methods is likely to be too high in order for implementation in standard EMS architectures and therefore a PS single sensitivity design technique would be preferable. Similar advantages to those obtained in the design example should accrue to the application of the PS design method in other industrial problems especially where low order or fixed structure controllers are required.

Chapter 6

Mixed Sensitivity Parameter Space Control

6.1 Introduction

Many powertrain applications require a good level of transient performance whilst at the same time demonstrating robustness. This robustness is required due to: system-to-system variation; the wide range of environmental conditions that the system must operate in; and, plant degradation over the lifespan of the vehicle. Furthermore, this 'performance in the presence of uncertainty' must generally be achieved with a limited amount of control action due to physical constraints on the hardware.

To achieve multiple constraints on a problem, it is usually necessary to use several weighted sensitivity constraints. For many design $\mathcal{H}_\infty$ techniques, including algebraic Riccati approaches multiple constraints are combined into a single $\mathcal{H}_\infty$ norm cost function by stacking the weighted sensitivity functions constraints. The $\mathcal{H}_\infty$ standard problem is expressed as

$$\left\| \begin{matrix} W_S S \\ W_T T \end{matrix} \right\|_\infty \leq 1$$

where W_S and W_T are weighting functions acting on the primary and complementary sensitivity functions S and T respectively. This combination of sensitivity functions can add conservatism into the design, since weighting functions are specifically designed to shape a single sensitivity function. For example, a controller could meet all the individual sensitivity requirements without satisfying the combined $\mathcal{H}_\infty$ norm

$$\begin{cases} W_S S \leq 0.9 \\ W_T T \leq 0.9 \end{cases} \quad \text{without satisfying} \quad \left\| \begin{matrix} W_S S \\ W_T T \end{matrix} \right\|_\infty \leq 1$$

Multiple sensitivity functions can readily be included in parameter space (PS) designs by superimposing each set of sensitivity bounds. Accordingly, the admissible region reduces to

the set of gains which simultaneously meet all the sensitivity constraints. Overlaying each of the sensitivity constraints on the parameter plane has the additional advantage of revealing to the designer any weighting choices which may be over constrained or problematic.

This chapter extends the multivariable PS technique presented in Chapter 5 to non-square systems. In addition left and right hand weighting functions are included in the theory for the full set of possible sensitivity functions. To accommodate high order controller design in the technique a method for including multiple controller elements is considered.

To highlight the significant benefits of multivariable control a simple example compares a SISO loop design to the multivariable technique developed here based on singular values.

A design procedure for minimising one of more sensitivity functions is detailed. This process is demonstated in a second comparative example which illustrates the capability of the technique both for direct design of low order, PID and fourth order controllers and for retuning a reduced order Riccati designed $\mathcal{H}_\infty$ controller, by application to a well known benchmark problem for an experimental highly maneuverable aircraft (HiMAT).

The organisation of this chapter is as follows. The complete set of sensitivity functions for all eight possible feedback transmissions is derived in section 6.2. Conditions necessary for internal stability based on the closed loop transmissions and the general singular value conditions for each sensitivity are given. Section 6.3.1 presents the controller structure and details the updating scheme when selecting controller coefficients and includes an extension for higher order controllers. Solutions for computing controller loci for the six unique sensitivity function are presented. A suggested design procedure for minimising sensitivity function(s) is given in section 6.4.4. The differences between single-input-single-output (SISO) loop designs and multiple-input-multiple-output (MIMO) controller designs is graphically presented in section 6.5. A sensitivity minimisation design for the benchmark problem for an experimental highly maneuverable aircraft (HiMAT) is shown in section 6.6. The merits of the PS technique for direct controller design and retuning reduced order controllers are evaluated and compared with full order algebraic Riccati designs. Some concluding remarks are given in section 6.7.

6.2 System Requirements

This section derives the full set of possible sensitivity functions which can be considered for controller design purposes.

In the sequel we will consider the negative unity feedback system of figure 6.1 with plant G and feedback controller K. Since the method presented in the sequel uses only the non-parametric frequency response of the plant, both discrete and continuous systems can be

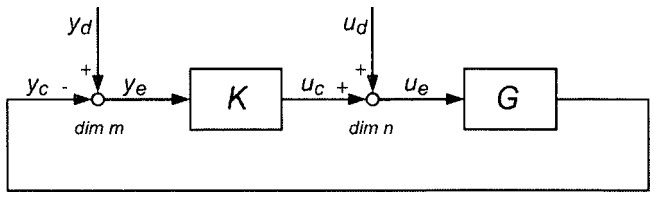

Figure 6.1: Negative unity feedback control block diagram

handled uniformly, however for simplicity of exposition we will present only the continuous case. Accordingly let the plant be characterised by an $n \times m$ non parametric frequency response matrix $G(j\omega) = [G_{i,j}(j\omega)]$ where ideally $\omega \in [0, +\infty)$ but which in practice will be characterised at carefully chosen [15] discrete frequencies $\omega \in \Omega = \{\omega_1, \omega_2, \ldots, \omega_N\}$. Throughout the paper we will consider the controller to be designed to be characterised by a $m \times n$ continuous rational transfer function matrix $K = [K_{i,j}(s)]$.

6.2.1 Internal Stability

Internal stability of a system requires that all transmissions of inputs to nodes in the feedback loop are stable. The conditions are normally stated in either state-space form or in terms of coprime polynomial representations of the controller and plant. In the case of the parameter-space design of systems of non-parametric frequency response transmissions (possibly irrational transfer functions), internal stability is more appropriately established in terms of the complete set of system closed loop transmissions.

For the linear irrational negative unity feedback system of figure 6.1, by exhaustion, internal stability is completely determined by the stability of the six transmissions

$$y_d \rightarrow y_e \;:\; S = [I + GK]^{-1} \tag{6.1}$$

$$y_d \rightarrow y_c \;:\; T = GK[I + GK]^{-1} \tag{6.2}$$

$$y_d \rightarrow u_c, u_e \;:\; U = K[I + GK]^{-1} \tag{6.3}$$

$$u_d \rightarrow u_e \;:\; Q = [I + KG]^{-1} \tag{6.4}$$

$$u_d \rightarrow u_c \;:\; R = KG[I + KG]^{-1} \tag{6.5}$$

$$u_d \rightarrow y_c, y_e \;:\; V = G[I + KG]^{-1} \tag{6.6}$$

for which the associated sensitivity functions are termed: Primary S, Complementary T, Control-Effort U, Dual-Primary Q, Dual-Complementary R and Plant Input Disturbance V.

Now since $GK[I + GK]^{-1} = I - [I + GK]^{-1}$, stability of $[I + GK]^{-1}$ establishes the stability of $GK[I + GK]^{-1} = [I + GK]^{-1}GK$. Similarly stability of $[I + KG]^{-1}$ establishes the stability of $KG[I + KG]^{-1} = [I + KG]^{-1}KG$. Thus (as is well known for rational finite

state space systems [100, 115]), internal stability is established solely by the stability of the four transmissions

$$[I + GK]^{-1} \tag{6.7}$$

$$K[I + GK]^{-1} = [I + KG]^{-1}K \tag{6.8}$$

$$[I + KG]^{-1} \tag{6.9}$$

$$G[I + KG]^{-1} = [I + GK]^{-1}G \tag{6.10}$$

Now the stability of a MIMO transfer function is determined from the irrational system multivariable Nyquist criterion [23, 32] by the encirclements and intersections of the origin by $|I + L(j\omega)|$. For G, $n \times m$, and K, $m \times n$, the eigenvalues of $I + L$ for $L = GK$ and $L = KG$ are identical excepting for $|n - m|$ eigenvalues at unity. Consequently the stability boundaries found from both $|I + L(j\omega)| = 0$ (or equivalently $\bar{\sigma}(I + L(j\omega)) = 0$) are identical. Internal stability can thus be established solely by the transmissions 6.7, 6.8 and 6.10.

6.2.2 Sensitivity Constraints

In application of $\mathcal{H}_\infty$ methods, general closed loop system performance including transient performance and stability robustness are formulated by weighted sensitivity function constraints. In general a sensitivity function F, determined by G and K, will be weighted on both the left and the right by invertible weighting function matrices W and M. In general they may be required to be bounded from both above [46, 100, 115] or below [65] according to

$$\underline{\gamma} \leq ||W(j\omega)F(j\omega)M(j\omega)|| \leq \overline{\gamma} \quad \forall\, \omega \in [0; +\infty) \tag{6.11}$$

with different weighting functions generally applied to the upper and lower constraints.

For ease of exposition we will discuss only constraints, $\gamma = \overline{\gamma}$, from above [1]. In order to ensure internal stability it is only necessary to consider three sensitivity functions as above. On the other hand for general performance design constraints, although it is often found necessary to consider only two or three sensitivity functions, in practice constraints on all six sensitivity functions, equations 6.1 to 6.6 can on occasion be found to be necessary.

At any discrete frequency there exists a complex locus that divides the parameter space into two distinct sets, one of which contains the admissible solution. The boundary condition leading to these sets is found from the complex controller loci for a sensitivity function F meeting the condition set by left and right weighting functions W and M. This is done by inspection of the maximum singular values.

[1] In fact the proposed MIMO method of this thesis can be used to give both upper and lower boundaries.

Subsuming the iterating parameter γ in the weighting functions, by the continuity of eigenvalues with respect to matrix parameters [13] the non-singular parameter boundary conditions for upper sensitivity function constraints of equation 6.11 for K can be determined by the solution of the equality

$$\overline{\sigma}(W(j\omega)F(j\omega)M(j\omega)) = 1, \quad \forall\, \omega \in [0; +\infty) \tag{6.12}$$

For evaluation purposes this is evaluated for $\forall\ \omega \in \Omega$ on a finite set Ω of N frequencies where, as mentioned earlier, the number and range of particular frequencies depends upon the application complexity and dynamics. Dropping reference to the arbitrary frequency point ω under consideration we can write equation 6.12 as either one of the eigenvalue equalities

$$\overline{\lambda}(M^*F^*W^*WFM) = 1$$

or

$$\overline{\lambda}(WFMM^*F^*W^*) = 1$$

Now the solutions to these equalities are each one of the solutions from the set of m or n solutions respectively of the determinant equations

$$\left|M^{-1}F^{-1}W^{-1}W^{*-1}F^{*-1}M^{-1} - I\right| = 0 \tag{6.13}$$

or

$$\left|W^{*-1}F^{*-1}M^{-1}M^{-1}F^{-1}W^{-1} - I\right| = 0 \tag{6.14}$$

6.3 Controller Structure and Constraint Locus

6.3.1 Controller Updating Scheme

The proposed interactive design method is an iterative scheme, in common with other parameter space approaches, in which the parameterised $m \times n$ fixed order rational transfer function controller matrix $K(s) = [K_{i,j}(s)]$ is updated. The proposed update scheme is of the form

$$K(s) = k(s)E(s) + K_0(s) \tag{6.15}$$

where $K_0(s)$ is an initial controller, $K(s)$ the resulting updated controller, and $k(s)$ a parameterised scalar transfer function component which is located by some fixed basis matrix $E(s)$, where $E(s)$ is of rank one at each frequency $s = j\omega;\ \forall\, \omega \in [0, \infty)$.

For the remainder of the chapter we will use the basis $E = [\delta_{i,j}]$, and $K(s)$ will consist of elements $K_{i,j}(s)$ comprising of M second order elemental controllers [15] of the form

$$K_{i,j}(s) = \sum_{k=1}^{M} K_{i,j,k}(s)$$

where

$$K_{i,j,k}(s) = \frac{b_{2_{ijk}}s^2 + b_{1_{ijk}}s + b_{0_{ijk}}}{a_{2_{ijk}}s^2 + a_{1_{ijk}}s + a_{0_{ijk}}} \tag{6.16}$$

For physical implementation we will in practice deal here only with proper controllers [2] and so by convention choose $a_{2_{ijk}} = 1$. At each iteration $K_0(s)$ will accordingly be reintialised to $K(s)$, except at the chosen element location i, j where it is set to zero.

The complex locus k corresponding to the sensitivity constraint boundaries which are determined by the initial controller and plant matrices K_0 and G are mapped to the parameter planes of $k(s)$. In the sequel it is shown that for any update scheme of the form of 6.15, at a particular frequency, the problem of finding k for equation 6.13 or 6.14 to be satisfied can always be reduced to a generalised Hermitian matrix pencil problem, either of the form

$$|A + kBE + k^*E^*B^* + kk^*E^*CE| = 0 \tag{6.17}$$

or of the form

$$\left|\bar{A} + kE\bar{B} + k^*\bar{B}^*E^* + kk^*E\bar{C}E^*\right| = 0 \tag{6.18}$$

Both equations 6.17 and 6.18 are found to have particularly convenient structures due to the rank deficient nature of E (refer to section 6.3.8).

6.3.2 Primary Sensitivity S

For constraints on the primary sensitivity function $S = [I + GK]^{-1}$ shaped by suitable left and right performance weighting functions W_S and M_S such that

$$||W_S S M_S|| \leq 1$$

the nonsingular parameter boundary condition is

$$\overline{\sigma}(W_S[I + GK]^{-1}M_S) = 1 \tag{6.19}$$

Equation (6.19) is equivalent to the eigenvalue equality

$$\overline{\lambda}(M_S^*[I + KG]^{*-1}W_S^{*-1}W_S[I + GK]M_S) = 1$$

which may be solved by identifying the appropriate solution for K of

$$|[I + GK]^*M_S^{*-1}M_S^{-1}[I + GK] - W_S^*W_S| = 0 \tag{6.20}$$

Now making the substitution for $K = kE + K_0$ equation 6.20 may then be rewritten as

$$\begin{aligned} &| \,[I + GK_0]^*M_S^{*-1}M_S^{-1}[I + GK_0] - W_S^*W_S \\ &+ k[I + K_0^*G^*]M_S^{*-1}M_S^{-1}GE \\ &+ k^*E^*G^*M_S^{*-1}M_S^{-1}[I + GK_0] \\ &+ kk^*E^*G^*M_S^{*-1}M_S^{-1}GE \,| = 0 \end{aligned}$$

[2] though not mathematically necessary

Hence for this case the matrices A, B and C of equation 6.17 for the primary sensitivity function constraint are

$$A = [I + GK_0]^* M_S^{*-1} M_S^{-1} [I + GK_0] - W_S^* W_S \quad (6.21)$$

$$B = [I + K_0^* G^*] M_S^{*-1} M_S^{-1} G \quad (6.22)$$

$$C = G^* M_S^{*-1} M_S^{-1} G \quad (6.23)$$

6.3.3 Complementary Sensitivity T

For constraints on the complementary sensitivity function $T = GK[I + GK]^{-1}$ shaped by suitable left and right performance weighting functions W_T and M_T such that

$$||W_T T M_T|| \leq 1$$

the nonsingular parameter boundary condition is

$$\overline{\sigma}(W_T GK[I + GK]^{-1} M_T) = 1 \quad (6.24)$$

Equation 6.24 is equivalent to the eigenvalue equality

$$\overline{\lambda}(M_T^*[I + GK]^{*-1} K^* G^* W_T^* W_T GK[I + GK]^{-1} M_T) = 1 \quad (6.25)$$

which may be solved by identifying the appropriate solution of

$$|[I + GK]^* M_T^{*-1} M_T^{-1} [I + GK] - K^* G^* W_T^* W_T GK| = 0 \quad (6.26)$$

which is equivalent to

$$|M_T^{*-1} M_T^{-1} + M_T^{*-1} M_T^{-1} GK + K^* G^* M_T^{*-1} M_T^{-1} + K^* G^* [M_T^{*-1} M_T^{-1} - W_T^* W_T] GK| = 0 \quad (6.27)$$

Hence for this case by making the substitution for $K = kE + K_0$ the matrices A, B and C of equation 6.17 for the weighted complementary sensitivity function constraint are found to be

$$A = K_0^* G^* W_T^* W_T GK_0 - [I + GK_0]^* M_T^{*-1} M_T^{-1} [I + GK_0] \quad (6.28)$$

$$B = M_T^{*-1} M_T^{-1} G + K_0^* G^* [M_T^{*-1} M_T^{-1} - W_T^* W_T] G \quad (6.29)$$

$$C = E^* G^* [M_T^{*-1} M_T^{-1} - W_T^* W_T] GE \quad (6.30)$$

6.3.4 Control Effort Sensitivity U

For constraints on the control effort sensitivity function $U = K[I + GK]^{-1}$ shaped by suitable left and right performance weighting functions W_U and M_U such that

$$||W_U U M_U|| \leq 1$$

the nonsingular parameter boundary condition is

$$\overline{\sigma}(W_U K[I+GK]^{-1}M_U) = 1$$

This has an equivalent eigenvalue equality

$$\overline{\lambda}(M_U^*[I+GK]^{*-1}K^*W_U^*W_U K[I+GK]^{-1}M_U) = 1$$

which may be solved by identifying the appropriate solution of

$$|[I+GK]^*M_U^{*-1}M_U^{-1}[I+GK] - K^*W_U^*W_U K| = 0$$

or equivalently

$$|M_U^{*-1}M_U^{-1} + M_U^{*-1}M_U^{-1}GK + K^*G^*M_U^{*-1}M_U^{-1} + K^*[G^*M_U^{*-1}M_U^{-1}G - W_U^*W_U]K| = 0$$

Hence for this case by making the substitution for $K = kE + K_0$ the matrices A, B and C of equation 6.17 for the weighted control effort sensitivity function constraint are

$$A = [I+GK_0]^*M_U^{*-1}M_U^{-1}[I+GK_0] \quad (6.31)$$

$$B = M_U^{*-1}M_U^{-1}G + K_0^*[G^*M_U^{*-1}M_U^{-1}G - W_U^*W_U] \quad (6.32)$$

$$C = [G^*M_U^{*-1}M_U^{-1}G - W_U^*W_U] \quad (6.33)$$

6.3.5 Plant Input Sensitivity V

For constraints on the plant input sensitivity function $V = G[I+KG]^{-1}$ shaped by suitable left and right performance weighting functions W_V and M_V such that

$$||W_V V M_V|| \leq 1$$

the nonsingular parameter boundary condition is

$$\overline{\sigma}[W_V G[I+KG]^{-1}M_V] = 1$$

which has an equivalent eigenvalue equality

$$\overline{\lambda}(M_V^*[I+KG]^{*-1}G^*W_V^*W_V G[I+KG]^{-1}M_V) = 1$$

This may be solved by identifying the appropriate solution of

$$|[I+KG]^*M_V^{*-1}M_V^{-1}[I+KG] - G^*W_V^*W_V G| = 0$$

or equivalently

$$|M_V^{*-1}M_V^{-1} + KGM_V^{*-1}M_V^{-1} + M_V^{*-1}M_V^{-1}G^*K^* + KGM_V^{*-1}M_V^{-1}G^*K^* - G^*W_V^*W_V G| = 0$$

Hence for this case by making the substitution for $K = kE + K_0$ the matrices $\bar{A}, \bar{B}$ and $\bar{C}$ of equation 6.18 for the weighted plant input sensitivity function constraint are found to be

$$\bar{A} = [I+K_0G]^*M_V^{*-1}M_V^{-1}[I+K_0G] - G^*W_V^*W_V G \quad (6.34)$$

$$\bar{B} = GM_V^{*-1}M_V^{-1}[I+G^*K_0^*] \quad (6.35)$$

$$\bar{C} = GM_V^{*-1}M_V^{-1}G^* \quad (6.36)$$

6.3.6 Dual Primary Sensitivity Q

For constraints on the dual primary sensitivity function $Q = [I + KG]^{-1}$ shaped by suitable left and right performance weighting functions W_Q and M_Q such that

$$||W_Q Q M_Q|| \leq 1$$

the nonsingular parameter boundary condition is

$$\overline{\sigma}[W_Q[I + KG]^{-1} M_Q] = 1$$

This has an equivalent eigenvalue equality

$$\overline{\lambda}(W_Q[I + KG]^{-1} M_Q M_Q^* [I + KG]^{*-1} W_Q^*) = 1$$

which may be solved by identifying the appropriate solution of

$$|[I + KG] W_Q^{-1} W_Q^{*-1} [I + KG]^* - M_Q M_Q^*| = 0$$

or equally

$$|W_Q^{-1} W_Q^{*-1} + KG W_Q^{-1} W_Q^{*-1} + W_Q^{-1} W_Q^{*-1} G^* K^* + KG W_Q^{-1} W_Q^{*-1} G^* K^* - M_Q M_Q^*| = 0$$

Hence for this case by making the substitution for $K = kE + K_0$ the matrices $\bar{A}, \bar{B}$ and $\bar{C}$ of equation 6.18 for the weighted plant input sensitivity function constraint are

$$\bar{A} = [I + K_0 G] W_Q^{-1} W_Q^{*-1} [I + K_0 G]^* - M_Q M_Q^* \quad (6.37)$$

$$\bar{B} = G W_Q^{-1} W_Q^{*-1} [I + G^* K_0^*] \quad (6.38)$$

$$\bar{C} = G W_Q^{-1} W_Q^{*-1} G^* \quad (6.39)$$

6.3.7 Dual Complementary Sensitivity R

For constraints on the dual complementary sensitivity function $R = [I + KG]^{-1} KG$ shaped by suitable left and right performance weighting functions W_R and M_R such that

$$||W_R R M_R|| \leq 1$$

the nonsingular parameter boundary condition is

$$\overline{\sigma}[W_R[I + KG]^{-1} KG M_R] = 1$$

which has an equivalent eigenvalue equality

$$\overline{\lambda}(W_R[I + KG]^{-1} KG M_R M_R^* G^* K^* [I + KG]^{*-1} W_R^*) = 1$$

This may be solved by identifying the appropriate solution of

$$|[I + KG]W_R^{-1}W_R^{*-1}[I + KG]^* - KGM_RM_R^*G^*K^*| = 0$$

or equivalently

$$|W_R^{-1}W_R^{*-1}+KGW_R^{-1}W_R^{*-1}+W_R^{-1}W_R^{*-1}G^*K^*+KGW_R^{-1}W_R^{*-1}G^*K^*-KGM_RM_R^*G^*K^*| = 0$$

Hence for this case by making the substitution for $K = kE + K_0$ the matrices $\bar{A}, \bar{B}$ and $\bar{C}$ of equation 6.18 for the weighted plant input sensitivity function constraint are

$$\bar{A} = [I + K_0G]W_R^{-1}W_R^{*-1}[I + K_0G]^* - K_0GM_RM_R^*G^*K_0^* \quad (6.40)$$

$$\bar{B} = GW_R^{-1}W_R^{*-1}[I + G^*K_0^*] - GM_RM_R^*G^*K_0^* \quad (6.41)$$

$$\bar{C} = G[W_R^{-1}W_R^{*-1} - M_RM_R^*]G^* \quad (6.42)$$

6.3.8 Complex Controller Bounds

The controller bounds are found by solving the determinant equation for each sensitivity of interest. Accordingly it is necessary to consider solutions of equations in the formats 6.17 and 6.18.

Case 1

For any rank one $p \times p$ matrix E there exists a full rank $p \times p$ matrix $\tilde{E}$ so that $E\tilde{E}$ is a matrix of structure $[e|0(p \times p - 1)]$, that is with zero elements excepting for the first column. In this case it is possible to determine the solutions for equation 6.17 from

$$\left|\tilde{E}^*A\tilde{E} + k\tilde{E}^*BE\tilde{E} + k^*\tilde{E}^*E^*B^*\tilde{E} + kk^*\tilde{E}^*E^*CE\tilde{E}\right| = 0 \quad (6.43)$$

Because of the resulting structure the coefficient matrices of equation 6.43 can then be partitioned as

$$\tilde{E}^*A\tilde{E} = \begin{bmatrix} a_{11} & a_{21}^* \\ a_{21} & A_{22} \end{bmatrix}, \quad \tilde{E}^*BE\tilde{E} = \begin{bmatrix} b_{11} & 0_{12} \\ b_{21} & 0_{22} \end{bmatrix}, \quad C = \begin{bmatrix} c_{11} & 0_{12} \\ 0_{21} & 0_{22} \end{bmatrix}.$$

which in the determinant equation becomes

$$\begin{vmatrix} a_{11} + kb_{11} + k^*b_{11}^* + kk^*c_{11} & a_{21}^* + k^*b_{21} \\ a_{21} + kb_{21} & A_{22} \end{vmatrix} = 0 \quad (6.44)$$

By virtue of the occurrence of nonsingular right weighting terms of the form $M^{*-1}M^{-1}$in A, then either $|A_{22}| \neq 0$ or this can be obtained by an arbitrarily small perturbation[3] of this nonsingular term. and therefore the solution to equation 6.44 is equivalent to

$$a + kb + k^*b^* + kk^*c = 0 \quad (6.45)$$

[3]In practice such a perturbation appears to be almost always unnecessary.

where a and c are real

$$a = a_{11} - a_{21}^{*} A_{22}^{-1} a_{21} \qquad ; \qquad c = c_{11} - b_{21}^{*} A_{22}^{-1} b_{21}$$

and b is complex

$$b \equiv b_R + j b_I = b_{11} - a_{21}^{*} A_{22}^{-1} b_{21}$$

Thus with $k = k_R + j k_I$ equation6.45 is equivalent to the real coefficient equation:

$$a + 2k_R b_R - 2k_I b_I + (k_R^2 + k_I^2) c = 0 \tag{6.46}$$

which is the equation of a conic section [15] defining the complex controller bounds k_R and k_I for the controller k associated with the basis matrix E.

Case 2

Now also for any rank one $p \times p$ matrix E there exists a full rank $p \times p$ matrix $\bar{E}$ so that $\bar{E}E$ is a matrix of structure $[e|0(p \times p - 1)]^T$, that is with zero elements excepting for the first row. In this case it is possible to determine the solutions for equation 6.18 from

$$\left| \bar{E}\bar{A}\bar{E}^{*} + k\bar{E}E\bar{B}\bar{E}^{*} + k^{*}\bar{B}^{*}E^{*}\bar{E}^{*} + kk^{*}\bar{E}E\bar{C}E^{*}\bar{E}^{*} \right| = 0 \tag{6.47}$$

Because of the resulting structure the coefficient matrices of equation(6.47 can then be partitioned as

$$\bar{E}\bar{A}\bar{E}^{*} = \begin{bmatrix} a_{11} & a_{21}^{*} \\ a_{21} & A_{22} \end{bmatrix}, \quad \bar{E}E\bar{B}\bar{E}^{*} = \begin{bmatrix} b_{11} & b_{12} \\ 0_{21} & 0_{22} \end{bmatrix}, \quad \bar{E}E\bar{C}E^{*}\bar{E}^{*} = \begin{bmatrix} c_{11} & 0_{12} \\ 0_{21} & 0_{22} \end{bmatrix}.$$

which results again in a conic equation in the k_R and k_I, for controller bounds, of the form of 6.46 where now a and c are the reals

$$a = a_{11} - a_{21}^{*} A_{22}^{-1} a_{21} \qquad ; \qquad c = c_{11} - b_{12} A_{22}^{-1} b_{12}^{*}$$

and b is the complex

$$b \equiv b_R + j b_I = b_{11} - b_{12} A_{22}^{-1} a_{21}$$

6.4 Controller Parameter Plane Mapping and Design

6.4.1 Element Selection and Multiple Controller Elements

The conic sections defined by equation 6.46, with the coefficients of Case 1 and Case 2 above, have an circular solution since there is no cross product term $k_R k_I$ and both k_R^2 and k_I^2 share the same coefficient c. The solutions to such conics which constitute the complex controller

boundaries may be conveniently determined by trigonometric parameterization over a range of discrete points $\theta \in [0, 2\pi)$.

In the case of finding the complex gains for an element in a specific row and column of the controller, that is when using $E = [\delta_{i,j}]$, the result allows a complex locus $K_{i,j}(j\omega)$ to be plotted for any element i, j of the $m \times n$ controller matrix frequency response $K = [K_{i,j}(j\omega)]$. A locus is produced for each sensitivity function constraint. To determine the appropriate locus for mapping any chosen elemental controller $K_{i,j,\hat{k}}$ from M elemental controllers it is necessary to divide the locus by the response of the other fixed controller elements so that we use

$$K_{i,j}(j\omega)/\Pi_{k=1,k\neq\hat{k}}^{M} K_{i,j,k}(j\omega)$$

as the mapping locus for the $\hat{k}$th elemental controller.

6.4.2 Mapping Constraint Boundaries to the Parameter Plane

The complex controller bounds determined by the conic equations 6.46 can now be mapped into convenient parameter planes by equating the complex gains to the controller element defined in equation 6.16. For a continuous controller we make the substitution $s = j\omega$ and denoting the circular mapping locus for the required elemental controller $k_R(j\omega) + jk_I(j\omega)$ the parameter planes are then determined from

$$k(j\omega) = \frac{b_2\omega^2 + jb_1\omega + b_0}{a_2\omega^2 + ja_1\omega + a_0} = \frac{(b_0 - b_2\omega^2 + jb_1\omega)(a_0 - a_2\omega^2 - ja_1\omega)}{(a_0 - a_2\omega^2 + ja_1\omega)(a_0 - a_2\omega^2 - ja_1\omega)}$$

from which

$$k_R(j\omega) = \frac{(b_0 - b_2\omega^2)(a_0 - a_2\omega^2) + b_1a_1\omega^2}{(a_0 - a_2\omega^2)^2 + a_1^2\omega^2} \tag{6.48}$$

$$k_I(j\omega) = \frac{-a_1\omega(b_0 - b_2\omega^2) + b_1\omega(a_0 - a_2\omega^2)}{(a_0 - a_2\omega^2)^2 + a_1^2\omega^2} \tag{6.49}$$

where for the continuous case one coefficient must be an odd power of s and the other coefficient be an even power of s. The odd and even pairs (b_0, b_1), (b_1, b_2) and (a_1, a_0) are particularly useful. Similar results can be obtained for mapping discrete controllers.

6.4.3 Stability Boundaries

Complex loci defining stability bounds can be determined from the generalised Nyquist criterion [23, 32] and boundaries derived using the method for the sensitivities, although non-singular boundaries coincide with the centre of the sensitivity function solutions and therefore are generally not necessary. However, singular boundaries and conditions for ω at 0 and ∞ need to be considered. A detailed study of these conditions is described in [92], which presents

the conditions by which parameter plane axes may become stability boundaries. The principal singular boundary occurs as a zero frequency singular boundary due to the use of integral control action, and makes all zero integral gain axes stability boundaries.

6.4.4 Design Procedure

For controller design purposes the results for each of the discrete frequencies $\omega \in \Omega$ over the range of interest, are superimposed onto a single parameter plane. Each of the ellipses divides the plane into two regions. Testing the centre of the conic section can determine which side of the boundary the solution lies on [15]. Superimposing the boundaries for different weighting functions onto the same plane allows the designer to find a multiple sensitivity constraint solution.

Once the region satisfying all the frequencies has been identified the designer is able to select a set of gains. An obvious approach adopted by both [14] and [88] is to use either a manual or numerical optimisation technique to maximise some multiplier γ acting on the weighting function. A significant advantage of the parameter plane method in such an optimisation problem is that it can reveal convexity in the constraints. The optimisation approach adopted here involves selecting the gains at the centre of each permissible region. Once a pair of controller coefficients are selected these are then incorporated in the fixed part of the controller, K_0. With the updated controller the designer can then either select a different element to tune or a different pair of controller gains.

The method to maximise γ for a given specification is then:

1. Start with a stabilising controller. For a stable plant the start controller can be $K = 0$, that is $b_{2ij} = b_{1ij} = b_{0ij} = 0$. If the plant is unstable the parameter partitions may be used to first obtain a stabilising start controller. Choose a low initial value of γ.

2. Select a controller row-column and parameter pair combination which is admissible in the fixed structure.

3. Select a pair of parameters values from the geometric centre of the admissible region.

4. Iterate between the planes for any admissible controller row-column and any admissible parameter pair combinations selecting new controller row-column and parameter pair combinations. Return to step 3 unless the parameter planes have been exhausted.

5. If possible increase γ a small enough amount to ensure increased specifications can be met for all frequencies. Stop if the admissible region shrinks to the empty set and specifications can not be tightened further or if sufficient performance is achieved.

6. Return to step 2.

6.5 Comparison of SISO and MIMO Techniques

SISO methods can be used to design controllers for MIMO systems by sequential loop design. Using such a sequential loop design the loop function for the system is calculated with all but the current controllers in place. The designer works through one loop at a time ensuring performance or robustness in that specific loop. However, it is known that SISO methods cannot assure optimal levels of robustness in MIMO systems by this approach since they ignore variations which simultaneously affect multiple loops [33]. In fact in such a scheme PS SISO techniques have unique advantageous features over other SISO methods since multiple loop functions can be mapped onto the same parameter plane. Nevertheless SISO techniques only bound the gain of that particular loop [78] and no SISO methodology can guarantee an optimised level of robustness. True MIMO design methods based on the multivariable system norm are required. This can be illustrated by comparing the MIMO parameter space method developed above with a SISO PS method.

Consider the 2 x 2 plant transfer function matrix (taken from [33])

$$G(s) = \begin{bmatrix} \frac{-47s+2}{(s+1)(s+2)} & \frac{56s}{(s+1)(s+2)} \\ \frac{-42s}{(s+1)(s+2)} & \frac{-47s+2}{(s+1)(s+2)} \end{bmatrix}$$

One obvious stabilising feedback controller is

$$K = \begin{bmatrix} K_1 & 0 \\ 0 & K_2 \end{bmatrix} = \begin{bmatrix} 1 & 0 \\ 0 & 1 \end{bmatrix} \tag{6.50}$$

In this example consider the case that the primary sensitivity function is required in the design to give a guaranteed robustness across all frequencies and that the chosen primary sensitivity weighting function is $W_S = 0.2$. Assuming the current controller to be the stabilising controller of equation 6.50, as in [33], parameter planes for K_1 can be plotted using the multivariable approach above or alternatively using a SISO method such as [15, 86] and considering *both* SISO loops affected by the controller element.

Figure 6.2 shows the SISO parameter plane for $b_1 = k_P$ and $b_o = k_I$. Shown are permissible regions for selecting PI controller gains to meet the weighting function constraints. With the benefit of the PS superposition, boundaries for both outputs are overlaid. The first is for selecting gains to limit the maximum singular values for the y_1 output loop. The second is for the same controller for the y_2 loop. The parameter plane for the same controller element using the gains of the maximum singular value of the MIMO system rather than SISO loops is presented in figure 6.3. If we now consider the highest permissible proportional gain suggested

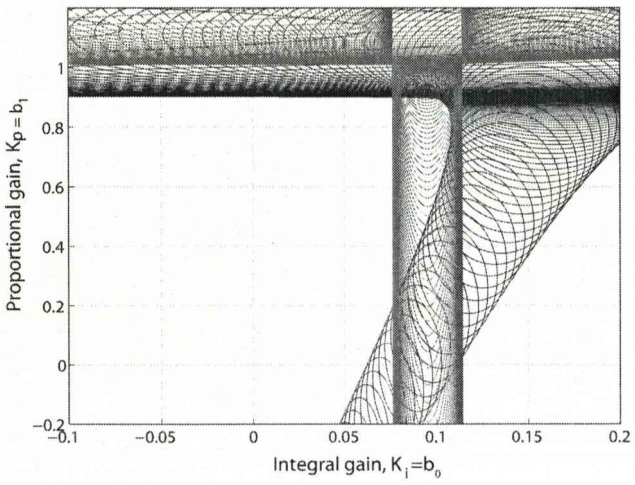

Figure 6.2: SISO parameter plane

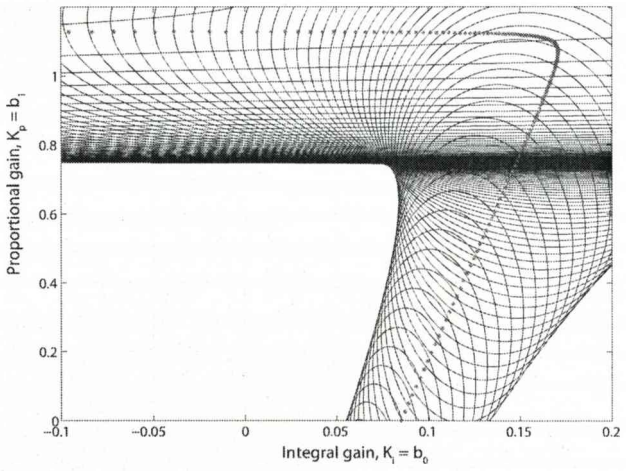

Figure 6.3: MIMO parameter plane

by both techniques it can be seen that the maximum gain from the MIMO parameter plane is significantly lower than that of the SISO technique. Accordingly the resulting robustness would therefore be significantly lower using the loop at a time technique. A plot showing maximum singular values of the primary sensitivity functions for both controllers together with the weighting function used for both designs is depicted in figure 6.4.

6.6 Design Example - HiMAT

A 2 × 2-pitch axis controller problem for an experimental highly maneuverable aircraft, HiMAT is taken from [28]. Only the longitudinal dynamics of the aircraft are considered in the

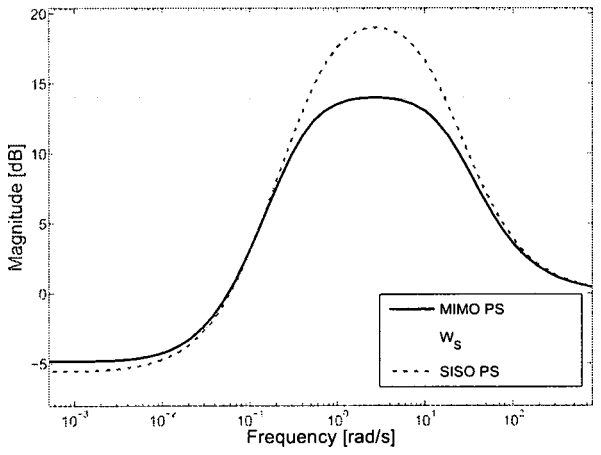

Figure 6.4: Maximum singular values using proportional gain from MIMO and SISO parameter planes

trimmed condition at 25,000 ft and 0.9 Mach. For this flight condition the linear model is unstable. State-space matrices describing the plant dynamics are given as:

$$A = \begin{bmatrix} -0.022567 & -36.617 & -18.897 & -32.090 & 3.2509 & -0.76257 \\ 9.2572 \times 10^{-5} & -1.8997 & 0.98312 & -0.00072562 & -0.17080 & -0.0049652 \\ 0.012338 & 11.720 & -2.6316 & 0.00087582 & -31.604 & 22.396 \\ 0 & 0 & 1 & 0 & 0 & 0 \\ 0 & 0 & 0 & 0 & -30 & 0 \\ 0 & 0 & 0 & 0 & 0 & -30 \end{bmatrix}$$

$$B = \begin{bmatrix} 0 & 0 \\ 0 & 0 \\ 0 & 0 \\ 0 & 0 \\ 30 & 0 \\ 0 & 30 \end{bmatrix}$$

$$C = \begin{bmatrix} 0 & 1 & 0 & 0 & 0 & 0 \\ 0 & 0 & 0 & 1 & 0 & 0 \end{bmatrix}$$

The given singular value design specifications [28] are:

1. Robustness : -40 db/decade roll-off and at least -20 db at 100 rad/s.
2. Performance: Minimise the primary sensitivity function as much as possible.

The primary sensitivity weighting function is given as

$$W_S = \gamma_S \begin{bmatrix} \frac{s+100}{100s+1} & 0 \\ 0 & \frac{s+100}{100s+1} \end{bmatrix} \tag{6.51}$$

and a suitable complementary sensitivity weighting function to meet the robustness requirements given as

$$W_T = \gamma_T \begin{bmatrix} \frac{s^2}{1000} & 0 \\ 0 & \frac{0.5\times10^{-3}+s^2}{1000} \end{bmatrix} \tag{6.52}$$

It is emphasised that for comparative purposes, as in [28], subject to item 1 being satisfied the sole objective here is the minimisation in item 2, without regard to any further engineering considerations. The example is used to determine the difficulties in applying optimal control methods if constraints are made on the controller order. To investigate the effects of pure time delays on the system outputs due to possible transport lags, actuator dead-times and computation delays, in a second case delays of 0.01s and 0.02s are applied to outputs 1 and 2 respectively. A second order Padé approximation is used to estimate the delay when performing the Riccati controller designs.

6.6.1 2nd Order PS Controller

For the case with no time delay a 2nd order PS controller was designed element by element using $E = [\delta_{i,j}]$. To constrain the controller to 2nd order the denominator coefficients are fixed with $a_2 = 1$, $a_1 = 10$, $a_0 = 0$. Starting with $b_2 = b_1 = b_0 = 0$ and $\gamma_S = 0.001$ a stabilising set of controller gains is readily found from the diagonal elements in the first 2 iterations. γ_S can then be gradually increased until no further increase is possible since the feasible area becomes empty with a final value of $\gamma_S = 1.2$, resulting in the controller

$$K = \frac{1}{s^2+10s} \begin{bmatrix} (-2.115s^2 - 31.66s - 51.71) & (0.1897s^2 + 14.43s + 205) \\ (1.835s^2 + 4.78s + 3.683) & (4.291s^2 + 22.54s + 466) \end{bmatrix}$$

For the case with time delays the resulting controller with a final value of $\gamma_S = 1.0$ is

$$K = \frac{1}{s^2+10s} \begin{bmatrix} (-0.1996s^2 - 20.91s - 68.52) & (-3.493s^2 + 0.4007s + 174.1) \\ (2.495s^2 + 1.179s - 60.75) & (-0.4189s^2 + 6.383s + 375) \end{bmatrix}$$

In these designs 500 discrete frequencies were used in the generation of the parameter planes. The algorithm was implemented on Matlab 2006a running on a Microsoft Corporation Windows based PC equipped with an AMD Athlon 2800XP processor and 512MB RAM. The generation of each parameter plane in this problem takes less than 2s for each sensitivity function.

6.6.2 Reduced Order Riccati Controller

A full order Riccati design for the problem is described in [28]. The design achieved a $\gamma_S = 16.8$ and resulted in an 8th order controller. This 8th order controller can be reduced using several order reduction methods. None of the order reduction algorithms found in the

Matlab Robust Control Toolbox [28], including frequency weighted methods, irrespective of choice of frequency weight could produce a stable controller below 4th order. A balanced stochastic truncation (BST) model reduction method was however found to obtain a stable reduced 4th order controller, at the cost of a reduction in γ_S to 0.53 and a failure to achieve the required robustness. Whereby the complementary sensitivity function only achieved $\gamma_T = 0.36$. This large reduction in γ_S and γ_T is largely due to a poor fit at low frequencies. Nevertheless frequency weighted methods irrespective of choice of frequency weight could not produce a stable controller even at 4th order. This large reduction in performance highlights the difficulties with order reduction techniques when a significant reduction in orders is required.

When the time delays are included in the problem the maximum γ_S that can be achieved by the full order Riccati controller on the corresponding plant with the Padé approximation is reduced to 13.1[4] and the controller order is increased to 12. A 4th order stabilising controller can be realised from a BST controller reduction, but again leads to very low values of gamma at $\gamma_S = 0.49$ and $\gamma_T = 0.20$.

6.6.3 PS Tuned Riccati Controller

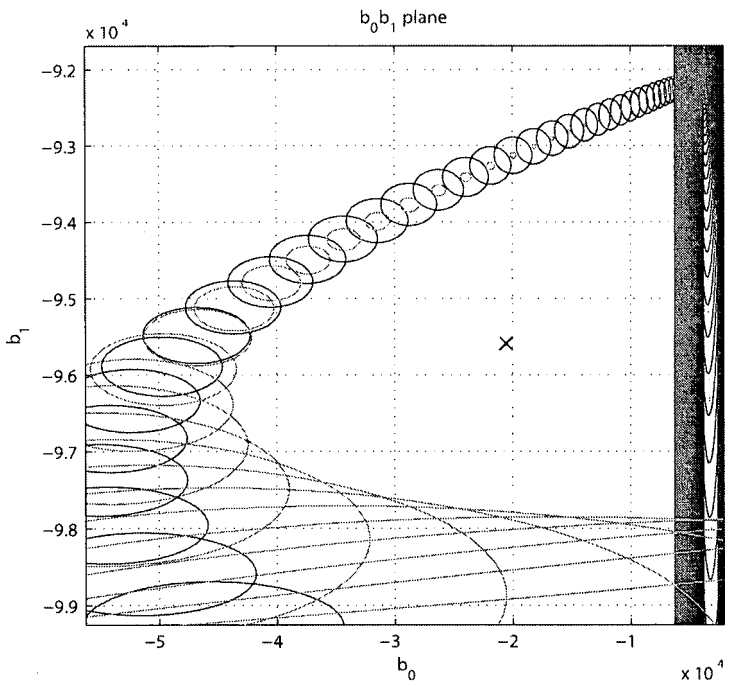

Figure 6.5: HiMAT example with time-delay: $b_0 b_1$ parameter plane, $k = 2$ iteration 4, $\gamma_S = 1.2$

[4]Evaluated using the plant with pure time delay

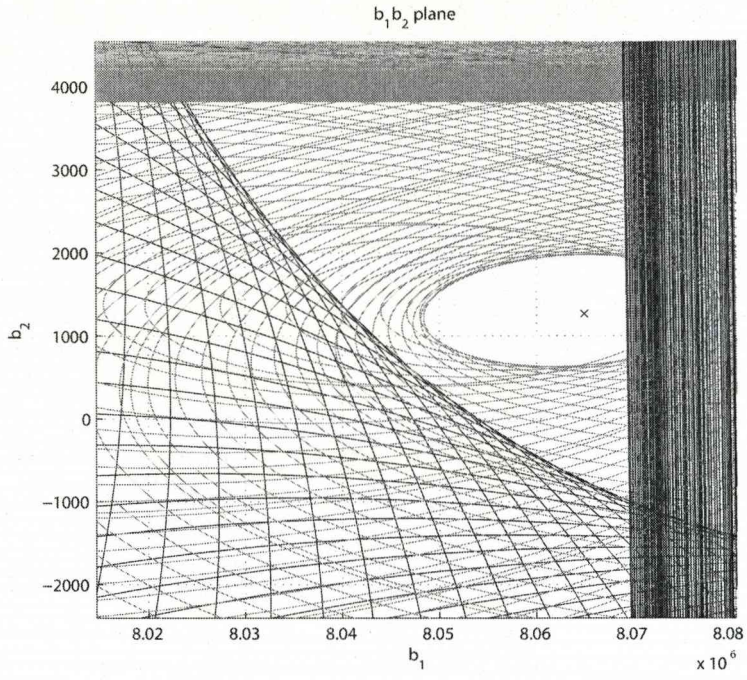

Figure 6.6: HiMAT example with time-delay: $b_1 b_2$ parameter plane, $k = 2$ iteration 75, $\gamma_S = 9.0$

For the PS retuning method, coefficients from the reduced order Riccati design are used as the start controller. The numerator coefficients of the reduced order transfer function matrix was fixed to maintain a 4th order controller. The robustness requirement is not satisfied for this start controller and so it is necessary to try and improve this, but also to reduce the primary sensitivity as much as possible. For the problem without time delays the PS tuning process was started with $\gamma_S = 0.5$; the planes with a significant impact on the sensitivity functions soon become evident to the designer. The final parameter space controller achieved $\gamma_S = 11.5$ and also significantly reduced the peak exceeding the complementary sensitivity weight, to result in $\gamma_T = 0.58$. The resulting parameter space tuned controller matrices for the system without time delay were

$$
\begin{aligned}
K_{i,j} &= K_{i,j,1} \bullet K_{i,j,2} \\
&= \begin{bmatrix} \frac{9.109s^2+618.6s+3.133\times10^5}{s^2+2266s+5.727\times10^5} & \frac{1.337s^2-2056s-1.878\times10^5}{s^2+2266s+5.727\times10^5} \\ \frac{0.8934s^2-229.4s-7.392\times10^4}{s^2+2266s+5.727\times10^5} & \frac{1.472s^2+217.6s+1.311\times10^4}{s^2+2266s+5.727\times10^5} \end{bmatrix} \\
&\bullet \begin{bmatrix} \frac{-13.47s^2-2.794\times10^4s-1.397\times10^4}{s^2+60.94s+0.006236} & \frac{-1.487s^2-3.288\times10^4s-1676}{s^2+60.94s+0.006236} \\ \frac{21.31s^2+1.684\times10^5s+7.711\times10^4}{s^2+60.94s+0.006236} & \frac{100.5s^2+7.033\times10^5s+1.979\times10^5}{s^2+60.94s+0.006236} \end{bmatrix}
\end{aligned}
$$

where $\bullet$ denotes Hadamard product (ie element-by-element multiplication).

Frequency response data for the case of the plant with a pure time delay is readily determined and rational approximations are not necessary. For this case the design was started

with $\gamma_S = 0.4$ and $\gamma_T = 0.2$. In just four parameter plane iterations it was possible to get over 100% increase of γ_S and obtain a value of 1. Figure 6.5 shows the associated $b_0 b_1$ parameter plane at this design stage and the admissible region from which a subsequent pair of such gains may be selected. After 75 iterations the design could not be improved further with a resulting $\gamma_S = 4.2$ and $\gamma_T = 0.29$. Figure 6.6 shows the associated $b_1 b_2$ parameter plane where the admissible region at this final stage effectively disappears for any small increase in either of the weighting functions.

$$
\begin{aligned}
K_{i,j} &= K_{i,j,1} \bullet K_{i,j,2} \\
&= \begin{bmatrix} \frac{22.64s^2-1133s+5.651\times10^5}{s^2+4980s+6.035\times10^6} & \frac{-0.06383s^2-2463s-1.428\times10^5}{s^2+4980s+6.035\times10^6} \\ \frac{1.216s^2-148s-33.08}{s^2+4980s+6.035\times10^6} & \frac{1.404s^2+188.9s+9251}{s^2+4980s+6.035\times10^6} \end{bmatrix} \\
&\bullet \begin{bmatrix} \frac{2.285s^2-9.354\times10^4 s-4.401\times10^4}{s^2+44.7s+0.007776} & \frac{593s^2-3.488\times10^5 s+6.89\times10^4}{s^2+44.7s+0.007776} \\ \frac{-1253s^2+2.878\times10^6 s+4.961\times10^8}{s^2+44.7s+0.007776} & \frac{4341s^2+8.073\times10^6 s+1.093\times10^6}{s^2+44.7s+0.007776} \end{bmatrix}
\end{aligned}
$$

Possible alternative compromises between the final values of γ_S and γ_T are evident to the designer at all stages of the PS design. It is straightforward for example to retune the reduced order Riccati design to meet the complimentary robustness weighting if this is deemed more important.

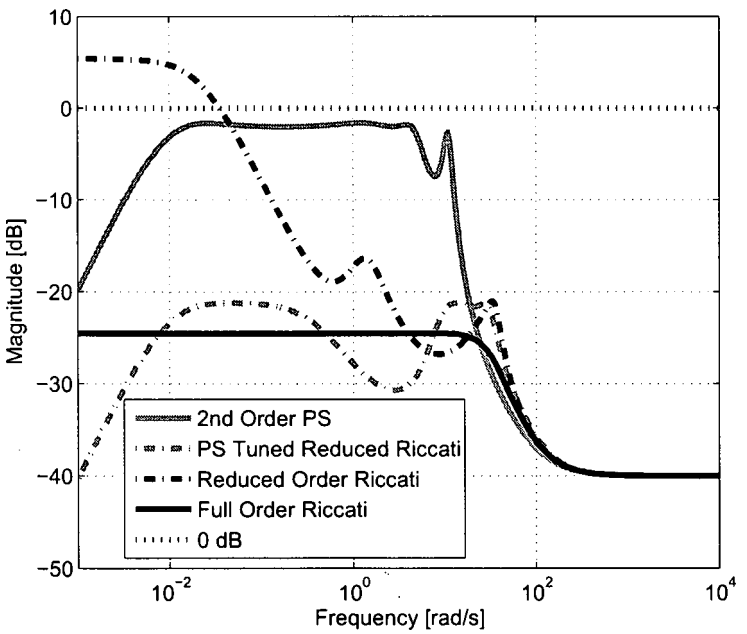

Figure 6.7: Weighted primary sensitivity functions

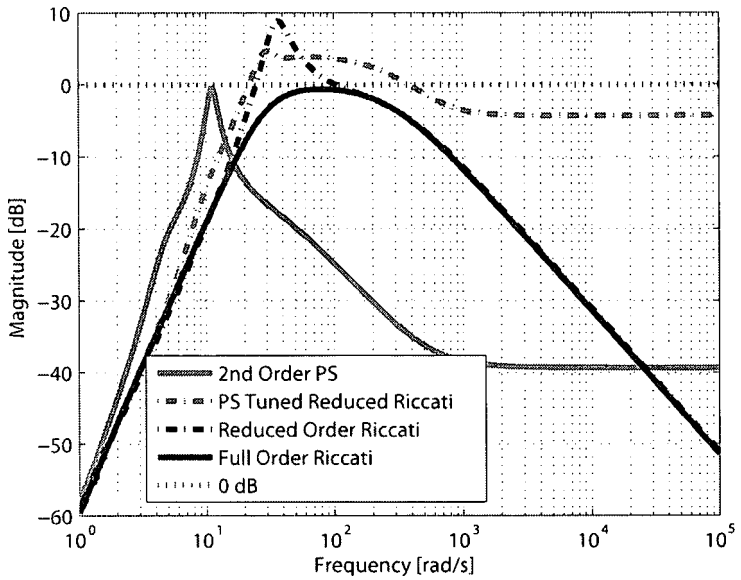

Figure 6.8: Weighted complementary sensitivity functions

6.6.4 Comparison of Controllers

The design requirements for the HiMAT problem, taken from [28] and used in section 6.6, were to reduce the specified primary sensitivity function as much as possible, whilst obtaining the specified complementary weighting function. The corresponding weighted primary and complementary sensitivity plots for the different designs for the HiMAT problem (shown for the system without the time delay) are given in figures 6.7 and 6.8. It can been seen from figure 6.7 that for the given specifications the full order Riccati solution achieves the lowest peak-magnitude primary sensitivity function of all the designs ($\gamma_S = 16.8$) and is of order 8. However, when considering a BST reduced order version of the same controller it is apparent that it becomes relatively poor at minimising the sensitivity function ($\gamma_S = 0.53$) and moreover, it exceeds the robustness constraint as shown in figure 6.8. It is also found that the optimal full order Riccati design cannot be reduced below an order of 4 without making the system unstable. In contrast to this it was shown that a 2nd order PS controller not only acts to stabilise the system but also achieves a greater reduction in primary sensitivity function than the 4th order reduced Riccati controller in both the weighted primary and weighted complementary sensitivity function as shown figures 6.7 and 6.8.

By using the reduced-order design as a start controller the PS technique significantly reduced the weighted primary sensitivity function whilst at the same time improving the weighted complementary sensitivity function robustness levels. During the design iterations the PS technique allows the designer to observe the trade-off between the two sensitivities and tighten the different constraints independently as necessary. For the same order controllers it

is apparent that an improvement in magnitude in excess of 10 times can readily be obtained on the primary sensitivity function by using the PS method to retune the reduced order Riccati controller.

6.7 Conclusions

The frequency response based technique presented in this chapter graphically determines regions in the parameter space meeting one or more $\mathcal{H}_\infty$ MIMO norm specifications. Internal stability conditions for the irrational unity feedback system are developed. Both sensitivity function constraint and internal stability results are conveniently stated directly in terms of the plant and weighting function frequency response matrices. The maximum singular value constraints at discrete frequencies yield elliptical loci which readily map into the parameter planes of any general format fixed low order controller structure to populate the matrix controller elements.

The technique has some significant advantages over current algebraic Riccati $\mathcal{H}_\infty$ methods since the method requires only non-parametric frequency response information. The technique allows the significant benefits of SISO parameter space, for interactive graphical design of fixed low order controller to be extended to multivariable systems which may be irrational and possibly non-square with arbitrary numbers of multivariable norm, mixed sensitivity function specifications.

Boundaries which are parameterised with frequency are superimposed graphically to give the designer a greater insight into the trade-offs between performance and robustness which is often hidden in other techniques. Moreover the proposed method treats continuous and discrete systems uniformly. The technique can be used either indirectly as a tuning tool for improving low-order controllers designed by other methods or for direct design. The superiority of the MIMO norm based design technique over SISO sequential loop design was demonstrated by a simple example.

In a comparative study the proposed MIMO PS method was demonstrated by application to the indirect retuning of an $\mathcal{H}_\infty$ Riccati designed order-reduced controller and the direct design of fixed low order controllers for a highly maneuverable aircraft (HiMAT) benchmark example.

Chapter 7

MIMO Idle Speed and AFR Control System Design

7.1 Introduction

The air-to-fuel ratio (AFR) in a port fuel-injection (PFI) engine must be maintained close to stoichiometric at all times in order that the three-way catalytic converter in the exhaust system operates efficiently. The AFR path is controlled by adjusting the fuel injected into the inlet manifold prior to the inlet valves opening. Because of transport lag this requires accurate and fast feedforward control [45] in addition to any feedback action. Engine management systems (EMS) implement this feedforward control using an estimate of air entering a cylinder and any manifold wall wetting dynamics to determine the correct length of fuel pulse. Standard engine strategies use look-up tables for calculating the fuel pulse width based on air-estimation from either manifold absolute pressure (MAP) or mass air flow (MAF) sensors and engine speed. These tables are generated empirically by a number of static operating point dynamometer mappings for a large number of speeds and loads. Not only is this static mapping process expensive in resource and time [12] but also dynamic effects are not fully addressed. An over-reliance on the feedforward element in the conventional calibration process means that the resulting look-up tables require extensive modification for environmental effects such as temperature or humidity [22]. An example static fuelling map for the idle region (based on the method presented in the sequel) is shown in figure 7.1.

An alternative method for generating the feedforward controller is proposed in the sequel based on a directly identified inverse engine model. An early use of direct inverse control was considered in [50] for nonlinear QFT designs to reduce the size of uncertainty templates due to nonlinearity. A later example of a neural network controller design with direct inverse control can be found in [1]. More recently a technique based on using an ordinary least squares (OLS) to identify a inverse nonlinear auto-regressive with moving average (I-NARMA) structure was

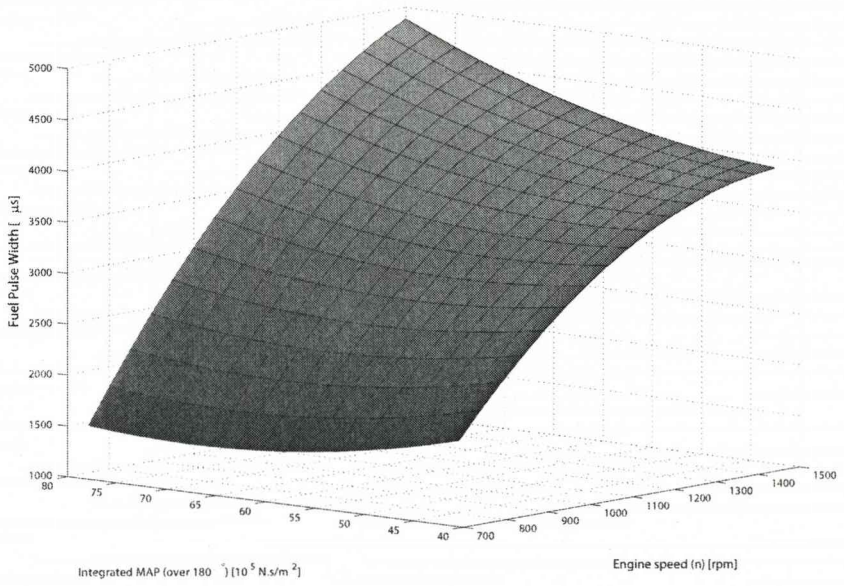

Figure 7.1: Fuelling map obtained from I-NARMA model

proposed and successfully applied to a SISO idle speed problem in [83].

As in conventional fuelling control the proposed identified controller contains a feedforward element to respond quickly to any changes in demand or disturbances that can be measured in the air path. A significant difference in implementation of the proposed controller is however, that a multivariable feedback control element is applied through a linearising inverse compensator. A distinctive feature is that the proposed controller employs the combination of both multivariable control and linearising action in the fuelling path.

The following chapter is organised as follows. In section 7.2 the idle speed control problem is explained and the typical control approaches discussed. The requirements for an idle speed and AFR controller are given in section 7.3 for the multivariable problem as posed here. A rapid calibration technique for developing the feedforward AFR controller based on a directly identified inverse model is given in section 7.4. In section 7.5 a linear multiple-input-multiple-output (MIMO) plant model is identified for the system with the linearising compensator coupled to the fuel path. Section 7.6 details the feedback controller design for regulation of engine speed and AFR. The performance of the feedforward and feedback system is critically evaluated in section 7.7. Suggestions and comments for cylinder balancing control using the proposed technique is discussed in section 7.8. Some conclusions on the technique are given in section 7.9.

7.2 Idle Speed Control

The idle speed problem is a compromise between low engine speed to economise on fuel and the ability to satisfactorily reject disturbances [54]. Torque disturbances due to electrical demand on the alternator, power-steering pump or air conditioning units can quickly load the engine causing a reduction in speed which can cause undesirable noise and vibration characteristics for the driver, or possibly engine stall. The problem of regulating speed has typically required careful control of the air entering the engine by either an electronic throttle or air-bypass valve. For faster response to disturbances, though at the cost of engine efficiency, the spark channel may be used where this is retarded from 'maximum best torque' (MBT) under the idling strategy to allow additional control action as necessary. This multiple-input-single-output (MISO) formulation is most widely used in practice [54]. During disturbances the fuel channel is typically used to maintain the AFR as close to stoichiometric as possible on a separate single-input-single-output (SISO) control loop.

An alternative approach to the idle speed problem is to incorporate the fuel channel into a multivariable scheme. A 3x3 MIMO formulation of the idle speed problem is addressed in [45] where throttle, spark and fuel are used to control engine speed, AFR and manifold pressure for a $1.8l$ normally aspirated SI engine. This scheme has the greatest potential for tracking and disturbance rejection at the expense of setting the spark below its optimal angle. A simplified 2x2 throttle and fuel scheme is presented in [40] where the the engine speed and AFR are controlled in a multivariable scheme for a natural gas engine. The multivariable treatment of the engine in these formulations provides additional actuation for disturbance rejection and tracking. Furthermore, incorporating the fuel in such a way also avoids having sequential SISO designed loops which can often give lower performance or stability.

The AFR in a PFI engine must be maintained close to stoichiometric at all times in order that the three-way catalytic converter in the exhaust system operates efficiently as shown in figure 7.2. When operating efficiently a significant reduction of harmful emissions at the tailpipe is achieved by providing the environment for chemical reactions to take place rapidly. The three-way catalytic converter (TWC) is given its name because of the three reactions which take place [45, 48]

1. Conversion of nitrous oxides to oxygen and nitrogen: $2NO_x \rightarrow xO_2 + N_2$

2. Oxidation of carbon monoxide to carbon dioxide: $2CO + O_2 \rightarrow 2CO_2$

3. Oxidation of hydrocarbons (HC) to carbon dioxide and water: $C_xH_y + zO_2 \rightarrow nCO_2 + mH_2O$

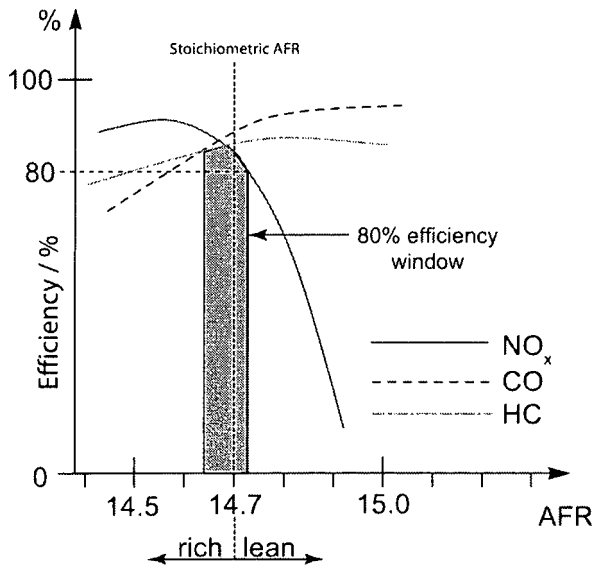

Figure 7.2: Efficiency of TWC for NO_x, CO and HC reduction

7.3 MIMO AFR and Idle Speed Control Objectives

A feedforward controller is required on the fuel path to speed up the response to changes in air flow or load. It is crucial that the feedforward element of the control scheme responds quickly to any changes thereby returning the AFR to stoichiometric as quickly as possible to ensure the TWC converter works at optimal efficiency.

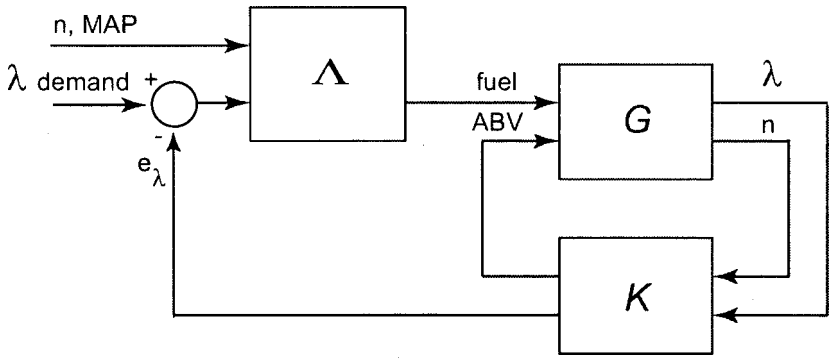

Figure 7.3: Inverse compensator and MIMO feedback controller configuration

Figure 7.3 illustrates how the two-input-two-output problem can be formulated with a fast feedforward fuelling controller Λ, together with a feedback controller K for precise regulation. The requirements for the feedback controller K are primarily to compensate for any error in the feedforward controller due to modelling deficiencies, manufacturing tolerances, mechanical wear or environmental effects. Therefore, the primary requirement for both the speed and AFR channels is for tracking with zero steady-state error. The target idle speed for the Zetec engine used here when fully warmed up is 880 rpm and the target for the AFR channel is to

keep λ no more than 0.1% from its optimal setting of 1 during steady state [45], where λ is defined as

$$\lambda = \frac{AFR_{measured}}{AFR_{stoichiometric}}$$

7.3.1 Time Delays

Large time delays exist between inputs entering the engine and the response at the outputs. One of the main control difficulties associated with engines is due to these time delays. The discrete nature of engines introduces a very significant induction to power stroke (IPS) delay [45] which for a four cylinder engine is approximately two combustion events or

$$\tau_{IPS} \approx \frac{2\pi}{\omega_e}$$

where ω_e is engine speed measured in rad/s. Any AFR effects in the gas can only be observed after the induction to exhaust gas (IEG) delay

$$\tau_{IEG} \approx \frac{3\pi}{\omega_e}$$

These delays are obviously most significant at low idle speeds. Transport delays are the other major delay in engine applications due to the physical distance that fluids are transported. Other delays include wall wetting dynamics, actuator response times and sensor time constants as discussed in Chapter 1.

7.4 Inverse MISO Feedforward Compensator

Standard engine strategies use look-up tables for calculating the fuel pulse width based an air-estimation using either MAP or MAF sensors and engine speed. These tables are generated by a number of static mapping sweeps for a wide range of speeds and loads. For these tables to be accurate this is an extensive experimental effort and requires a large number of operating conditions to be mapped. Furthermore, since these mappings are obtained at steady-state conditions any dynamic affects are subsequently not included in the controller.

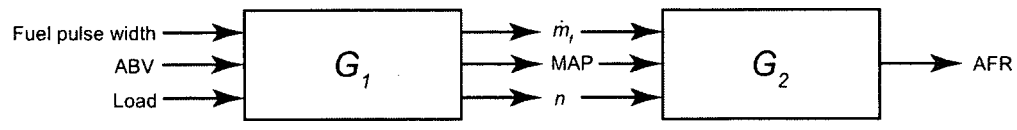

Figure 7.4: Open loop AFR path

An alternative method for generating the feedforward controller is presented here based on nonlinear black box modelling. This behavioural approach attempts to characterise the systems dynamics in a single nonlinear identification. The AFR path on an SI engine, over the idle range and at fully warmed up conditions can be assumed to be dependent upon the amount of air entering the engine, the fuel mass injected and the load applied. Therefore, by perturbing the air, load and fuel mass sufficiently and recording the engine outcome it is possible to identify the relationships between these and the MAP, engine speed and AFR as shown in figure 7.4. Here we are interested in determining the relationship between the AFR from engine load, speed and fuel mass. Since in general a direct measure of load would not normally be available in a production vehicle we can instead consider the MAP signal[1] since this is proportional to engine load. Similarly the fuel mass is not directly controlled or measured, instead an injection pulse width is considered.

Changing the causality (input-output assignment) of the identification data allows direct inverse models to be generated. The inverse models can then be used directly as feedforward controllers. This method of generating a feedforward controller is quicker than for a series of static mappings, since only one set of identification data is required followed by the generation of a single inverse model. Furthermore, transient behaviour of the system is captured in the model and therefore included in the controller. The structure of the feedforward compensator Λ is depicted in figure 7.5, where it can be seen that for a measured MAP, at a particular engine speed the fuel is calculated to generate a desired AFR. The compensator has the further advantage of linearising the plant dynamics over the identified range, and thus ideally creates a unity feedforward path excepting for the inherent time delay.

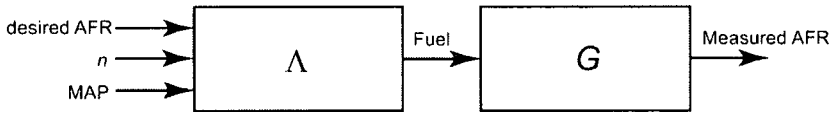

Figure 7.5: Feedforward compensator

7.4.1 Nonlinear Excitation Signals

The presence of directions in multivariable systems make it it necessary to identify the output channels from all the inputs simultaneously [100]. The output of a particular channel is dependent on the frequency of the input and the specific channel(s) these enter the system. Accordingly multivariable system identification approaches are necessary to ensure the directions associated with the plant, disturbances and delays are fully established.

The input signals used in the identification process must be sufficiently rich to excite

[1]The actual values used in the identification and control is MAP integrated over 180 degrees and sampled in the sequel but for clarity will be referred to as MAP.

the important frequencies of the system. Furthermore, since the process is nonlinear it is necessary to use input signals which excite these nonlinearities. Random binary sequences are used for linear systems since they have an auto correlation similar to that of white noise with a spectrum similar to that of a Gaussian signal. These properties are desirable for identification, however for amplitude dependencies it is important that the input signals have more than two levels. Accordingly, in the experimental work scaled random numbers with a DC bias were applied to the inputs. These signals have the advantages of using switching signals and also of picking up amplitude dependencies.

For MIMO and MISO identification it is important to ensure the different input signals are not correlated with each other, therefore different sequences with different seeds are necessary for each channel [39]. The rate at which the signals can change between levels depends on the system's dynamics. A signal which changes too rapidly can make it difficult to distinguish a reaction, on the other hand a signal which changes too slowly can fail to pick up the higher frequency dynamics. After consideration of the physical processes including the significant time delays, a matrix of candidate signals with different switching lengths were trialled. It was found that the signal lengths for achieving the best model fit required the ABV to change no faster than every 0.6s, the fuel pulse length every 0.7s and the load every 0.65s.

The range and switching period of the signals was determined based on *a priori* understanding of the system. Additionally several signals were trialled to ensure the system was sufficiently excited at all important speeds and loads, without significantly leaving the idle region or causing the engine to stall. Table 7.1 gives the maximum, minimum, mean and variance of each of the three inputs.

Table 7.1: Statistics of nonlinear identification signals

	Minimum	Maximum	Mean	Variance
ABV [$\%_{duty}$]	0.30	0.48	0.39	7.8×10^{-4}
Fuel Pulse [μs]	2635	3975	3191	5.4×10^{4}
Load (voltage) [V]	2.1×10^{-3}	0.12	0.07	5.0×10^{-4}

7.4.2 NARMA(X) Models

An algebraic NARMA (nonlinear auto-regressive with moving average) model structure is proposed for the inverse compensator. A NARMA model generates an output based on previous and current inputs and outputs. A number of linear and nonlinear terms can be considered for the structure including delayed terms, power terms, cross products or combinations thereof. The general form of a SISO NARMA model [19] is

$$y(k) = F(y(k-1), \ldots, y(t-n_y), u(k), u(k-1), \ldots, u(k-n_u))$$

where F is a nonlinear function in the output y at time step $k-1$ and up to the maximum lag of n_y and the input u, at the current time step k_m and previous inputs up to a maximum delay of n_u. Noise terms can also be included into the model to extend to a NARMAX structure. In contrast to linear models these terms in general are included with the nonlinear function and are not simply additive at the output.

The nonlinear function will use various cross products of terms with lags up to some maximum of n_y and n_u. This becomes considerably more complicated when a MIMO NARMA(X) model structure is considered. A convenient and simple representation of an algebraic MIMO NARMAX structure [93] is

$$y_h(t) = \sum_{i=1}^{I} \theta_{i,h} \prod_{j=0}^{J-1} \prod_{h=1}^{K} y_k^{l_{h,i,j,k}}(t-j) u_k^{m_{h,i,j,k}}(t-j) e_k^{n_{h,i,j,k}}(t-j) \tag{7.1}$$

This representation is of the algebraic NARMAX (NARMA with exogenous) expressions in K output, input, and noise, in discrete-time variables $y_1, y_2, \ldots, y_K$, $u_1, u_2, \ldots, u_K$ and $e_1, e_2, \ldots, e_K$ for each output $y_{h,t} \;:\; h = 1, 2, \ldots, K$ at time t. Each summation term $i = 1, 2, \ldots, I$ is expressed in the powers of all the $j = 0, 1, \ldots, J-1$ delays of each of the variables $k = 1, 2, \ldots, K$. There is a maximum of I terms in any expression and if the maximum delay in any term is β then $J = \beta + 1$. For each term i of each expression there can then be formed an $K \times I \times J \times K$ array $l = [l_{h,i,j,k}]$, an $K \times I \times J \times K$ array $m = [m_{h,i,j,k}]$, an $K \times I \times J \times K$ array $n = [n_{h,i,j,k}]$, and an $I \times K$ array of parameters $\theta = [\theta_{i,h}]$. The NARMAX expression can therefore be represented by the 4-tuple $\langle \theta, l, m, n \rangle$.

7.4.3 Ordinary Least Squares

An ordinary least squares algorithm (OLS) is used for estimating the parameters $\theta_{i,h}$ in equation 7.1. This algorithm is well understood and documented [109]; parameter coefficients for a set of regressors can be readily solved using

$$\Theta = (X^T X)^{-1} X^T y$$

where y is the measured output data that is to be modelled and X is a matrix of regressors. Each regressor is a single column with a length equal to that of the dataset under consideration. The resulting Θ is a column consisting of identified parameter coefficients $\theta_{i,h}$.

7.4.4 Inverse NARMA MISO Compensator Identification

The identification process was based on datasets of 6000 points each sampled every 180 degrees of crank. Half of this data was used for identification and the remaining used for validation. Relatively long data lengths of 3000 points were used for the identification to ensure all nonlinearities were sufficiently captured. Due to significant time delays in the plant, AFR displays a delayed response to changes in MAP, engine speed and fuel. Therefore, to create a causal identification data set, it is necessary to shift the data. The measured fuel signal is shifted by the amount of the pure time delay on the measured AFR signal. Making the fuel an *output* and the AFR an *input* creates a causal MISO system, where engine speed and MAP are now automatically causal due to the shift in fuel signal. However these inputs also now contain a time delay relative to this new output. Accordingly, these signals must also be shifted so that no pure time delay exists between any of the altered causality inputs and the output if the compensator is to respond as quickly as possible.

On the other hand for the compensator to operate successfully online the various time delays must also be synchronised. This is necessary since the dynamic compensator relies on a number of delayed and cross-coupled terms. One way to guarantee synchronicity is to shift all the data by the largest time delay. However, in doing so fast inputs such as speed and MAP are delayed excessively and the resulting compensator becomes very slow. Accordingly, after shifting the fuel signal to make the inverse system causal the MAP and engine speed signals are then subsequently shifted by an *equal* amount to ensure no delay occurs between the fastest of these, yet also ensuring both are synchronised with each other. In doing so the AFR becomes unsynchronised, however, since in general for a PFI engine this value will be regulated to a fixed value. Thus creating a compensator with a suitable trade-off between a fast response time due to the undelayed, faster inputs of MAP and engine speed, at the cost of absolute model accuracy when the AFR is perturbed due to disturbances.

Figure 7.6(a) indicates the number of pure time delays found from identification of the forward system.[2] The largest delay between the fuel signal and an observed response at the lambda sensor was found to be 20 samples. The response to changes in MAP and engine speed were observed after only 12 engine events. Accordingly, to get an inverse model which can predict the fuel signal it was necessary to alter the causality by shifting the fuel signal by the longest delay of 20 samples as depicted in figure 7.6(b). The fastest compensator was obtained by removing the resulting delay between the MAP and speed signal by shifting these signals forward by 8 samples as shown in figure 7.6(c).

The structure for the NARMA model was found using *a priori* understanding of the system dynamics to gain a basic model structure. Only input terms were used in the model since

[2]For simplicity the time delays are shown to act before the dynamics of the system.

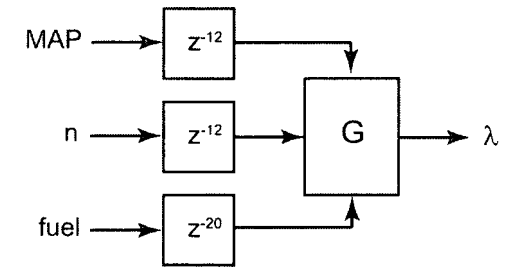

(a) Forward Model

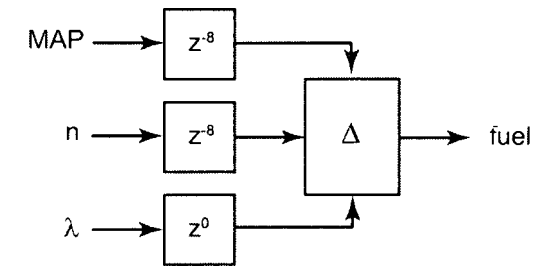

(b) Synchronised Partial Inverse Model

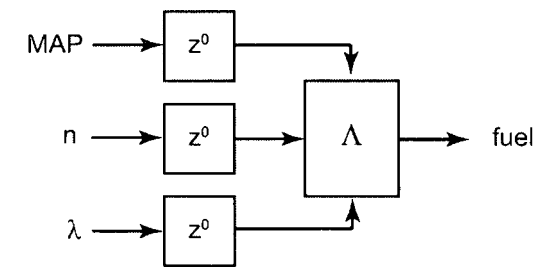

(c) Unsynchronised Partial Inverse Model

Figure 7.6: Progression to partial inverse model

the previous output terms were found to make the model only suitable for next step prediction. The inclusion of cross-product terms containing the output were found to be heavily weighted by the OLS algorithm which resulted in a good model fit but this was subsequently rejected since validation using the *simulated* output rather than the measured output revealed suitability only as a next step predictor. This effect occurs since the output is generated by the compensator and therefore any error in generating the 'correct' output is fed back and is further compounded. Therefore, heuristic tuning of the input parameters was undertaken by consideration of which parameters would improve the model fit and also improve the transient performance. Fit functions and residual analysis were used to ensure the inverse dynamics were adequately modelled. The regression terms selected for the compensator are given in table 7.2.

Regressor	Parameter Coefficient
Constant	3.88×10^3
$u_1(t)$	-62.1
$u_1(t-2)$	178
$u_1(t-4)$	147
$u_1(t-8)^2$	0.198
$u_2(t)$	12.4
$u_2(t-2)$	7.15
$u_2(t)^2$	0.0013
$u_3(t)$	-1.44×10^4
$u_3(t-1)$	-2.06×10^3
$u_3(t-2)$	-3.71×10^3
$u_3(t-5)$	-150
$u_3(t-8)$	1.11×10^3
$u_3(t-10)$	7.96×10^3
$u_3(t)^2$	5.43×10^3
$u_1(t)u_1(t-2)$	-1.52
$u_1(t)u_2(t)$	0.0758
$u_1(t)u_2(t-6)$	-0.0508
$u_1(t)u_2(t)u_3(t)$	0.120
$u_1(t-2)u_2(t-2)u_3(t-2)$	0.0319
$u_1(t-1)u_3(t)$	26.0
$u_1(t-1)u_3(t-10)$	-105
$u_1(t-4)u_2(t-2)u_3(t)$	-0.131

Table 7.2: Inverse compensator regressor terms and associated coefficients

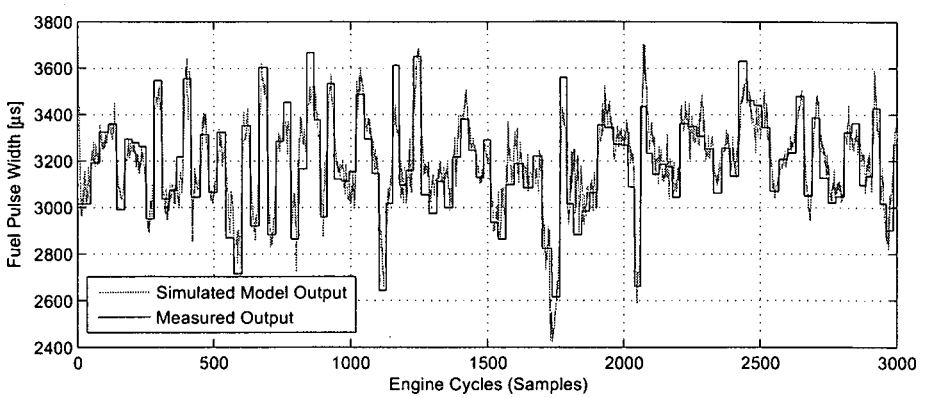

Figure 7.7: Inverse model fit to measured data using unseen validation data

Figure 7.7 shows the fit of the model using validation data. The identification data resulted in a model with an R-squared value of 0.72, indicating the model picked up 72% of the system dynamics. Inverse models are difficult to accurately model since input data for the inverse has been subject to disturbances when captured and therefore this fit was considered satisfactory. The validation data was found to have an R-squared value of 0.64. The residuals of the validation dataset were tested for whiteness and cross-correlation with the three model inputs. Examination of the residuals displayed in figure 7.8 shows some correlated dynamics with the input, however the correlation is relatively small. The mean of the residuals was within 0.5 % of the mean of the measured signal. The correlation coefficients between the residuals and the inputs were calculated to be 0.02, 0.05 and 0.10 corresponding to the speed, MAP and AFR respectively. The speed and MAP values were, within sufficient statistical bounds to be considered un-correlated, with the AFR channel demonstating the most correlation. This correlation is however relatively small and was not found to significantly reduce with larger model structures.

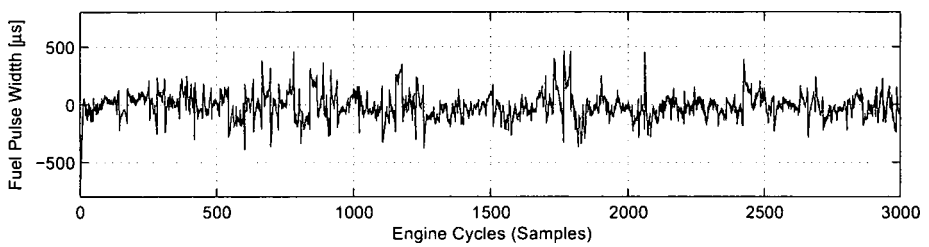

Figure 7.8: Residuals from fitting unseen data to the inverse model

7.4.5 Experimental Validation of Inverse Compensator

The inverse compensator was applied to the engine to observe its ability to adequately and quickly reject disturbances on the AFR path before the feedback controller was added. The AFR results are displayed in figure 7.9 which shows how the compensator responded to load disturbances of approximately 5 Nm. The results were collected every 2 degrees of crank and the raw signal is displayed together with a filtered version which removes frequencies above the controller operating frequency of 30 Hz (180° at 880 rpm). The results show that the compensator quickly responds to disturbances and removes most of the DC offset, however it can also be observed that the compensator does not fully return the AFR to stoichiometric when step loads were applied. The compensator was also assessed for tracking to different reference set points as can be seen in figure 7.9. Examination show the compensator reacts very quickly to demand changes and also tracks closely to the demanded values. The compensator demonstrated a linear response to tracking demands, verifying the effectiveness at linearising the AFR channel and the disturbance rejection capability illustrated an effectiveness as a fast feedforward controller. The DC error which is observed demonstrates the requirement for an

additional feedback scheme.

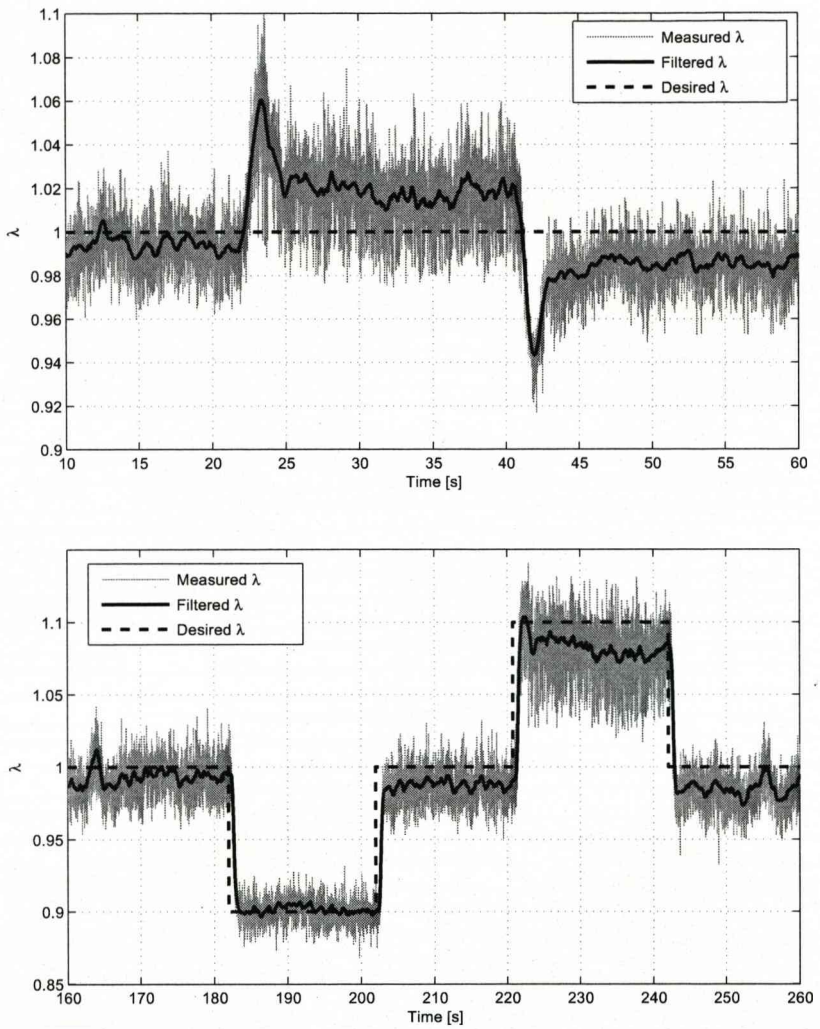

Figure 7.9: Disturbance rejection (top) and tracking (bottom) performance of inverse compensator

7.5 Compensated Engine MIMO Identification

In order to design the feedback controller it was necessary to obtain a suitable linear model of the system. The inclusion of the inverse compensator has the effect of linearising the AFR channel and therefore it is useful to consider the compensator dynamics in the identification. Accordingly, perturbation of the AFR therefore requires an perturbation of the compensator, rather than the fuel pulse directly. The inputs to the system are now desired λ and ABV and the outputs are the measured λ and engine speed. A static operating point ('spot point') model linearised at the middle of the desired engine speed and load operating point was

thus identified. A set of spot point models over the entire operating range can result in improvements in robustness and performance. One particular advantage of the parameter space technique based on frequency response information allows nominal models to be generated from uncertainty discs in the complex plane. Such discs are generated over a range of finite frequencies based upon the frequency response of the set of spot point models. The disc radii is also useful for shaping weighting functions since it gives frequency based information of the spread of uncertainty in the various channels.

Frequency rich pseudo-random binary sequence (PRBS) signals were selected to excite the system inputs. The period of switching for the PRBS was selected by collecting data for a range of switching rates. The best trade-off between fit quality and high frequency information was obtained by perturbing the ABV no faster than 0.6s and the desired λ at 0.7s. The magnitude of the ABV signal was 0.01 which was added and subtracted to the mean value of 0.38. The desired λ input to the compensator was perturbed by 0.075 around a mean value of 1. The relatively slow changing signals required a dataset of 2000 points for identification to ensure the input signals displayed a sufficiently white autocorrelation characteristic. The section of data used for the identification is shown in figure 7.10.

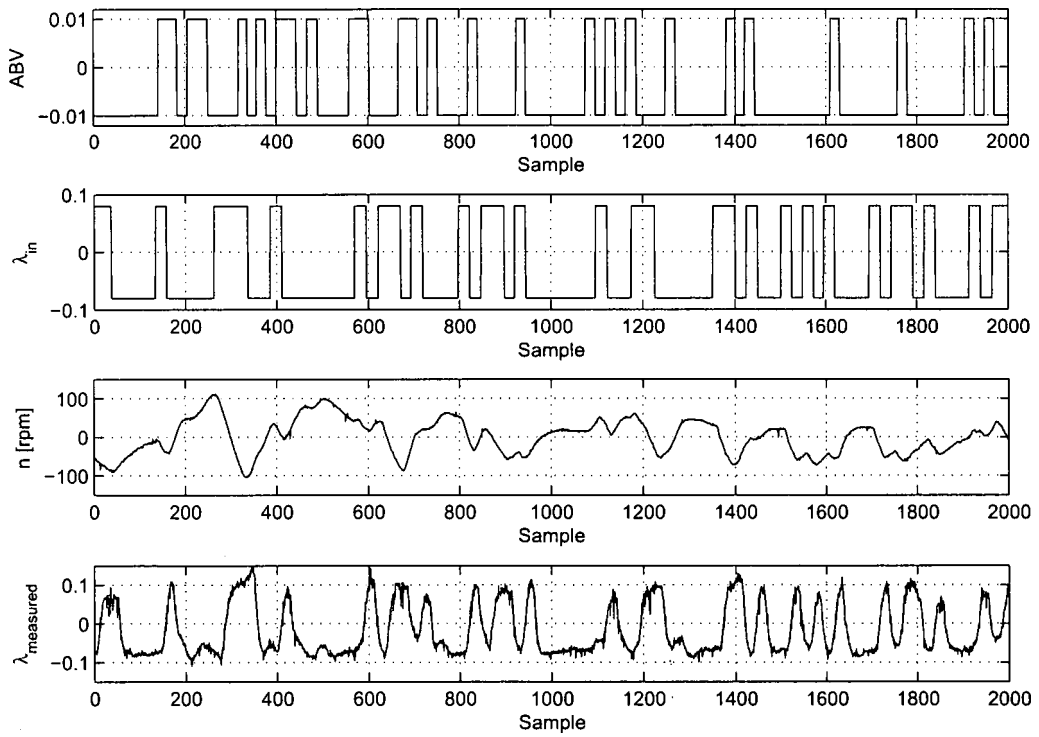

Figure 7.10: Identification data for the compensated engine

Step tests were used to estimate the time delay between the two inputs and outputs. Two linear ARMAX MISO identifications were used to capture the plant dynamics. The exogenous input in the model was used here to improve the accuracy of the identified plant dynamics. The Matlab System Identification toolbox [70] was then used to generate a linear model of the plant based upon *a priori* understanding of the system dynamics and the delay. The final structure and exact number of delays was found using the order selection utility with a focus based upon model prediction which maximised the Akaike's information criterion (AIC). An example of the model fit using unseen validation data for the speed and AFR channels is displayed in figures 7.11 and 7.12 respectively.

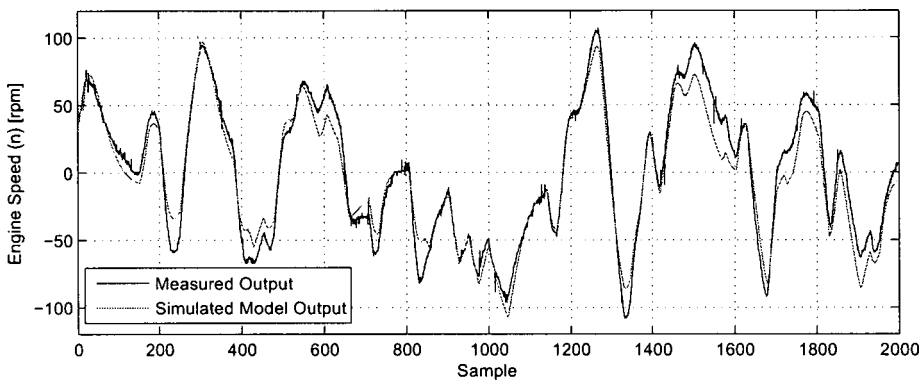

Figure 7.11: Speed output (y_1) model fit using unseen validation data

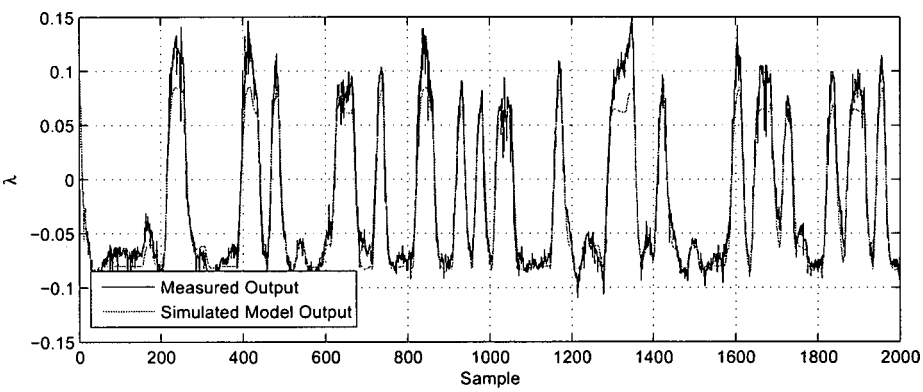

Figure 7.12: λ output (y_2) model fit using unseen validation data

Acceptance of the model was based upon model fit and analysis of the residuals. The quality of the fit was judged from a visual perspective and consideration of the calculated R^2 value. R^2 values of 0.998 and 0.977, corresponding to $y1$ and $y2$ respectively were calculated from validation data, therefore suggesting that virtually all the output variance in the recorded output can be explained by the model. The residuals for each output which could not be accounted for in the model are displayed in figure 7.13. The residuals from each output were observed to have a strong whiteness characteristic. Cross-correlation checks based on a

5% stastical certainty bound demonstrated the inputs in general to be uncorrelated with the outputs; only the ABV to speed was not within these bounds. This remaining correlation was within the lags covered by the model and therefore was most likely due to a small degree of nonlinearity in the plant [82]. Cross-correlation plots are shown in figure 7.14.

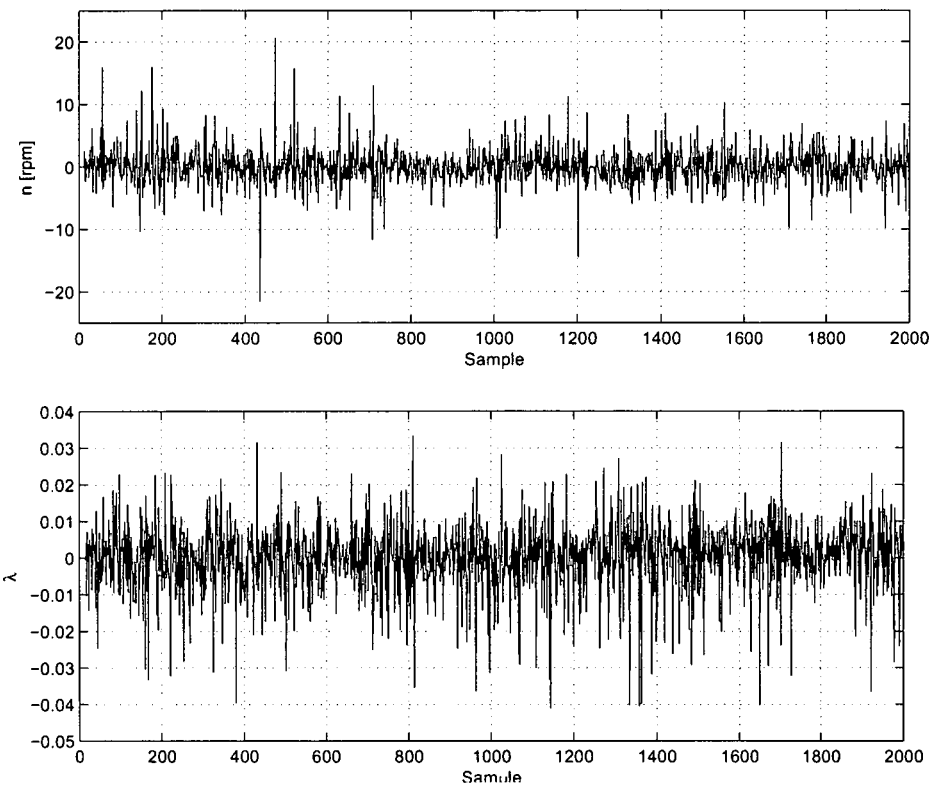

Figure 7.13: Residuals from unseen data to model (Top: y_1 Bottom: y_2)

The resulting discrete plant transfer function model $G = [g_{i,j}]$ was

$$g_{11} = \frac{71.15z^4 - 68.7z^3 - 42.83z^2 + 88.02z - 37.26}{z^{11} - 1.736z^{10} + 0.5075z^9 + 0.1703z^8 + 0.1554z^7 - 0.09607z^6} \quad (7.2)$$

$$g_{12} = \frac{-10.27z^7 + 3.822z^6 + 5.33z^5}{z^{11} - 1.736z^{10} + 0.5075z^9 + 0.1703z^8 + 0.1554z^7 - 0.09607z^6} \quad (7.3)$$

$$g_{21} = \frac{0.08092z^3 - 0.09787z^2 + 0.1558z - 0.1129}{z^{16} - 1.376z^{15} - 0.1624z^{14} + 0.7917z^{13} - 0.2259z^{12}} \quad (7.4)$$

$$g_{22} = \frac{-0.01476z^5 + 0.03945z^4}{z^{16} - 1.376z1^5 - 0.1624z^{14} + 0.7917z^{13} - 0.2259z^{12}} \quad (7.5)$$

Bode plots of the compensated system dynamics can be seen in figure 7.15.

The degree of interaction in the model was assessed by computing the relative gain array

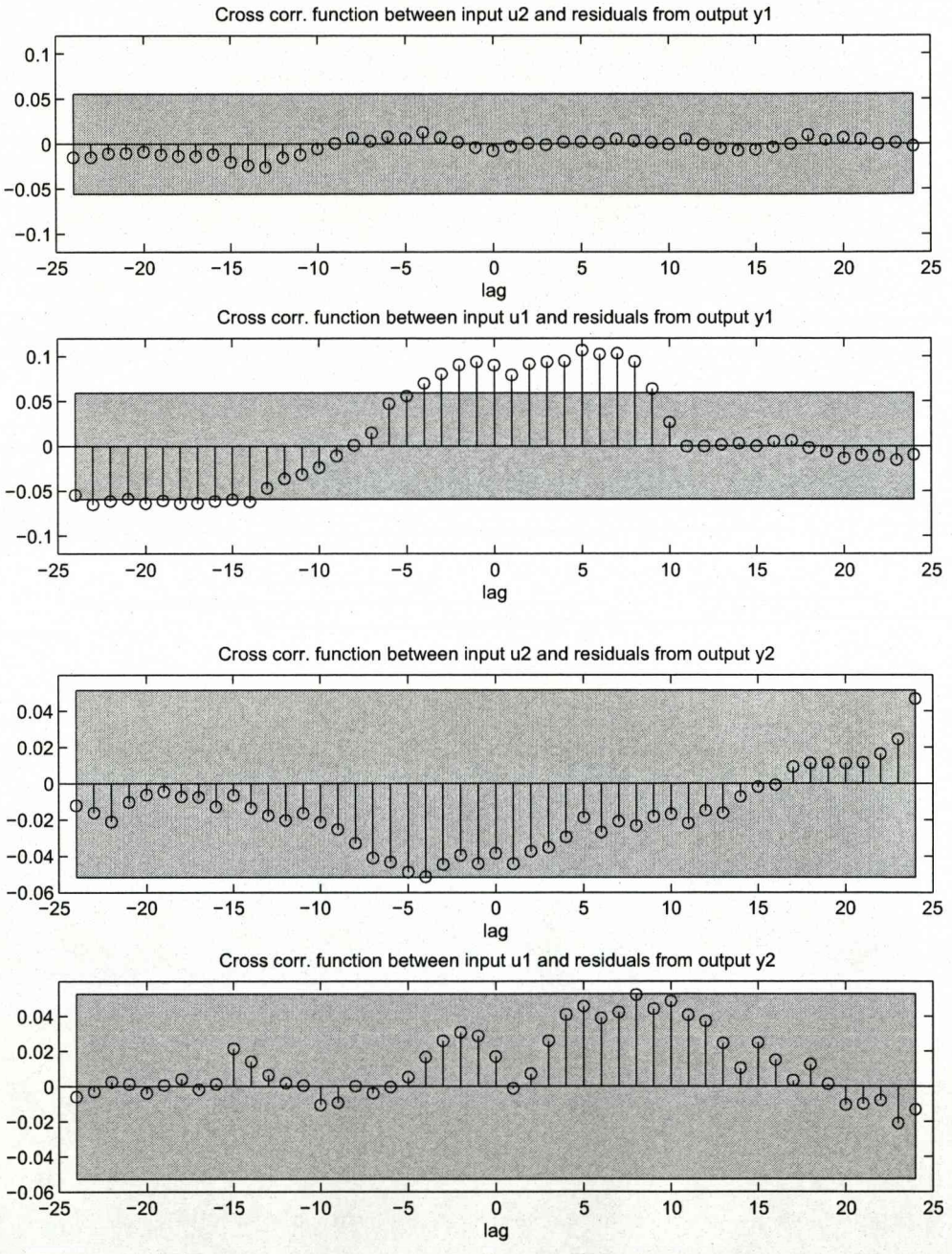

Figure 7.14: Cross-correlation of validation model residuals with the inputs

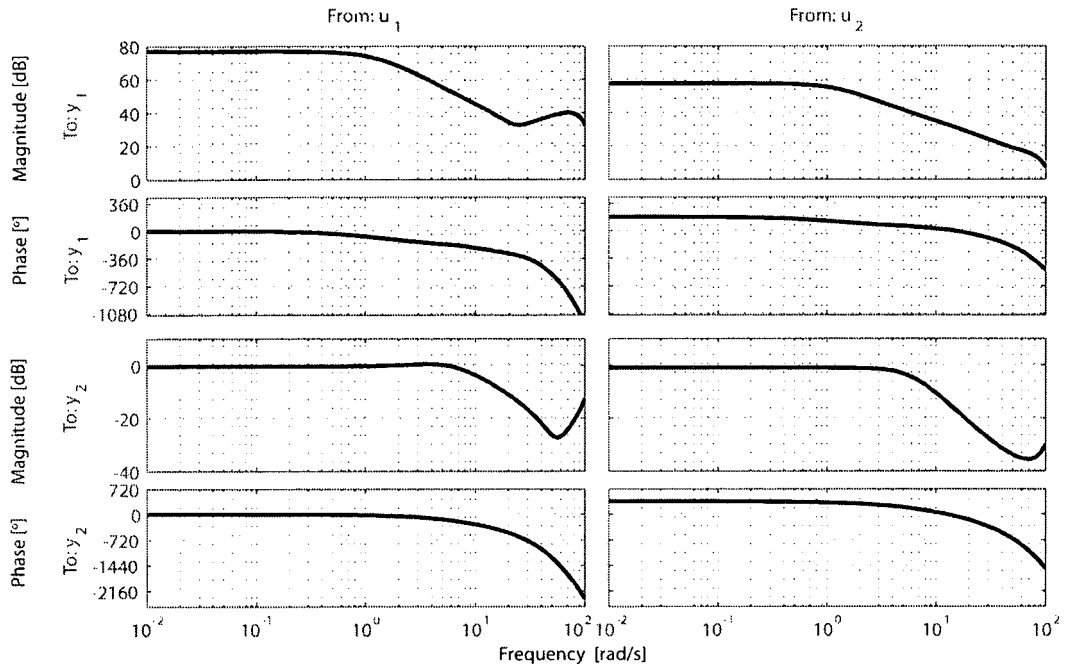

Figure 7.15: Bode plot of the compensated system

(RGA) over a range of frequencies of interest. The RGA is defined in equation 4.45, where for a 2×2 matrix it can been observed that only one element is necessary to assess the degree of cross channel interaction.

$$\Lambda(G) = \begin{bmatrix} \lambda_{11} & \lambda_{12} \\ \lambda_{21} & \lambda_{22} \end{bmatrix} = \begin{bmatrix} \lambda_{11} & 1 - \lambda_{11} \\ 1 - \lambda_{11} & \lambda_{11} \end{bmatrix} \tag{7.6}$$

Figure 7.16 displays the elements λ_{11} and λ_{12} of the RGA for frequencies up to the Nyquist frequency. At low frequencies the interaction is relatively low and therefore the input-output pairing is optimal since integral action can cause stability problems when the relative gains are small [100]. The high degree of interaction at the higher frequencies indicates the benefits of considering the problem in a multivariable formulation. Both channels are affected at high frequencies by both control inputs and therefore combining the inputs can create a fast response to disturbances. Furthermore, as both channels are active at these higher frequencies the RGA demonstrates the necessity to consider MIMO techniques rather than loop-at-a-time methods, to prevent instabilities or low robustness.

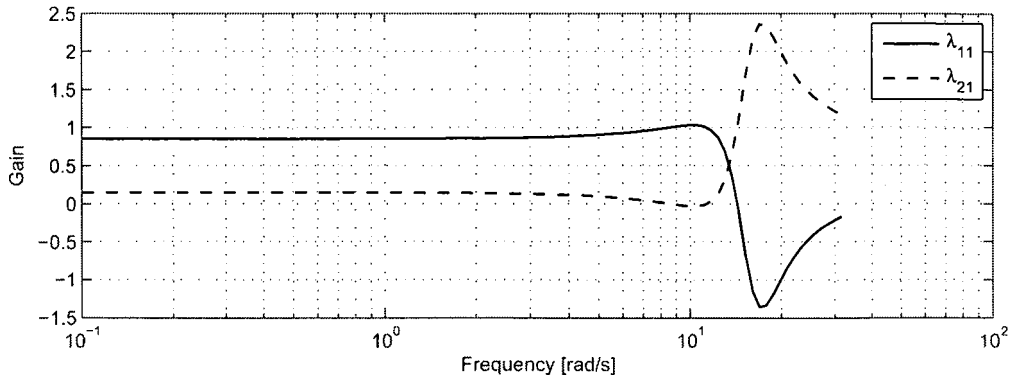

Figure 7.16: Frequency varying RGA values $\lambda 11$ and $\lambda 12$

7.6 PS Controller Design

The feedback controller was designed using the multivariable parameter space (PS) technique developed in the previous chapters. The frequency response of the linear compensated MIMO model is obtained directly from the discrete transfer functions (equations 7.2 - 7.5) for the frequency range of interest. In this application 200 frequencies up to the Nyquist frequency, logarithmically spaced in the range

$$10^{-3} \leq \omega \ [rad/s] \leq 10^{1.5}$$

were considered.

The controller specification outlined in section 7.3 are translated into appropriate weighting functions to guide the designer to a solution. Once suitable weights are selected the designer can iterate through the planes to converge on a local optimal solution. At each step the designer can tighten or relax one or more of the weighting functions as necessary to achieve the final goal. Ultimately for this application the aim is to achieve good disturbance rejection and tracking on the outputs and therefore, the weighting functions defining an admissible region act only to steer the designer towards suitable gains for the best time response.

In practice the automotive industry favours low order controllers due to their low computational requirements and therefore the controller designed here is constrained to 2nd order PID type. The controller is intended to operate once per fuelling event (every 180° of crank), which corresponds to a sample time between 0.02 and 0.05s. The elemental controllers structure was constrained to represent a PID with an appropriate time constant on the derivative gain, therefore the tuning parameters are $b_{2_{ij}}, b_{1_{ij}}$ and $b_{0_{ij}}$ in each element

$$k_{ij} = \frac{b_{2_{ij}} s^2 + b_{1_{ij}} s + b_{0_{ij}}}{0.07s + s}$$

7.6.1 Weighting Function Design

Since the AFR channel was linearised to obtain a theoretical unity path, the requirements on this channel vary considerably compared to the speed channel. For this particular problem only diagonal, right-hand weighting functions were found to be necessary. The primary sensitivity was used in the design to achieve the performance requirement together with the complimentary sensitivity function to ensure robustness. Other sensitivity requirements such as the control effort were not found to aid in the design due to the relatively large amount of actuation of the ABV and fuel at idle.

Weightings choices are intended to guide the designer to a solution though various iterations. At each iteration time response and weighting functions can be reviewed and adjusted as necessary. Indeed one of the strengths of the interactive approach is the freedom the designer has to move around the design space. This flexibility removes some of the difficulties in selecting weighting functions and graphically the designer can evaluate which frequencies are problematic.

Primary Sensitivity

The basic transient performance of the feedback controller is determined by the primary sensitivity function. For good tracking performance and disturbance rejection large gains at low frequencies are essential. Large integral gains achieve fast response to step or load changes and particularly important for AFR control is the zero steady-state error characteristic. Typically, low gains at frequencies greater than the gain cross over frequency are desirable for attenuation of high frequency noise.

The selected weightings were the 1st order low-pass functions of

$$W_S = \gamma_S \begin{bmatrix} \frac{s+1}{100s} & 0 \\ 0 & \frac{s+1}{10s} \end{bmatrix} \tag{7.7}$$

where γ_S is a scalar acting on the primary sensitivity weighting function.

Complementary Sensitivity

The complementary sensitivity function was designed to roll-off at high frequencies where plant interactions are most severe thereby adding the necessary robustness. This also has the effect of bounding the control effort at high frequencies and accordingly, control effort sensitivity functions were not necessary in this design. At low frequencies the complementary function allows high gains and therefore does not compromise steady-state tracking performance. The selected target weight for the complementary sensitivity function was chosen

as

$$W_T = \gamma_T \begin{bmatrix} \frac{10s+1}{100} & 0 \\ 0 & \frac{10s+1}{100} \end{bmatrix}$$

where γ_T is a scalar acting on the complementary sensitivity weighting function.

7.6.2 Parameter Plane Iterations

The parameter plane iterations began with relaxed scalars γ_S and γ_T applied to the primary and complementary sensitivity functions respectively. During the design these were gradually increased until the design met the requirements. No start controller was used in the design, ie the start controller was set to

$$K = \begin{bmatrix} \frac{0}{0.07s^2+s} & \frac{0}{0.07s^2+s} \\ \frac{0}{0.07s^2+s} & \frac{0}{0.07s^2+s} \end{bmatrix} \tag{7.8}$$

Since the input-output pairings were matched for low frequencies the design was started with $\gamma_S = 0.01$ and $\gamma_T = 0.01$ in the $b_0 b_1$ plane for the diagonal elements to create a PI-type decentralised controller. The following two iterations were for the off-diagonal elements, after which γ_S was increased to tighten the design space. During the initial iterations gains are selected from the centre of the admissible region as this is the obvious selection to meet the weighting functions. The four subsequent iterations were carried out in the $b_1 b_2$ plane before the constraint on the complementary sensitivity was tightened. As the design progresses the designer can choose to try different control gains within the admissible regions. This allows the designer some flexibility for improving the time response without violating the sensitivity functions.

The design required 34 iterations in total to provide a satisfactory design. Further tightening of the sensitivity functions after this point was found to have detrimental effect on the time response. Table 7.3 displays the 34 parameter plane iterations including the values of γ_S and γ_T and the gains selected in each parameter plane. Singular values plots of the resulting weighted primary and complementary sensitivity functions are illustrated in figures 7.17 and 7.18 respectively.

The resulting controller in continuous transfer function form was

$$K = \begin{bmatrix} \frac{6.222\times10^{-5}s^2+0.0002056s+0.0002178}{0.07s^2+s} & \frac{0.001921s^2+0.02001s+0.05124}{0.07s^2+s} \\ \frac{-0.0001274s^2-0.0002292s-0.000257}{0.07s^2+s} & \frac{-0.002172s^2+0.05905s+0.4001}{0.07s^2+s} \end{bmatrix} \tag{7.9}$$

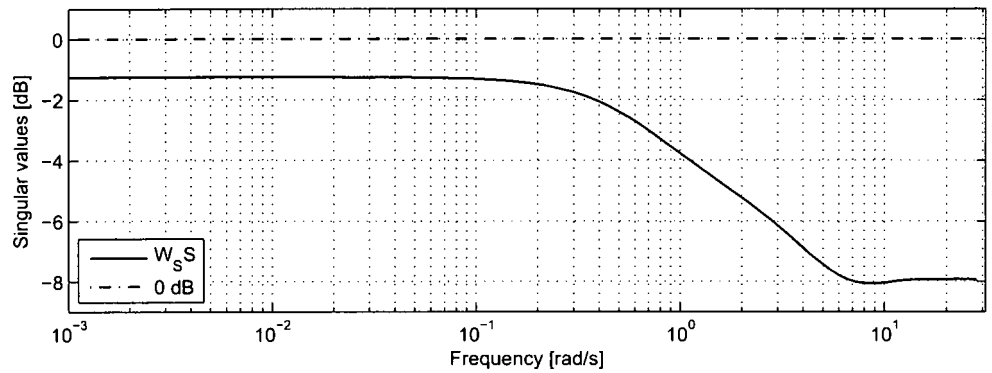

Figure 7.17: Maximum singular values of $W_S S$

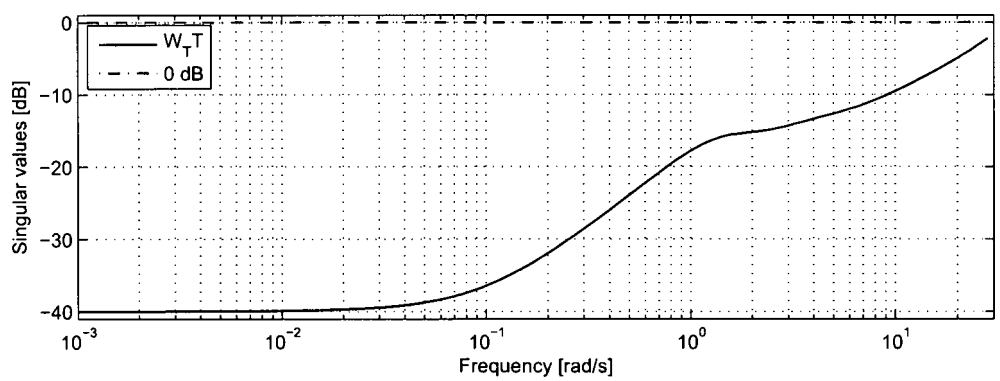

Figure 7.18: Maximum singular values of $W_T T$

It	Element	Plane	γ_S	γ_T	coeff-x	coeff-y
01	k_{11}	b_0b_1	0.01	0.01	$b_0 = +2.131 \times 10^{-4}$	$b_1 = +2.940 \times 10^{-4}$
02	k_{22}	b_0b_1	0.01	0.01	$b_0 = +3.255 \times 10^{-1}$	$b_1 = -6.141 \times 10^{-2}$
03	k_{21}	b_0b_1	0.05	0.01	$b_0 = +4.069 \times 10^{-2}$	$b_1 = +1.829 \times 10^{-2}$
04	k_{12}	b_0b_1	0.05	0.02	$b_0 = -1.210 \times 10^{-4}$	$b_1 = -6.227 \times 10^{-4}$
05	k_{11}	b_1b_2	0.05	0.02	$b_1 = +2.913 \times 10^{-4}$	$b_2 = +4.519 \times 10^{-5}$
06	k_{11}	b_1b_2	0.05	0.02	$b_1 = +2.913 \times 10^{-4}$	$b_2 = +4.519 \times 10^{-5}$
07	k_{22}	b_1b_2	0.1	0.02	$b_1 = +5.794 \times 10^{-2}$	$b_2 = +1.474 \times 10^{-2}$
08	k_{12}	b_1b_2	0.1	0.02	$b_1 = -3.441 \times 10^{-4}$	$b_2 = -1.387 \times 10^{-4}$
09	k_{11}	b_0b_1	0.2	0.1	$b_0 = +1.757 \times 10^{-4}$	$b_1 = +1.633 \times 10^{-4}$
10	k_{22}	b_0b_1	0.4	0.1	$b_0 = +3.998 \times 10^{-1}$	$b_1 = +5.865 \times 10^{-2}$
11	k_{21}	b_0b_1	0.4	0.1	$b_0 = +4.387 \times 10^{-2}$	$b_1 = +1.799 \times 10^{-2}$
12	k_{12}	b_0b_1	0.4	0.1	$b_0 = -2.760 \times 10^{-4}$	$b_1 = -2.652 \times 10^{-4}$
13	k_{11}	b_1b_2	0.5	0.1	$b_1 = +1.879 \times 10^{-4}$	$b_2 = +6.183 \times 10^{-5}$
14	k_{22}	b_1b_2	0.5	0.1	$b_1 = +6.212 \times 10^{-2}$	$b_2 = -7.343 \times 10^{-4}$
15	k_{21}	b_1b_2	0.5	0.1	$b_1 = +1.976 \times 10^{-2}$	$b_2 = +1.426 \times 10^{-3}$
16	k_{12}	b_1b_2	0.5	0.1	$b_1 = -1.554 \times 10^{-4}$	$b_2 = -1.532 \times 10^{-4}$
17	k_{11}	b_0b_1	0.8	0.3	$b_0 = +1.762 \times 10^{-4}$	$b_1 = +2.151 \times 10^{-4}$
18	k_{22}	b_0b_1	0.8	0.3	$b_0 = +3.727 \times 10^{-1}$	$b_1 = +6.459 \times 10^{-2}$
19	k_{21}	b_0b_1	0.8	0.3	$b_0 = +4.503 \times 10^{-2}$	$b_1 = +1.970 \times 10^{-2}$
20	k_{12}	b_1b_2	0.8	0.3	$b_1 = -2.644 \times 10^{-4}$	$b_2 = -1.492 \times 10^{-4}$
21	k_{11}	b_0b_1	0.8	0.5	$b_0 = +2.178 \times 10^{-4}$	$b_1 = +2.196 \times 10^{-4}$
22	k_{22}	b_0b_1	0.8	0.5	$b_0 = +4.001 \times 10^{-1}$	$b_1 = +6.520 \times 10^{-2}$
23	k_{21}	b_0b_1	0.8	0.5	$b_0 = +5.124 \times 10^{-2}$	$b_1 = +2.047 \times 10^{-2}$
24	k_{12}	b_0b_1	0.8	0.5	$b_0 = -2.570 \times 10^{-4}$	$b_1 = -2.705 \times 10^{-4}$
25	k_{11}	b_1b_2	1	0.7	$b_1 = +2.056 \times 10^{-4}$	$b_2 = +6.222 \times 10^{-5}$
26	k_{22}	b_1b_2	1	0.7	$b_1 = +5.905 \times 10^{-2}$	$b_2 = -2.172 \times 10^{-3}$
27	k_{21}	b_1b_2	1	0.7	$b_1 = +2.001 \times 10^{-2}$	$b_2 = +1.921 \times 10^{-3}$
28	k_{12}	b_1b_2	2.5	0.7	$b_1 = -2.292 \times 10^{-4}$	$b_2 = -1.274 \times 10^{-4}$
29	k_{11}	b_0b_1	2.5	0.7	$b_0 = +2.217 \times 10^{-4}$	$b_1 = +2.039 \times 10^{-4}$
30	k_{22}	b_0b_1	2.5	0.7	$b_0 = +4.071 \times 10^{-1}$	$b_1 = +5.923 \times 10^{-2}$
31	k_{21}	b_0b_1	2.5	0.9	$b_0 = +5.145 \times 10^{-2}$	$b_1 = +2.005 \times 10^{-2}$
32	k_{21}	b_0b_1	2.5	0.9	$b_0 = +5.145 \times 10^{-2}$	$b_1 = +2.005 \times 10^{-2}$
33	k_{21}	b_0b_1	4	1	$b_0 = +5.135 \times 10^{-2}$	$b_1 = +2.013 \times 10^{-2}$
34	k_{12}	b_0b_1	4	1	$b_0 = -3.150 \times 10^{-4}$	$b_1 = -2.311 \times 10^{-4}$

Table 7.3: Parameter plane design iterations for PID type feedback controller

7.7 Controller Performance

The controller performance was critically evaluated on the engine for tracking, disturbance rejection and control effort. The system response was assessed with both the feedforward compensator and feedback controllers acting. Before the feedback controller could be implemented on the engine it was necessary to convert it to discrete form. For simplicity the continuous controller of equation 7.9 was converted into state-space form, followed by a bilinear transformation to give the discrete realisation

$$A = \begin{bmatrix} 0.99133 & -0.082060 & 1.3586 \times 10^{-13} & -3.6455 \times 10^{-14} \\ -0.031093 & 0.70564 & -1.4372 \times 10^{-14} & -2.9569 \times 10^{-13} \\ 5.1361 \times 10^{-14} & 3.0008 \times 10^{-14} & 0.69697 & -0.10100 \\ -1.3653 \times 10^{-14} & -1.2916 \times 10^{-13} & -3.1301 \times 10^{-6} & 1.0000 \end{bmatrix}$$

$$B = \begin{bmatrix} 0.022187 & -9.3040 \times 10^{-16} \\ 0.13090 & 1.6345 \times 10^{-12} \\ -2.1588 \times 10^{-13} & 1.0471 \\ 5.7440 \times 10^{-14} & 0.21089 \end{bmatrix}$$

$$C = \begin{bmatrix} -0.00052298 & -0.0012416 & -0.0025348 & 0.0052292 \\ 0.00077701 & 0.0029794 & 0.014281 & 0.052193 \end{bmatrix}$$

$$D = \begin{bmatrix} 0.00078574 & 0.026409 \\ -0.0015795 & -0.016623 \end{bmatrix}$$

Disturbance rejection was evaluated by applying positive and negative load steps to the system acting at the mean load value of the compensator's range. During these steps the idle speed demand was set to the reference value of 880 rpm and the λ at 1. Step loads of approximately ± 6 Nm were applied to the engine through the low inertia dynamometer. The time response of the system to the positive step (decreasing the load on the engine) is displayed in figure 7.19. The response to negative step load (increasing the load on the engine) is displayed in figure 7.20. Both loading and unloading show similar response times, where the engine returns to ± 10 rpm of the nominal engine speed in around 3s. The AFR channel settles to within ± 0.01 of the mean after approximately 2s.

Tracking performance was assessed by applying a series of step tracking demands. Speed demands of ± 100 rpm were applied to the system operating at the nominal operating speed of 880 rpm, the AFR demand was fixed at $\lambda = 1$. The measured outputs for positive and negative step demands are displayed in figures 7.21 and 7.22 respectively. The response time to within 90% is around 2s, where a small deviation of approximately 0.03 is observed in λ. The negative step demand reveals slower performance. This can be assumed to be due to the longer sample periods at lower engine speeds and due to the lower stability at the near-stall region that the engine is taken into.

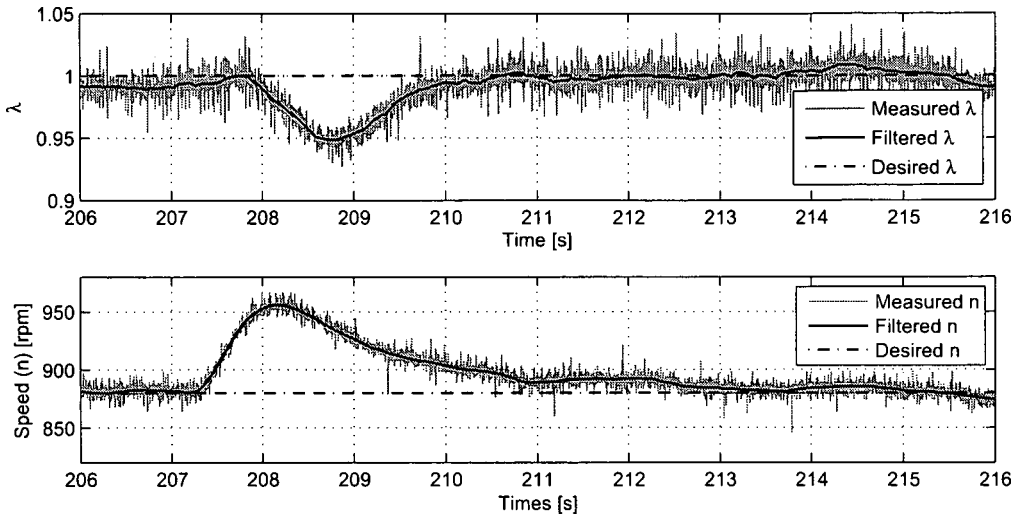

Figure 7.19: Closed loop system response to positive step load

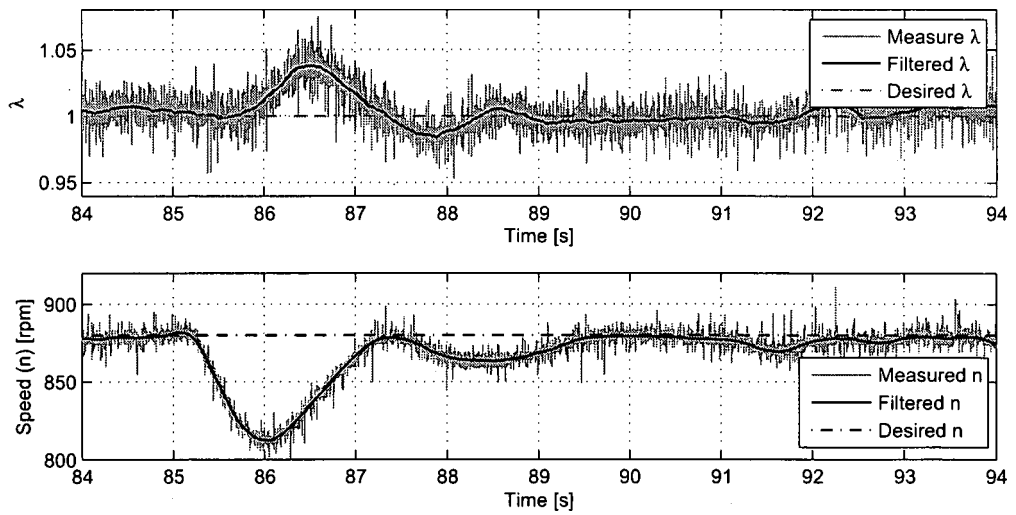

Figure 7.20: Closed loop system response to negative step load

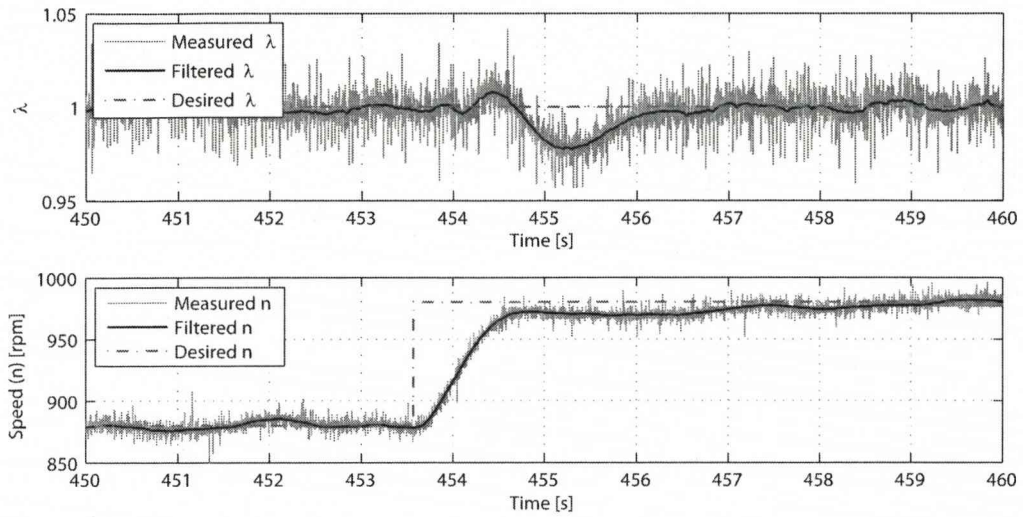

Figure 7.21: Closed loop system response to positive speed demand

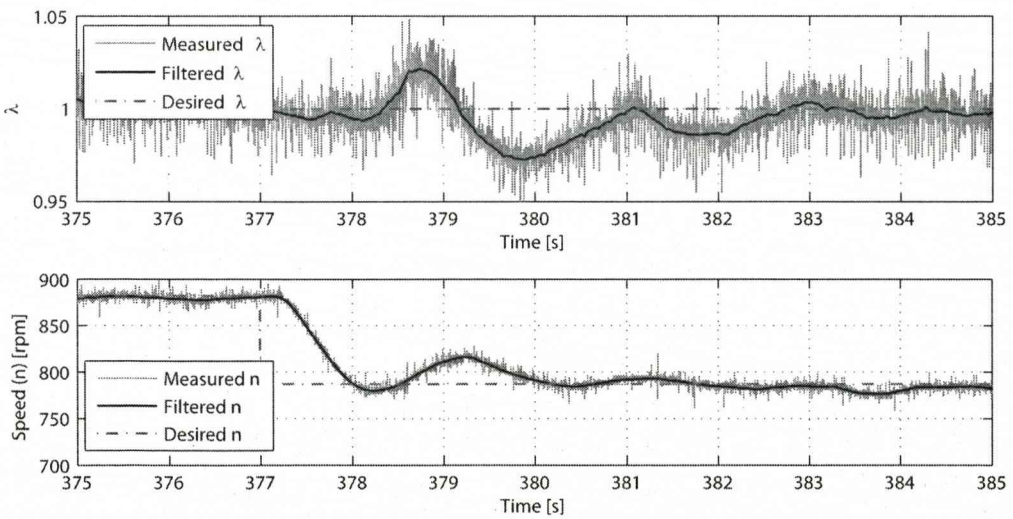

Figure 7.22: Closed loop system response to negative speed demand

Similar step tests were carried out on the AFR channel. During these tests the speed command was set to the constant nominal level of 880 rpm. Steps of ± 0.1 corresponding to lean and rich demands are displayed in figures 7.23 and 7.24 respectively. The step to $\lambda = 1.1$ takes over 3s to settle to within 0.01 of the demand and the speed channel is perturbed by approximately 50 rpm. This strong interaction is caused by a reduction in torque since the AFR becomes lean. When rich demand steps are applied the engine speed is almost unaffected and the response to the new set point is much sharper.

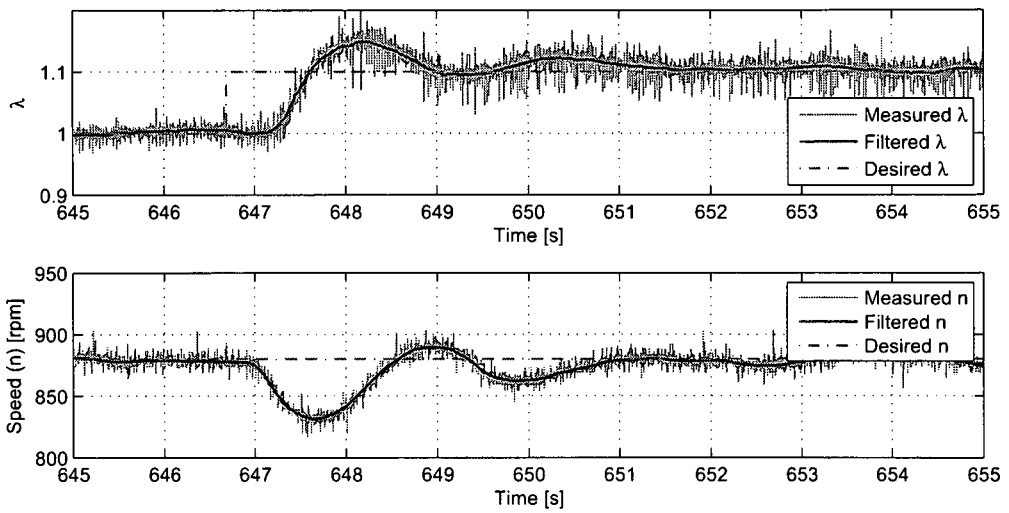

Figure 7.23: Closed loop system response to lean λ demand

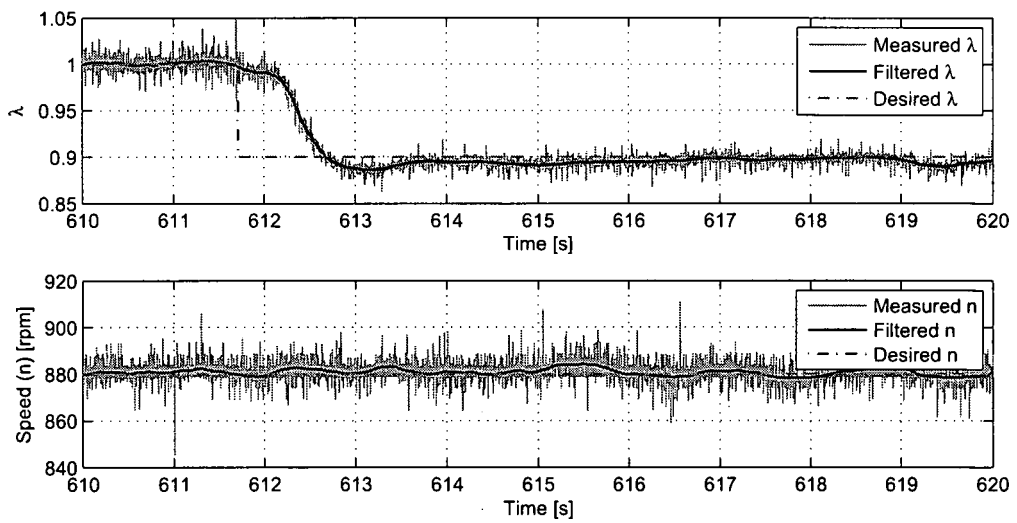

Figure 7.24: Closed loop system response to rich λ demand

For comparative purposes, load steps were applied to the engine using the standard EMS controllers, with the exception of the spark advance (SA) which was fixed. It is noted that the

EMS AFR feedback is through a standard switching type heated exhaust gas oxygen (HEGO) sensor and the strategy is from circa. 1995. Time response plots for positive and negative load steps are shown in figures 7.25 and 7.26 respectively. It can be seen that the settling time for the engine speed is significantly slower than with the methodology presented above. However, the slow response of the air channel allow the AFR to return to stoichiometric quickly, with a time response comparable to the multivariable control scheme. It is also worth noting the steady state response of the AFR channel under the EMS strategy is oscillatory due to the switching nature of the HEGO used in the feedback scheme.

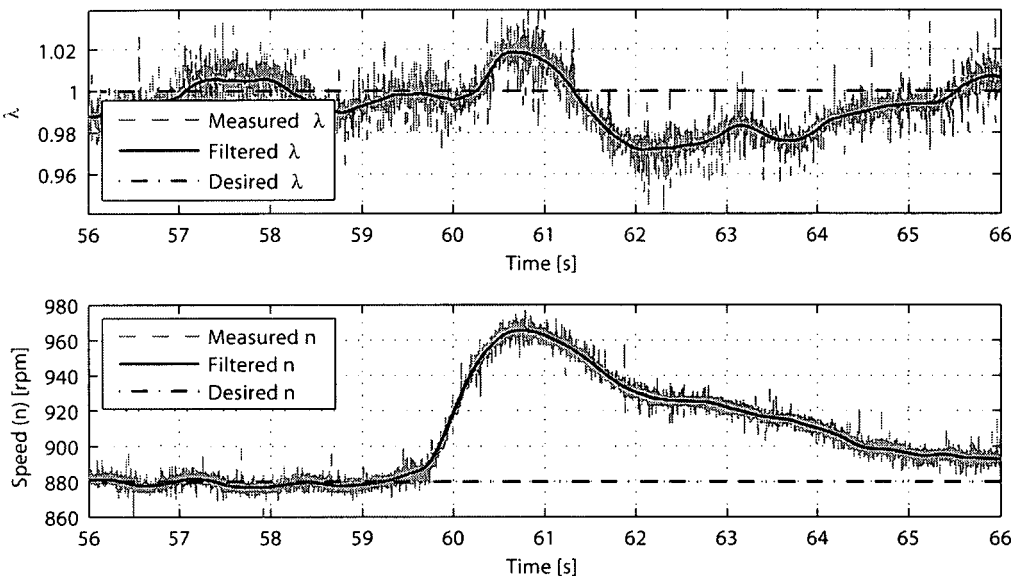

Figure 7.25: Closed loop EMS system response to positive step load

7.8 Cylinder Balancing

Significant performance gains can be achieved from the engine if each cylinder is balanced [60]. Manufacturing tolerances, variation between plants and different wear rates can lead to large differences in AFR (up to 5% [48]) between cylinders. With additional sensors available on each exhaust runner it is possible to optimise the combustion in each cylinder leading to greater torque production and better emission levels.

Faster feedback control is also possible if the oxygen sensor is moved closer to the exhaust port of the cylinder. Placing the sensors as close to the exhaust port as possible minimises any transport delays. Moreover, placing the sensor prior to the confluence point reduces cylinder-to-cylinder exhaust gases mixing and therefore allows each cylinder to be balanced to produce a stoichiometric AFR. Since the engine setup used here has only cylinder one

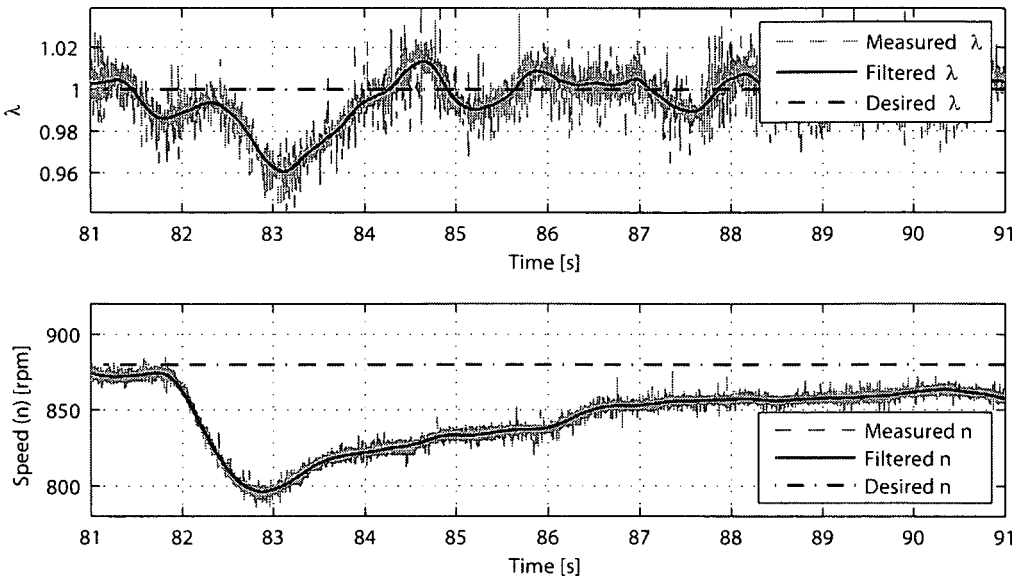

Figure 7.26: Closed loop EMS system response to negative step load

fitted with a close-coupled mounting point, the confluence point was used for measurement of the AFR. This placement is also more typical of a production engine due to the economics of using multiple sensors for feedback, moreover using the confluence point helps to smooth the signal due to mixing and therefore a feedback scheme is less affected by the stochastic nature of combustion.

However, it is anticipated that the above methodology could easily be extended to control each of the cylinder's fuel separately and therefore gain performance benefits from cylinder balancing. The close-coupled sensors would also improve the transient behaviour of the system as it would remove some of the significant time delays.

7.9 Conclusions

A novel system identification approach for the systematic calibration of a fuelling and speed controller strategy in the PFI SI engine was presented. Nonlinear black-box parameter identification directly produces a dynamic inverse multivariable NARMA feedforward controller and linearising feedback compensator to control AFR based on manifold pressure and engine speed. In contrast to traditional approaches of retarding the SA to gain fast actuation to disturbances it has been demonstrated that using both the air and fuel channels in a multivariable control scheme can result in fast regulation of the AFR and engine speed. Moreover this approach does not require the SA to be backed off from MBT position.

For the linearised feedback component, any linear robust feedback controller design method can be used to exploit the potential performance and robustness benefits of the multivariable linearising compensator. In this chapter a multivariable parameter space feedback controller technique was employed using a mixed sensitivity parameter space approach. Suitable weighting functions were used to guide the design toward suitable controller gains. With this interactive approach the designer can try different points in the design space achieving the required robustness and ultimately also achieve the desired time response.

The resulting identified feedforward and feedback compensator combined with the robust linear $\mathcal{H}_\infty$ controller scheme was experimentally demonstrated on a four cylinder 1.6l engine over the idle region. In the forward case different time delays are observed between MAP, engine speed and fuel and therefore a compromise between tracking performance and time response is necessary. The controller accurately determined the required fuel pulse width from engine speed and manifold pressure to jointly maintain stoichiometric air-to-fuel ratio and set engine speed. It regulated these by incorporation of a linear multivariable feedback controller. The resulting controller was demonstrated to perform quickly to remove disturbances.

In comparison to current industrial techniques of developing fuel maps the method is based entirely on rapidly obtained dynamically perturbed input-output data and thus not only saves considerable time but also captures dynamic effects.

Chapter 8

Conclusions and Recommendations for Future Work

8.1 Conclusions

Detailed in this thesis is the development and implementation of several engineering controller 'design tools'. Within the automotive industry, increased competition, greater demands from consumers and increasing environmental legislation is increasing the necessity to be able to rapidly design control systems with high performance requirements. Despite the trend for lower cost improved capability in modern electronics the EMS still remains a relatively constrained piece of hardware. Additionally, the requirement for ease of understanding and tuning by relatively non-expert control engineers means that industry strongly favours PID type feedback controllers. Accordingly, as engine systems become more complex and additional systems are added the control engineer is still faced with the difficulty of achieving high performance with low order controllers for complex systems.

There is no single solution for the different powertrain control problems. Many applications such as combustion control are subject to persistent noise disturbances and are suited to minimum variance type controllers. Many systems contain strong cross coupling between the various input-output relationships and as such it is necessary to consider multivariable feedback techniques. Fuelling control requires a fast feedforward controller in order to realise the performance requirements. Rapid calibration tools can greatly assist in developing such controllers.

The following contributions and conclusions for powertrain control can be drawn from this work:

- The fourth chapter of this thesis presented a constrained and minimum variance PS control technique suited to SISO systems with discrete or continuous formulations. Use

is made of the mean-squared value, evaluated from the spectral density function and Leverrier's algorithm to compute loci for a given closed loop output variance, provided the closed-loop system is rational and strictly proper. Loci of constant variance can thus be readily computed and mapped into parameter planes for any rational two term controller. Making use of the PS, additional constraints can be superimposed and therefore a robust, constrained-variance environment is created.

The technique was demonstrated to be useful for the design of an idle speed controller, where robustness constraints in terms of phase margins were superimposed on a constrained variance to non-conservatively obtain an idle speed controller which also acted to lower the closed-loop output variance.

A discrete example was used to compare a MV design, a tracking MV design and the parameter space technique. The parameter space technique was demonstrated to have improved tracking properties over both algebraic MV designs. Moreover, this was achieved with a significantly lower output variance than the MV controller with tracking.

A design example for controlling the PPP from the SA demonstrated the merits of the technique for designing low order controllers. SISO constrained variance controllers were designed and implemented on all four cylinders of an engine. Experimental validation showed the advantages of using closed loop control for the problem by balancing the cylinders and accurate tracking to an optimal set-point without excessively exciting the noise dynamics.

- In chapter 5 a low order, parameter space, controller design technique was developed. The technique allows for nominal performance and robust stability using MIMO $\mathcal{H}_\infty$ norm specifications on the weighted functions. The maximum singular value constraints at discrete frequencies yield circular loci which readily map into the parameter planes of any general format fixed low order controller structure to populate the matrix controller elements. The proposed method is uniformly adapted to producing controllers in continuous and discrete systems. The technique designs fixed, low order controllers through an interactive PS method for MIMO plants which are invertible and square in the input and output feedback channels. Regions satisfying the performance and stability constraints are superimposed graphically to give the designer insight in the design process.

  A multivariable idle speed disturbance rejection example for a natural gas engine demonstrated that using the PS method to map only the primary sensitivity function to the parameter plane can yield large improvements over existing low order and reduced order controller design methods. The PS approach demonstrated performance close to a full order algebraic Riccati solution using a mixed primary and control sen-

sitivity formulation. The PS and Riccati controller design techniques were shown to give better time response performance for the same level of robust stability than an eigenvalue PI tuning method.

When designing controllers the interactive nature of PS techniques allows the designer to select controller gains to meet time response criteria from a basic weighting function. This is in contrast to alternative techniques which require carefully selected weighting functions to achieve a good time response. The PS method was shown to alleviate much difficulty in selecting the weighting functions since only a basic first order weighting function was required for the primary sensitivity.

- In chapter 6 the multivariable PS technique was extended for non-square systems. Internal stability conditions for irrational unity feedback system were developed. Both sensitivity function constraint and internal stability results were conveniently stated directly in terms of the plant and weighting function frequency response matrices.

  The technique requires only non-parametric frequency response information and therefore has some significant advantages over current algebraic Riccati $\mathcal{H}_\infty$ methods. The technique allows the significant benefits of SISO parameter space, for interactive graphical design of fixed low order controllers, to be extended to multivariable systems that could be irrational and non-square problems with any number of MIMO mixed sensitivity function specifications. The superiority of the MIMO norm based design technique over SISO sequential loop design was demonstrated by a simple example. In a comparative study the proposed MIMO PS method was demonstrated by application to the indirect retuning of a reduced order $\mathcal{H}_\infty$ Riccati designed controller and the direct design of fixed low order controllers for a highly maneuverable aircraft (HiMAT) benchmark example.

- In chapter 7 a novel system identification approach for the systematic calibration of a fuelling and speed controller strategy in a PFI SI engine was presented. Use was made of nonlinear black-box parameter identification to directly obtain a dynamic inverse multivariable NARMA feedforward controller and linearising feedback compensator to control AFR by regulation of the fuel pulse width from the manifold pressure and engine speed.

  Using the linearised AFR path a multivariable controller was designed using the mixed sensitivity PS approach developed in chapter 6 to regulate the idle speed and AFR. Suitable weighting functions were used to guide the design towards suitable controller gains. With this interactive approach the designer can try different points in the design space achieving the required robustness and ultimately also achieving the desired time response.

The resulting identified feedforward and feedback compensator combined with the robust linear $\mathcal{H}_\infty$ PS controller scheme was experimentally demonstrated on a four cylinder 1.6l engine over the idle region. In the forward case different time delays are observed between the inputs MAP, engine speed and fuel and the AFR, therefore a compromise between tracking performance and time response was necessary. The controller accurately determined the required fuel pulse width from engine speed and manifold pressure to jointly maintain stoichiometric air-to-fuel ratio and engine speed and regulated these by incorporation of a linear multivariable feedback controller. The resulting controller was demonstrated to perform quickly to disturbances.

In comparison to current industrial techniques of developing fuel maps, the method is based entirely on identifying a nonlinear compensator from rapidly obtained dynamically perturbed input-output data and thus not only saves considerable time but also captures dynamic effects.

8.2 Recommendations for Future Work

It is recommended that some methods presented in this thesis are extended to improve the scope of the techniques and further validate the usefulness of the approaches. The following suggestions are made:

PS Robust Performance: Two Disc Problem

The mixed sensitivity approach developed in chapter 6 could be further developed to solve the non-conservative, robust-performance, two disc problem. Since the PS technique directly handles frequency response information this would allow uncertainty information obtained through identification techniques to be used to define the system uncertainty. It is anticipated that linear matrix inequalities (LMI) would be useful for such an extension.

Automated Parameter Space Search

For systems with a large number of inputs and outputs, or for systems with complex dynamics an automated PS search technique would make the technique more attractive. Provided a set of stablising gains are included at the start of the design the admissible region could readily be detected. An algorithm which detects boundaries and then locates the centre would be extremely useful in sensitivity minimisaton problems. Alternatively, an automated search which reduces the sensitivity functions to a pre-determined level would speed up the design process but also allow the designer the freedom to choose gains away from the centre in

final iterations and therefore maintain the benefits gained by the interactive nature of the technique.

Full engine range I-NARMA

It is recommended that the fuelling controller obtained using the inverse-NARMA black box modelling approach presented in chapter 7 is extended over the entire engine operating region. It is anticipated that the nonlinearities and model structure would be significantly more complex and therefore a systematic structure selection method would be necessary.

Due to the large speed range of the engine it is recommended that a study is made into appropriate input signals to ensure sufficient balance is achieved between high and low frequency dynamics across this range. Furthermore, care must taken to ensure the load applied during the identification does not cause engine stall at low speeds or cause the engine speed to saturate at the maximum speed of its range. To avoid these problems it could be necessary to consider several small speed and load ranges which are subsequently scheduled.

It is also suggested that alternative identification algorithms are evaluated for suitability to the problem. Other least squares algorithms could be advantageous to the problem. Neural networks could also be particularly useful since they can handle specific nonlinearities.

Away from the idle region, speed regulation is not required. However, it would be interesting to continue the multivariable feedback control for torque and AFR control since these outputs are highly coupled through the air and fuel paths.

References

[1] G.C.M. De Abreu, R.L. Teixeira, and J.F. Ribeiro. A neural network-based direct inverse control for active control of vibrations of mechanical systems. *IEEE Proceedings. Sixth Brazilian Symposium on Neural Networks*, pages 107–112, 2000.

[2] J. Ackermann. Parameter space design of robust control system. *IEEE Transactions on Automatic Control*, 25(6):1058–1072, 1980.

[3] J. Ackermann, P. Blue, T. Bünte, L. Güvenç, D. Kaesbauer, M. Kordt, M. Muhler, and D. Odenthal. *Robust Control: The Parameter Space Approach.* Springer, 2002.

[4] M.A. Aizerman. *Theory of Automatic Control.* Pergamon Press, London, 1963.

[5] B.D.O Anderson and Y. Liu. Controller reduction: Concepts and approaches. *IEEE Transactions on Automatic Control*, 34(8):802–812, 1999.

[6] K. A. Åstrom. *Introduction to Stochastic Control Theory.* Academic Press, 1970.

[7] K. A. Åstrom. *Introduction to Stochastic Control Theory.* Academic Press, 1979.

[8] A.C. Atkinson and A.N. Donev. *Optimum Experimental Designs.* Clarendon, Oxford, 1992.

[9] J.-I. Bae and S.-C. Bae. A study on the engine downsizing using mechanical supercharger. *Journal of Mechanical science and technology*, 19(12):2321–2329, 2005.

[10] G. Balas, R. Chiang, A. Pickard, and M. Safonov. *Robust Control Toolbox 3 User's Guide.* The MathsWorks, Inc., 2007.

[11] G.J. Balas, J.C. Doyle, K. Glover, A. Packard, and R. Smith. *μ-Analysis and Synthesis Toolbox - User's Guide.* The MathsWorks, Inc., 1993.

[12] A.G. Bell. *Four-Stroke Performance Tuning.* Haynes, Sparkford, UK, 2002.

[13] R. Bellman. *Introduction to Matrix Analysis.* McGraw Hill, 1960.

[14] V. Besson. *Parameter Space Robust Control for S.I. Engine Idle Speed.* PhD Thesis, The University of Liverpool, England, UK, 1998.

[15] V. Besson and A.T. Shenton. Interactive control system design by a mixed $\mathcal{H}_\infty$-parameter space method. *IEEE Transactions on Automatic Control*, 42(7):946–955, 1997.

[16] V. Besson and A.T. Shenton. An interactive parameter space method for robust performance in mixed sensitivity problem. *IEEE Transactions on Automatic Control*, pages 1272–1276, 1999.

[17] V. Besson and A.T. Shenton. Interactive parameter space design method for robust performance of MISO control systems. *IEEE Transactions on Automatic Control*, pages 1917–1924, 2000.

[18] S.A. Billings, S. Chen, and R.J Backhouse. The identification of linear and non-linear models of a turbocharged automotive diesel engine. *Mechanical Systems and Signal Processing*, 3(2):123–142, 1989.

[19] S.A. Billings and I.J. Leontartitis. Parameter estimation techniques for non-linear systems. *Proceedings of 6th IFAC Symposium on Identification and System Parameter Estimation*, pages 505–510, 1982.

[20] S.A. Billings and Q.M. Zhu. A structure detection algorithm for nonlinear dynamic rational models. *International Journal of Control*, 59(6):1439–1463, 1994.

[21] C. Borghesani, Y. Chait, and O. Yaniv. *Quantitative Feedback Theory Toolbox.* The MathsWorks, Inc., 1994.

[22] Bosch. *Gasoline-engine management.* SAE International, 1999.

[23] F.M. Callier and C. Desoer. Necessary and sufficient conditions for the stability of n-input n-output convolution feedback systems with a finite number of poles. *IEEE Transactions on Automatic Control*, 18(3):295–298, 1973.

[24] C. Carnevale and A. Moschetti. Idle speed control with h-infinity technique. *SAE Technical Papers*, 930770, 1993.

[25] S.D Carroll. *Control of S.I. Engines Using In-Cylinder Pressure.* PhD Thesis, The University of Liverpool, England, UK, 2003.

[26] C.H. Chang and K.W. Han. Gain margins and phase margins for control systems with adjustable parameters. *Journal of Guidance, Control and Dynamics*, 15(4):404–408, 1990.

[27] C.H. Chang and K.W. Han. Gain margins and phase margins for sample-data control systems with adjustable parameters. *IEE Proceedings. Volume: D*, 138:285–291, 1991.

[28] R. Chiang and M. Safonov. *Robust Control Toolbox User's Guide.* The MathsWorks, Inc., 1992.

[29] D.W. Clarke and P.J. Gawthrop. Self-tuning control. *IEE Proceedings. Volume: D*, 122:929–934, 1975.

[30] R. Cook. Gain and phase boundary routine for two-loop feedback systems. *IEEE Transactions on Automatic Control*, 11(3):573– 576, 1966.

[31] H. Demuth and M. Beale. *Neural Network Toolbox.* The MathsWorks, Inc., 1998.

[32] C.A Desoer and M. Vidyasagar. *Feedback Systems: Input-Output Properties.* Academic Press, 1975.

[33] J.C. Doyle. Robustness of multiloop linear feedback systems. *Proceedings of the Conference of Decision and Control*, 1978.

[34] J.C. Doyle. Quantitative feedback theory (QFT) and robust control. *IEEE Proceedings of the American Control Conference, New York*, 3:1691–1689, 1986.

[35] J.C. Doyle and B.A. Francis. *Feedback Control Theory.* Macmillan, 1992.

[36] J.C. Doyle, K. Glover, P.P Khargonekar, and B.A Francis. State-space solutions to standard $\mathcal{H}_\epsilon$ and $\mathcal{H}_\infty$ control problems. *IEEE Transactions on Automatic Control*, 38(8):831–847, 1989.

[37] R.D. Fruechte, F.E. Coats, and C.H. Folkerts. Idle speed control for automobiles. *IEEE 17th Inter-Society Energy Conservation Engineering Conference*, pages 467–472, 1983.

[38] L. Gould G. Newton and J. Kaiser. *Analytical Design of Linear Feedback Controls.* Wiley, 1957.

[39] S. Gaikwad and D. Rivera. Control-relevant input signal design for multivariable system identification: Application to high-purity distillation. *Proceedings of the 13th IFAC World Congress*, M:349–354, 1996.

[40] A. Ganagopadhyay and P. Meckl. Multivariable PI tuning for disturbance rejection and application to engine idle speed control simulation. *International Journal of Control*, 74(10):1033–1041, 2001.

[41] A. U. Genç. A state-space algorithm for designing $\mathcal{H}_\infty$ loop shaping PID controllers. http://www-control.eng.cam.ac.uk/aug20/hinf_pid.pdf, 2000.

[42] M.J. Grimble. Restricted structure controller tuning and performance assessment. *Control Theory and Applications, IEE Proceedings*, 1(149):8–16, 2002.

[43] M.J. Grimble. Optimal restricted structure control with prespecified gain or phase margins. *Control Theory and Applications, IEE Proceedings*, 3(151):271–277, 2004.

[44] L. Güvenç and J. Ackermann. Links between the parameter space and frequency domain methods of robust control. *International Journal of Robust and Nonlinear Control*, 11:1435–1453, 2001.

[45] L. Guzzella and C. H. Onder. *Introduction to Modeling and Control of Internal Combustion Engine Systems.* Springer, 2004.

[46] J.W. Helton and O. Merino. *Classical Control Using $\mathcal{H}_\infty$ Methods; Theory, Optimization and Design and Classical Control Using $\mathcal{H}_\infty$ Methods; An Introduction to Design.* SIAM, Philadelphia, 1998.

[47] E. Hendricks and S.C. Sorenson. Mean value modeling of spark ignition engines. *SAE Technical Papers*, 900616, 1990.

[48] J. Heywood. *Internal Combustion Engine Fundamentals.* McGraw-Hill, 1988.

[49] H. Hong, G.B. Parvate-Patil, and B. Gordon. Review and analysis of variable valve timing strategieseight ways to approach. *Proc. Instn Mech. Engrs Part D: J. Automobile Engineering*, 218:1179–1200, 2004.

[50] I. Horowitz. Improvement in quantitative non-linear feedback design by cancellation. *International Journal of Control*, 34:547–560, 1981.

[51] C.H. Houpis. Horowitz: bridging the gap. *International Journal of Robust and Nonlinear Control*, 12(4):295–302, 2002.

[52] C.H. Houpis and S.J. Rasmussen. *Quantitative feedback theory: fundamentals and applications.* Marcel Dekker, New York, 1999.

[53] C.H. Houpis and R.R. Sating. Mimo qft cad package (version 3). *International Journal of Robust and Nonlinear Control*, 7:533–549, 1997.

[54] D. Hrovat and J. Sun. Models and control methodologies for IC engine idle speed control design. *Control Engineering Practice*, 11:279–290, June 2002.

[55] S.C. Hsieh, A.G. Stefanopoulou, J.S Freudenberg, and K.R. Butts. Emission and driveability tradeoffs in a variable cam timing SI engine with electronic thottle. *Proceedings of the American Control Conference*, 1:284–288, 1997.

[56] M. Jankovic, F. Frischmuth, A. Stefanopoulou, and J.A. Cook. Torque management of engines with variable cam timing. *IEEE Control Systems Magazine*, 8(5):34–42, 1998.

[57] M. Jankovic and S.W. Magner. Variable cam timing: Consequences to automotive engine control design. *IFAC 15th Trienninal World Congress*, pages 271–276, 2002.

[58] S. Jayasuriya and M.A. Franchek. A qft type design methodology for a parallel plant structure and its application in idle speed control. *International Journal of Control*, 5(60):653–670, 1994.

[59] R. Jurgen. *Automotive Electronics Handbook.* McGraw Hill, 1995.

[60] J.L. Kainz and J.C. Smith. Individual cylinder fuel control with a switching oxygen sensor. *SAE Technical Papers*, 1999-01-0546, 1999.

[61] M. Kerr and S. Jayasuriya. An improved non-sequential MIMO QFT design method. *American Control Conference*, pages 2857–2862, June 2005.

[62] P.P Khargonekar and M.A Rotea. Mixed h2/h-infinity control - a convex optimization approach. *IEEE Transactions on Automatic Control*, 36:824–837, July 1991.

[63] H. Kwakernaak. Robust control and $\mathcal{H}_\infty$-optimization-tutorial paper. *Automatica*, 29(2):255–273, 1993.

[64] T.H. Lake. Turbocharging concepts for downsized di gasoline engines. *SAE Technical Papers*, 2004-01-0036, 2004.

[65] I.D. Landau and A. Karimi. Robust digital control using pole placement with sensitivity function shaping method. *International Journal of Robust and Nonlinear Control*, 8:191–210, 1998.

[66] B. Lecointe. Downsizing a gasoline engine using turbocharging with direct injection. *SAE Technical Papers*, 2003-01-0542, 2003.

[67] D.P. Lindorff. *Theory of Sampled-Data Control Systems.* Wiley, 1965.

[68] L. Ljung. *System Identification.* Linköping University, 1995.

[69] L. Ljung. *System Identification Theory for the User - 2nd edition.* Prentice Hall, 1999.

[70] L. Ljung. *System Identification Toolbox User's Guide.* The MathsWorks, Inc., 2005.

[71] P.D. Dobson M. Hubbard and J.D. Powell. Closed loop control of spark advance using a cylinder pressure sensor. *ASME Journal of Dynamic Systems, Measurement and Control*, pages 414–420, December 1976.

[72] C. Manzie and H.C. Watson. A novel approach to disturbance rejection in idle speed control towards reduced idle fuel consumption. *IMechE Part D: Journal of Automobile Engineering*, 217:677–690, 2003.

[73] Mathworks. *Genetic Algorithm and Direct Search Toolbox 2 User's Guide.* The MathsWorks, Inc., 2007.

[74] D. McFarlane and K. Glover. A loop shaping design procedure using H_∞ synthesis. *IEEE Transactions on Automatic Control*, 37(6):759–769, 1992.

[75] D. McLean. *Automatic Flight Control Systems.* Prentice Hall, Hemel Hempstead, 1990.

[76] D. Mitrović. Graphical analysis and synthesis of feedback control systems, I - theory and analysis, II - synthesis.

[77] M. Muhler. Mapping MIMO control system specifications into parameter space. *Proceedings of the 41st IEEE Conference on Decision and Control*, pages 4527–4532, 2002.

[78] S. Sánchez-Pe na and M. Sznaier. *Robust Systems Theory and Applications.* Wiley, 1998.

[79] Y.I. Niemark. On the problem of the distribution of roots of polynomials. *Dokl. Akad. Nauk. SSSR*, 58:357, 1947.

[80] Y.I. Niemark. Structure of the D-partition of the space of polynomials and the diagrams of vishnegradskii and nyquist. *Dokl. Akad. Nauk. SSSR*, 59:853, 1948.

[81] G. Obinata and B.D.O. Anderson. *Model reduction for control design.* Springer, 2001.

[82] A.P. Petridis. *Non-linear robust control of S.I. engines.* PhD Thesis, The University of Liverpool, England, UK, 2000.

[83] A.P. Petridis and A.T. Shenton. Inverse-NARMA: a robust control method applied to SI engine idle-speed regulation. *Control Engineering Practice*, 7:279290, 2003.

[84] B. Porter. *Stability criteria for linear dynamical systems.* Academic Press, London, 1968.

[85] J.D. Powell. Engine control using in-cylinder pressure: Past, present and future. *ASME Journal of Dynamic System, Measurement, and Control*, 115:343–350, June 1993.

[86] M. Saeki. Fixed structure PID controller design for standard h_∞ control problem. *Transactions of the Institute of Systems Control and Information Engineers*, 7(12):520–527, 1994.

[87] M. Saeki. Fixed structure PID controller design for standard h_∞ control problem. *Automatica*, 42:93–100, 2006.

[88] M. Saeki and K. Aimoto. PID controller optimization of $\mathcal{H}_\infty$ control by linear programming. *International Journal of Robust and Nonlinear Control*, 10:83–99, 2000.

[89] S.Barnett and C.Storey. *Matrix Methods in Stability Theory.* Thomas Nelson and Sons Ltd, London, 1970.

[90] Z. Shafiei and A.T. Shenton. Tuning of PID controllers for stable and unstable systems with time delay. *Automatica*, 30(10):1609–1615, 1994.

[91] Z. Shafiei and A.T. Shenton. *MES/ATS/FMC/101/96/1996: Advanced Control Methodology Program.* Department of Engineering, University of Liverpool, England UK, 1996.

[92] Z. Shafiei and A.T. Shenton. Frequency-domain design of PID controllers for stable and unstable systems with time delay. *Automatica*, 33(12):2223–2232, 1997.

[93] A.T. Shenton. *Internal report, MES/ATS/INT/045/2003: Internal Report NARMAX system representations.* Department of Engineering, The University of Liverpool, England UK, 2003.

[94] A.T. Shenton. Automotive applications of control. *EPSRC/UKACC Postgraduate Workshop, 28-29 August UKAC International Control Conference*, pages 1–24, 2006.

[95] A.T Shenton and Z. Shafiei. Relative stability for control systems with adjustable parameters. *Journal of Guidance Control and Dynamics, AIAA*, 17(2):304–310, 1994.

[96] D.D. Siljak. Analysis and synthesis of feedback control systems pts I,II,III. *IEEE Transactions on Applications in Industry*, 83:449–473, 1964.

[97] D.D. Siljak. Parameter space methods for robust control design: A guided tour. *IEEE Transactions on Automatic Control*, 34(7):674–688, 1989.

[98] J. Sjöberg, H. Hjalmarsson, and L. Ljung. Neural networks in system identification. *Department of Electrical Engineering, Linkping University, Sweden*, 1994.

[99] J. Sjöeberg, Q. Zhang, L. Ljung, A. Benveniste, B. Delyon, P.Y. Glorennec, H. Hjalmarsson, and A. Juditsky. Nonlinear black-box modeling in system identification: a unified overview. *Automatica*, 31(12):1691–1724, 1995.

[100] S. Skogestad and I. Postlewaite. *Multivariable Feedback Control Analysis and Design.* Wiley, 2004.

[101] T. Söderstöm and P. Stoica. *System Identification.* Prentice Hall, 1989.

[102] A. Stefanopoulou. *Modeling and Control of Advanced Technology Engines.* PhD Thesis, The University of Michigan, 1996.

[103] J. Sun, I. Kolmanovsky, J.A. Cook, and J.H. Buckland. Modeling and control of automotive powertrain systems: A tutorial. *Proceedings of American Control Conference*, pages 3271–3283, 2005.

[104] G.J. Thaler and R.G. Brown. *Analysis and Design of Feedback Control Systems.* McGraw Hill, 1960.

[105] G. Triantos. *NARMAX Modelling and Control With Powertrain Applications.* PhD Thesis, The University of Liverpool, England, UK, 2006.

[106] G. Triantos and A.T. Shenton. NARMAX structure selection for powertrain control. *Proceedings IFAC symposium on: Advances in Automotive Control, Salerno*, pages 1–4, 2004.

[107] G. Triantos, A.T. Shenton, and S.D. Carroll. Minimum variance control of cylinder peak pressure position. *Proceedings IFAC symposium on: Advances in Automotive Control, Salerno*, pages 158–163, 2004.

[108] U.I. Ukpai and S. Jayasuriya. Using controller reduction techniques for efficient PID controller synthesis. *Transactions of ASME, Journal of Dynamic Systems, Measurement, and Control*, 126:692–696, 2004.

[109] P.E Wellstead and M.B Zarrop. *Self-tuning Systems: Control and Signal Processing.* Wiley, 1991.

[110] S.J. Williams, D. Hrovat, C. Davey, D. Maclay, J.W. Crevel, and L.F Chen. Idle speed control design using and H-infinity approach. *Proceedings of ACC*, pages 1950–1956, 1989.

[111] S. Yamato and I. Hashimoto. Present status and future needs the view from japanese industry. *Proceedings of CPCIV, 4th International Conference Chemical Process Control*, 1991.

[112] G. Zames. Feedback and optimal sensitivity: Model reference transformation multiplicative seminorms and approximate inverses. *IEEE transactions on Automatic Control*, 26(2):301–320, 1981.

[113] F. Zhao, D.L. Harrington, and M.-C. Lai. *Automotive Gasoline Direct-injection Engines.* Society of Automotive Engineers, 2002.

[114] F. Zhao, M.C. Lai, and D.L. Harrington. Automotive spark-ignited direct-injection gasoline engines. *Progress in Energy and Combustion Science*, 25:437–562, 1999.

[115] K. Zhou, J.C. Doyle, and K. Glover. *Robust and Optimal Control.* Prentice Hall, 1996.